ROMAN LEAD SILVER SMELTING AT RIO TINTO

The case study of Corta Lago

Thesis submitted by Lorna Anguilano
For PhD in Archaeology

University College London

I, Lorna Anguilano confirm that the work presented in this thesis is my own. Where information has been derived from other sources, I confirm that this has been indicated in the thesis.

To my parents

Ai miei genitori

Abstract

The Rio Tinto area is famous for the presence there of a rich concentration of several metals, in particular copper, silver and manganese, which were exploited from the Bronze Age up to few decades ago. The modern mining industry has been responsible for both bringing to light and destroying signs of past exploitation of the mines and metal production there.

The Corta Lago site owes its discovery to the open cast exploitation that reduced the whole mount of Cerro Colorado to an artificial canyon. This exploitation left behind sections of antique metallurgical debris as well as revealing the old underground workings. The Corta Lago site dates from the Bronze Age up to the 2nd century AD, consisting mainly of silver and copper production slag, but also including litharge cakes, tuyéres and pottery.

The project focused on the study of silver production slag from different periods using petrograhical and chemical techniques, such as Optical Microscopy, X-Ray Diffraction, X-Ray Fluorescence, Scanning Electron Microscopy associated to Energy Dispersive Spectrometry and Multi-Collector Inductively Coupled Plasma Mass Spectrometry. The aim of the project was to reconstruct the metallurgical processes of the different periods, detecting any differences and similarities.

The mineral exploited was jarosite, $XFe^{3+}{}_3(OH)_6(SO_4)_2$, where X can be K, Na, Pb, Ag and NH_4, and the results show that the system of production was much more similar to iron production than silver. In the slag, the main mineral is fayalite, and the concentration of lead is around 1%.

These results and study of the jarosite suggest the possibility of different sources of lead for the collection of silver in the system, and this is the reason for the utilization of the MC-ICP MS for the analysis of the lead isotopes. The results for the isotopes indicate the addition of a second source of lead used as lead metal in the system to increase the amount of lead and improve the collection of silver.

The differences in the processes used at different periods are the amount of lead coming from another site that was added, and the level of standardization of the system. While the first difference is evident in a comparison between the pre-Roman process and one of the Republican phases, the second is mainly visible between the pre-Roman and Roman processes. At this stage the aim of the project was to attempt

to correlate the differences in the processes, metallurgical skills and geological knowledge.

Table of contents

List of figures

List of tables

Acknowledgements

Several people have supported and helped me through the years, in the time spent in the lab and in the time spent reading and writing. First of all I would like to thank my supervisor Thilo Rehren for the patience, the support and the intellectual stimuli. I would like to thank all the people that have worked in Rio Tinto, Paul and Brenda Craddock, Phil Andrews, Aurelio Perez Macias, they all have helped me reconstructing the history of the material as well as giving me some flavours of how the environment was during the excavations. I want to remember here also the support obtained by Aquilino Delgado, director of the Rio Tinto Museum, and Professor Saez, from the University of Huelva. Dr Delgado escorted me around the Rio Tinto area, showing me, where possible the smelting areas and telling me about the more recent history of the mining district, and Professor Saez supported me with the geological understanding of the area.

I want to thank Simon Groom and Kevin Reeves for the help in the lab, with the instruments, and for the company during the long hours preparing samples and in front of the SEM. I want to thank Anna Karatzani, Fatma Mari and Mike Charlton both professionally and as friends.

I do not believe any of this would have been possible without the presence of my dear friends David, Olga, Simon, Elpida and Lunia that accompanied me through this adventure.

Finally, this project was funded by the Marie Curie Early Stage Training fellowship which made it possible for me to focus in the learning process of a doctorate.

CHAPTER 1

Introduction

1.1 The importance of Iberian metal production in Antiquity

The study of mines and metal production constitutes a speciality far removed from the field of the historical sciences. The main reason for this separation seems to be the difficulty in handling the technical questions for a classical historian. It is easy to find treatments of the administrative and economic aspects of the subject, but general works treating the entire picture are rare. A purely archaeometallurgical treatment is unlikely to revolutionise the field of history, but it can provide significant specialist information and data to historians and theoretical scholars that would contribute to the overall understanding of the organisational processes of metal production.

Within this framework, this thesis does not claim to provide definite answers to historical questions. This is a comparative thesis that aims to establish the metallurgical processes in place at the sites of Corta Lago between the Orientalising period (700-300 BC divided in Late Bronge Age, Phoenician and Ibero-punic for the rest of this thesis) and the 2nd century AD, and Tharsis during the Roman Republican and Imperial periods, in order to highlight the differences and similarities in terms of the technical processes involved, as they changed over time and within the geological constraints of the region. These observations form the basis for a greater understanding of improvements in geological and metallurgical knowledge across time. In turn, the knowledge and subsequent organisation of metallurgical production represents one of the underlying causes of socio-economic change.

The subject is vast, as vast as the Iberian Peninsula that in Roman times was considered as a discrete entity (Hispania), without the modern distinction between Spain and Portugal. The time scale of the exploitation of the area is vast as well, covering at least six centuries, from before the Roman conquest (197 BC) to the late Empire. The present study is not limited to the Roman occupation, because it is important to show that the Roman exploitation and production of metals was not imposed on virgin territory, but followed what in the region, and in Europe as a

whole, was an old tradition dating back to the Eneolithic. In addition, it is also important to understand how Roman knowledge interacted with older techniques.

Several Roman authors refer to the importance of the Hispanic mining district, from historians such as Polybius, Diodorus, Appianus and Livy, to authors of technical treatises such as Vitruvius and Pliny, and to the ethnographer Strabo. In terms of mines and metals, the Iberian Peninsula was the place most often referred to by such authors; it was, in fact, the land of metal par excellence in Antiquity. The legendary stories of Herodotus, the historical chronicle of Polybius, the essays on economic geography by Strabo, the lists drawn up by Livy as inventories of the great quantities of gold and silver entering the *aerarium* through the conquests, the encyclopaedic compilations by Pliny, Catullus and Ovid, all point out the richness in precious metals of the Iberian peninsula. For instance, "(In Spain) the precious metals like gold and silver are abundant", "as well as the useful metals like lead, copper and iron" (Pliny, 3, 30; Pomponius Mela, 2, 86), to which Pliny adds the tin in the north-western part of the peninsula (Pliny, 4, 112).

In these early sources, silver was already commonly associated with lead minerals, frequently galena (see Appendix 1 for the chemical composition of the minerals referred to in the text). Strabo, for instance, mentions this association specifically for New Cartago as well as the mines in Sierra Morena, poor in silver, while Pliny mentions the argentiferous lead of Spain.

Lead was sought for on its own in Roman times, as mentioned by Etechiel, who located one of the primary areas of production in western Tharsis. In Pliny's time, Spain, Gaul and Britannia were the main regions producing lead, and several sources refer to the frequency of lead in these areas.

Classical sources also mention the infertility of these areas so rich in ores. Strabo, for instance, states "for the same reason they are rich in metals, the soils of this region are necessarily stony and very poor" (Strabo, 3, 2, 3). Pliny states the same for "the mountains of Spain which are dry, sterile and do not allow anything to grow, we force them to produce this precious thing", meaning gold (Pliny, 33, 67). And again "(silver) can be found almost in every province, but the most beautiful in Spain, and (as well as the gold) in a poor soil in the mountains" (Pliny, 33, 96). These quotes not only indicate that the mines were found in sterile areas, but also that they were in the mountains. This second aspect, in particular, is helpful for prospecting, and is due to the endogenic processes of mineral formation, geological processes related to the

formation of the mountains themselves. This naturalistic observation of the landscape provided 'geological' and mining connotations to the landscape itself, already in Antiquity. We know that three endogenic processes may be involved here:

- Magmas rising through the pre-existing rocks, coming from the base of the crust and carrying a variety of minerals;
- Volcanic phenomena linked to metal-bearing (copper, gold, silver, lead, zinc, etc.) mineral deposits formation.
- Detrital deposits accumulated in the basins where the climate and the environment may have created favourable conditions for the concentration of metal-bearing minerals. This is because superficial phenomena are strictly linked to the sedimentation following alteration and erosion periods.

Volcanic and orogenetic tectonic processes can lead to the concentration of mineralisation through two different effects (Julivert et al. 1974, 37; Monseur 1977, 340-341):

- Fractures which affect at every scale (micron to kilometre) the rocks and their mineralisation, favouring the solubility of the latter and its fluid circulation. Thus, the selective concentration of the elements in solution takes place following the thermal gradients in the fractures created in the rocks (veins).
- Folds and dislocations affecting the sedimentary and/or volcano-sedimentary deposits can increase the thickness of an ore layer through the piling of successive folds. They can also prompt the surfacing of mineralised deposits and their exposure to superficial alteration, which can induce the enrichment of the deposit through cementation.

The sulphuric masses of the Iberian pyrite belt in the south-west of the peninsula, the subject of this thesis, are linked with Hercynian pre-orogenic volcanism. The formations in which the mineralised deposits are included were then folded and raised during the Hercynian orogeny, and during this same period the majority of the granitic plutons set in place. The association of these phenomena resulted in the geology and geomorphology visible even today.

In short, this meant that every mineral deposit formed in whichever geological period is located in either mountains or plateaus, as the abovementioned ancient sources state. This observation is important for ore prospecting in Antiquity, regarding which we can distinguish two levels:

- A regional level defined in Strabo and Pliny, directing prospectors towards the mountains;
- A district level on the technical side, which restricted the prospection grid in order to localise the ores with precision.

1.2 Information on the ancient mines of the Iberian Peninsula and the paucity of information on the ancient production techniques

It is from the first reports published during the 19th century by mining engineers, who initiated modern mining activities in the Sierra Morena, Huelva, Murcia and Almeria (Madoz 1948-1950), that we obtain our first detailed information regarding the exploitation of the area. These reports are very important because they are from a period when ancient features in and around the mines were still intact. Furthermore, these engineers were mostly well-educated and thoroughly acquainted with the classical sources (Strabo, Diodorus, Pliny), and as a result they tried to relate these sources to their practical knowledge of the mines (Domergue 1990, XIII-XIV).

Two works attempted a comprehensive study of the mining exploitation in the Iberian Peninsula before Domergue's (1987) *Catalogue de mines et des fonderies antiques de la Peninsule Iberique*. These studies are *Apuntes para una biblioteca Espanola de libros, folletos y articulos, impresas y manuscritos, relatives al conocimiento y explotacion de las riquezas minerals y a las ciencias auxiliaries* (Maffei and Rua Figueroa 1871) and *Bibliografia de mineria, metalurgia, geologia y ciencias afinos 1778-1961* (Lopez de Azcona 1962).

Domergue's catalogue includes 565 sites, a number to which the author strongly believed others would be added (Domergue, 1987; 1990, XIV), confirming the intense exploitation of the peninsula in Antiquity, as already stated in the written sources mentioned in the previous section.

He also gives ample space to Rio Tinto (Domergue, 1987), where the mines are catalogued and the analyses of slag and ore samples are listed. As the title suggests, Domergue's *Catalogue* does not attempt to reconstruct the metallurgical processes, but represents a useful tool for tracing their spatial and temporal distribution within the Iberian Peninsula.

In 1981, Rothenberg and Blanco Freijeiro published a catalogue of mining and metallurgical activities focussed on the Huelva province. This is the result of a survey of the mining as well as the metallurgical sites in the area. The survey constituted the basis for the subsequent excavation of the site of Corta Lago, and provides my basic knowledge about the site and the area. Based on the survey, Rothenberg and Blanco Freijero (1981) provided some indications regarding the production processes, but these are not exhaustive of the topic. Following the survey, several excavations were carried out, and these are the sources of the material under consideration in this thesis, following initial studies and process reconstructions by Craddock (1995) and Keesman (1993) that will be presented in Chapter 4.

1.3 Archaeometallurgical data within cultural and socio-economic reconstructions

Several scholars have pointed out the benefits that could be gained from collaborations between historians, archaeologists and earth scientists for the study of ancient mines. Such collaborations could help elucidate issues such as:

- Aspects pertaining to the pre-Roman exploitation of mines that are still unclear;
- The role played by small private societies and individual enterprise in the development and improvement of the silver mines in Spain during the period covering the end of the Roman Republic and the beginning of the Empire;
- The importance of silver and gold mines and their relative metal production during the Empire from administrative, economic and technical perspectives.

As will be discussed in more detail in the following chapters, an archaeometallurgical approach adds to the technical data available for a certain area and a certain period, enhancing our appreciation of the following spheres:

- cultural (metallurgical and geological knowledge – metallurgical answers to geological constraints);
- socio-economic (work organisation, uniformity/standardisation of production, small scale/industrial production);
- exchange patterns, local production vs. export-import (isotopes as well as calculation of the scale of the production).

The reconstruction of metallurgical processes provides in the first instance an insight into the metallurgical knowledge of the smelters. However, smelting, and more generally metallurgy, is obviously intimately linked to the availability of raw materials, mainly ore and fuel, and these are natural elements, the availability of which cannot be changed. Consequently, every area has constraints imposed upon it by its geology and fuel availability. The metallurgical results in that area thus not only depend on the metallurgical skills and knowledge of the smelters, but also on their 'geological' knowledge, however empirical that might have been, of how to overcome the natural constraints of the ore.

In this case, for instance, the ore in question is jarosite, that is, as we are going to see in more detail later on in this thesis, an iron mineral treated to produce silver. The nature of the ore itself provides an initial constraint. If the amount of lead in the system was insufficient to mobilise all the silver, the smelters needed to respond to this. Their response may have differed depending on their knowledge, as well as on political and economic factors prevailing at the time. For instance, times of efficient state control of the mines and production may allow more movement of resources from one mining district to another.

Lead isotope analyses can indicate such movements of resources, while chemical analyses of slag can show the degree of uniformity and standardisation of the production process. A high degree of standardisation suggests an industrialised process involving large capital investment and most likely control by the Roman state.

As already mentioned at the beginning of this chapter, several authors have discussed the laws of the time regarding ore mining and silver minting, but these do not touch upon smelting, the intermediate step. Thus, although lead isotope analysis may indicate the movement of raw materials, and we can hypothesise a state control of this aspect, this does not necessarily mean that the smelting was under the control of the state.

Within an industrialised process, several possibilities exist in this regard. There may have been large numbers of individual smelters, professional craftsmen who worked within a state-controlled framework, achieving state determined production goals, or, conversely, 'state-workers' simply 'employed' by the state. Whether and how archaeometallurgical studies can elucidate this matter will be discussed later on in this thesis (Chapters 9 and 10).

1.4 Aims and approaches

Within this framework, the following paragraphs provide a preliminary discussion of the choice of the site and the material to be analysed in order to answer the following two questions:

What was the process employed for the production of silver in the Rio Tinto area during the Roman occupation?

What metallurgical and geological knowledge was applied and what links can be drawn between the production and the economic and socio-political framework within which this production set?

In more detail: what are the changes in the process from the pre-Roman local production to the one carried out during the Roman occupation? Does the smelting process evolve and change at the passage between Republican and Imperial Rome? Can we suggest a change in workshop organisation through time, from individual enterprise to state-controlled industrial scale? Can we observe changes due to cultural traditions? And, conversely, can we point out changes due to 'natural' constraints, such as changes in ore and/or fuel availability?

The choice of Rio Tinto and Tharsis, which will be discussed in detail in Chapters 4 and 5, is motivated by the massive production of silver in this area during Roman times, as emphasised by the ancient sources mentioned above. This production of silver on an industrial scale was due to the high demand for the precious metal, for purposes of coinage. For instance, it is estimated that around 9 million *denarii* per year were produced at New Cartago in the middle of the 2nd century AD (Jones 1974, 115). If we extrapolate this number to the entire Roman Empire, even considering the recycling of the metal, the amount of silver needed for coinage was so considerable that only an industrial scale process could meet it. As a result, we observe the extensive exploitation of silver-bearing minerals all across the Empire: in Rio Tinto and Tharsis in Spain, Lavrion in Greece, Sardinia in Italy, and in Serbia and Anatolia, to mention only the main provinces involved in this production. The choice of Rio Tinto as the principal site and of Tharsis as a secondary site for comparison is motivated by the presence of a well-defined stratigraphy at Rio Tinto that allows for

a general screening of the silver smelting processes through time, including the pre-Roman periods.

The amount of slag produced, based on previous reconstructions (Rothenberg and Blanco Freijero 1981; Salkield 1987; Domergue 1990), is estimated to have been between 6 and 16 million tonnes and will be discussed in further detail in Chapter 4. This estimate, although far from accurate, gives a strong indication of the 'industrial' scale of the production at the site under consideration. The study of the production process at this site allows a description of the 'industrial' and standardised process of silver production in Roman times as compared to the one employed during the previous period of occupation of the area.

The peculiar characteristics of the ore offer an insight into the geological and chemical knowledge of the metallurgists over time. Their ability to plan a standardised production process using such a peculiar raw material allows observation of the practice of balancing between efficiency and geological and economic constraints. In this area, the silver is linked to an iron mineralisation rather than the more common lead one, as will be explained in detail in Chapter 3. This feature requires geological and metallurgical knowledge different from other areas, and possibly more complex, in order to achieve the appropriate proportions between ore, flux and additional lead used as collector for the silver, as will be explained in Chapter 8. All these factors constitute the premises for the choice of this site.

1.5 Slag as primary material for the reconstruction of the metallurgical process

The choice of slag as the primary material for reconstructing the metallurgical process is well-established in the archaeometallurgical world. Slag is the waste resulting from the metallurgical process, and it collects all the elements that were part of the system except for the desired metal. Therefore, slag provides information on the raw material. Sometimes slag can trap semi-reacted or non-reacted ore portions, and this allows for a reliable identification of the mineralisation.

The limited amount of non-reacted or semi-reacted material provides an overall understanding of the material itself. The flux/mineralisation ratio employed in the smelting depends on the concentration of the metal that needs to be extracted, as well

as on the mineralogical association constituting the raw material (for instance sulphidic or oxidic ore). Thus, if no residues are detected in the slag, this gives a strong indication that the comprehension of the ratio was correct, and consequently that the 'chemical' and 'geological' knowledge and understanding of the raw material was clear.

Chemical analyses of the portion of the slag that was liquid, meaning all the material that underwent melting and therefore observable as newly formed, crystalline or amorphous, phases, allows the reconstruction of the temperature reached by the system.

Petrographic analysis of the newly formed crystalline phases allows identification of the main mineralogical associations. Such associations depend directly on the oxygen pressure in the system during the transformation from liquid to solid, its temperature and its cooling conditions.

The morphological analysis of the main minerals, olivine in particular, allows the reconstruction of the cooling speed of the slag, and thus provides an indication of the continuity of the process and the amount of material involved.

All of the above aspects constitute the reasons for the choice of slag as study material.

This thesis is divided into ten chapters. Following this first introductory chapter, Chapter 2 will focus on the Roman economy within which the silver production developed and was so important.

Chapter 3 compares the major silver-bearing minerals with jarosite. The focus is mainly on the chemical behaviour of the minerals during the smelting, indicating how the slag is produced, what to expect in them and why.

In Chapter 4 we narrow the focus to production at Corta Lago, describing the site in its geological and archaeological context, and providing a detailed stratigraphy for it.

Chapter 5 presents the methodology of the sampling approach and the analytical methods employed, as well as detailing the analytical instruments used and their properties, thus justifying their choice.

Chapters 6 and 7 present the analytical results, the former focussed on Corta Lago and the latter on Tharsis, as well as a comparison between the two sites. Both chapters are structured according to a chronological framework and present the description of the samples firstly from a macro-morphological point of view, followed by chemical, mineralogical and petrographic observations. The chapters

conclude with summaries initiating the comparisons that are expanded in more detail in the discussion chapter (Chapter 9).

The lead isotope analysis results are presented separately in Chapter 8, due to the need for a more coherent discussion of specific chemical data within the jarositic mineralogical context.

While Chapter 9 discusses the results within the framework of the procedural approaches, in Chapter 10 (Conclusion) the picture is enlarged to take into consideration the socio-economic contextualisation of the hypothesis resulting from the discussion of the analytical data.

CHAPTER 2

Silver mining and smelting in the Roman economy

The aim of this chapter is to consider the site of Corta Lago within the more complex socio-political and economic picture of silver production during the Roman period. There are several questions pertaining to this topic that need to be addressed, such as how the inhabitants of the Rio Tinto area were perceived by the Roman colonists, and, following this, how the ownership and organisation of the mines and the smelting workshops changed through time.

If we consider mine ownership, a question comes to mind: is there any difference between the ownership of the mines and of the smelting workshops? In other words, who was exploiting the former and who was running the latter? Most of the literary sources, as we shall see in this chapter, focus exclusively on the mines and the mints, but not on the intermediary stage – smelting – even though it is of crucial importance for the production of silver coins.

Another group of questions, or mainly comments, is related to a broader topic: the importance of archaeometallurgical studies and technology reconstruction for the understanding of socio-political and economic factors. This topic will be discussed focusing on a debate already initiated in 1986 by Greene in his book *Archaeology of the Roman Economy*. The author of the present work believes that archaeometallurgical studies should be used by historians and theoretical archaeologists, at least in order to clarify gaps and raise doubts about our current understanding of economic and social factors.

2.1 The Rio Tinto silver production within the Roman Economy

Roman economic history is the subject of a fluorising literature. One of the most preeminent description, given by Jones (1974) is the one used here to sketch the changes elapsing within the Republic and the Empire for what concerns the ownership of the mines connected to minting and coinage and the relative taxation.

During the Republican period, the early Roman provinces consisted of autonomous communities grouped and placed under the military control of a Roman magistrate. The Spanish provinces comprised some Greek, Punic and native city states in the more civilised coastal areas, and Iberian and Celtic tribes in the interior (Jones 1974, 1). During this time, Spanish clans also moved from their hill forts and built modern cities on the plains (Jones 1974, 6).

The integration of the provinces was carried out by conferring the Latin status to native communities. A considerable number of these, located in the western provinces, such as Sicily, Narbonese, Gaul and Spain, were conferred the Latin status by Caesar and Augustus. Later emperors continued the process, granting the status both to individual communities and sometimes to entire provinces; an example is provided by the case of Vespasian extending the *ius latii* to all the stipendiary communities of Spain. On receiving the Latin status, a community was issued a *lex data*, prescribing for it a constitution based on the Roman model, and its citizens became subject to Roman private law (Jones 1974, 7).

On the other hand, colonies of Roman citizens were 'planted' in the provinces in considerable numbers from Caesar's time onwards, and the native inhabitants of the communities in which they were settled shared the same status as the colonists (Jones 1974, 7).

Within this social system, laws were applied to mines and metal production. Pliny provides an account of the mines in Spain as being rich in silver and very important for the minting of coins in Roman times. However, there is scarcely any information on some very elementary questions, such as where and how governments obtained the bullion needed for their mints, about the organisation and techniques employed for coin production, and also regarding how governments put the coins they struck into circulation. If we look at Classical Greece as an example, some states, like Athens, had silver mines on their territory, but there is no precise information on the production steps between mining and the mint, smelting and cupellation. It is probable that the lessees of the mines had to pay 5% of the gross yields of silver to the state by way of royalty. The remaining 95% of the silver must have belonged to the lessee, but he presumably got it minted – perhaps he was obliged to do so, although there is no evidence in this respect, and perhaps he paid some commission on this. If this is true, than the lessee also possessed some metallurgical knowledge, and could smelt the mineral and cupel the bullion on his own; otherwise, he would

have needed to sell to a 'smelting' company, or pay a skilled smelter to do so. On the other side of this hypothesis, we have to consider then that most of the coins struck by the Athenian mint would thus have come back into circulation by the fact that the lessees of the mines would spend them. A small proportion would belong to the state, and would pass into circulation via public expenditure – paid to magistrates, soldiers, and so forth. Another problem is related to the ways in which cities like Corinth and Aegina, which had no internal source of silver, produced their large currencies; this aspect remains unknown to this date. It can only be suggested that foreign currency or bullion circulating in the market was recycled in the mint and struck as Corinthian or Aeginetan staters (Jones 1974, 61).

By the 2nd century BC, the Roman Republic owned important silver mines in Spain, and the silver stock in the form of bars of the treasury was significant, as Pliny tells us. Some of it may have been derived from the payment of taxes from the mines done by the *publicani*, tax farmers in the provinces, while some may have represented war indemnities levied from Carthage, Philip and Antiochus. By the end of the reign of Tiberius (37 AD), state property was extended by confiscation of the most important gold and silver mines, but the method of their exploitation remains mysterious. If they were still leased to *publicani*, it may be guessed that the lessees paid part of the bullion extracted to the state under their contract, as just described for Athens, but we do not know what happened to the rest. The *Metallum Vispacense* mentions two ownership possibilities: first, it was possible for a contractor to buy a shaft outright from the *fiscus* for cash; second, he could work a shaft on a 50-50 basis. Unfortunately there is no information on what happened to the silver which the contractor extracted under the former arrangement, nor to the half share of the contractor under the latter. During the 4th century AD, gold-washers had to pay the state 8 *scruples per annum* and sell the rest to the treasury. It is, however, probable that most of the bullion used in the Roman mints consisted of the old coins received in taxation and melted down. This was certainly the case under the late Empire, when the *solidi* received in taxation were melted down in the province in which they were collected, and sent up to the treasury in the form of bars. The treasury also usually reserved to itself the gold and silver plate that formed part of the confiscated properties (*bona vacantia, caduca, damnatorum*), even when the rest of the property was granted to petitioners. The mint also occasionally received huge quantities of bullion, such as the Dacian hoard of gold that Trajan captured, or the vast quantities

of gold Constantine confiscated from the pagan temples, where they had been stored for centuries in the form of dedications and cult-statues (Jones 1974, 68-69).

It appears, then, that the Imperial government in the 4th century AD normally refused to mint privately-owned gold for the owner. He could, however, use it to pay his taxes, or sell it to the treasury for debased *denarii*. For silver the practice may have been different. Otherwise, it is difficult to explain a rather curious phenomenon that numismatists have noted, regarding the fact that a very large number of silver coins from the 4th century minted in Gaul or even farther afield have been found in the neighbourhood of the silver mines of the Mendips. Either the mines were privately exploited, or, if they were state owned, the miners were entitled to keep a proportion of the silver extracted. The miners must have sent their own silver, after smelting the bullion and cuppeling it in workshops around the mining area, to the nearest mint (which may have been located a long way away) and got it back (almost certainly less minting charges) in coins (Jones 1974, 72). These sources all seem to highlight two aspects: the importance of individuality for the production, mainly prior to the Empire, and the extreme importance of metal movement and recycling.

It must be borne in mind that the economy of the Empire was primarily agricultural, that the vast majority of its inhabitants were peasants, and that the national income was mostly derived from the land. Its main tax, which seems to have produced over 90% of the revenue, was likewise imposed on agriculture. It was a combined land and poll tax, being assessed partly on criteria related to agricultural land (*iugatio*) and partly on the rural population (*capitatio*) (Jones 1974, 83).

Within this agricultural system, 'industrial' mining enterprises that could bring big revenue existed. For instance, as already mentioned above, in the middle of the 2nd century AD the silver mines of New Carthage brought the Roman people 25,000 *denarii* a day, which adds up to about 9 million a year (Jones 1974, 115). This gives us an idea of the scale of production, as does the case of Rio Tinto, to be discussed further, where the amount of metal produced can be inferred from the fact that several million tons of slags were produced. But how did the individual enterprise fit in this industrial framework?

Another interesting factor is the amount of free labour available, because the Empire set in motion certain important population changes. During the wars, from the first Punic war to Caesar's conquest of Gaul, vast numbers of prisoners were sold as slaves and the majority were imported into Italy, though very considerable numbers

went to Sicily to work on the land, and to Spain for service in the mines (Jones 1974, 122).

The Roman aristocracy craved for land, and this need promoted the formation of large estates in Italy at the expense of the surviving small holders. This trend quickly extended into the provinces. Was agricultural land addressed by the same approach as 'mining land'? An example from the literary sources states that Sextus Marius, an aristocrat, owned considerable properties in Spain, including mines (Jones 1974, 125). This represents an interesting insight into the ownership of the mines, possibly not different from the ownership of agricultural land. The Empire was possibly distributing resources among the members of its aristocracy, believing that this was a way to distribute democracy, and that the government would be more stable if vested in the better sort of citizens, whom Romans identified with the richer sort (Jones 1974, 95). Was the aristocrat creating then a small enterprise for the exploitation of the mines and production of the metal, or was he leasing the shafts and the workshops to experienced miners and metallurgists?

An important change in the slave trade policy occurring at a time between the Republic and the Principate (27 BC) provoked a subsequent major change in mining exploitation and farming. The slave trade, greatly stimulated by wars and conquests during the Republic and by its negligence of public security by sea and land, was greatly reduced under the Principate. After Augustus, wars of conquest were few and internal rebellions rare, hence the number of prisoners of war put on the market was greatly reduced. Within the Empire, piracy was virtually abolished and brigandage well controlled, so kidnapping became rare. The result was that by the 2nd century AD the number of slaves decreased and became largely dependent on breeding, and, as the demand was still high, prices rose very steeply. The profitability of employing slaves in agriculture and mining decreased and, instead, the estates became usually cultivated by dividing them into small holdings and leasing them to tenant farmers, and by using free indentured labourers in the mines, or even by leasing shafts to free miners (Jones 1974, 128).

We do not want to enter here into a debate on the primitivism or modernity of the Roman economy (summarised in the following sub-chapters), because this is not the purpose of this study. However, it is still significant to highlight the fact that precious metals were very important in Roman times, whether for prestige, wealth or the

market. Being the base of the actual coinage, silver, gold, tin and copper obviously constituted a very important part of the Roman economy.

The Roman government was interested in revenue, and in acquiring precious metals, as well as the mines which produced them, but in very little else in the economic sphere (Jones 1974, 137).

To understand the importance of the metals originating from the mining industry, it is useful to highlight some numbers. There are some contradictory elements in Jones' *Roman Economy* (1974). On page 115, they assert that "it is extremely difficult to estimate the volume of production of gold and silver, but it does not seem to have been very high, nor to have varied greatly from period to period". Yet, they had just mentioned a production of silver in New Carthage of 9 million *denari* a year during the 2nd century AD, a figure which fits with the attempt to calculate the amount of Roman slag in Rio Tinto, attested to be at least 6 million tons (Rothenberg and Blanco-Freijeiro 1981; Salkield 1987; Domergue 1990). It is agreed that in the absence of any literary sources it is extremely difficult to estimate the volume of production, but the scale of the production, even considering only these two estimations, does not look small. The statement that production did not vary greatly from period to period can also be doubted because, using as examples the sites of Corta Lago and Tharsis, we notice an increase in the scale of production between the Republic and the Empire (a detailed discussion of this point will be carried out in chapters 6, 7 and 9). An aspect that is worth noting here is the acquisition (following Trajan's conquest of Dacia) of a large hoard of gold and of the Transylvanian gold mines, which remained in the possession of the Empire until 270 AD. All mines were imperial property, and newly produced gold and silver were therefore directly available for minting if the smelting process was carried out by state companies as well. It is then very probable that the quantity of precious metals owned by the Empire would remain fairly constant, "new production being balanced by wastage and export" (Jones 1974, 190-191). There are still questions related to these aspects, in particular whether property laws regarding mines varied from province to province. In the inflationary period, much of the pure silver coinage would have been withdrawn from circulation, thus increasing the amount available for plates and other luxury uses, but the debased coinage still continued to absorb a considerable quantity of metal. This is the reason why the price of silver decreased only half as much as that of gold (Jones 1974, 202). It seems here that at least three different stages of

social organisation of the mining work are visible: from a state-controlled slave work system, a passage is made to a small entrepreneurs system, and then back into the rigidity of a state-controlled one.

Another important question concerns the social status of the miners and the question whether it was the same for smelters.

"The hereditary classes fell into two main categories: those whose personal service was required by the government, such as soldiers, agricultural labourers and workers in the mints, the state factories, and in public posts; and those like the *decurions*, the shippers (*naviculari*) and the guilds of Rome, who, though they might have to perform certain personal services, were mainly required to make a financial contribution to various essential activities" (Jones 1974, 396).

The miners and the gold-washers of the later Empire seem on the other hand to have been free men, even though their counterparts, the minters, were part of the hereditary class. By the 2nd century AD, due to the lack of slaves and the consequent social changes, mines had ceased to be operated by a large servile labour force, and they became largely privately managed, while remaining state owned. Quarries were still often worked by convicts, and so were some mines, but for the most part the government appears to have leased individual shafts to *coloni*, as attested at Vipasca. The *coloni* were evidently working miners, even though they might have had partners or employed a few slaves or indentured labourers. Later on, some mines and quarries were still worked by convicts or by corvée labour, but most mines seem to have been operated by descendants of the *coloni* of the Principate, making mining a hereditary work. There is actually no law enforcing work in the mines on miners earlier than 369/370 AD (the site of Corta Lago had ceased to be a smelting area at this time and had become a workshop area, but mining activities in the area were still going on), when Valentinian and Valens carried out a general settlement of the mine working forces, and no specific mention of miners' sons is made until 424 AD, but all the laws assume a pre-existing obligation. Miners in most societies have tended to form close hereditary groups, passing on skills and knowledge (Jones 1974, 402), and this may well have been the case in the Roman Empire. When Valentinian and Valens, who were greatly interested in building up stocks of gold, found that miners had been leaving the mines and taking up agriculture, they apparently thought it natural and proper to recall them to their traditional work (Jones 1974, 402).

The depopulation that resulted from the great plagues of the late 2nd and early 3rd centuries AD, as well as the barbarian invasions and civil wars of the 3rd century with their resultant famines, produced a general shortage of manpower. As a result, miners were tempted to take up agriculture, soldiers' sons to cultivate their fathers' allotments instead of enlisting, and tenants to abandon their old holdings and seek better farms. The shortage of manpower was increased by the rising demands for recruits, which reached a climax when Diocletian doubled the size of the army (Jones 1974, 409).

The natural reaction of the government to the crisis was first to 'freeze' the persons engaged in each threatened occupation, next to recall to each threatened occupation those who had recently left it, and finally, as the crisis persisted, to draft their sons into it (Jones 1974, 409). Miners also continued to be tied on by similar criteria (not only by birth but by age and skill) during Justinian's reign (Jones 1974, 411). The political and economic changes forced subsequent changes in terms of production and 'professionalism', as we can see from 200 AD onwards. More than possibly, similar alternating cycles took place in the previous 400 years, the ones covered in the Corta Lago section under consideration.

It is possible that smelting followed the same legal changes as mining, where the ownership and the managing of the process were concerned. Hence, we can attest a passage from individual smelters linked to the miners in one way or another, to private companies employing skilled metallurgists, and to state-controlled smelting completely related to mining and minting in the case of silver production. There are several mixed possibilities, such as private companies which had to reach an efficiency level dictated by the state, private companies different from the companies owning/managing the mines, or a professional group of metallurgists/smelters in a sort of free-lance state, as opposed to a highly prepared management ruling poorly skilled labour.

2.2 Archaeometallurgy and the Economy: potential insights

A multidisciplinary approach, combining anthropology, ethnography, archaeology and history, should constitute an ideal battery of research tools for investigating the Roman Empire, particularly its economy. There is an attractive convergence between

the thinking of Braudel (1985) and that of ethno-archaeologists like Binford (1962, 1972) or Hodder (1987), who believe that small items of everyday life, such as artefacts associated with burial practices or forms of pottery and metal objects, reflect wider aspects of society, for instance social structure and religious beliefs.

A growing number of scientific techniques assist archaeologists in their task. Thus, for the study of agricultural systems, there are methods of locating, recording and excavating the sites of farms, studying the bones and plant remains recovered, and analysing the potential of the soils in relation to the geography of a settlement pattern. Populations can be studied according to skeletal remains, which reveal traces of their diet, diseases and mortality. Technology can be investigated by means of the analysis of metals (and metallurgical debris), building stone or pottery, and trade can be detected from the distribution of artefacts away from their sources. All of this information can be placed into the general context of the climate and other prevailing environmental conditions (Greene 1986, 9).

What archaeology cannot do is achieve certainty. All of the known sites and artefacts are merely a surviving sample of what once existed, and not necessarily a representative one (Greene 1986, 9). Thus, the most that archaeology can achieve is putting forth hypotheses that can be validated or not by subsequent evidence, and not a definite answer to our research questions.

Finally, the relevance of archaeometric studies of Imperial materials within the general archaeological study of the Roman Empire may be called into question. This study, although representing only a small detailed snapshot, is part of this broader picture. One important issue is the assessment of Roman technology, agriculture and related aspects of military activity and urbanisation. The improvements in the understanding of such issues brought about by archaeological information are fundamental to the further interpretation of their social implications. A concerted effort on behalf of many disciplines is necessary to advance our understanding of the economy of the Roman Empire. The thinking involved in the task can only be of benefit in a world of differing economic development, technological and demographic change, and varying relationships between states, societies and their economies. “Perhaps there is as much to be learned from the question of why the Roman Empire did not experience an Industrial Revolution as from why 18th century England did” (Greene 1986, 13).

We have to start our enquiry by taking into consideration the main contrasting theories on the Roman economy. To simplify, two of the most authoritative models have been chosen within the multitude of studies on Roman economy because they summarise, generalising, most of the points raised in the literature debating this vast subject. The Finley (1973, 1992) and Jones (1974) models, and the Hopkins model (1980, 1983) will be briefly described and discussed.

The Finley and Jones models state that agriculture was the dominant form of economic activity in the Roman Empire, as already described in sub-chapter 1.1. Agriculture was pre-eminent, but most of its products were consumed locally, not traded. Inter-regional trade was limited in volume because of poor transport links and the lack of specialisation resulting from the uniform farming conditions that existed around the Mediterranean. Traders and craftsmen were modest in their operations and of low social status. Any of them who did make fortunes promptly bought land and became 'respectable' landowners for whom commerce was a secondary activity. Land brought status, and status involved displays of wealth by private consumption and expenditure on public benefaction, never productive investment. Looking at this model, one wonders where mining and metal production fit into the economy, considering that the 'respectable' landowners were also the owners of the mines.

Hopkins (1980), on the other hand, while accepting the basic validity of this model, has introduced a significant modification. He contends that there was genuine economic growth that increased surplus production by means of political change and technical or social innovations. The period of growth corresponded to the late first millennium BC and the first two centuries AD (a period when we also observe the maximum level of activity at the site of Corta Lago). Its results were felt in production, consumption and trade. Hopkins' proposition (1983) that there was a trend towards greater surpluses is set out in seven clauses that provide a useful framework for the examination of the relevance of archaeology to the study of the economy of the Roman Empire:

1) Agricultural production rose, and more land was cultivated. Hopkins (1983) notes the relevance of pollen analysis and the study of settlement patterns.
2) The population was more numerous in the first two centuries AD than 1000 years earlier or 500 years later. A combination of literary evidence and archaeological research into patterns of settlement and mortality is relevant here.

3) A greater proportion of workers was involved in non-agricultural production and services, both in the towns and countryside. Excavation of rural and urban workshops, as well as the study of their products, is important here.
4) High division of labour promoted increased production, and a high-point in the distribution of luxuries and more mundane goods occurred in the first two centuries AD. Very detailed quantitative archaeological studies of finds from occupation sites, and centres of manufacture of items like pottery or bricks (particularly those where items were stamped with workers' names) can allow further exploration of this clause.
5) Production per capita rose, in both agriculture and other spheres, as a result of a wide range of stimuli, including taxation, slavery, business practices, prolonged peace and technical developments.
6) The intensity of exploitation increased because of the amount and proportion of production that was diverted into taxes or rents.
7) In core provinces, the levying of monetary taxes, which were spent on the frontiers (to pay for armies) or in Rome (for state activities), stimulated long-distance trade, the development of means of transport, production of goods for sale, increased use and volume of coinage, and the rise in importance of towns. Archaeology can assist in the study of each of these results of taxation and expenditure, although literary evidence is needed to establish the level and nature of taxation. Archaeometallurgy can assist in the study of metallurgical techniques in order to establish change and improvement. Isotopic studies can assist in understanding the network of exchanges of raw materials and artefacts.

Roman skills and knowledge were extensive and diffused across many areas of technology. We can use different examples to assess this, one being the Venetic ships, described by Strabo (Geography IV, 4, 1). Strabo states about these ships that they were water-proofed by caulking, rather than through the precise carpentry of the close-fitting planks of Mediterranean builders. He writes: "…they do not bring the joints of the planks together but leave gaps; they stuff the gaps full of sea weed, however, so that the wood may not, for lack of moisture, become dry when the ships are hauled up. Furthermore, a shell-first ship can be constructed without a precise design by experienced builders; the internal frames need only be roughly prepared, and can be trimmed and fitted individually into a completed shell. In contrast, if a

keel and ribs are to be completed first, it is necessary to have a much more detailed concept and precise plans of the finished vessel, because all of the main timbers have to be cut to the correct shape in advance" (Geography IV, 4, 1). This indicates a change in production, from a technology where only very skilled craftsmen could produce artefacts to a technology that can allow more people to practice a certain craftwork. This is possibly the case in different fields of production in Roman times, when the dimension of the industry became important and a standardised process allowed the use of 'poorer' skills to be spread instead of basing the process on the abilities of a few people. Observations of the variability of the processes within the same period are used in this thesis to indicate the employment of higher or lower skilled metallurgists.

Another aspect of the debate is the diffusion of coinage in cities and the countryside. This is important because it does change the amount of coinage itself, and thus the amount of metal needed, as well as the policy on mining and smelting. The *denarius* was to remain the principal silver coin until the 3rd century AD. The first *denarii* seem to have been issued shortly before 211 BC (Greene 1986, 48).

Crawford (1970, 47) concludes: "the use of coined money as a means of exchange was largely limited to the cities of the Empire, and the Roman government had no policy concerning the supply of coinage and no monetary policy except in matters which directly affected its own interest or standing". Lo Cascio (1981), on the other hand, proposed that the Roman government not only had an awareness of financial issues arising from coinage, but actively controlled the relationships between different denominations with considerable success from the time of Augustus to the early 3rd century AD. The means of control included the limitation of mining operations, and adjustments to the supply, weight and purity of the gold, silver and bronze coinage, perhaps even with the needs of the economy as well as state finances in mind; in other words, through a monetary policy. Thus, in little over a decade, numismatists and ancient historians have been able to present two opposing views of the Roman economy: one minimising rural coin use or the state's understanding of monetary affairs, the other proposing a thoroughly monetised imperial system in which the government strove to maintain the stability of coinage for economic reasons (Greene 1986, 50).

The richness of resources in some areas could have changed the economic and socio-political environment locally. For example, writers such as Pliny and Strabo

celebrated the fertility of Baetica (Spain), as well as its important mineral resources (Greene 1986, 110).

It may be argued that Baetica is a special case of a rural settlements located in an area benefitting from the demand for olive oil and metals. The rapid development of intensive oil production in Roman Baetica is impressive, not least for the considerable impact that locally-spent profits must have had on other sections of the economy, both rural and urban. The organisation of transport on land and on the Guadalcuivir, the supply of exotic stone, mosaics and fine tableware to villa dwellers, and the dynamic cycle of harvesting, processing and exporting olives, must all have brought large numbers of individuals into the economy during the early period of the Empire, and stimulated the use of coinage and markets. However, the potential 'multiplier effect' brought no further advance or economic 'take-off'. Much of Baetica went out of intensive cultivation until the 20th century (Greene 1986, 114).

It has been said that almost all of the Roman population was involved in low-level agriculture "…while industry depended on a backward technology and was rarely organised in large units" (Duncan –Jones 1974, 1). "Did Roman technology allow the Romans to exploit the resources they needed? If it is found that the answer is affirmative, and that labour and resources were quite adequate without any elaborate technical developments, we can hardly judge the Roman Empire harshly for not making them" (Greene 1986, 142). Later in this work, Roman technological improvements in silver production are going to be the focus of the discussion, and indeed it has to be said that there is no need to invest time, effort and capital in research for technological improvements when the results obtained are already satisfactory. And, as we will see in chapter 6, in terms of the effectiveness of the smelting of lead bullion from jarosite, the results were very satisfactory.

Metals were put to a wide variety of uses in the Roman Empire. Gold and silver were used for making coins, jewellery, ornaments and high class tableware (Painter 1977). Bronze was far more common, and provided the bulk of the coinage, cheaper jewellery, and all manner of fittings for vehicles, military armour, furniture, etc. It was also the principal metal used in casting statues and in making a range of cast and sheet metal vessels and containers, from cauldrons to jugs. Lead and tin provided metal for alloying with copper to make bronze, or with each other for pewter or solder (Hughes 1977; Blagg and Read 1977). Lead on its own was invaluable for sealing roofs or water tanks, and for making the pipes that were important in the

construction of the water-supply systems and baths (Boulakia 1972). Iron had an universal use for the production of strong, sharp and durable tools for agriculture and crafts, many of which are remarkably similar to their modern counterparts; their range of specialisation was also noticeably greater than in the pre-Roman Iron Age (Gaitzsch 1980, 259-261). The Roman period brought about intensification rather than innovation in terms of methods of exploitation. Under Augustus, existing mines expanded and new mines were dug, using extensive shafts and underground galleries. The Roman period did not coincide with any great new invention and developments in metal technology, except for the introduction of brass, but the Roman occupation brought a greater intensity of exploitation and production than had ever been seen before (Greene 1986, 143).

To summarise: the most important aspects of the socio-economic framework on which archaeometallurgy can elucidate are:
- specialisation of the work, lower or higher levels of skill, importance of the individual or chain work of low skilled workers within an industrial scene;
- movement of the material at the district, regional or even larger inter-regional level;
- technological improvements as a reaction to natural constraints, which in this case would be ore and fuel related.

As we have already mentioned, what archaeometallurgy can do is indicate and suggest certain hypotheses, while only a holistic and multidisciplinary approach would be able to offer a certain or at least plausible answer.

2.2.1. Archaeometallurgy and the Economy in the Rio Tinto area

The guiding principle in the collection of ores for smelting is, naturally, the expenditure of minimum effort. Underground mining in the Roman period was, therefore, a last resort, reserved for precious metals. Despite several thousand years of metal use, many sources of ores were probably still being exploited by means of opencast workings on surface outcrops of rocks containing ores. Some sites associated with Roman gold mines in Wales and Spain show a progression from simple to complex methods, as the deposits that were easier to reach became exhausted (Greene 1986, 144).

In terms of scale, the most spectacular mining activities in all of the Roman Empire were undoubtedly found in the Huelva district of southern Spain, notably at the Rio Tinto mines. Modern exploitation has uncovered many traces of earlier activity, and mainly destroyed them as well, as it is the case with the Corta Lago section itself. An extensive dark area of copper ore is being totally removed by blasting, and the exposed workface which is over 100 m high has revealed several Roman mine shafts that have been cut through by the process. Although mining occurred at the site in earlier times, the exploitation during the Roman period was unrivalled in its intensity until modern times (Greene 1986, 144). Analysis of waste and slag from a deeply stratified deposit has shown the development of the working pattern from prehistoric to Carthaginian and Roman times (Rothenberg and Blanco-Freijero 1981, 163-182; see also chapter 6 of this work). In these historical times, silver was the principal attraction, but copper continued to be extracted as well. "Huelva was the most important metal producing area in the Roman Empire and one of the most important metallurgical regions in the ancient world…almost all of the presently operating and most of the old abandoned copper mines of Huelva had previously been operated in Imperial Roman times and had produced silver as well as copper" (Rothenberg and Blanco Freijero 1981, 173). Southern Spain and Portugal have provided examples of actual tools and other artefacts used in mines (Healy 1978, 21-37), and technical equipment used in drainage, including substantial remains of water-wheels of the kind known from Dolaucothi (Luzon 1968, 106-7, Figs. 4-6). Mechanical bucket-chains, Archimedean screw-pumps, and even double-acting pumps with non-return valves were in use (Luzon 1968, 111-120). The organisation of the mines and their labour is an interesting question, and the synthesis of information that can be inferred from references to Spain in the works of Roman writers has been extended by the discovery of the remarkable inscribed bronze tablets from Vipasca, in the modern district of Aljusterel, Portugal. These provide many details pertaining to mining practices in the course of the regulations which they record (Domergue 1987), as we have seen in the previous section.

In general, metal resources in the Roman Empire seem to have been under state control, following the precedent of many earlier states and kingdoms (Finley 1973). In many cases, mines were not worked directly by the state, although the army may have been involved in the initial exploitation of newly-conquered provinces (Noeske 1977). Richardson (1976, 151-152) has discussed the 'gold-rush' of Italians to Spain

in the Republican period, and has stressed the importance of exploitation by comparatively small-scale lease-holders rather than huge companies which 'farmed' taxes. The names of individuals and companies (*societates*) have been found cast or stamped on unused ingots (Colls et al. 1975). In a study of stamps on lead ingots recovered from the sea near part of Cartagena ('New Carthage') in south-eastern Spain, Domergue (1966, 65-66) has observed the shift from large companies to individuals by the time of Augustus. During the Empire, state control increased, and new mining areas were exploited directly (Domergue 1966, 67-68). New conquests evidently affected the output of different mining areas, for ingots in south-western Gaul implying that the port of Narbonne changed from acting as a transit point for Spanish metal on its way north to being an intermediary for supplies from Britain on their way to Italy and the Mediterranean (Laubenheimer-Leenhardt 1973, 199-201). Ideally, the Roman authorities should have been able to meet their requirements of metal of all kinds without having to undertake any direct mining at all, by balancing the demands made upon lease-holders against the need to encourage mining when necessary. It has been suggested that the massive scale of exploitation undertaken at Rio Tinto was too great for the operation of companies with leases, rather than directly by the state (Rothenberg and Blanco-Freijero 1981, 173), and the scale of some of the north-western Spanish mining activities has led to the same conclusion (Tranoy 1981, 133).

However, it must be remembered that the Roman government felt able to run the vital supply of grain to the capital, as well as the distribution of stone, on a very large scale on a contract basis (Rickman 1980; Ward-Perkins 1980, 334), so it may have applied the same system to mining, even if it is not clear how the system worked for the smelting. Some areas were placed under the control of an official, entitled *procurator metallorum*, who regulated mining activities and supervised the leasing of such operations to individuals and companies (Dusanič 1977, 79-85). Many of the leases were operated on a system similar to agricultural tenancies, based on the sharing of the products with the state. In the provinces along the river Danube, it has been suggested that the state organisation of mining inhibited 'normal' progress towards town-centred Romanisation (Dusanič 1977, 93). Labour in mines must always have been dangerous and unpleasant, and the ancient writers provide frequent examples of the use of slaves, criminals and forced labour for this type of work (Healy 1987, 135-137). The use of free contracted labour may well have been

underplayed for dramatic effect, however, and holders of leases in mining areas would have needed to secure skilled and experienced labour (Mrozek 1977, 102-109). This would apply even more for what concerns the smelting; an analysis of inscriptions from Galicia in north-west Spain shows that workers were attracted from other parts of the Peninsula (Tranoy 1981, 233). The Vipasca tablets give details of leasing arrangements (Healy 1978, 130, 138; excerpts translated in Lewis and Reinhold 1966, 188-194). There are mining regulations relating to safety, measures aimed at reducing fraud by mine owners, and even details about other occupations in the area, such as the operation of the baths, shoemakers and tax concessions for teachers. They give the impression of a community possessing the essential facilities to attract lease holders and labourers to a remote district (Greene 1986, 146-147). However, Rothenberg and Blanco Freijero (1981, 173) argue that the documents only apply to a small community, and need not be representative of what happened at large centres of exploitation. It is interesting to note how smelting is not mentioned alongside the other occupations, as mining and metallurgy were under the same label. The use of a wide variety of metals in Roman metalwork demonstrates a clear control over technology, and it is, of course, implicit that similar competence existed in the entire *chaîne operatoire*, from mining through to the preparation and smelting of the ores. For example, Cope (1971) found that Roman copper smelting for coinage reached a level of purity comparable to the very best modern practices. Improvements in technique are apparent, but not revolutionary. It is the scale of extraction and use that distinguishes the exploitation of metals in the Roman period from that of earlier times, or indeed pre-Industrial Europe. For example, although the mining of iron and its subsequent processing into steel made the province of Noricum famous in Roman times (Alföldy 1974, 113-114), the technique of producing cast iron in Europe was not perfected until the late 18th century, when it allowed significant advances in the manufacture of train rails and building elements of great strength (Greene 1986, 149).

The fact that there is no serious discussion of Roman pottery in the Roman literary and epigraphic sources demonstrates the importance of archaeology for expanding the range of information upon which an understanding of the economy can be based (Greene 1986, 167), and it would be interesting to explore whether the same can be said about archaeometallurgy and the reconstruction of metallurgical technology.

The exploitation of the resources of the Empire did not involve revolutionary technology. The consistent features of mining, quarrying and pottery-making are the extent of operations and the quantity of output. The Roman state constructed marble buildings on an unprecedented scale, and minted millions of gold, silver and bronze coins. Thousands of ordinary Roman farmers had more iron tools, architectural stonework and fine tableware than ever before, to an extent that would not be matched again until the post-medieval period. The technology applied to the extraction and processing of raw materials was evidently adequate to meet this high level of demand, at prices that could be afforded by a wide section of society. The combination of effective transport links and appropriate coin denominations, which has been noted above, would obviously have helped to sustain trade in these materials, far beyond the requirements of the state and the army alone. Archaeology is of fundamental importance in examining all aspects of this phenomenon (Greene 1986, 170).

CHAPTER 3

The technology of Roman silver smelting: galena, cerussite and jarosite

In the course of time, metal mining produces a variety of waste materials, including waste rock, flotation tailings and slag. Slag is either dumped on site or may be used as road ballast or backfill material, as sandblasting agents, as cement additives, or as material for roofing shingles (Patiak et al. 2004, 1039). The waste material depends on the raw material as much as on the processing conditions, and these differences are going to be the focus of this chapter.

It is possible that ancient peoples were initially attracted by native metals, which appeared on surface areas of the metallic ore bodies. The subsequent evolution of exploitation from native metals through oxides to sulphides follows the zoning of the ore bodies themselves. Furthermore, the progress of metallurgical techniques follows the same trajectory, the oxides being easier to treat than the sulphides that also appear in the mineralisation underneath the oxidation cap.

A huge brown iron cap, composed of more than 80% iron oxides (haematite-goethite), covers the pyritic body in the south-west of Spain, the area under consideration in this study (a more detailed description of the geological situation in the area of interest will follow in chapter 4). This brown cap, because of its strong coloration, allowed recognition of the presence of a mineralisation in the past (Fig. 4.3, Lago open pit, Rio Tinto and Fig. 4.5 Peña del Hierro, Rio Tinto). The iron cap was 'hiding' the secondary enrichment zone containing the jarositic minerals, which represent our primary concern.

Jarosite is basically an iron sulphate with the general composition $XFe_3(SO_4)_2(OH)_6$, where X could be K, Na, Ag, Pb or NH_4 (Amoros et al. 1981, 206; Bachmann 1982, 3). Thus, the jarosite group includes the isomorphous plumbojarosite, natrojarosite and argentojarosite (Fernandez Caliani and Requena Abujeta 1993, 69), types which have been identified by XRD (Williams 1950, 8). The yellow jarositic bands, together with the black ones, give the major concentrations of silver (bright yellow) and gold (black - Williams 1934, 631-632; 1950, 8). Jarositic bands are also rich in Pb, Sb, Bi, Se and Ba, and normally also in silica (Salkield 1987, 90), Sn and As

(Jenkin 1911, 1). On the other hand, they are also characterised by their low Cu and Zn content (Williams 1934, 632). Mineralogically, jarosite would be mainly associated with iron oxides and hydroxides, plus quartz (SiO_2), and varying quantities of barite as gangue minerals; cerussite, anglesite; and scorodite, the only arsenate, as secondary minerals.

Argentojarosites have also been identified, as red and yellow 1 m thick earth bands, located above the sterile porphyry in the southern part of Cerro Salomon. They present a high gold content, more than 30 g per ton, and large quantities of silver, as well as abundant barite (Williams 1934, 633). These earthy layers, on which the Roman exploitations were concentrated, were also identified between South Lode and Dehesa Opencast, in North Lode (Allan 1968, 48), and, to a minor extent, over the sulphide deposits of Lago and Salomon (Fig. 4.2). It has been estimated that the amount of jarositic earths in Rio Tinto was around 1 million metric tons (Allan 1968, 48), although other authors give the higher figure of 3 million tons (Dutrizac et al. 1985, 78), of which perhaps some 2 million were exploited by the Romans (Salkield 1987, 13).

Records from the late 19th and early 20th century indicate silver concentrations of around 0.2% in the ore (Douglas 1924; Salkield 1987, 15; Perez Macias 1998). This concentration of silver in geologically determined zones is, as mentioned above, by no means a phenomenon confined exclusively to the Rio Tinto deposits: jarosite was discovered in the Cueva de la Mora, and was doubtlessly exploited in the South and Central Lodes of Tharsis (Fig. 4.1 - Checkland 1967, 26, 50). Following the archaeological work carried out in the Aznalcollar mine (Seville), the same range of silver concentration has been detected in exploitations (in the gossans that still remain in the western part of the present opencast) dated to the Late Bronze Age/Phoenician Colonisation Period (Hunt Ortiz 2003, 39).

As the importance of jarosite has been signalled by several scholars in the Rio Tinto area, a brief insight into the chemistry and mineralogy of this mineral is necessary in order to provide a better understanding of what to expect from slag resulting from its processing.

As already mentioned above, jarosite is an iron sulphate that can contain different cations in its structure. For this reason, its formula is rendered as $XFe_3(SO_4)_2(OH)_6$, where X indicates the different cations that can be found in the structure, which could be K, Na, Ag, Pb or NH_4.

Looking at the formula, we see that there are three main "compounds" that we need to separate in order to obtain the metallic part of the mineral: the XFe, the sulphate and the hydrate portion. Then, we need to separate the X cation from the iron, as well as, within the X cation, separate the lead (silver) metal from the alkali. The hydroxide portions separate as vapour during a 'roasting' phase, which could be a preliminary one or take place within the smelting process, when the minerals are broken during their first heating in the furnace. The sulphate portion follows this step and the cation separates from it at a temperature around 800 ºC in a reducing environment. The earthy form of the jarosite facilitates the entire process, since the material is already of a 'sandy' consistency.

In order to separate the iron and the other cations from the desired metal, a more reducing state is necessary. This state is obtained deeper in the furnace, and fluxing elements need to be added to the system. All the cations contained in the jarosite, with the exception of silver, enter into silicated structures at a temperature around 1100/1200 ºC (that is the temperature of interest for the processes studied in this project, as we will discuss in chapters 6, 7 and 8). The iron mainly forms fayalite and magnetite crystals; the former can contain a low amount of Mg and Ca, normally less than 1%. The association fayalite/magnetite indicates a partial oxygen pressure below the buffer curve Fe^{3+}/Fe^{2+}, at a temperature of 1150 ºC (Fig. 3.1 – line FMQ); this oxygen pressure is too reducing for the lead to be in an oxidised form, and therefore at these conditions lead would be in a metallic state, as would the silver. The alkalis deriving from the jarosites are normally incorporated into a pyroxenitic phase (pyroxene mineral – Na - or glass with a pyroxene-like composition – K). When the cooling speed is too fast, or the silica is not sufficient, the pyroxenitic phase does not crystallise and the alkalis and the calcium are incorporated into a glassy matrix interstitial to the olivinic phase.

This chemical process would leave the lead and the silver that do not enter in the silicatic phase free to collect as bullion. Associated to these two metals we also find antimony and bismuth when the exploited ore is polymetallic, as is the case with those of Rio Tinto.

The jarositic earths present a further problem, involving the variability of the amount of lead. The earths are of mixed composition and normally it is impossible to distinguish between the different compositions during mining, even more so underground. The different cations confer a different colour to the jarosites, but only

thick lenses of one composition would be possible to distinguish, while a mixture of them would be impossible to differentiate. The case study of Corta Lago is characterised by high chemical variability, since a concentration of plumbojarosite ranging from 3 to 30% has been reported (Hunt-Ortiz 2003, 39). In cases where the level of plumbojarosite is very low, there would be a lack of lead in the system, preventing a satisfactory collection of silver. This problem would need to be addressed by adding lead rich minerals (galena, as Domergue (1990) suggests for other sites) or lead ingots into the system. These possibilities will be discussed in chapters 8 and 9.

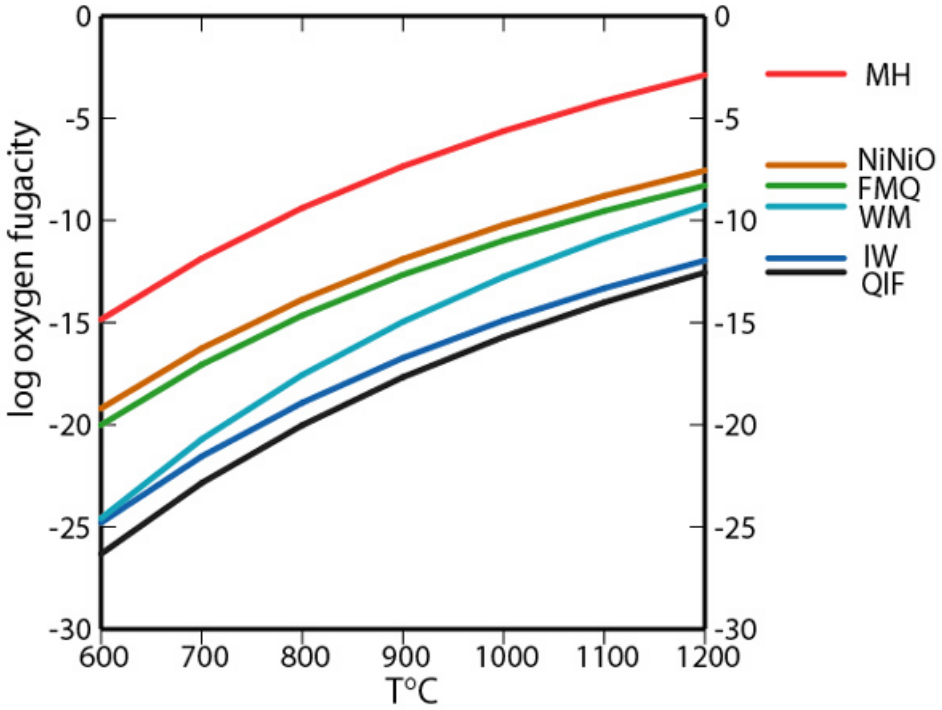

Figure 3.1 Diagram of temperature/oxygen pressure for major mineralogical phases association (MH, magnetite-hematite; NiNiO, Nickel-nickel oxide; FMQ, fayalite-magnetite-quartz; WM, wustite-magnetite; IW, iron-wustite; QIF, quartz-iron-fayalite – Frost, 1991).

Because of the distinctiveness of the deposits and mineralogy of the Laurion area in Attica, Greece, we will use it here as an example to describe the exploitation of different lead (silver) minerals, galena and cerussite, as well as the re-use of more ancient lead (silver) slag to obtain silver in Roman times.

In Laurion, the practical process of metal production was separated into three interrelated stages: 1) discovery and mining of the ores; 2) processing and cleaning

of all constituents that were not silver-bearing lead; 3) smelting in order to produce the metals (Kakavoyannis 2001, 365).

Many ores and non-metallic minerals are present in the Laurion substratum, but not always in exploitable amounts. The most common are those containing argentiferous lead, that is galena (PbS) and cerussite ($PbCO_3$), often associated. Many of these ores are, as a rule, mixed together in the stratification already discussed at the beginning of this chapter. Deposits of pure galena or cerussite exist, but are relatively rare and small. Galena or cerussite usually constitute, on average, 20% of the deposit; this is a rather small percentage, indicating that overall the region had a low argentiferous lead concentration (Kakavoyannis 2001, 365).

There is evidence in the ancient literary sources that the pre-Classical furnaces disappeared almost completely. Their inferior smelting technology, however, had produced slags or *scoriae* that were rich in argentiferous lead. The Classical and post-Classical metallurgists at Lavrion, who possessed a superior technology to that of their predecessors, systematically sought out these *scoriae* to smelt them and obtain the argentiferous lead they contained. There is a revealing testimony to this in Strabo (IX.I.23), who is certainly writing of his own period: "… the silver mines in Attica were originally valuable but now have failed. Moreover, those who worked them, when the mining yielded only meagre returns, melted again the old refuse, or dross, and were still able to extract from it pure silver, since the workmen of earlier times had been unskilful in heating the ore in furnaces".

Different minerals leave different metallurgical remains after processing, not only due to differences in their mineral chemistry, but also to the different mineralogical associations in the geological formations.

If we compare galena (PbS) and cerussite ($PbCO_3$) with jarosite ($XFe_3(SO_4)_2(OH)_6$), we observe that the main problem with jarosite is removing the iron from the structure, while galena and cerussite only require the breakage of the structure to free SO_2 and CO_2 as gases and to keep the lead, as oxide in the first step and metal in the second. Thus, if we roast galena, we observe the reaction $2PbS+3O_2 = 2PbO+2SO_2$; the lead oxide can then react directly with the remaining galena ($2PbO+PbS = 3Pb+SO_2$ and $2PbS+4O_2 = 2PbSO_4$ followed by $PbS+ PbSO_4 = 2Pb+2SO_2$), with Pb collecting as metal and SO_2 leaving the process as gas. The process for cerussite would be similar, starting from $2PbCO_3 = 2PbO+2CO_2$, and then reducing the lead oxide into lead metal. If these minerals are completely pure, then we should obtain

virtually no metallurgical debris, as we see for instance at Copa Hill, Wales (Anguilano et al., 2010). In reality, when smelting galena, lead oxide can be reduced back to newly formed PbS, as well as facilitate the formation of a pyroxenitic phase. The high chemical reactivity of the lead oxide that forms in the more oxidising conditions around the wall of the furnace can attack the clay linings of the furnace or the technical ceramics (tuyères), forming a lead silicatic phase. In this case the slag would be very rich in lead, but only a very small amount of slag would form (Anguilano et al., 2010). Where the galena is associated with other sulphides, as is often the case, it would need to be washed in order to be more concentrated, but also some flux would need to be added in order to free the system from impurities. If the impurities are iron-rich, quartz would need to be added. The opposite may happen if minerals from the gangue are the impurities, as may happen mainly where stockwork ores of minute size are used, or where gangue and veinlets are inter-mixed and difficultly separable. In such cases, iron would need to be added to avoid the forming of lead silicates, which would increase the lead loss in the case of quartz. On the other hand quartz would need to be added in the other cases in order to form silicates of calcium and magnesium. As for cerussite, the same discussion applies, because this mineral normally contains the same types of impurities as galena, as it is a transformation product due to oxidation and carbonation of the sulphidic phase.
The third material we have mentioned above as being used in Lavrion as a source of silver in Roman times is slag left over from earlier times. These are calcium rich silicates, and were re-smelted as self-fluxing material within more controlled temperature and oxygen pressure conditions in order to keep the slag in a liquid condition as long as it was required for the lead droplets to collect in a bullion.

Only lead has been discussed in this section because lead and silver are connected in the system under consideration, and, thus, if there is a loss of lead, this would influence the efficiency of the collection of silver from the ores. Therefore, as regards smelting, the main point is to produce lead metal that would collect all the silver from the system; thus, it is important that any loss of lead as oxide or silicate is avoided. Also, the loss of lead as newly formed sulphide should be avoided because this would mean losing not only the lead as collector, but also silver, which is stable in the lead sulphide structures. Furthermore, not only is there a need to produce lead metal in order to collect the silver, but conditions in the system also need to be

maintained that allow the slag to stay as fluid as possible, avoiding both residual crystals, normally of gangue minerals (quartz and barite), and the crystallisation of silicates of such dimensions that they would limit the movement of the liquid part of the system, impeding the flow of the metal droplets toward the bullion and hence the collection of lead (silver).

A typical example would be a deposit including a polymetallic vein and replacement deposits, most of which are hosted by slate, dolomite and quartzite. Granitic rocks may also be associated with many of the deposits, since normally the sulphidic deposits are related to hydrothermal activity after the intrusion of plutons. The major sulphide minerals are galena, sphalerite, pyrite, tetrahedrite and chalcopyrite; both galena and tetrahedrite may be argentiferous (Patiak et al. 2004, 1041).

The slag samples resulting from the process of such mineralogical associations are normally grey, glassy to coarsely crystalline, and commonly display a metallic lustre. These samples, such as those from the Vermont copper belt, Idaho Clayton (USA) in recent times (Patiak et al., 2004, from Cwmystwith (Wales) – both Roman and Medieval (Anguilano et al. 2010), from Porco-Potosí (Bolivia) – both archaeological and modern (Cohen, 2009), from Mont Lozere (France – Ploquin et al., 2003), and several others deriving from the smelting of lead sulphides, display few textures, having glassy chilled margins containing vesicles and coarse-grained crystalline interiors. The silicates present in these samples include olivine group minerals and pyroxene. Olivine is present as radial laths up to several centimetres long, whereas pyroxene occurs as subhedral crystals scattered throughout the sample. The examined sample may contain only interstitial glass or can be completely glassy. The associated spinel can be euhedral or dendritic, depending on the speed of the process, once there has been an increase in oxygen pressure. The sulphides (which are mainly of Pb, or Cu-Fe) occur as discrete grains disseminated throughout the silicate matrix, or as admixtures with native metals and alloys of various metals (Ploquin et al., 2003; Patiak et al. 2004; 1044; Cohen, 2009; Anguilano et al. 2010).

The substitution of Ca or Mg for Fe in natural fayalitic olivine is limited, but olivines with a composition similar to those found in the Clayton smelting slag samples have been reported in slag from the Pribram mining district in the Czech Republic (Ettler et al. 2009) and in Roman slag from the Colline Metallifere (Tuscany, Italy – Manasse et al. 2001). Also, quenched experimental studies have demonstrated the

formation of a complete solid solution between fayalite and kirschteinite at temperatures above 1040 °C (Mukhopadhyay and Lindsley 1983; Patiak et al. 2004, 1044).

These are a few archaeological examples of metallurgical sites associated with lead production, randomly chosen so as to give an idea of how variable the lead smelting waste scenario can be, but also of how specific the case of the smelting of jarosite is within this framework. In fact, looking at the lead smelting slag derived from the smelting of galena and cerussite, it is interesting to note that they show great variability in their lead contents, while jarosite smelting slags are mainly iron slags, and look much more similar to copper slag than to the lead slag described in the literature.

CHAPTER 4

The study sites: Corta Lago and Tharsis

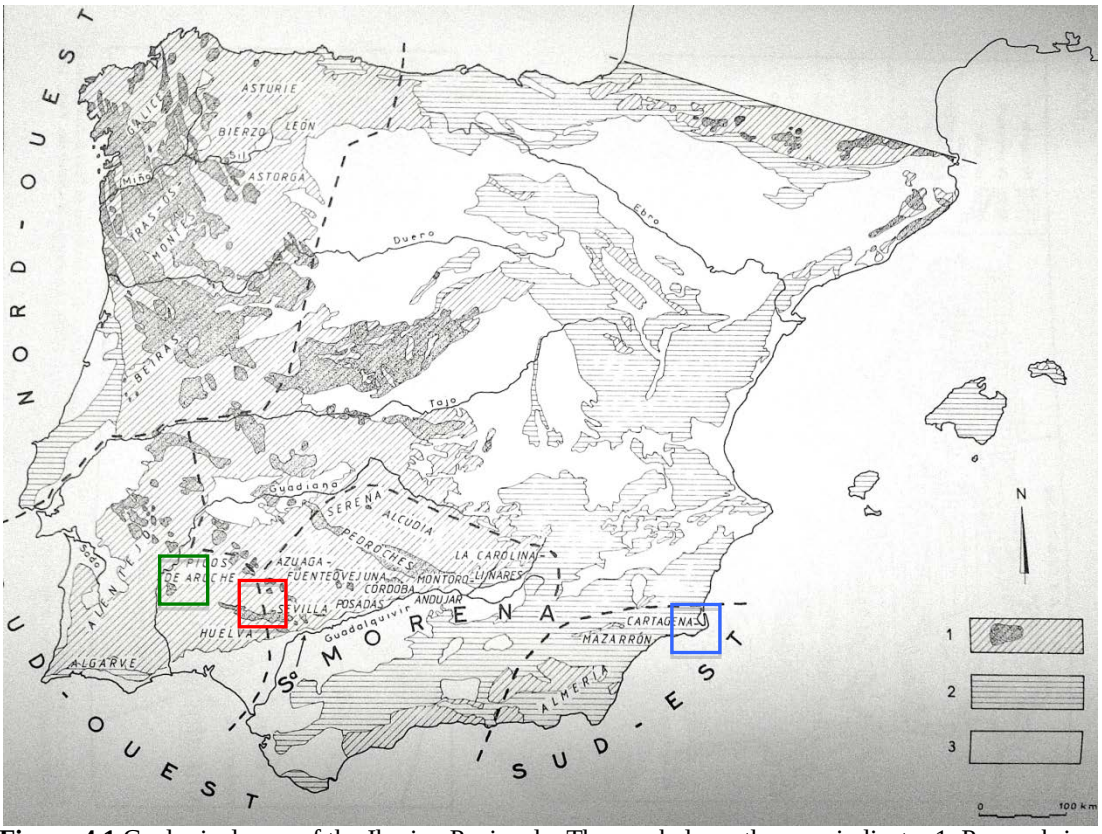

Figure 4.1 Geological map of the Iberian Peninsula. The symbols on the map indicate: 1. Precambrian, the dotted areas indicate granites; 2. Mesozoic; 3. Cenozoic. (Domergue, 1990, 518). The blue square highlights the location of Cartagena, the red one indicates the location of Rio Tinto, and the green one of Tharsis, the main sites involved in this thesis.

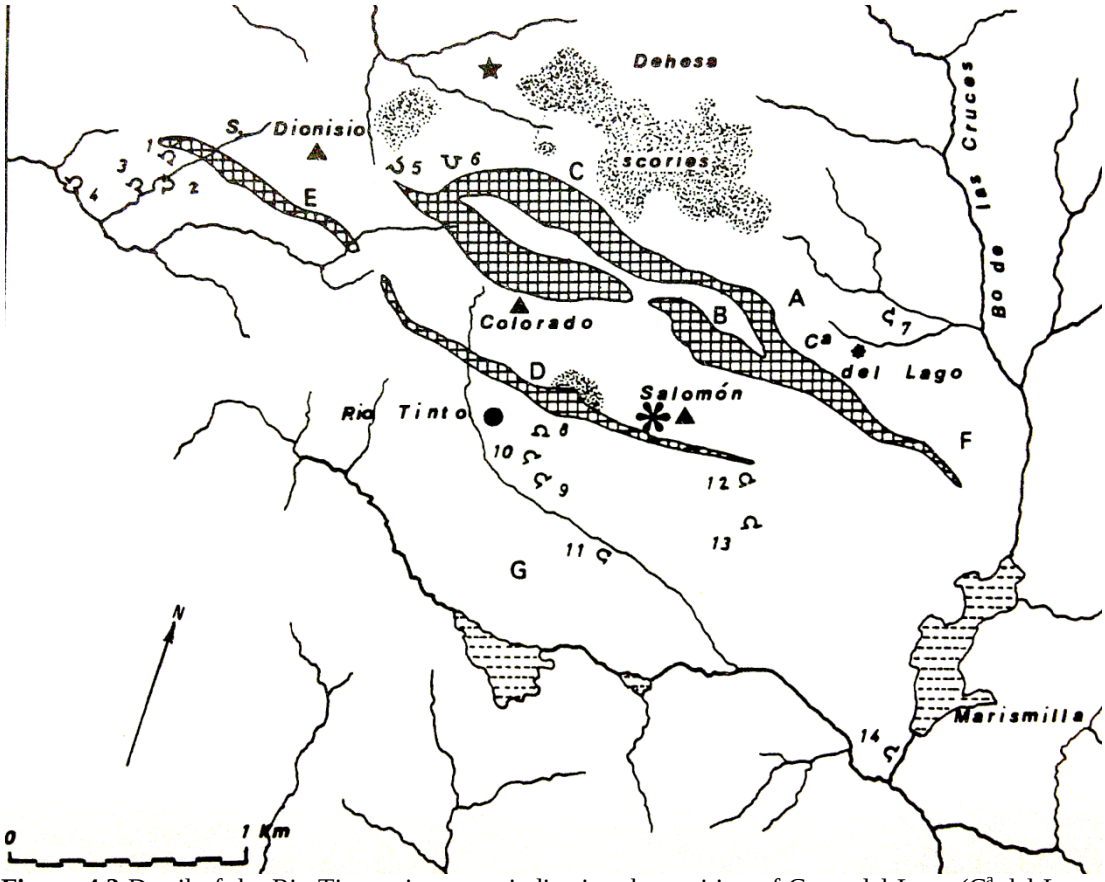

Figure 4.2 Detail of the Rio Tinto mines area indicating the position of Corta del Lago (C[a] del Lago in the figure) and the position of the main exploitation works (squared areas) and slag heaps (dotted areas) (Domergue, 1990, 531)

4.1 The Geology of Corta Lago

The site of Corta Lago was discovered more than thirty years ago during the Huelva Archaeo-Metallurgical Survey coordinated by Professor Beno Rothenberg. The survey was focused on the identification of archaeo-metallurgical sites within the large pyrite belt deposit that characterises the area. This is a unique geological lineament extending over an arch-shaped area of about 250 km by 35 km in southern Portugal and south-west Spain (Fig. 4.1). This belt is one of the most important metallogenic provinces in Europe, and over the centuries iron, copper, silver and gold were produced in great quantities from a number of large-scale mines (Rothenberg and Blanco-Freijeiro 1981, 33). The volcanic-hosted massive sulphide deposit mineralisation constituting the metallogenic core consists of 1700 Mt of sulphides, from which the following reserves have been calculated: 14.6 Mt of copper, 13.0 Mt of lead, 34.9 Mt of zinc, 46100 t of silver and 880 t of gold (Leistel et al. 1998, 2).

Typical geological vocabulary will be used in the following section, and thus it is important to begin by explaining some of the terms used:

- "Veins" are flat mineral masses contained between two sub-parallel planes cutting through the stratification of the surrounding deposits.
- "Stockworks" consist of randomly oriented complexes of veinlets and small sized mineralisations (sulphide-bearing inclusions) surfacing over a large area. The vast diameter of the excavations left by the miners of the ancient world may be used as an index of the exploitation of this type of deposits.
- "Stratiform ore" bodies consist of mineralised strata – more or less inter-stratified – within other rock formations, whether of a sedimentary origin or not. They are located within two beds, or within a layer. A stratiform ore body is called "concordant" when it is located between two planes parallel to the stratification. The ore can also be present as an irregular mass within the host-rocks; in this case, the ore bodies are defined as "stratabound".

Figure 4.3 Lago open pit (Rio Tinto). Massive sulphides were present in the pit, forming the core of a syncline, and stockwork is still visible on both sides of the pit. Drifts are of Roman age (Leistel et al. 1998, 10).

4.1.1 Geological sequence

The geological setting of the Iberian Pyrite Belt consists of a sequence of Devonian Carboniferous rocks deposited in the central part of a large geosynclinal basin. They include basal phyllites and quartzites, followed by a series of volcano-sedimentary

rocks (already mentioned as the location of the massive sulphide deposit mineralisation), which are overlain by a greywacke series (*greywacke* – grey, earthy rock – is a variety of hard sandstone characterised by dark colour and a compact, clay-fine matrix with inclusions of poorly-sorted, angular grains of quartz - see Appendix 1 for the chemical composition of the minerals referred to in the text -, feldspar, and small rock fragments – the series is shown in Fig. 4.4). It is a texturally-immature sedimentary rock generally found in the area in Palaeozoic strata. The larger grains are sand-to-gravel-sized, and matrix materials generally constitute more than 15% of the rock by volume (Rothenberg and Blanco-Freijeiro 1981, 33). The rocks forming the lower portion of this complex (called the Phyllite-Quartzite Group) consist mainly of grey phyllites with variable amounts of interbedded quartzites and some greywacke. Small limestone lenses occur near the top of this Group. The associations of rocks suggest that, during this period, the area was tectonically inactive (Rothenberg and Blanco-Freijeiro 1981, 33). The Volcanic Siliceous Complex overlying the Phyllite-Quartzite Group just described contains all of the large-scale pyrite deposits. The Pyritic Belt includes more than 75 polymetallic deposits, forming a metallogenic province (Fernandez Alvarez 1975, 66; Barriga 1990, 369;) – i.e. a group of deposits with geological affinities concentrated in one particular geographic area (Anguita Virella and Moreno Serrano 1991, 201) – considered to be one of the most important in Europe (Strauss and Gray 1986, 304). The complex is characterised by lenses and layers of sub-marine volcanic rocks, such as tuffs and pillow-lavas, intermixed with fine-grained siliceous sediments including quartzites, cherts, jaspers, radiolarites and greywackes. The deposits of polymetallic sulphides appearing in this domain are large lenses of iron sulphides containing mainly chalcopyrite, galena and sphalerite, and other accessory minerals (MGMA 1985, 37) containing the precious metals gold and silver. In addition, another series of metals is also present, such as Sn, Cd, Co, Hg, Bi and Se, with contents ranging from tens to thousands of ppm (Barriga 1990, 369). A more detailed description of the sulphide mineralogical associations will follow in section 4.1.3.

The thicker jasper beds contain manganese carbonates and manganese silicate minerals that have at some time been exploited for their manganese content. Dolomite and siderite beds occur in very restricted parts of the volcanic siliceous complex. They often contain fossil crinoid debris and may be closely associated with the pyritic ore bodies. The overlying rocks, called the Culm Group, form a thick

sequence of greywacke and phyllites, and probably represent a turbidite sequence that was deposited in deep water (Rothenberg and Blanco-Freijeiro 1981, 33).

All the rocks in the Pyrite Belt underwent an intense metamorphic process during the Hercynian Orogeny of later Carboniferous times, and were intensely folded, thrust and faulted. The resulting broad geological pattern is made up of narrow and very complex isoclinal folds with a roughly east-west trend, and which are overturned to the south or south-west. Widespread low-grade regional metamorphism was associated with these orogenic movements (Rothenberg and Blanco-Freijeiro 1981, 33; Barriga 1990).

4.1.2 Mineralised rocks

All of the mineralised rocks of the area occur in the Volcanic Siliceous Complex. Two main types of major sulphide ore bodies have been recognised. The first type consists of massive pyritic lenses up to several hundred meters thick, overlying stockworks of small sulphide veins. The pyrite has a fine-grained colloidal texture with little evidence of banding or other sedimentary features. The deposits contain up to one percent of copper and smaller proportions of lead and zinc, and have been classified as autochthonous (formed *in situ* – Rothenberg and Blanco-Freijeiro 1981, 33).

The second type of massive sulphide deposit is also very fine-grained, but shows well-developed sedimentary structures such as banding, cross-bedding and slumping, and the sulphides are interbedded with carbonaceous slates, volcanic tuffs and breccias. This type of sulphide deposit contains up to 3% of combined lead and zinc, and has been classified as allochthonous (formed elsewhere and re-sedimented) (Rothenberg and Blanco-Freijeiro 1981, 33).

In recent geological times, the entire area was eroded to form a nearly flat surface that was later covered with thin layers of sand and gravel. Only a few of the large metal-rich deposits outcrop at the surface, and those that are exposed weather to produce ‘gossans’ up to 30 m thick, which overlie secondary enrichment zones that can be up to 100 m thick (Rothenberg and Blanco-Freijeiro 1981, 33).

These gossans consist of red and yellow iron oxide and iron sulphate minerals (mainly goethite and, at the base, jarosite) that have been derived from the original iron sulphide (Fig. 4.3 shows the gossan at the site of Corta Lago). The zones of secondary enrichment beneath the gossans tend to contain much higher

concentrations of copper, silver and gold than the unaltered primary deposits, which occur at greater depths. The copper-bearing minerals include chalcocite and covellite. In their unaltered, primary form, the massive sulphidic mineral deposits of the Huelva region contain a complex assemblage of sulphide minerals. The dominant mineral is always pyrite, and for this reason the deposits are often called 'pyritite' rocks. These pyritites are remarkably homogeneous over large areas, and their overall chemical compositions vary very little over the entire area of the Pyrite Belt.

S 44-48%

Fe 39-43%

Cu 0.4-1.5%

Zn 0.6-4.5%

Pb 0.2-1.8%

As 0.3-0.9%

Au 0.1-1.5 g/ton

Ag 10-70 g/ton

4.1.3 Mineral association

Although the main mineral is pyrite, these rocks (pyritites) also contain economically interesting amounts of chalcopyrite, fahlerz, sphalerite and galena, along with smaller amounts of arsenopyrite, pyrrhotite, cassiterite, stannite and native bismuth (Rothenberg and Blanco-Freijeiro 1981, 34). The gangue minerals include quartz, chlorite, calcite, dolomite and clay minerals (Rothenberg and Blanco-Freijeiro 1981, 34).

Many of the pyritite deposits show mineralised stockworks of veins in the footwall (originally the base of the deposit), often with cores of massive pyrite and outer shells containing economic amounts of chalcopyrite and minor lead- and zinc-bearing minerals. These veins, and the rocks immediately surrounding them, sometimes show hydrothermal alteration in which a chloritised core is surrounded by zones of silicisation and sericitisation (Rothenberg and Blanco-Freijeiro 1981, 34).

Disseminated pyritic veins also occur in volcanic tuffs, and some of these contain appreciable chalcopyrite with smaller amounts of sphalerite, galena, quartz, calcite and ankeritic carbonates ($Ca(Fe,Mg,Mn)(CO_3)_2$). These thin veins may, nevertheless, have been of great significance during the earliest period of metalworking, since the chalcopyrite weathers at the level of outcrop to produce a number of 'oxidised'

copper minerals that include malachite, azurite and, occasionally, chrysocolla and native copper (Rothenberg and Blanco-Freijeiro 1981, 34), visible due to their bright green/blue colours. Generally accessory minerals of this dominant association are tetrahedrite-tennantite, cassiterite and pyrrhotite, and numerous trace minerals, including electrum. Furthermore, the stockwork zone and the interaction zone at the base of the massive sulphide mounds in the Iberian Pyrite Belt contains bismuth and cobalt minerals not found in the overlying massive sulphides: cobalt sulpho-arsenides (cobaltite, alloclasite, glaucodot) formed at the beginning of the massive sulphide genesis; and bismuth sulphides (bismuthinite, hammarite, wittichenite, cosalite, kobellite, joseite, etc., and rare species such as nuffieldite, giessenite, jaskolkiite) deposited from late-stage high-temperature (> 300 ºC) copper-bearing fluids containing Bi (Te, Se). The late-stage fluids also precipitated chalcopyrite with Cu, Bi, Te and traces of Se sulphosalts at the base of the sulphide mound to form a high-grade copper zone, a few metres thick, showing chalcopyrite disease textures (Leistel et al. 1998, 13).

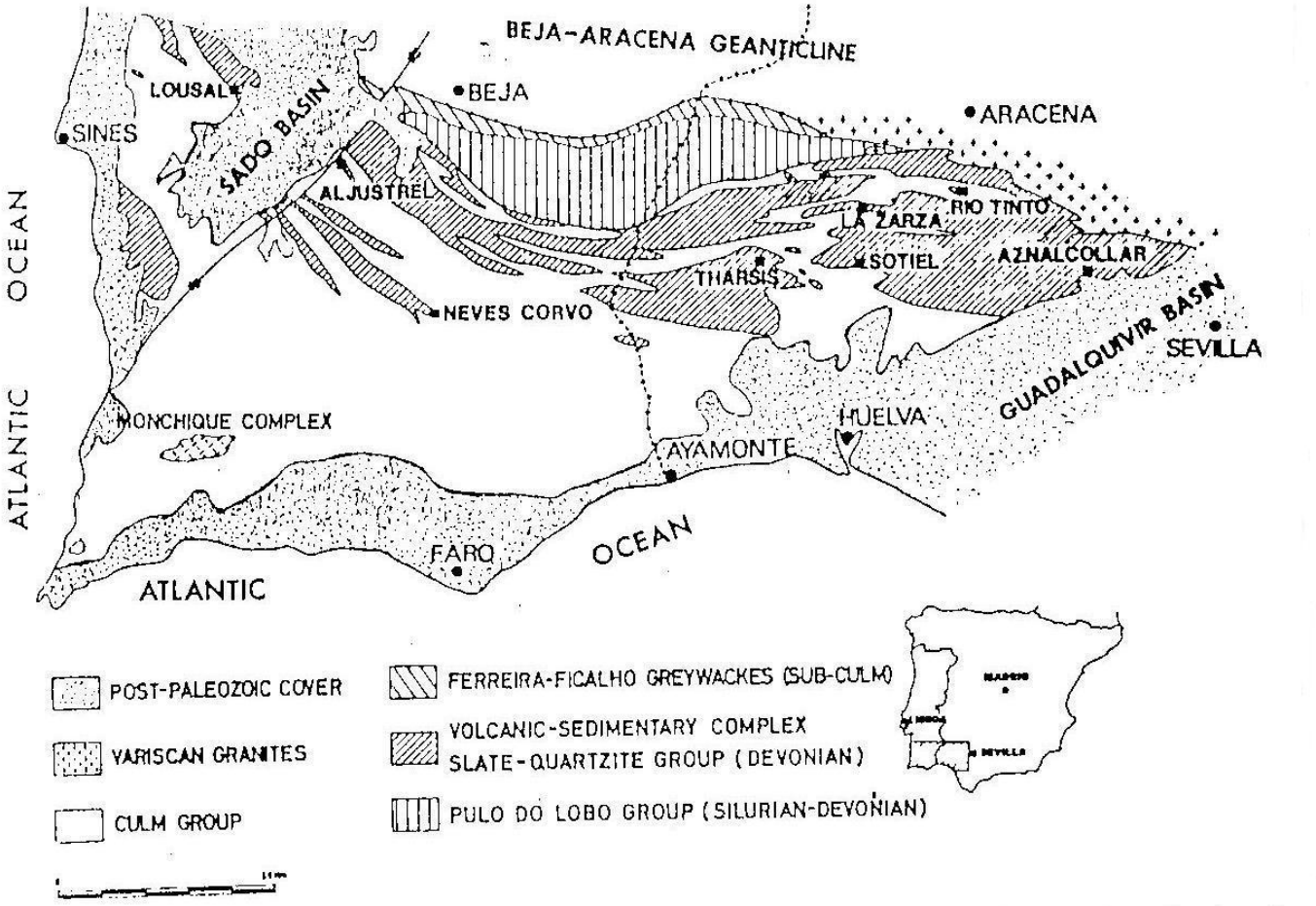

Figure 4.4 Map of the Iberian Pyrite Belt (Strauss and Gray 1986). Corta Lago is located within the Rio Tinto area, south of Aracena.

4.1.4 The secondary enrichment zone

The Cerro Colorado North Lode-South Lode deposit, where the site of Corta Lago is situated (Fig. 4.1), is located in the centre of the Rio Tinto anticline, and is the most extensive mineralisation of the area (Fig. 4.4). It consists of deeply altered massive sulphides, essentially pyrites, more or less cupriferous, in connection with an enormous iron hat of iron oxides and hydroxides (gossan), and an extensive mineralisation of stockwork (Figs. 4.3 and 4.5 - Garcia Palomero 1990, 24). In these deposits, practically all the original sulphide (between 70% and 90%) has been weathered or altered by external agents, producing the great gossan capping, of between 100-150 million tons, formed from some 400-500 million tons of original sulphides (Garcia Palomero 1990, 26). The existence of this gossan is one of the characteristics of the outcropping ore bodies, in which the sulphide minerals are weathered to form iron oxides and hydroxides, releasing practically all the sulphur, zinc, and arsenic, and partially copper and silver. At the same time, this process produces a residual enrichment in the less soluble elements, including gold, barium, lead and zinc, some of which are enriched as much as five times when compared with their contents in the massive sulphides (Garcia Palomero 1990, 26). What is obtained is a layered deposit:

- Zone of Oxidation or Infiltration. Above the piezometric surface is the area where water circulates. Charged with oxygen and carbonated gases from the atmosphere, the water attacks the rocks, oxidising the sulphides in particular (Domergue 1990, 29).
- Secondary Enrichment Area. Under the piezometric surface is the phreatic table, where the rocks and minerals are in permanent contact with water, and where the water circulation slows down. The elements taken in solution in the oxidation area above deposit in this area (Domergue 1990, 29).
- Primary Zone. The quantity and circulation of water decreases and becomes almost nil due to the stronger cohesion of the rock. The primary minerals are not attacked and remain in their primary state (Domergue 1990, 29).

Figure 4.5 Ore vein in Rio Tinto: the grey area on the left side of the picture is the massive pyrite mineralisation, the red area on the top part is the gossan, and the brownish layer between the two is the jarositic layer (Peña del Hierro – Rio Tinto).

Important chemical phenomena within the two superior zones of oxidation and cementation (secondary enrichment zone) accompany the chemically very active water enriched in oxygen and carbonated gases on its way down. The sulphides form sulphates, among which iron sulphates are very important, being very abundant due to the presence of pyrite as the main mineral. Thus, within the oxidation zone, where the superior part of the mineralisation is oxidised into gossan (Figs. 4.3 and 4.5), after several reactions iron sulphate transforms into siderite, limonite, and sometimes into complex sulphates like jarosites. In this form, soluble in water, the oxygen can reach depths that meteoric water cannot, contributing to the oxidation of other sulphides. According to this process the oxidation zone is leached (Domergue 1990, 29).

The descending sulphate solutions deposit their metallic content both in the lower part of the oxidation area and in the cementation area. During this deposition, a series of chemical reactions proceed both within the gangue in the oxidation area and within the massive sulphides in the cementation area. The results of these phenomena are:

a) In the oxidation area, formation of gossan, principally constituted by goethite, occurs. Furthermore, since the host-rock is a carbonate (limestone, dolomite, siderite, as mentioned above), the sulphates become carbonates.
b) In the cementation zone, the enrichment can be considerable. The most characteristic minerals would be secondary copper sulphides (covellite and chalcocite).
c) Underneath the cementation zone, hypogenic sulphides are not altered (Domergue 1990, 29).

Between the iron cap and the subjacent sulphides in the cementation zone, there is a small jarositic zone of varying thickness, normally around few decimetres, in which the gold and silver content is higher (Calderon 1910, 82). At Rio Tinto, this level appears as a band up to 1.5 metres thick at the base of the gossans, frequently composed of different coloured strata: yellow, red, grey and black, depending on the composition. The deposition of the bands was not always continuous, and they are in fact absent in specific zones. The yellow bands have been considered predominant and on occasion appear alone (Williams 1934, 631-632; 1950, 8). These zones of jarositic enrichment, formed by the alteration of massive sulphides, would have been exposed on some occasions by lateral weathering of the gossan, thereby becoming easily accessible (Dutrizac et al. 1985, 80). This is a very important aspect when considering its possible exploitation by ancient mining technologies. For Rio Tinto and other mines, it has been suggested that concentrations of jarosite existed near or at the surface in ancient times (Allan 1968, 48; Dutrizac et al. 1985, 78). Being able to include in their lattice different cations (K, Na, Pb, Ag, NH_4) in a solid solution, the jarosites have a variable composition; for example, the concentration of plumbo-jarosite may have varied between 3 and 30% (Hunt Ortiz 1987; Domergue 1990), as already mentioned above.

The chemical phenomena of oxidation, leaching and preferential accumulation of some elements (de Launay 1913; Routhier 1963) occurring in the superficial part of the ore bodies, as described above, are the cause of the metal enrichment, and thus of the interest shown by the miners of the ancient world in the area.

We are not concerned as to whether gold was produced in these pyrite mines of the south-west in antiquity. Undoubtedly, the mineral assemblage contained it. At Tharsis, the gossan of the south vein was rich in gold, and after obtaining the silver ingots through cupellation, the miners may have separated gold from the silver either

by the addition of some sulphide (like galena) during the smelting, or by some other method (Forbes 1964, 175-177). There is no evidence for this except for the south lode in Tharsis, where traces of mercury have been found that could have originated from amalgamation operations practiced by the miners (Pinedo Vara 1963).

4.1.5 The 'hydrothermal deposits'

In addition to the mineralisation described above, genetically associated with the volcano-sedimentary sequence, the Iberian Pyrite Belt hosts late-vein mineralisations of no economic (in modern terms) significance. These veins can be found within the volcano-sedimentary sequence or Culm facies. Their mineralogy is clearly different from that of the massive sulphides and their stockwork. The veins comprise quartz-galena-sphalerite (La Aurora), quartz-stibnite (La Esmeralda, Neron), quartz-cassiterite-scheelite (Bajo Carumbel, La Palma del Condado), fluorite-galena-sphalerite-chalcopyrite (Los Angeles), and quartz-pyrite ± chalcopyrite – grey copper (Lomo Chaparro, Valdeflores, Magalejo – Leistel *et al.*, 1998). These deposits will be referred to as 'hydrothermal deposits' in the following paragraphs.

4.2 The Archaeology of Corta Lago

As a result of this metal-rich geology, the exploitation of different areas of the Pyrite Belt was initiated very early. In the case of Rio Tinto, the metal workings can be dated from the Late Bronze Age, through the Roman era, until a few decades ago. This provides an indication as to why the site of Corta Lago is very important from an archaeological point of view, presenting a unique collection of ores, slags, furnace linings, tuyères and metal fragments representing metallurgical activities of approximately 1300 years (1100 BC – 200 AD).

Considering the entire area of Rio Tinto, the metal-producing sites with their mines, slag heaps and furnaces are now seen as a sequence of interrelated technological levels of silver, copper and iron production within the historical context of ancient south-western Iberia.

At Rio Tinto, following the evaluation of Williams (1950), the miners could have exploited around two of the three million tons of jarositic ore that originally existed in the area. Salkield (1970), on the other hand, calculated a total of 9 million tons of slag produced by silver metallurgy (only) in Rio Tinto. Previous authors (Rothenberg

and Blanco-Freijeiro 1981), following a systematic sampling of the slag, estimated a total of more than 15 million tons. A tentative discussion of these numbers will be attempted in Chapter 9.

The site of Corta Lago (Fig. 4.2), named site 44/5 during the Huelva Archaeometallurgical Survey in 1977 (Rothenberg and Blanco-Freijeiro 1981, 101), is a very large section about 8 m high and more than 500 m long (Fig. 4.6). The archaeological excavations, directed by Beno Rothenberg, and carried out by Paul Craddock and Brenda Craddock, took place over four seasons, between 1977 and 1985.

The uppermost 6 m of the section (Fig. 4.6) presented a straight 'cliff' of slag, facing the uppermost step of the mine, with some building remains visible in the uppermost 2-3 m of the section. A trench dug into this uppermost step of the mine revealed 2 m of ancient slag layers overlying the bedrock of decomposed porphyry (Figs. 4.7 and 4.8 - Rothenberg and Blanco-Freijeiro 1981, 101).

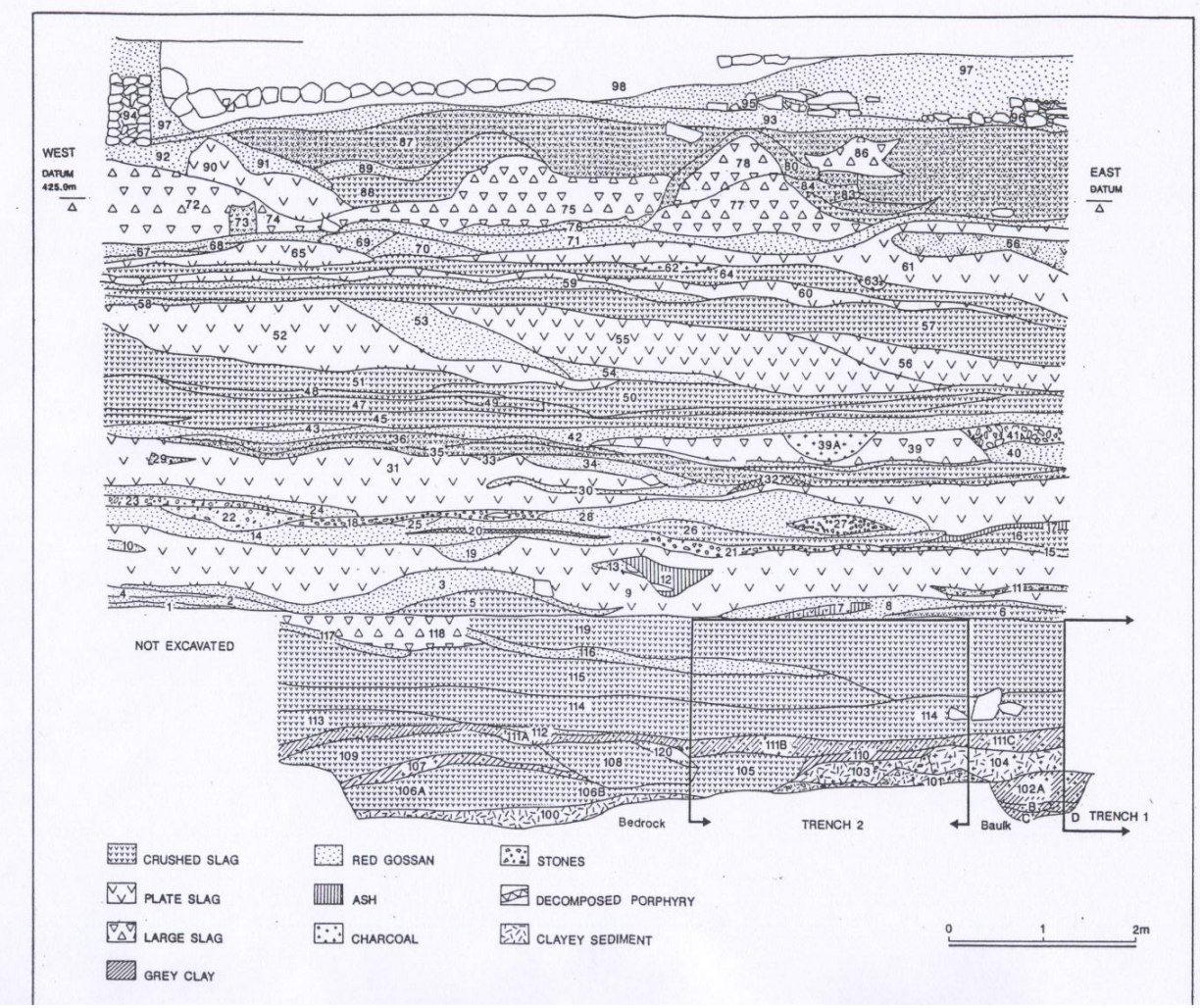

Figure 4.6 Corta Lago section as drawn by Brenda Craddock (Rothenberg and Blanco-Freijeiro 1981). The label 'plate slag' in the legend does not reflect the label 'plate slag' used in this thesis. The term 'plate slag' in this map mostly indicates tapped slag, while in this thesis 'plate slag' refers to the macro-morphology of the single sample.

Sherds and tile fragments visible in many of the slag layers and among the building debris sticking out of the section provided dating evidence. The smelting activities at Corta Lago had already been initiated in the Late Bronze Age (12th-9th centuries BC), and continued in the Early Iron Age, during the Tartessian and Phoenician periods, right up to Ibero-Punic times. Many superimposed layers of slag indicated a long history of metal production by the local Ibero-Punic inhabitants of the area, which continued well into the days of the Roman Republic. With Imperial Rome, and up to the end of the 2nd century AD, Corta Lago became the site of a very extensive and sophisticated metal production. However, by the 1st century AD, at least part of the area of the huge open air operation at Corta Lago was covered by solidly built workshops and industrial installations, and it must be assumed that by this time the smelting operation had been moved elsewhere.

The stratigraphy of the Corta Lago section and the description of the material found were first published by Rothenberg and Blanco-Freijeiro (1981), as follows:

- layers 100-106 Late Bronze Age;
- layers 107-119 Phoenician / Ibero-Punic;
- layers 1-99 Republican / Imperial Roman.

Despite the fact that Phoenician and Punic are synonyms Rothenberg and Blanc-Freijeiro (1981) use the two different wordings relating them to the two distinct periods: Phoenician for the highest Orientalising phase where the strongest cultural influence from the population occupying the area from Carthage(on the Tunisian coast) is visible. In this case then Phoenician and Orientalising indicates the same period. A later period is indicated by the synonym Punic. This indicates the decline of the Phoenician influence, that is nevertheless still visible, and reintegration of local influence in the area, hence the period is called Ibero-Punic. For continuity with the literature, Rothenberg and Blanco-Freijeiro (1981) in particular due to the importance of their text on the sites under study, the author considers crucial to maintain the same wording for these two periods that will be called throughout the thesis Phoenician and Ibero-Punic.

The excavation was carried out in different seasons. In September 1977, a section of ancient deposits (Fig. 4.6), exposed during the opening of the Corta (open cast), was discovered during the Huelva Archaeo-Metallurgical Project survey on the north side of the first mining terrace at Corta Lago. The section was called RT 25 and measured

10 m in length and 7 m in height. Another 2 m of archaeological deposits were hidden below this terrace. In 1978, the section was cut back in 1.5 m wide steps to record and sample it. The composite section was numbered from the bottom upwards (layers 1-99 – Fig. 4.6). The recorded layers were intensively sampled for metallurgical debris. Charcoal was collected for radiocarbon dating, and a few potsherds were found. The recording and sampling were undertaken by P. Craddock, B. Craddock and P. Andrews.

In 1979, the lower deposits hidden by the terrace were excavated archaeologically. Two trenches (Figs. 4.7 and 4.8) were cut through the deposits concealed at the bottom of the main section using an earthmoving scraper. These trenches were cleaned, recorded and sampled by P. Craddock and B. Craddock, and they showed that the activity began in the period of Phoenician contact, in the 7th century BC, also known as the Orientalising period. The layers were numbered consecutively with the main section in 1977 (layers 100-119, starting from 100 at the bottom and going upwards until layer 1 – Figs. 4.7 and 4.8). The discontinuity in the drawing of the main section in 1977/78 and 1979 arises because the section projects 3 m at the bottom (Fig. 4.7).

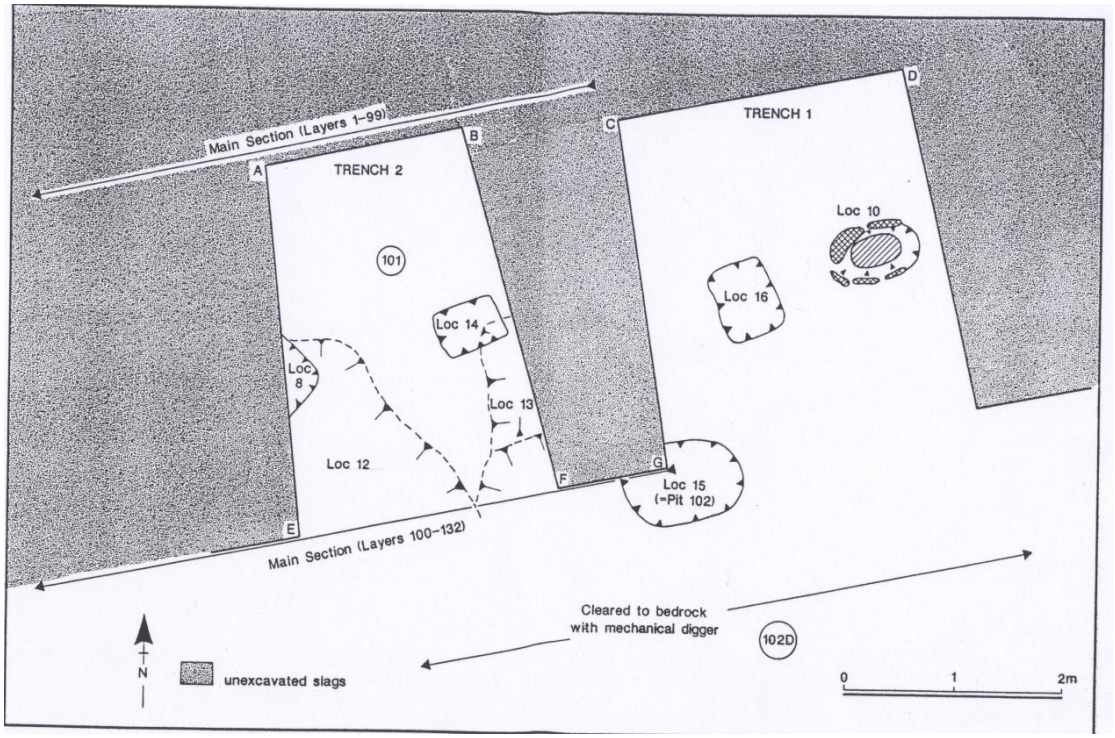

Figure 4.7 Plan of trenches T1 and T2 and location of the main section at Corta Lago.

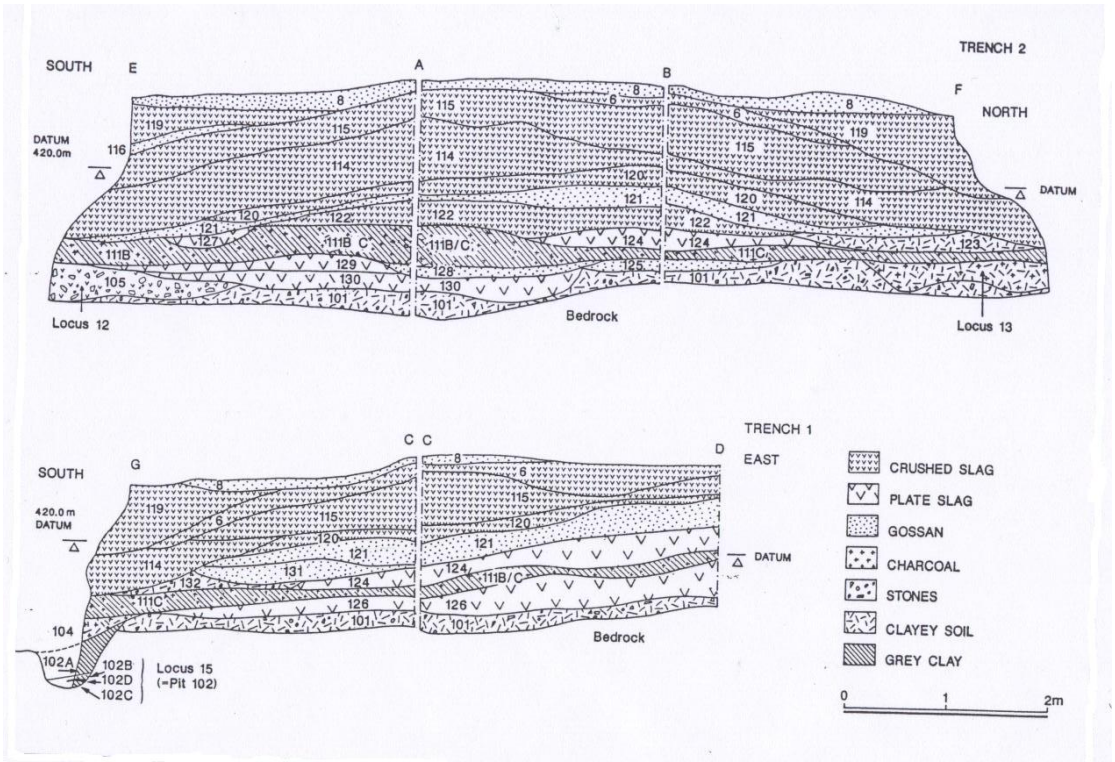

Figure 4.8 Section of trenches T1 and T2 at Corta Lago.

This huge composite section is the only complete record of the sequence of ancient deposits at Corta Lago. They are principally large slag deposits piled upon and

against each other. There is some occupation debris in the bottom and top levels, but the general impression is that the slags originate from rapid and continuous disposal of industrial waste and smelting debris.

Although a number of installations that were unearthed in the Corta Lago section were described as furnace remains, no unquestionable furnace structures have been identified so far, and there is insufficient archaeological data for a reconstruction of smelting furnaces. However, in most layers of the section, thick lumps of slagged clay lining, heavily tempered with calcite gravel, and many burnt slate and granite fragments were observed. It is clear that from the very bottom layer of Corta Lago, dating to the Late Bronze Age, up to the Roman layers at the top, furnaces built with stones and lined with clay were used. Some thick fragments of crucibles, associated either with a casting or a cupellation process, were also found (Rothenberg and Blanco-Freijeiro 1981, 106).

Studying the slag layers in the section, it became obvious that this was not one large heap of slag, but numerous superimposed metallurgical working-surfaces onto which small slag piles had been dumped, each probably representing one distinct furnace. It was only under Imperial Rome, when Rio Tinto had become the site of a huge metal industry, that large slag tip heaps were formed, evidence for a very sophisticated industrial organisation (Rothenberg and Blanco-Freijeiro 1981, 106).

Later studies by Richard Harrison (personal communication) defined the stratigraphy and materials from Corta Lago in more detail. This revision of the stratigraphy is used in this study to identify the layers and the periods associated with the chosen samples. The earliest levels include pottery of the Final Bronze Age together with imported Phoenician amphorae. They are followed by Iberian and Roman Republican deposits, again dated by pottery and a Punic coin (layer 105 and 107-32). Above them lie 6 m of Republican and Imperial Roman deposits (layers 1-98). The pottery suggests that layers 114-92 were Republican Roman of the 1st century BC, and layers 93-98 were Imperial Roman of the 1st century AD (Fig. 4.6). The uppermost deposits may have been truncated recently, and thus we do not know with certainty when the Roman activity ceased. The latest pottery recovered suggests that the activity continued at least until the mid to late 2nd century AD. Mining and smelting were resumed at this site in the 19th century AD.

Many slags lie horizontally in section, and discrete heaps were only found in the top layers (for example, layers 77 and 78; 75 and 88; and 90 and 91). Some horizontal

layers stretched for tens of metres along the section face. Perhaps there was a period of smelting when the slag was spread evenly over the surrounding area, or there was occasional smelting and earlier slag heaps were levelled. Whichever of these is the correct interpretation, and both might be, smelting took place here repeatedly from the 7th century BC until the 2nd century AD. Sometimes the hillocks of slag were levelled with a lot more slag (layers 85 and 87) to make way for Roman buildings (top layer of Fig. 4.6).

The extensive Roman buildings of the 1st century AD, excavated in 1985 by Paul Craddock, Brenda Craddock and Phil Andrews under the coordination of Beno Rothenberg and Blanco-Freijeiro, show that the dumps shifted to other areas, and they are not visible anymore on the Corta Lago section. No structures were found in the earlier levels. Perhaps they were built of timber and no traces have survived, or perhaps contemporary structures lay elsewhere and remain undiscovered. They may also have been destroyed by later mining.

Most deposits were slags of varying sizes. Some were separated by thin layers of charcoal, ash or stone associated with smelting, although the stone could have originated from demolished buildings. In addition, there were several thin deposits of gossan spread extensively (for example, layers 8, 42 and 59). These layers were fine sediments probably washed down during rainstorms. They could be deposited very rapidly, and need not be interpreted as a period of abandonment of the site. The slags from layer 106 towards the top of the section were all tap slags of three basic types: complete tap slags such as those found in layers 76, 77, and 78; thin plate slags such as those found in layers 52, 53, 55 and 56; and broken tap slags of varying size. Some of the layers were entirely composed of tap or plate slags, but most slag layers also contained ash, stones and gossan silt that had filtered in after deposition. Similarly, other layers always contained some slag (Fig. 4.6). Although the large slags were concentrated towards the top of the section, they also occurred much lower down, such as in layer 9, and large pieces of tap slag were found in layer 106, the earliest slag heap in the section. Therefore, it seems that these distinctive slag types (fragments of large tapped slag and large tapped slag heaps) do not have chronological significance, but were produced over a wide timespan, even though their major concentration in pre-Roman (small fragments) and Imperial Roman (large heaps) layers may be an indication of different processes. These aspects will be discussed later. However, the plate slags (mentioned in layers 52, 53, 55 and 56)

were concentrated together in specific layers and rarely found isolated. The process producing such debris appears limited to a short time span. It is possible that the different slags originate from the smelting of different ores. This aspect will also be discussed later.

There is a fourth type of slag found mainly at the bottom of the section, the so-called 'free silica' or ball slag, and it is associated with tap slag. This type takes its first name from the significant number of large siliceous rock inclusions it contains (Fig. 4.9), and the second name from its shape, which is often that of a ball or a bun (Fig. 4.10).

Figure 4.9 Quartz inclusion in the fresh fracture of a free-silica slag from Corta Lago.

Figure 4.10 Clear ball shape of a ball-shaped slag from Corta Lago.

This type of slag has been found at a number of sites throughout south-western Spain. It was found in the Tartessian Sites of Huelva – La Esperanza (Fernández Jurado and Garcia Rincon 1988, 192), San Bartolomé de Almonte (Ruiz Mata and Fernández Jurado 1986, 260), Salomon Ridge (Salkield 1987, 142), Tejada la Vieja (Rothenberg and Blanco-Freijeiro 1981, 85), Sierrecilla (Rothenberg and Blanco-Freijeiro 1981, 94), Monte Romero (Kassianidou 1992), and in other sites presented by Hunt Ortiz (2003). A more detailed list of locations for ball slag finds and their pottery associations is presented in Chapter 6.

Almost all of the known examples are related to silver smelting sites, while their presence is attested from the 7th century BC until the 3rd century BC, but not into the Roman period. Thus, it could be argued that this slag is related to the smelting technology and production of silver as it was practiced in Spain for most of the Phoenician and Iberian periods. A few examples of free silica-looking slag were recovered from RT 24, dated as Roman Imperial according to their stratigraphic position, and are probably ancient slags taken to the site in antiquity.

The stratigraphy can be summarised as follows (Harrison personal communication):

- layers 100 to 107 Phoenician;
- layers 111B and C, and 124 Iberio-Punic;
- layers 114 to 119 Iberians (Fig. 4.8);
- and 1-50 Republican Phase I tapped slag;
- layers 51 to 66 Republican Phase II plate slag;
- layers 67 to 90 Republican Phase III tapped slag;
- layers 91 to 99 Imperial tapped slag period.

This more detailed chronological sub-division of the stratigraphy of the Corta Lago section will be followed throughout the thesis. This stratigraphy was initiated by Richard Harrison using the field notes of the excavators as well as Rothenberg's, in addition the small amount of ceramics and coins recovered at the site were studied, typologically recognised and helped the dating of the section. Unfortunately the study was never published. Nevertheless this detailed study was completed before the author abandoned the project, hence it will be preferred here instead of the stratigraphy published by Rothenberg and Blanc-Freijeiro in 1981 because of its more thorough completeness.

Summarising the stratigraphy of the Corta Lago section is composed of the following chronological period: it starts with a Late Bronze Age/Early Iron Age phase, divided in one early section presenting slag of a specific typology (ball slag) the clear belonging of which is disputed, they could be attributed to a local technology or an early Phoenician one, the argument is expressed in section 6.1, and the samples are denominated Late Bronze Age and Phoenician in the summary table 9.1. From Middle to Late Iron Age a decline of the Phoenician influence is observed and the local input becomes more important we pass then to an Ibero-Punic phase and thenphinally to an Iberian (completely local) phase. At this point the Roman occupation starts (mid 2nd century BC) and both Roman Republican and Roman Imperial periods are present at the site. The Republican period can be divided in three different phases that present slag with different morphology. The different morphologies create also three chronological groups so at a first period (Republican Phase I) of tapped slag, follows a period (Republican Phase II) where the morphology of the slag is plate. In the last phase (Republican Phase III) the morphology of the slag is tapped as in Phase I.

4.3 First Archaeometric Studies of the Corta Lago remains

The physical appearance of the slag in almost each of the Corta Lago layers showed great variance: there were crushed platy slag fragments next to large lumps of solid tapped slag and rather viscous looking slag pieces that contained unburned charcoal, bits of furnace lining and gas holes that could not possibly have run out of a furnace, i.e. furnace slag which was mechanically raked out of the hearth. In some of the layers, mainly in the lower part of the section, there were also pockets of nodular slag pieces. Numerous large slag ‘cakes’ showed several superimposed layers, which must be considered as an indication of repeated tapping, obviously from the same furnace. There were often small ripples of slag on top of a solid body of tapped slag. While some of these large cakes carried the impression and even remains of a wooden pole across their otherwise flat top – obviously traces of the pole used to keep the tap hole open – many conical slag cakes had a tubular, very smooth hole, 3-4 cm in diameter, penetrating vertically 10-25 cm into the centre of the slag cone from its peak. The latter, mostly a very large slag body, seemed to have been formed

by numerous distinct tapping operations running down along a stick or tube from a furnace directly above, although to date there is no explanation for this extraordinary arrangement (Rothenberg and Blanco-Freijeiro 1981, 106).

A few archaeometric studies were carried out after the excavations and published in Rothenberg and Blanco-Freijeiro (1981). These results will be presented first and compared with the results of the present study in Chapter 6. Already in the Late Bronze Age, at the very bottom of the Corta Lago section, proper tapped slags indicate a sophisticated smelting process. Samples of typical slag shapes from layer 102 and 110 were analysed, and proved to be rich lead-silver slag. Only silver smelting slag was found in the Late Bronze Age layers of Corta Lago (Rothenberg and Blanco-Freijeiro 1981, 106).

The Phoenician-Ibero-Punic layers showed a continuation of the same smelting technology. One sample analysed from layer 119 is a typical rich lead-silver slag of this period, containing around 20 kg of Ag in a ton of lead. Once again, only silver appears to have been produced during this period at Corta Lago (Rothenberg and Blanco-Freijeiro 1981, 106).

The Roman layers of the section (i.e. about 6 m of its total height of 8 m) showed that during this period of major metal production in Rio Tinto, the area of Corta Lago was again mainly a silver smelting plant. Production processes, reflected by the appearance of the slag, remained essentially the same as those in operation during the preceding periods, although it seems that perhaps larger or better-constructed furnaces were used at this time, allowing a longer sequence of smelting runs that produced larger cakes of tapped slag. The Roman slag also showed a higher efficiency in metal production, i.e. less metal was lost in the slag.

Copper was also produced at Corta Lago. Significantly, copper and silver smelting slag appeared at least once in the same layer (layer 53 – Rothenberg and Blanco-Freijeiro 1981, 106). It is obvious that the Romans knew how to extract copper as well as silver from occasional pockets of complex ore in the secondary enrichment zone underneath the gossan.

The third metal produced during the Roman period was iron. Several layers of typical fayalite iron smelting slag were identified in the Corta Lago section. Gossan could well have been the ore used for this iron production. One sample from layer 64 and one from layer 72 are the first indications of iron smelting slag in the Rio Tinto area, further evidence for the sophisticated diversification of the Roman Imperial

enterprise at Rio Tinto. To date, no remains of large-scale iron production have been found at Corta Lago, nor elsewhere in the immediate Rio Tinto area. The quantities involved may have been sufficient for the local production of mining tools and implements of daily use.

Further archaeometric studies were carried out by Craddock and co-authors and published in 1985. These studies identified the mineral exploited in the Rio Tinto area in order to produce silver as jarosite. The smelting temperature was calculated at 1200 °C. The most interesting results obtained by Craddock et al. (1985) are the bulk chemical analyses, which will be compared with the results of the present study in the chapters that follow:

	Plate slag (wt%)	Plate slag	Plate slag	Ropey slag	Slag inclusion in wedge	High PbO glass
SiO_2	23.20	30.66	33.31	28.42	36.29	19.24
Al_2O_3	2.66	4.46	4.19	5.91	4.94	5.83
FeO	42.00	36.57	34.97	50.54	38.89	1.66
MgO	0.32	0.70	0.83	0.20	0.50	0.34
CaO	1.95	3.75	3.82	0.15	3.09	0.62
BaO	11.12	8.56	5.92	1.36	9.70	b.d.
Na_2O	0.07	0.20	0.20	0.13	0.70	b.d.
K_2O	0.73	1.75	n.a.	0.71	3.27	1.37
PbO	0.55	1.12	1.07	0.66	1.02	67.57
CuO	0.13	0.09	0.03	0.05	n.a.	n.a.
TiO_2	0.19	0.36	0.38	0.32	n.a.	b.d.
	82.97	88.30	84.79	88.49	100.04	99.67

Table 4.1 Craddock et al. (1985) bulk analyses of slags from site 19 A, located slightly further west of Corta Lago.

As for their phase analyses, all slags contained fayalite, but fayalite was not invariably dominant, depending on the chemistry of the sample. Instead, the rare mineral andremeyerite, $BaFe_2Si_2O_7$ (Sahama et al. 1973), was dominant in one sample. Other phases present included barium-potassium feldspars in the series celsian ($BaAl_2Si_2O_8$, "Cn") – sanidine ($KAlSi_3O_8$, "Sa"), iron oxides (magnetite or wüstite), and iron sulphide (pyrrhotite FeS). It is interesting to note that Craddock and co-authors, both in 1985 and 1995, highlighted the non-local isotopic signature of lead isotopes in the slags, as compared to the local ore signature. This problem will be discussed thoroughly in Chapter 8 of this study.

Results published by Ingo Keesmann (1993, 110) show a similar bulk composition for the slag and the feldspars (Fig 4.10). In agreement with Paul Craddock (1995),

the reconstruction of the process places considerable importance on the production of speiss (Fig. 4.11), which Craddock (1995) presents not as a waste by-product, but as a useful intermediary material for the production of silver. However, speiss is not the object of this project, due to the lack of samples (samples recorded as speiss were in fact slags), and only arsenic will be discussed as a component of the slag in Chapter 6.

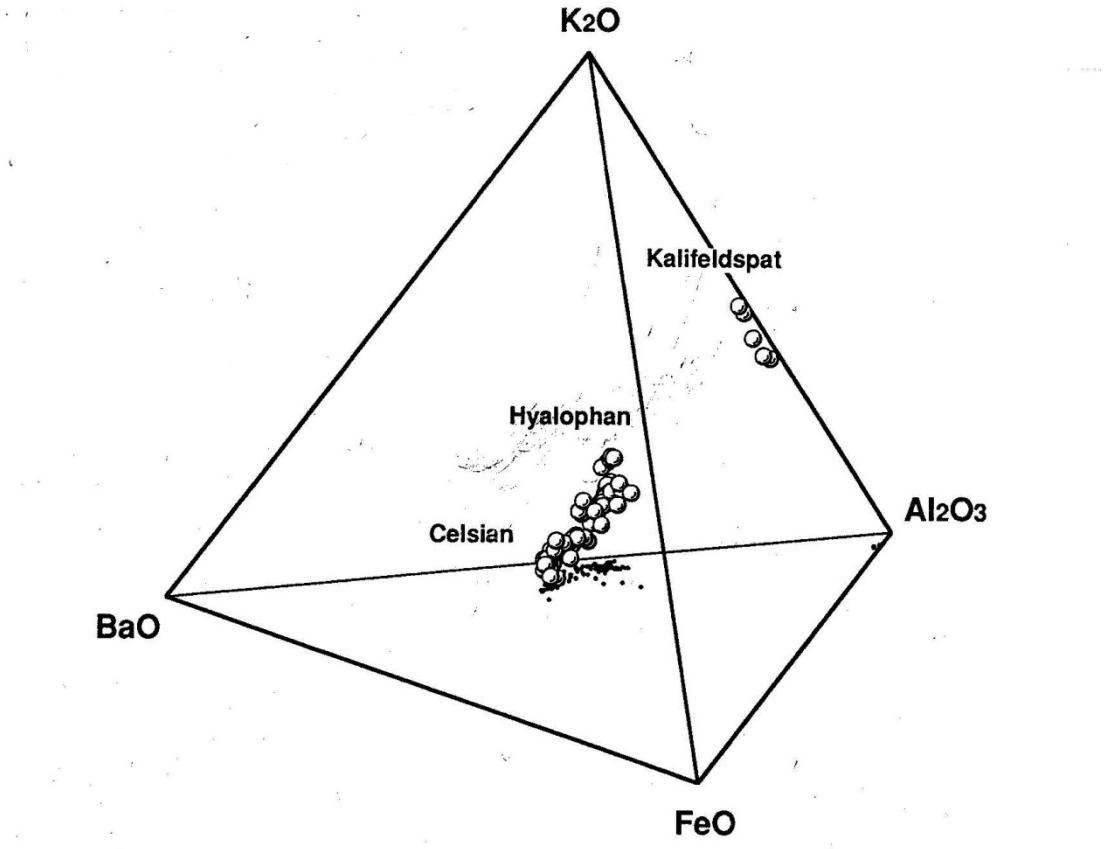

Figure 4.11 Keesman's (1993) chemical description of the feldspars detected in the slag from Rio Tinto, their main composition varying between hyalophane and celsian.

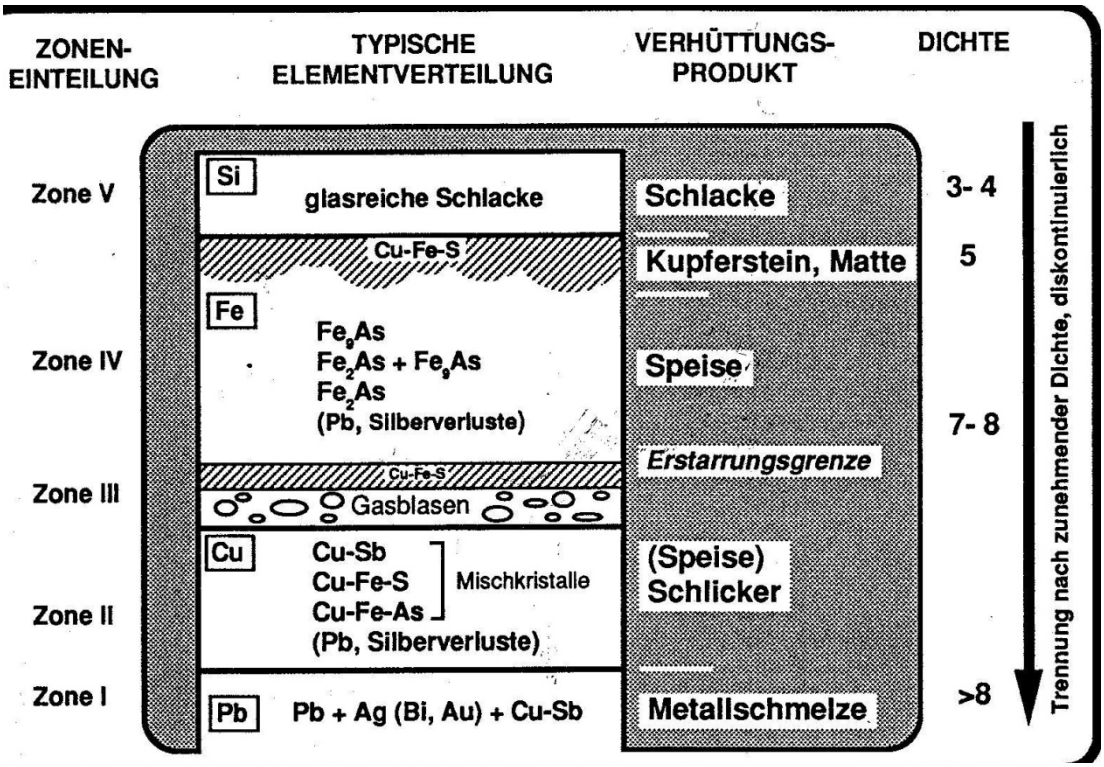

Figure 4.12 Keesman's (1993) description of the reaction zones in the furnace, indicating where the formation of the speiss and of the metal occur.

4.4 The site of Tharsis

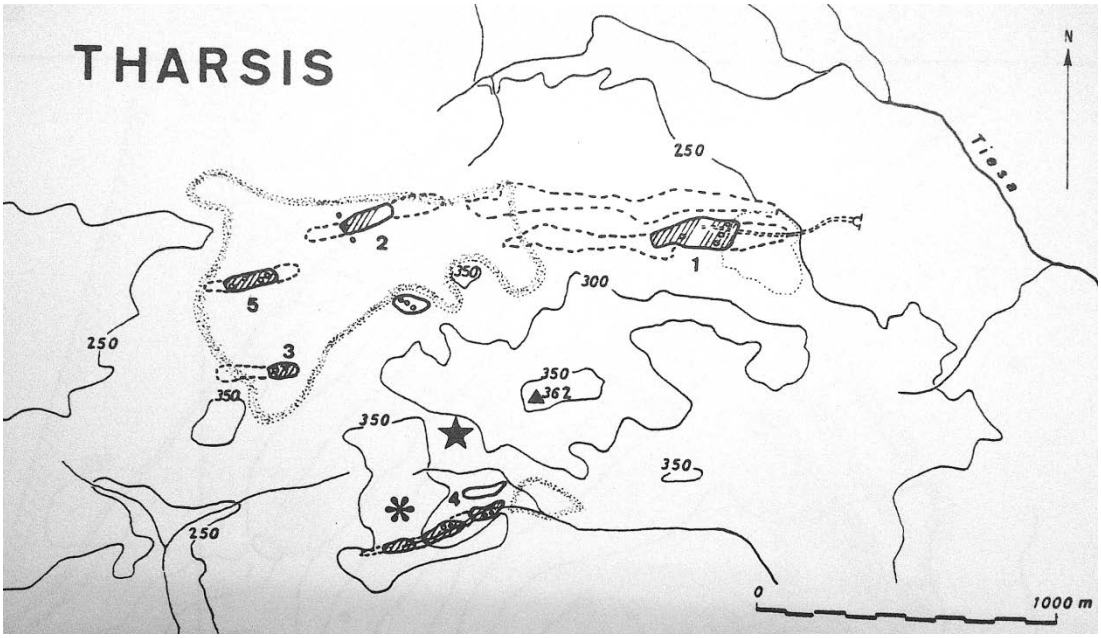

Figure 4.13 The site of Tharsis. The areas highlighted with diagonal lines indicate the pyritic zones (mineralisations), the dotted areas indicate the extension of the slag heaps, and the star indicates the position of the Roman settlement (Domergue 1990, 526).

4.4.1 Brief summary of the geology and mineralogy of ores at Tharsis

The orebody at Tharsis is one of the largest pyrite-rich massive sulphide deposits of the world (Fig. 4.13). There are three major tectonic units separated by thick fault zones, each unit with its own lithologic and hydrothermal features. The mineralisation is located within the Lower Unit and is composed of several stacked sheets of massive sulphides and shales hosting a stockwork zone with no obvious zonation. This deposit is a typical example of the sheet-like, shale hosted, anoxic, low temperature and Zn-rich massive sulphides developed in an ensialic extensional basin (Tornos et al. 1998, 150).

As a whole, the massive sulphide orebodies constitute a deposit of about 1500 m total length and about 80 m mean thickness. The total original proven reserves are 86 Mt, with an average grade of 46.5% S, 2.7% Zn and Pb, 0.7% Cu, 35g/t Ag and 0.9g/t Au (Tornos et al. 1998, 151). The mine has been exploited since approximately 4500 BC. There is important evidence of Tartessian (from 1200 to 130 BC) and Roman (from the 1st century BC to the 5th century AD) mining, which worked the gossan and the cementation zones; some mining works and between 3 and 4 Mt of slag remain from that epoch (Tornos et al. 1998, 151-152).

As for Rio Tinto, the geology of the Tharsis district has been described as follows: the oldest rocks belong to the PQ Group (Phillitic-Quartzite Group), composed of phyllites and quartzites of Upper Devonian Age. The mineralised Volcano-Sedimentary (VS) Complex overlies the PQ Group. It is very heterogeneous and, at a regional scale, it has been dated as of lower Tournaisian – Middle Visean age. However, recent palynologic dating of shales interbedded with massive sulphides in the Aznalcollar mine suggests that the hydrothermal events can be as old as Upper Devonian (Strunian – Tornos et al. 1998, 152).

The volcanism of the area is divided into acid and basic: the acid volcanism is dominated by rhyolites and dacites of calc-alkaline composition, while basalts are alkali or tholeiitic (Tornos et al. 1998, 152).

Within the PQ Group, the fault rocks can be easily mapped. There are two major tectonised bands bounding respectively the Lower and Intermediate Units (Lower Deformation Band) and the Intermediate and Upper Units (Upper Deformation Band). These bands are not only characterised by the presence of phyllonites, but

also limit tectonic units with different lithologic and hydrothermal features (Tornos et al. 1998, 155). The phyllonites are black shaly rocks with a highly penetrative foliation. They are made up of dominant strained phyllosilicates (white micas and some chlorite) and abundant organic matter accumulated along tectonic planes. Common accessory phases are rutile, magnetite and chalcopyrite, but they are very rich in pyrite, which occurs disseminated in the rock or as lenses or veins forming asymmetric, sigmoidally shaped and boudined bodies. Also typical of these rocks are the abundant pre-tectonic and syn-tectonic quartz and ankerite veins along the tectonic foliation (Tornos et al. 1998, 153).

In contact with the PQ Group just described is the Lower Unit, focus of the mining and of our interest. The Lower Unit includes the massive sulphides, which are embedded with shales showing a millimetre thick banding defined by alternating black and grey shades. The orebody is made up of superimposed 10 to 30 m thick stacked slices of homogenous massive sulphides separated by minor and anastomising fault rock bands, described above (Tornos et al. 1998, 155).

The hydrothermal alteration due to the volcanism is restricted to some shale slices intercalated with the sulphides. They show a pervasive chloritisation and pyritisation associated with the formation of abundant and unoriented millimetre to centimetre thick sulphide-rich veins; ankerite may also locally replace the shales. These rocks are interpreted as a stockwork or stringer zone.

At the contact with the massive sulphide, the stockwork zone grades laterally and downwards to unaltered shales, which are progressively less chloritised and veined. Generally the sulphide veins increase in size and proportion towards the massive sulphides.

The stockwork zone consists of almost monomineralic and highly oriented ripidolitic chlorite with minor amounts of quartz, sericite, ankerite, rutile (sometimes replacing ilmenite), and some graphite and zircon. Most of the sulphides in the stockwork zone occur within the veins. Their mineralogy is complex: pyrite occurs intergrown with abundant Co-As-Fe-S minerals (cobaltite-glaucodot, arsenopyrite, alloclasite and löllingite). These brittle minerals are cemented and replaced by others. The most common phase is chalcopyrite, but also sphalerite, pyrrhotite, bismuthinite, native bismuth, bournonite, tetrahedrite, cassiterite and rare haematite. Galena is scarce, and complex Bi-Pb-Cu-(Sb) sulphosalts and tellurides (joseite, tetradymite) can be locally important (Tornos et al. 1998, 156).

The massive sulphides occur as huge lensoidal bodies within the previously described Lower Unit. Different types of ore have been described from the economic and mesoscopic points of view. Most of the ore consists of recrystallised fine-grained pyrite with low content of base metal sulphides (pyritic ore). Some zones of the deposit are enriched in base metals (complex ore) or siderite (carbonate ore – Tornos et al. 1998, 157).

The mineral assemblage consists of pyrite, accounting for more than 95% of the sulphides; chalcopyrite and sphalerite are common phases, galena is accessory, and cassiterite, magnetite, bournonite, meneghinite, arsenopyrite, tetrahedrite, bismuthinite, haematite, ilmenite, cubanite, stannite, famatinite, pyrrhotite, mackinawite and bornite occur only sporadically. Non-metallic minerals are irregularly distributed, but they are accessory. Quartz and siderite are the most common, but sericite, chlorite, calcite and rutile are also present (Tornos et al. 1998, 157, 159).

4.4.2 The archaeology of Tharsis

All the authors indicate the density and extension of the ancient mining works (tunnels, shafts, etc.) within the huge gossan cap of this mineralisation. Most of these ancient mining works are now obliterated by modern works.

On top and around the gossan, slags can be detected. This discovery indicates that the minerals were processed *in situ*.

Part of these works is surely Roman: a large Roman settlement extended in a necropolis is located in the valley, between the administration quarter of the modern mine and the eastern extremity of the mineralisation itself. The recovered objects show that the site was occupied at least between the 1st and the 4th century AD (Domergue 1987, 202). Several thousand tons of slags (4.5 million tons) have been detected at Tharsis. Two classes have been recognised: one consists of quite thin slag, showing superficial roughness with indication of partial melting of the material, containing around 2.5% copper. The other, consisting of heaps, indicates a complete melting of the material and contains around 0.5% copper. Both initially considered as deriving from copper production and identified as Phoenician (the first category) and Roman (the second one), these slags were later interpreted as deriving from

production of copper (the first category) and from production of silver (the second one – Domergue 1987, 204).

CHAPTER 5

Methodology

The primary aim of this research is to reconstruct the process of silver production at Rio Tinto and Tharsis. In order to reconstruct the production process, a chemical, mineralogical and petrographic analysis of the slag was carried out. Chemical and micro-structural analyses of slag have long been recognised as playing an important role in clarifying archaeometallurgical processes. The understanding of the non-equilibrium processes quenched and preserved in the slag allows the reconstruction of the process itself (Bachmann 1982). The chemical composition of the slag primarily reflects the furnace charge, and hence the ore composition and any additives. Slags often trap small residual or semi-reacted fragments of the ore, providing further indications of the mineralisations used as ore, gangue or flux. The methodology was selected in order to provide as much relevant information for this research as possible.

5.1. Analytical Methods and Sample Preparation

5.1.1. Sampling strategy

The remains which will be presented in this thesis originate from two sites, Corta Lago and Tharsis, each with its own sampling history.

After the excavation of the site of Corta Lago thirty years ago, the resulting material was kept partly in museum storage at Rio Tinto and partly in off-site storage at the Institute of Archaeology, University College London, UCL, in London. The material in storage at the Rio Tinto Museum originated from the excavations carried out by IAMS (Institute for Archaeo-Metallurgical Studies) during the Huelva Archaeo-Metallurgical project, from 1977 until 1985, and the excavations carried out by Perez Macias in 1985 and 1990. The material kept for study was selected during the excavation by the archaeologists in charge, Beno Rothenberg, Paul Craddock, Brenda Craddock, and Philip Andrews. The material at the Institute of Archaeology

originates only from the IAMS excavations and underwent a second selection on transfer to the UK. This selection was based on field identification of the different classes of material in such a way as to include examples of all the defined categories (i.e. stratified sampling). The finds were stored in bags and labelled with a Find Box number, the layer or *locus* number, the year of the excavation, and the square in which they were found. However, most of the labels were found to be incomplete, further limiting the author's selection of material to analyse.

The material from Tharsis was chosen on-site by the author during a field trip to Huelva Province in May 2005. The aim was to collect typical materials that would allow characterising the most common smelting process carried out in the area. This was done in order to identify the standardised 'industrial' process at the site, rather than every type of smelting carried out.

All the chosen samples were washed with tap water and brushed to remove excess dirt. The samples were then photographed, weighed and catalogued with a new ID number.

As an initial approach, it was decided that mainly the slags would be processed further, and of these, the most typical (the ones representative of the majority of the slags recovered) have been subjected to the following procedure: the chosen samples were cut in three pieces using a diamond impregnated wheel, with one piece to be used for powder analysis, one for microscopy, and one stored as a reference for future studies.

The analytical techniques chosen for the study of the slags include X-Ray Powder Diffraction (XRD), Energy Dispersive X-Ray Fluorescence (XRF), and Optical Microscopy (OM), the latter one used for screening and descriptive analysis. Scanning Electron Microscopy associated with Energy Dispersive Spectrometry (SEM-EDS) was used for phase analysis; finally, Multi-Collector Inductively Coupled Plasma Mass Spectrometry (MC-ICP-MS) was used for isotope analysis of a small selection of samples.

5.1.2. Optical Microscopy

For this analytical technique, polished cross sections of the slags were used to study their internal structure and texture. The samples are set on the microscope stage, where they are illuminated by a beam of light. The light is then reflected, collected and magnified by the objective lens. A second set of lenses creates the image observed in the view plane of the human eye.
The method of using polished sections and a reflected light microscope is necessary for the study of phases that are completely opaque to transmitted light, and therefore cannot be analysed using the normal petrographic microscope (transmitted light). The most common opaque phases are sulphides and oxides.

Optical microscopy of some of the slag was used primarily as a preparation for the investigation of the samples by SEM. Thus, the different crystalline phases were observed and photographed when appropriate. The position of metallic prills, matte and speiss was noted, so that they could be located again when the samples were studied with the SEM.

5.1.3. X-Ray Diffraction

X-rays are electromagnetic radiations with wavelengths of about 100 Å, usually generated by a copper target in an X-ray tube. As the wavelengths are comparable with the distance of lattice planes in crystals, X-rays can be diffracted when passed through a crystal, forming a diffraction pattern characteristic of that crystal's lattice (Atkins 1990, 621). This is the main principle on which the X-ray diffraction method is based, and its main use is the identification of the crystalline phases present in a sample (Parkes 1986, 188).
To use an analogy, the lattice plane in a crystal may be regarded as a mirror and the crystal itself as a stack of such mirrors separated by a distance *d*. The incident beams of X-rays are reflected by each lattice plane and interact with each other either constructively (reinforcing each other) or destructively (cancelling each other out so that no X-ray is detected). This is described by Bragg's law: $n\lambda = 2d\sin\theta$, where n is an integer number indicating the level of diffraction, λ is the wavelength of the

incident beam, d is the inter-plan distance, and θ is the angle between the incident X-ray beam and the crystal plane (Atkins 1990, 621), so that every plane, indicated by a certain *d*, has its specific diffraction angle (2Θ).

In X-ray powder diffraction, monochromatic radiation is used and the sample is crushed into a fine powder. By using a beam of known wavelength and by changing the angle, one can then apply the above equation to calculate *d*. The sample is used as powder because in this form some of the crystallites will always be oriented so as to meet the conditions of Bragg's law (Atkins 1990, 622). The sample is spread on a flat plate and the diffraction pattern is monitored electronically (Atkins 1990, 623). From the resulting spectrum, the value of the incident angle at which a reflection has occurred can be measured, and, from that value, the *d* spacing can be calculated. Using appropriate reference databases, the mineral can thus be identified.

The X-ray diffraction analysis was carried out at the Mineralogy Department of the University of Milan, Italy. The diffractometer was an X'Pert Philips fully computer-integrated, with incident and anti-scatter optics completely programmable (Fig. 5.1). Two detectors were present: a proportional counter, and a position sensitive detector. They can be used for different purposes: the former for structural analyses, and the latter for fast reaction kinetics. For the purposes of this project, the proportional counter detector was used. The statistics of the interaction between the X-ray beam and the sample was improved by spinning the sample.

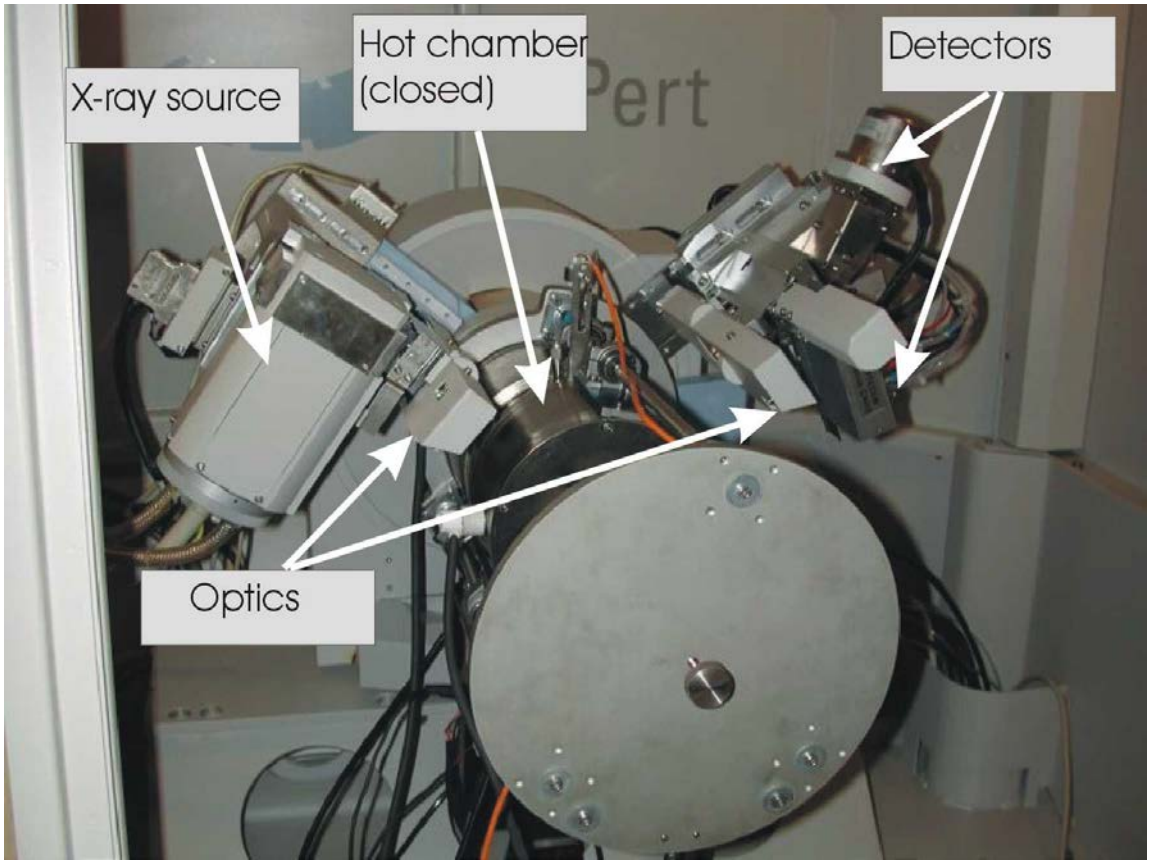

Figure 5.1 X'Pert Philips Diffractometer at the Dipartimento di Mineralogia, Università degli Studi di Milano.

A total of 33 finds, all from Corta Lago, were analysed by this method. They were mainly slags (27 samples), but also included clay lining, a cupellation dish fragment, and one tuyère sample. The samples from Corta Lago were the ones presenting the most heterogeneities, hence an insight of the mineralogical association (by XRD) mainly concerning the accessory minerals, was considered necessary in order to achieve a better understanding of the process forming the slag and the process altering it.

5.1.4. X-Ray Fluorescence

One way to excite characteristic X-rays is to bombard the specimen with X-rays of higher energy. This technique is known as X-ray fluorescence analysis. XRF has been a standard method of elemental analysis in geology for several decades, and it offers a good accuracy for major elements, as well as detection limits in the region of 1 ppm. In its usual form, it is a bulk method, requiring around 8 g of ground sample

material, and is therefore used principally for analysing entire rocks or separated minerals (Reed 1996, 5).

This method is used for quantitative chemical analysis after the definition of a purpose-built calibration curve. It consists of irradiating the sample with an X-ray beam produced by an X-ray tube or a radioactive source. When hitting the sample material, these X-rays excite the electrons of the atomic layers K and L to higher energetic levels. As electrons cascade down from the outer shells to fill the gaps, they emit secondary, fluorescent X-rays.

These fluorescent X-rays possess energies (or wavelengths) characteristic of the elements which have emitted them, so that by measuring those X-rays it is possible to identify each element and then determine the concentration of the different elements present in the sample. This is because the intensity of measurement is proportional to the concentration of a certain element (Parkes 1986, 151-152). X-ray fluorescence analysis can be used to determine elemental concentrations between 10 ppm and 100% with a confidence of ± 2 to 5% in the readings, although at lower concentrations the uncertainty levels increase significantly.

This technique can be carried out in a perfectly non-destructive manner, since the artefact can be analysed directly, with no previous extraction of samples. Surface irregularities, however, can complicate the calibration of the intensities, resulting in semi-quantitative/qualitative analysis.

A limitation of XRF surface analysis is the low penetration of the X-rays. As a result, the analysis only provides data concerning the superficial part of the sample, an aspect which can lead to distortions that need to be taken into account (e.g. variation for selective corrosion – Bui et al. 1986, 204).

The instrument used in this study was the Spectro X-Lab 2000 at the Wolfson Archaeological Science Laboratories of the Institute of Archaeology, UCL (Fig. 5.2). This X-ray fluorescence instrument is equipped with an energy dispersive spectrometer. For a comprehensive description of this machine, see Veldhuijzen (2003).

Figure 5.2 Spectro X-Lab 2000 X-Ray Fluorescence Instrument at the Wolfson Archaeological Science Laboratories, UCL Institute of Archaeology.

A total of 45 samples from Corta Lago and 4 samples from Tharsis in the form of pellets prepared from the powder of the sample (as described in section 5.1.9), were analysed by this method. The finds from Corta Lago included slags (44) – tapped, non-tapped and ball slag – and a fragment of litharge (PbO - 1). The chosen samples were as follows: 3 ball slags, 8 Phoenician, 5 Ibero-Punic, 6 Iberian, 8 Republican tapped slags of the first phase, 7 Republican plate slags of the second phase, 2 Republican tapped slags of the third phase, 6 Imperial tapped slags. The samples from Tharsis are only tapped slags, one Republican and one Imperial. The area of the specimen (pellet) irradiated by the X-ray beam is $0.5cm^2$ .The results for each of the two sites and the different materials will be discussed separately in the following chapters.

5.1.4.1. Accuracy and Precision

The accuracy and precision of X-ray fluorescence are dependent on the calibration curves used to correct the measured characteristic intensities. These intensities are

transformed into concentrations comparing the unknown measured intensities to a library of stored intensities/concentrations of known and certified reference materials (standards).

For the XRF instrument at the UCL Institute of Archaeology, several methods have been developed for various materials, including different kinds of slag. A 'method' is defined as the combination of characteristic measurement parameters, choice of standards, and deconvolution and correction procedures (see Veldhuijzen 2003 for details). The measurement parameters include the choice of secondary targets, the accelerating voltage for every target, which elements have to be measured by which target, and which elements have to be stripped from the spectrum for each target. The secondary targets are crystals located between the X-ray source and the sample. These crystals are used in order to modify the polychromatic X-ray coming out from the source so as to excite one particular region of the X-ray spectrum.

For the purpose of this thesis, several certified standards were chosen (BCS-CRM 381 Basic Slag, BCS-CRM 393 Limestone, BCS-CRM 313/1 High Purity Silica, USGS BCR-2 Columbia River Basalt, BCS 301/1 Lincolnshire Iron Ore), and measured quantities of lead oxide were added in 5% intervals ranging from 0 to 60% of lead. These standards were chosen in order to roughly reproduce the unknown material, because the interaction between the elements has to be considered as part of the corrections.

The second step was to reproduce an existing method ('Slag Fun', developed by Veldhuijzen between 2002 and 2005), and improve it by focusing on lead rich material. This was necessary because lead was the major element in the matrix of several of the slags that were analysed in the context of this project, instead of iron, as was the case with the 'Slag Fun' method. Every change in the method (addition of new standards, recalculation of calibration curves of different elements with different standards) was monitored by a re-evaluation of all the standards present in the library for the methods under construction, and the measurement of two standards used as reference material. After the evaluation of all the standards used in the new method, the author found the results unsatisfactory, due to the difficulty of correcting the matrix of such a material so rich in lead and consequently use it as a standard. Thus, a choice was made to measure the samples according to the 'Slag Fun' method implemented by Veldhuijzen (2003) and re-optimise the results for every change of X-ray source and targets.

5.1.5. Scanning Electron Microscopy with Energy Dispersive Spectrometry

The scanning electron microscope (SEM) is a close relative of the electron microprobe, but is designed primarily for imaging rather than analysis. Images are produced by scanning the beam in a television-like raster and displaying the signal from an electron detector on the screen. By selecting the appropriate detection mode, either topography (secondary electron) or compositional contrast (back scattering) can be emphasised ('composition' refers here to the mean atomic number: individual elements cannot be distinguished). A spatial resolution smaller than 10 nm in the topographic mode (secondary electron detector) and 100 nm in the compositional mode (back scattering detector) can be achieved, although in many applications the large depth of field obtained in SEM images (typically at least 100 times greater than for an OM image of comparable resolution) is more useful than high resolution. An important factor in the success of scanning electron microscopy is that SEM images of 3D objects are for the most part amenable to intuitive interpretation by the human eye and brain (Reed 1996, 1).

The SEM is very effective for studying crystal morphology on a micro-scale. The ability to produce compositional images of polished sections (showing differences in mean atomic number) is very useful in both sedimentary and igneous petrology, and we can argue that slags are relatively close to igneous rocks in this respect. The petrographic details thus recorded well exceed those obtainable with a polarised light microscope.

There are several reasons for using a scanning electron microscope in archaeometallurgy; in this case, the specimen preparation is straightforward and entails the use of existing techniques of section-making and polishing with only minor modifications. The SEM is also considered a non-destructive technique, unlike most other analytical techniques. The quantitative elemental analysis with Energy Dispersive Spectrometry has accuracy in the region of a few percent, and for major elements this can be obtained routinely. All the elements with atomic numbers above 10 can be determined with fairly uniform accuracy and sensitivity, and those between

4 and 10 with somewhat inferior sensitivity (H, He, Li are not determinable). The detection limits (typically in the region of 1000 ppm) are low enough to enable minor elements to be determined in many cases. The time of a single analysis is reasonably short, around 2 minutes. The spatial resolution of the order of 3-5 μm enables addressing most features of interest. Individual mineral grains can be analysed *in situ*, with their textural relationships undisturbed and visible to the analyst. A high specimen throughput rate is possible, with the time required for changing specimens being quite short (Reed 1996, 2).

Scanning electron microscopes incorporate an 'electron-optical column' for the purposes of generating the electron beam, focussing it on the specimen, scanning it to form images, etc. (Reed 1996, 21). The source of electrons in SEM instruments is an electron 'gun' consisting of an electron emitter at a negative potential of several kilovolts, which accelerates the electrons towards the sample. The effective source diameter obtained with the conventional (thermoionic) type of electron gun is about 50 μm. Magnetic electron lenses are used to project an image of the source onto the surface of the specimen, the image being demagnified by a factor ranging from 10^2 to 10^4 (Reed 1996, 21-24). In an SEM, the minimum attainable beam diameter is typically less than 10 nm (Reed 1996, 29).

As already mentioned at the beginning of this section, scanning images are produced by sweeping the beam across the sample in a television-like 'raster', while displaying the output of an electron detector on the screen of a synchronously scanned cathode ray tube. The frame scan frequency ranges from TV rate (50 or 60 Hz) to considerably lower frequencies. Instead of scanning a rectangular raster, the beam can be swept along a single line by using only one set of coils. The coils can also be used to move the beam around in 'spot' mode for X-ray point analyses (Reed 1996, 35-36), allowing the analyst to obtain different outputs from the sample.

X-ray spectrometers are of two types. The oldest is the wavelength-dispersive (WD) type, which makes use of Bragg reflection by a crystal. The energy dispersive (ED) type consists of a solid-state detector that produces pulses proportional in size to the X-ray photon energy, which are sorted electronically by intensity in order to produce a spectrum; the potentialities of the two spectrometers are also described in section 5.1.6. The pulses are processed in quick succession and the entire spectrum is effectively recorded 'in parallel'. This is different from WD spectrometers, which

operate in a 'serial' mode, the spectrometer being 'tuned' to only one wavelength at a time. The WD type has better spectral resolution, but the ED type is faster and more convenient to use. An ED spectrometer collects the entire X-ray spectrum at once, while 'windows' or energy bands containing the peaks of elements of interest can be defined and the outputs from these used for mapping (Reed 1996, 98), as described in the following sections.

One should keep in mind that owing to the broadness of the peaks in the ED spectrum, background is more important than for the WD spectrometer. It follows that significant X-ray intensity is recorded even in regions containing none of the elements concerned. Furthermore, the background (continuum) intensity varies with the mean atomic number, which may give a false impression of differences in concentration between areas actually containing negligible amounts of the relevant element, but varying in atomic number (Reed 1996, 102).

X-ray spectrometers attached to SEMs are usually of the ED type, although sometimes a single WD spectrometer is added (Reed 1996, 43). The ESEM used for the analysis of the slags within this project, is equipped with both ED and WD spectrometers. For the aim of this project only the energy dispersive spectrometer was used.

One of the parameters of the SEM to take into consideration is the 'dead-time', defined as the time interval (t) after the arrival of a pulse during which the system is unresponsive to further pulses (typically a few μs). This has the effect that the measured count-rate (n^1) is less than the true count-rate (n) by a value that becomes significant at high count-rates (Reed 1996, 63). In the case of the Philips ESEM used for this study, the dead-time was on average between 15 and 20%.

As already mentioned above, we can obtain two different types of images from a scanning electron microscope: secondary electron and backscattered electron images. Both secondary and backscattered electron images exhibit topographic contrast, although usually the former is used for this type of image, and the latter for displaying compositional differences (Reed 1996, 71). Secondary electrons are emitted from very near the surface of the sample, with energies of a few eV. The increase in SE yield with decreasing angle between the beam and the specimen surface gives rise to a three-dimensional effect in SE images (Reed 1996, 71).

As also stated in section 5.1.7, the fraction of electrons in the beam that are backscattered is strongly dependent on the atomic number, Z. Hence, the output of a

BSE detector reflects this dependence in somewhat modified form, because the detector is energy-sensitive and the energy distribution of backscattered electrons varies with Z. Brightness in a BSE image is thus a function of Z (or the mean atomic number, for compounds). For compositional imaging, the specimen should be well polished, so that interference from topographic effects is minimal. SE images also show some compositional contrast owing to secondary electron emissions caused by backscattered electrons (Reed 1996, 84).

Compositional BSE imaging is very useful in its own right as a petrographic technique, as well as serving to aid the selection of points for X-ray analysis; sometimes it is easier to distinguish different minerals by their mean atomic number than by their optical properties (Reed 1996, 85).

The spatial distribution of an element can be revealed by recording the intensity of the characteristic X-ray line of that element while the beam is moved across the specimen. If the beam is scanned in a rectangular raster, a two-dimensional element 'map' is produced. Compositional information is also contained in BSE images, but in this case it is related to the mean atomic number only, and is non-specific with respect to individual elements. Much longer recording times are required for X-ray images than for electron images, because the X-ray signal is several orders of magnitude less intense (Reed 1996, 96). For this study, an average time of 4000 s has been used to produce chemical maps of selected areas in order to highlight chemical distributions of different elements and different generations of crystallisation of the phases in the slag.

The simplest form of X-ray image is the 'dot-map', in which each recorded photon produces a bright dot on the display. Since the beam is scanned across the specimen in synchronism with the screen spot, the density of dots on the screen shows variations in the concentration of the selected element (Reed 1996, 96). In the case of the ESEM Philips, a spectrum is also registered for every dot in the map.

There are considerable advantages with digital recording systems in which the number of X-ray photons recorded at each point is stored in the computer memory. The image, or map, is generated by converting this number into the brightness of the screen spot. The image can be displayed continuously as the beam is repeatedly scanned, and acquisition can be stopped when a satisfactory result has been obtained (Reed 1996, 98).

The microanalysis proved to be a valuable method, especially in the case of heterogeneous materials, such as the ball slags from Corta Lago. The ESEM (Philips Scanning Electron Microscope with Oxford Instrument Energy Dispersive Spectrometer and Inca Analytical System – Fig.5.3) at the UCL Institute of Archaeology was used for the analysis of multi-phased metallic prills, matte and speiss, silicates and oxides in the slags. The main difference between an SEM and an ESEM is that with the latter analyses can be performed in a controlled atmosphere (variable pressure), and samples do not need to be coated in order to be analysed, the charging effect being minimised by the pressure present in the chamber. This function was not used during the analyses, and the samples were carbon coated and examined in high vacuum, as if we were using a normal SEM. This analytical choice was due for purposes of comparison, since all of the work on slag material performed at the UCL Institute of Archaeology was carried out using this method.

Figure 5.3 Philips ESEM and Oxford EDS instrument at the Wolfson Archaeological Science Laboratories, UCL Institute of Archaeology.

A total of 20 samples from Tharsis and 30 from Corta Lago were analysed by SEM-EDS. The selected samples from Corta Lago were as follows: 2 ball slags, 2 Iberian tapped slags, 4 Imperial tapped slags, 7 ore samples, 3 ingot samples, 2 Phoenician tapped slags, 6 tapped slags from the first Republican period, 2 plate slag samples from the middle Republican period, and 1 tapped slag from the last Republican period. The samples selected from Tharsis were 13 Imperial slag samples and 7 Republican slag samples. All the samples were subjected to a standardised process: 10 areas of 2 mm^2, avoiding residual phases if present, were analysed in order to obtain an image of the chemical homogeneity of the sample in its *liquidus* state; in addition, 10 analyses of each phase, and a few chemical maps per sample were performed, in order to obtain a better description of the dynamics of the chemical diffusion within the samples.

The area analyses associated with the imaging of the samples provide an indication of the uniformity of the samples, linked to two different factors:

- Presence of residual crystals that would indicate higher rigidity of the system and lower movement of the chemical elements within the system;
- Early crystallisation already inside the furnace and subsequent slow cooling speed, which allows for the crystallisation of big crystals that would make the diffusion of chemicals within the system impossible.

The performance of area analyses alone would not distinguish between these two completely different states of the material, but the correlation of these data with those resulting from image observation, both from OM and SEM, would provide more complete results.

5.1.6 Quantitative analysis with SEM and XRF

Two of the techniques described above, SEM-EDS and ED-XRF, can provide results pertaining to the chemical compositions of the analysed objects both qualitatively and quantitatively.

A ‘qualitative analysis’ entails the identification of the elements present in a given sample, or the identification of minerals from the elements which they contain. As mentioned in the previous section, there are two available types of X-ray spectrometry: the ED (Energy Dispersive) type is far superior for qualitative

analysis, owing to its ability to record a complete spectrum rapidly (Reed, 1996, 111), and WD (wavelength dispersive) spectrometers are more reliable for quantitative analysis (see section 5.1.5).

The energy range 1-10 keV typically covered by an ED spectrometer includes the K spectra of elements of atomic number 11 to 30 (Na-Zn). With a thin window, or in windowless mode, the atomic number range can be extended down to 4 (Be). The upper limit can be set to 20 keV, for elements with Z between 31 and 44; these elements also have L lines in the range 1-2.5 keV, which can be used for identification. The range of elements with L lines below 10 keV extends up to Z=80, and the only significant heavier elements are Pb, Bi, Th and U. M lines are detectable for Z>60 with a conventional Be-window detector. The simultaneous presence, within the normal range of an ED spectrometer of K and L lines for medium atomic number elements and L and M lines for heavy elements is sometimes useful in confirming identifications (Reed 1996, 111), as well as leading to line overlap. However, cases of possible ambiguity due to line overlap between α lines are few and occur only between lines of different shells, e.g. As Kα – Pb Lα, S Kα – Pb Mα and Ti Kα – Ba Lα (Reed 1996, 113).

'Quantitative analysis', on the other hand, entails measuring the intensities of the relevant X-ray lines generated in the specimen and in suitable standards, using identical instrumental conditions (accelerating voltage, beam current, specimen geometry, etc.). Element concentrations are calculated from the ratios of specimen and standard intensities and the known concentrations in the standards (Reed 1996, 126), via the prior construction of calibration curves.

The intensities are used to derive uncorrected concentrations and these are corrected by the usual ZAF procedures (see below). Owing to the simultaneous collection of the entire ED spectrum, relative peak intensities for different elements are unaffected by changes in beam current, which is a considerable advantage when using an instrument (SEM, for instance) lacking beam current stability. However, current variations will cause analysis totals to vary from the ideal 100%. Although normalisation to 100% may be acceptable in some cases, it is inappropriate when an undetermined component, such as H_2O, is present (Reed 1996, 130).

As mentioned in section 5.1.5, peak to background ratios are lower in ED spectra than in WD spectra, so rather than using a single channel for determining background, it is preferable to integrate over a number of channels in order to

improve the statistical precision. Likewise, linear background interpolation is less reliable in ED than WD spectra, owing to the greater energy range involved and the greater likelihood of overlap between peaks. A better approach is to represent the background by a more comprehensive expression for the continuum (Kramer's expression), with additional factors to allow for absorption in the sample itself and in the detector window, etc. This can be fitted to the observed background in peak-free regions (Reed 1996, 131).

Matrix corrections are also applied to measured concentrations in order to obtain 'true' concentrations corrected for composition-dependent matrix effects. Conventionally the corrections are expressed as three independent factors identified by the acronym 'ZAF', where Z indicates the atomic number, A absorption, and F fluorescence. These factors are dependent on the composition of the specimen, which is not known until the corrections have been calculated. This difficulty is solved by using an iterative procedure (Reed 1996, 134). These corrections can be carried out more effectively when the standards used to build the calibration curve have a matrix similar to the unknown sample measured.

The 'atomic number correction' is related to the dependence of the efficiency with which characteristic X-rays are excited on the mean atomic number of the specimen. Two distinct phenomena influence this correction: electron penetration and backscattering (Reed 1996, 134).

The mass penetrated by electrons of a given energy is not constant; instead, it actually increases with increasing Z. X-ray intensities (per unit concentration) therefore also increase with Z, and, when the sample has a higher mean atomic number than the standard, then the uncorrected concentration must be corrected downwards (and vice-versa – Reed 1996, 135).

Backscattered electrons leave the specimen owing to large-angle deflections resulting from encounters with the nuclei of target atoms, or the cumulative effect of numerous small-angle deflections. Backscattering is strongly dependent on atomic number: the variation of the backscatter factor η (the fraction of incident electrons that leave the specimen) increases exponentially with Z. The correction factor for X-ray intensities is closely related to η; backscattering thus causes a reduction in the X-ray intensity with increasing atomic number. The overall 'atomic number correction' acts in the direction of the backscattering effect since this predominates over the penetration effect (Reed 1996, 135).

Before leaving on their way to the spectrometer, X-rays travel a certain distance within the specimen itself and are consequently liable to absorption (Reed 1996, 136). Characteristic X-rays of atoms of a given element can be excited by other X-rays when the energy of the latter exceeds the critical excitation energy of the former. Fluorescence is always excited by a part of the continuum and sometimes by characteristic lines of other elements. Since the contribution of fluorescence generally differs between specimen and standard, a correction is necessary (Reed 1996, 138).

To calculate correction factors, a composition must be assumed. As an initial approximate, the uncorrected concentrations can be used. Having obtained a set of correction factors, updated concentrations are derived and used to recalculate the correction factors. When there are no further significant changes in the concentrations (typically after 3 to 6 iterations), the process is complete. Absorption factors, matrix effects, etc. must also be calculated for the standards, but since the true compositions of these are known from the start, iteration is unnecessary (Reed 1996, 141).

For the SEM, the accelerating voltage must be greater than the highest excitation potential of the elements present and preferably should be at least twice this value in order to provide reasonable intensities. Thus, for silicates containing iron, the accelerating voltage should not be inferior to 15 kV (Reed 1996, 145). In the context of the present study, a constant accelerating voltage of 20 kV has been used.

Peak intensities and peak to background ratios increase with increasing accelerating voltage (except when there is severe absorption of the emerging X-rays, in which case the intensity decreases beyond a certain point due to the predominance of absorption). It follows that, by operating at high accelerating voltage, better statistical precision can be obtained in a given counting time (or the same precision in a shorter time) and detection limits will be lowered (for a given counting time). These advantages are offset, however, by the increased electron range in the sample, which results in a decreased spatial resolution and increased absorption corrections. Balancing these considerations leads to a choice in the range of 15-25 kV in most cases. A lower value may be appropriate occasionally, e.g. for light elements subject to large absorption corrections. For trace elements, where detectability is more important than the size of the absorption correction, a higher value may be considered (Reed 1996, 145). For this study, only the estimation of major elements

was considered reliable when using the EDS-SEM technique. For the measurement of the trace elements in the bulk analysis, only the values obtained with XRF were taken into consideration.

A major limitation of quantitative EDS is the impossibility of distinguishing the valences of polyvalent elements such as Fe. Valency is important in determining crystal-chemical formulae, and uncertainty in Fe^{2+}/Fe^{3+} affects the validity of redox conditions calculations (Reed 1996, 156).

The 'detection limit' for a given element is the minimum concentration that can be positively detected, corresponding to a peak which can be distinguished from statistical background fluctuations. A suitable working definition for a just-detectable peak is that its height is greater than three standard deviations of the background count (the probability of this occurring by chance is less than 3% – Reed 1996, 159).

A cross-check of the quantitative results between the Philips ESEM and the Spectro XLab 2000 Pro XRF was carried out in order to identify the stability of the instruments and the precision/accuracy of the calibration methods used for the analyses. For the cross-check, certified standards and known samples were analysed by SEM and by two calibration methods of XRF. Furthermore, a cross-check of the chosen XRF method across a certain time span (the analyses were repeated in October 2005, January 2006 and February 2010) was carried out to inspect the consistency of the data after tube and target changing. For the SEM, 10 area analyses were carried out for each sample in order to calculate the consistency of the analyses, using the standard deviation as a numeric figure to describe the instability of the instrument. For the XRF, 3 or 5 runs per sample were carried out for the same reasons. All the results were normalised to avoid variability between instruments. Note that the tables summarising the results do not present the complete set of measured elements that were used for the normalisation.

The standard materials analysed by SEM were USGS BHVO 2 (Basalt Hawaiian Volcanic), BCR 2 (Basalt Col. River), BIR 1 (Basalt Icelandic) and Glass C. The known samples were produced mixing 9 g of USGS BHVO 2 with 1 g of $BaSO_4$, and 9 g of BCS 301/1 with 1 g of PbO, respectively. The two known samples were in the form of powder, and thus, in order to be analysed under the SEM, 1 g was mixed with resin, let to dry, and then mounted in resin, polished and analysed by SEM. A small portion of the powder was pressed into pellets and analysed under the SEM.

The two techniques employed to prepare the known samples for the SEM represent an attempt to establish a routine for cross-check analysis without production of glass pellets, which would have been the best solution for SEM, but were not available for this study.

The results of the certified material checks for the SEM (Table 5.1) show:

- silica consistently shows an average concentration that is 5% higher than the expected value;
- alumina values are on average 5% lower than the expected value for the standards, with a concentration of alumina of 12 and 14%; however, for Glass C, where the concentration of alumina is lower than 1%, the variation increases to more than 20%;
- the average concentration of magnesia varies between 8 and 4%, lower than the expected value;
- the average concentration of soda varies between 15% and 10%, lower than the expected value;
- phosphorous oxide is too close to the detection limit;
- the average concentration of potash varies between 1 and 4%, higher than the expected limit;
- the average concentration of calcium oxide varies between 3% lower than the expected value and 1% higher than the expected value;
- the average values of titanium oxide are up to 6% higher than the expected value;
- manganese oxide was never detected;
- the average concentration of iron oxide is up to 18% higher than the expected value.

The Glass C reference was chosen for its BaO (11.40 wt%) and PbO (36.70 wt%) contents. The results of the area analyses show an average concentration of barium oxide 15% higher than the expected value, and an average concentration of lead oxide about 6% lower than the expected value.

The high variation of the results is due to the instability of the beam, as demonstrated by a standard deviation always higher than 0.05 and in the majority of the cases higher than 0.1. If we consider the average of 10 area analyses in order to decrease the effect of the instrumental instability, we observe that most of the oxides show a difference of less than 5% between measured and expected values, except for soda,

where we still note a difference of 12%, iron, where the difference is as high as 18% in two of the samples, and barium oxide, for which the difference is around 15%. This effect seems to be appreciable in the area analyses, while it is not detectable in the spot analyses performed on the mineral and glass phases. In fact, as observable in Table 5.7, the analyses of one of the olivine's crystals (performed in this case on a polyhedral olivine in sample RT25 L101 S5) show very good coincidence with the stoichiometric composition of olivine.

The variability of the SEM-EDS analyses in the different samples, as we can observe in Table 5.1 and Figure 5.6, suggests the impossibility to calculate accurate and reliable correction factors and use the values obtained as bulk analyses. The area analyses performed with SEM-EDS will then be used as relative values, only to describe the variation within the samples. The SEM-EDS analyses will be used as absolute numbers for what concerns the phase analyses, as complementary to XRD phase identification.

The two known samples analysed by SEM did not provide satisfactory results as compared to the standard materials analysed. For the pressed pellets, the concentration of calcium oxide, for instance, was around 10% lower than expected, while alumina was 10% higher, and the list of examples could continue. The results were even worse for the powder mounted in resin, where we observed an increased variation between the ten area analyses, as well as a variance from the expected value of 16% for calcium oxide, and even a 100% higher value for alumina in one of the samples, using these two oxides as examples. The SEM images of the known materials, both as pellets and mounted in resin, showed a poor mixing of the two different powders in the first case, even though when examined with the naked eye the material looked completely mixed. The powder mounted in resin was not dense enough to provide a homogeneous layer of material for analysis (Figs. 5.4 and 5.5). The two maps showed that the surface was not a homogeneous layer of material, but that it was full of empty spaces (Figs. 5.4 and 5.5). This method of producing samples for SEM is thus not convincing, and the best solution would have been using a glass pellet. Nevertheless, the results show that, when only powder is available, the best method for it to be analysed with SEM is to press it (with no wax), and have an average of at least 5 area analyses to obtain an acceptable result.

Several cross-checks were performed for the XRF. Firstly, two different methods were compared (Table 5.4) in order to identify the one that was more suitable to our

material. After this choice was made, the chosen method was re-checked at the beginning and at the end of the project (as already mentioned) in order to verify the consistency of the results after engineering work on the machine. The consistency and repeatability of the results are considered crucial as a basis for the publication of the results.

The two methods under consideration were Turbo Quant (Table 5.3 and Fig. 5.8), a method developed by Spectro and sold as a general quantitative method for oxides, and 'Slag Fun' (Table 5.2, and Fig. 5.7), a method developed at the UCL Institute of Archaeology purposely for the analyses of iron slag (Veldhuijzen 2003). The uncertainty between the two methods derived from the presence in conspicuous quantities (few percentages) of barium and lead oxide in the slag under consideration, and the possibility that these two compounds could have invalidated the entire analysis, mainly due to the fact that they are composed of heavy cations creating different matrix and absorption effects. Matrix and absorption effects represent the bases of a calibration method, and 'Slag Fun' calibration curves are based on concentrations of less than 1% for both barium and lead oxide.

For the XRF, the analyses of certified standard material (Table 5.6) showed that the values of the 5 or 3 runs carried out per sample were very constant, demonstrating the stability of the instrument (the standard deviation is always lower than 0.1, except for soda, where it is slightly higher than 0.1).

For the Turbo Quant method, the difference between measured and expected values was much higher as compared to the average of the areas resulting from the SEM analyses; this difference was, in fact, between 40 and 10% for all the compounds analysed (Table 5.3, Fig. 5.8).

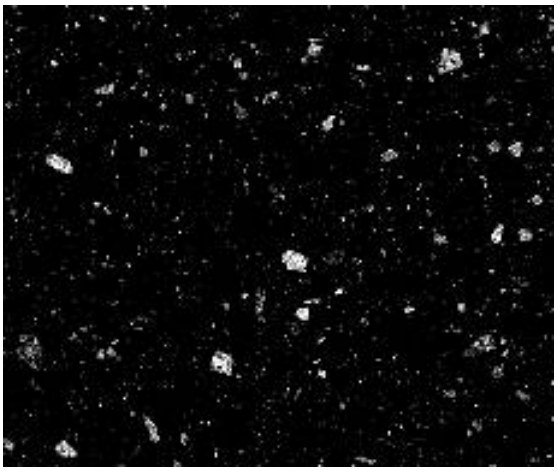

Figure 5.4 SEM map for iron (bright spots). The iron is only present in the certified material (BCS 301/2) mixed with lead oxide.

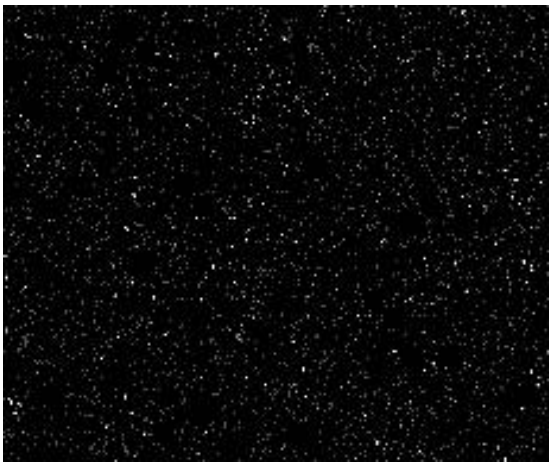

Figure 5.5 SEM map of the same area for lead in the known material BCS 301/1 plus 10% of PbO; the bright spots indicate lead oxide.

In contrast, Slag Fun shows very good consistency with the standards, with few percent errors noticeable between measured and expected values (Table 5.2 and Fig. 5.7). Since XRF is a calibration-based instrument and its calibration is very much linked to matrix and absorption, it is very important to focus mainly on the areas of interest (more similar to the unknown composition of the sample) and not to look at the entire composition range. This allows noting that the main oxides (SiO_2, Al_2O_3 and FeO) show very good correspondence between measured and expected values. These values can then be confidently used to estimate the temperature of the liquid during the process (smelting temperature) and its viscosity, as will be explained in detail in the following sections. The values measured for barium and lead oxide were cross-checked mainly with the known samples, since, as mentioned earlier, these concentrations were very low in the standard used for designing this method. More significant problems are found with respect to lead, which, being a very heavy cation, creates strong absorption effects. As we can observe in Table 5.5, the known samples used for the cross-check analyses were two standards, BCS 301/1 and BCS 381. These two known samples were formed by a mixture of different amounts of standard and lead oxide, the numbers following the standard identification name in Table 5.5: BCS 301/1 8.5-1.5 will have 8.5 g of the standard plus 1.5 g of lead oxide, BCS 381 5.5-4.5 will have 5.5 g of standard plus 4.5 g of lead oxide, and so forth. Unfortunately, the results obtained by this cross-check were highly unsatisfactory (Table 5.5), showing values at least one order of magnitude below the expected values. Table 5.5 also shows that a partial respect of the relative abundance is

maintained in the analyses performed by Slag Fun method, and for instance one sample (BCS 381, 5.5-4.5) is not even respecting this rule of thumb. This certainly indicates that Slag Fun is not adapt for analyses of high lead material. However, these cross-check samples have very high concentrations of lead oxide, and, as we can see in Figure 5.7, the calibration curve for XRF has a hyperbolic shape, but the method considers the calibration curve like a regression line. We can then infer that if the calibration curve is built with low values only, then for high values we will obtain a very strong underestimation, which is what is observed in these results. The attempt of creating a calibration curve for a large range of PbO concentration can then be considered vain, and only small segments of the curve can be obtained at the same time. By looking at Table 5.4, we can see that the values obtained for lead with the two different XRF methods are comparable, showing the correct relative relationship since the range of interest in the slag concerned by this study is still within the calibration curve of the methods. Moreover, as we can see in Table 5.3, the Turbo Quant method shows a 30% error from the expected value in the known sample. Combining these data leads us to think that the lead oxide value is not to be used as an absolute number. The lower value showed by the SEM-EDS analysis in the comparative Table 5.4 is due to the fact that lead is locally concentrated and highly variable in the samples. For the minor elements, and in particular for silver, there is no standard available for cross-checking the obtained results. Hence, as for barium and lead oxide, the measured values will be used only as relative comparison between the samples. When these values are used in the text, they should not be considered as absolute quantities, but as a simplification that allows discussing the enrichment and depletion linked to the efficiency of the process.
The verification of the Slag Fun method across the given time span presented above (Table 5.6) shows a satisfying concordance of the normalised results.

Overall, the three methods (SEM-EDS, XRF Turbo Quant, and XRF Slag Fun) show very different results for the collected data (Table 5.4). A decision was made to use the data from Slag Fun as bulk analyses, the data pertaining to the main compounds (SiO_2, Al_2O_3, FeO, alkali, MgO and MnO) as absolute values, while concentrations of PbO, Ba and Ag are used as comparative values only. Turbo Quant data will be dismissed. SEM-EDS data will be used only for the chemical characterisation of the crystalline and amorphous phases constituting the samples.

all compounds normalised	Na2O	MgO	Al2O3	SiO2	P2O5	K2O	CaO	TiO	MnO	FeO
BHVO 2 SEM	1.95	7.00	12.93	52.70	0.00	0.53	11.24	2.79	0.00	10.87
expected value	2.22	7.23	13.50	49.90	0.27	0.52	11.40	2.73	0.13	11.07
BCR 2 SEM	2.77	3.42	12.76	57.03	0.07	1.82	7.13	2.40	0.00	12.61
expected value	3.16	3.59	13.50	54.10	0.35	1.79	7.12	2.26	0.15	12.42
BIR 1 SEM	1.56	9.23	14.84	50.47	0.00	0.00	12.96	1.00	0.04	9.91
expected value	1.82	9.70	15.50	47.96	0.02	0.03	13.30	0.96	0.18	8.34

all compounds normalised	Na2O	MgO	Al2O3	SiO2	SO3	K2O	CaO	TiO	BaO	FeO
BHVO 2 + 10% BaSO4 pressed pellet	1.83	4.13	12.74	44.12	5.68	0.12	9.67	1.70	11.61	8.41
expected value	2.00	6.51	12.15	44.91	8.66	0.47	10.26	2.46	6.58	9.96

all compounds normalised	MgO	Al2O3	SiO2	SO3	K2O	CaO	As2O3	PbO	FeO	MnO
BCS 301/1 + 10% PbO pressed pellet	1.67	5.11	11.34	0.00	0.08	24.61	0.26	15.26	39.25	1.10
expected value	1.56	3.83	6.66	0.89	0.29	20.34	0.00	10.00	27.61	1.13

all compounds normalised	MgO	Al2O3	SiO2	CaO	TiO	BaO	FeO
BHVO 2 + 10% BaSO4 powder in resin	4.62	12.47	50.23	11.92	1.91	3.59	8.59
expected value	6.51	12.15	44.91	10.26	2.46	6.58	9.96

all compounds normalised	Al2O3	SiO2	CaO	PbO	FeO	MnO
BCS 301/1 + 10% PbO powder in resin	2.19	13.05	29.60	4.43	41.90	5.22
expected value	3.83	6.66	20.34	10.00	27.61	1.13

all compounds normalised	Na2O	MgO	Al2O3	SiO2	P2O5	K2O	CaO	TiO	FeO	CoO	CuO	ZnO	SrO	SnO2	Sb2O3	BaO	PbO
GLASS C	0.96	2.54	0.68	36.79	0.11	2.96	5.15	0.79	0.37	0.24	1.32	-0.07	0.47	0.12	-0.03	13.21	34.42
expected value	1.07	2.76	0.87	34.81	0.14	2.84	5.07	0.79	0.31	0.18	1.13	0.05	0.29	0.19	0.03	11.40	36.70

Table 5.1 Measured and expected values of Certified Reference Materials and prepared standards for the analyses performed with SEM-EDS.

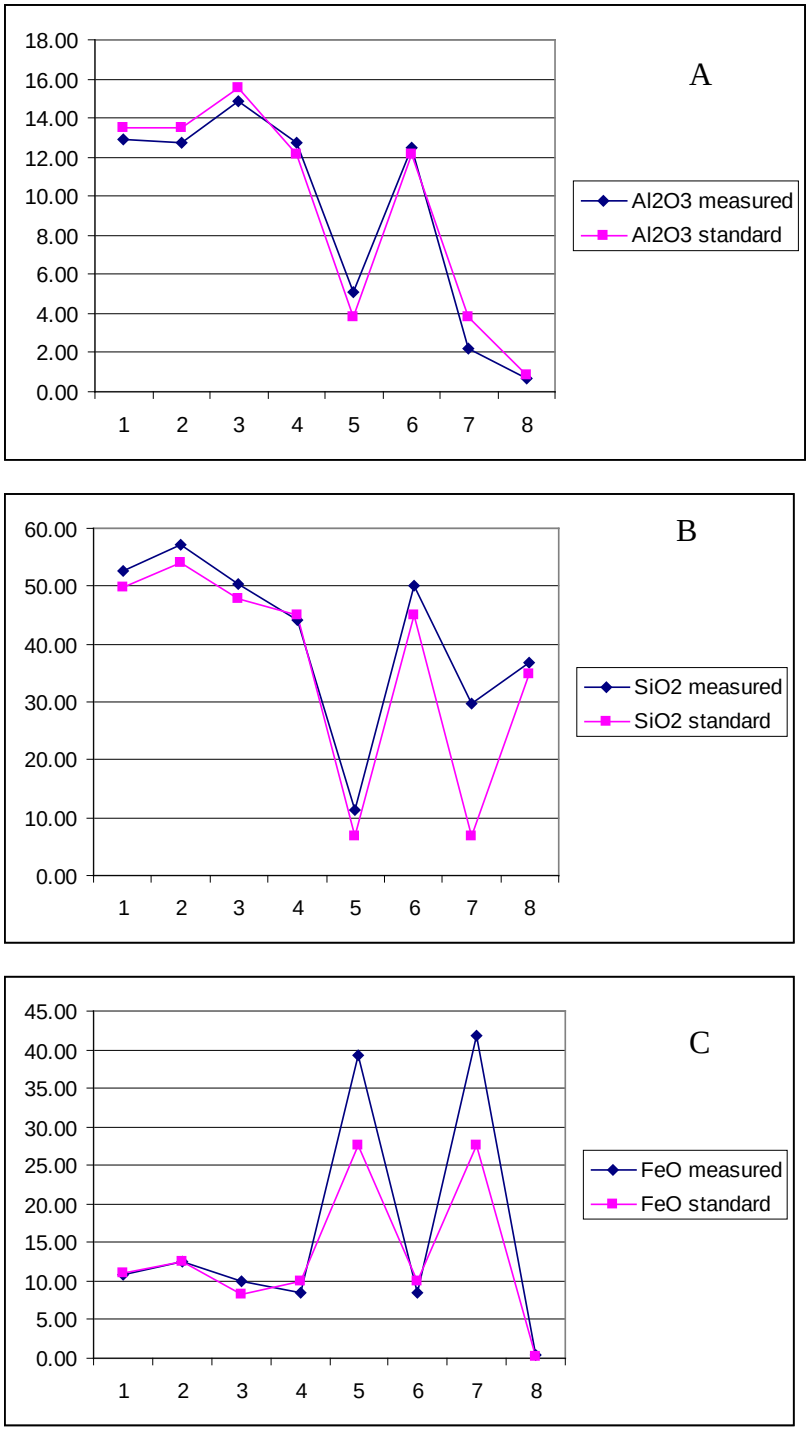

1) BHVO 2 SEM
2) BCR 2 SEM
3) BIR 1 SEM

4) BHVO 2 + 10% BaSO4 pressed pellet

5) BCS 301/1 + 10% PbO pressed pellet

6) BHVO 2 + 10% BaSO4 powder in resin

7) BCS 301/1 + 10% PbO powder in resin

8) GLASS C

Figure 5.6 Diagram presenting the behaviour of the values of the main compounds (A – alumina, B – silica, and C – iron oxide) measured by SEM-EDS in comparison with the expected values (standard values).

NORMALISED	Na2O	MgO	Al2O3	SiO2	P2O5	SO3	K2O	CaO	TiO2	V2O5	Cr2O3	MnO	FeO	SrO	Ba	PbO
	%	%	%	%	%	%	%	%	%	%	%	%	%	%	%	%
BCS 176/2	0.26	0.19	9.83	5.96	0.16	0.33	2.17	0.19	0.41	0.22	0.08	65.50	13.82	0.03	0.13	n.d.
expected values	0.14	0.05	6.48	3.15	0.11	0.05	1.62	0.11	0.37	0.00	0.00	76.42	11.00	0.00	0.21	0.01
BCS 309	0.73	0.34	59.65	34.28	0.15	0.11	0.54	0.24	1.96	0.04	0.07	0.02	1.61	0.00	0.00	0.00
expected values	0.34	0.17	61.27	34.20	0.00	0.00	0.46	0.22	1.93	0.00	0.00	0.03	1.36	0.00	0.01	0.00
BCS 381	0.92	n.d.	n.d.	7.93	16.09	0.69	0.05	51.55	0.25	0.89	0.35	2.96	18.23	0.04	0.02	n.d.
expected values	0.00	1.06	0.69	9.03	16.14	0.50	0.00	50.38	0.36	0.97	0.34	3.25	17.59	0.00	0.00	0.00
BCS RM 201a	7.20	0.07	22.84	58.46	n.d.	0.07	9.38	1.14	0.01	n.d.	n.d.	0.00	0.12	0.46	0.19	0.00
expected values	7.58	0.03	23.69	57.67	0.03	0.00	8.96	1.08	0.05	0.00	0.00	0.01	0.11	0.43	0.33	0.00
BCS-CRM 393	n.d.	0.14	n.d.	0.97	n.d.	0.05	0.02	98.69	n.d.	n.d.	n.d.	0.01	0.07	0.03	0.00	0.00
expected values	0.05	0.27	0.21	1.24	0.02	0.07	0.04	98.00	0.02	0.00	0.00	0.02	0.07	0.03	0.01	0.00
BCS-CRM375/1	7.81	0.39	18.49	69.32	0.06	0.11	2.04	0.99	0.28	n.d.	0.01	n.d.	0.39	0.02	0.00	0.01
expected values	8.96	0.18	18.02	69.77	0.23	0.00	1.48	0.79	0.31	0.00	0.00	0.00	0.26	0.00	0.00	0.00
BCS301	0.14	2.01	4.92	9.89	1.08	0.89	0.50	31.02	0.18	0.13	0.03	1.65	47.30	0.04	0.00	n.d.
expected values	0.10	2.50	6.15	10.69	0.51	1.45	0.46	32.65	0.23	0.00	0.00	1.81	44.32	0.00	0.00	0.00
BCS313/1	0.82	0.02	0.03	99.60	n.d.	0.07	n.d.	n.d.	0.01	n.d.	n.d.	n.d.	0.02	n.d.	n.d.	0.00
expected values	0.00	0.00	0.04	99.92	0.00	0.00	0.01	0.01	0.02	0.00	0.00	0.00	0.01	0.00	0.00	0.00
CCRM SL1	0.28	12.98	7.58	32.41	n.d.	4.16	0.64	39.83	0.30	n.d.	0.01	0.85	0.92	0.06	0.05	0.00
expected values	0.39	12.34	9.68	35.93	0.02	3.17	0.51	37.69	0.38	0.00	0.00	0.86	0.93	0.00	0.00	0.00
CaSO4	0.63	n.d.	n.d.	n.d.	n.d.	62.01	n.d.	37.21	n.d.	n.d.	n.d.	n.d.	n.d.	0.14	n.d.	0.00
expected values	n.d.	n.d.	n.d.	n.d.	n.d.	58.81	n.d.	41.19	n.d.	n.d.	n.d.	n.d.	n.d.	n.d.	n.d.	n.d.
ECRM 676-1	0.34	1.47	4.72	14.43	1.58	0.56	0.58	19.63	0.24	0.10	0.04	1.08	54.88	0.05	0.00	n.d.
expected values	0.13	2.03	6.77	14.43	1.42	0.80	0.55	18.84	0.33	0.13	0.00	1.13	53.91	0.00	0.00	0.00
ECRM 682-1	0.17	0.09	0.61	1.16	0.13	0.09	0.00	0.02	0.04	0.00	0.02	0.35	97.25	n.d.	n.d.	n.d.
expected values	0.01	0.03	0.43	0.54	0.09	0.02	0.01	0.02	0.06	0.00	0.00	0.30	98.50	0.00	0.00	0.00
ECRM 776-1	0.88	0.70	29.69	61.74	n.d.	0.04	3.23	0.33	1.62	0.01	0.03	0.00	1.49	0.02	0.06	0.01
expected values	0.49	0.48	29.47	63.16	0.06	0.00	2.94	0.31	1.63	0.00	0.02	0.00	1.29	0.00	0.11	0.00
ECRM681-1	0.31	1.51	13.66	20.99	2.67	0.36	0.69	4.71	0.51	0.17	0.09	0.35	53.52	0.15	0.01	n.d.
expected values	0.11	1.83	13.19	22.11	2.50	0.80	0.73	4.87	0.60	0.17	0.07	0.35	53.07	0.00	0.00	0.01
FER-1	0.72	0.40	0.45	23.90	5.23	0.72	0.01	4.37	0.00	0.00	0.01	0.25	62.77	0.01	0.05	0.54
expected values	0.03	0.32	0.56	18.60	2.56	0.70	0.02	3.53	0.03	0.00	0.00	0.24	73.10	0.00	0.10	0.60
FER-2	0.63	2.91	5.12	51.49	0.36	0.42	1.66	2.38	0.17	n.d.	0.02	0.13	34.60	0.01	0.01	n.d.
expected values	0.53	2.17	5.33	50.87	0.28	0.45	1.37	2.24	0.19	0.00	0.00	0.12	36.96	0.00	0.02	0.00
FER-4	0.38	2.31	2.40	54.27	0.08	0.27	0.39	3.08	0.04	n.d.	0.00	0.23	36.47	0.01	n.d.	n.d.
expected values	0.05	1.53	1.84	54.29	0.14	0.30	0.31	2.42	0.08	0.00	0.00	0.21	39.00	0.00	0.00	0.00
MnO2	0.16	n.d.	n.d.	0.49	n.d.	0.69	0.90	n.d.	n.d.	0.07	0.09	97.71	n.d.	n.d.	n.d.	n.d.
expected values	n.d.	n.d.	n.d.	n.d.	n.d.	n.d.	n.d.	n.d.	n.d.	n.d.	n.d.	81.62	n.d.	n.d.	n.d.	n.d.
NIST 76a	0.65	0.90	38.62	54.18	0.06	0.06	1.48	0.22	2.08	0.03	0.05	0.01	1.65	0.04	0.01	0.01
expected values	0.07	0.53	39.74	56.38	0.12	0.00	1.37	0.23	2.04	0.00	0.00	0.00	1.48	0.04	0.00	0.00
PbO	0.54	32.44	n.d.	1.39	n.d.	n.d.	0.05	n.d.	n.d.	n.d.	n.d.	n.d.	0.09	0.03	n.d.	61.54
expected values	n.d.	n.d.	n.d.	n.d.	n.d.	n.d.	n.d.	n.d.	n.d.	n.d.	n.d.	n.d.	n.d.	n.d.	n.d.	100.00
QLO 1	3.74	0.64	16.11	66.96	0.09	0.15	3.87	3.39	0.55	n.d.	n.d.	0.09	4.20	0.04	0.09	0.00
expected values	4.25	1.01	16.41	66.46	0.25	0.00	3.65	3.21	0.63	0.00	0.00	0.00	3.94	0.03	0.13	0.00
SARM 17	n.d.	5.23	n.d.	4.85	n.d.	0.11	0.19	25.73	n.d.	0.02	0.04	56.14	7.59	0.03	0.05	n.d.
expected values	0.14	4.75	0.38	7.36	n.d.	n.d.	0.14	n.d.	n.d.	n.d.	n.d.	78.61	8.62	n.d.	n.d.	n.d.
SCH 1	0.14	0.04	1.24	9.18	0.10	0.11	0.03	0.04	0.04	n.d.	0.01	0.88	88.12	n.d.	n.d.	n.d.
expected values	0.03	0.04	1.09	9.14	0.14	0.00	0.04	0.05	0.06	0.00	0.00	1.13	88.29	0.00	0.00	0.00
SO-1	2.57	5.00	17.50	57.72	0.02	0.16	3.67	2.82	0.87	0.00	0.03	0.13	9.27	0.05	0.06	0.00
expected values	2.72	4.07	18.84	58.54	0.15	0.00	3.43	2.68	0.93	0.00	0.00	0.12	8.20	0.32	0.00	0.00
SO-4	0.93	1.69	13.46	81.18	0.26	9.68	2.78	2.23	0.61	n.d.	0.01	0.10	4.12	0.03	0.05	0.07
expected values	1.52	1.03	11.65	77.27	0.24	0.00	2.34	1.74	0.62	0.01	0.01	0.09	3.44	0.02	n.d.	0.00
SRM-25d	0.16	n.d.	n.d.	0.28	0.47	0.08	0.36	0.09	98.52	n.d.	n.d.	n.d.	n.d.	n.d.	n.d.	0.00
expected values	n.d.	n.d.	n.d.	n.d.	n.d.	n.d.	n.d.	n.d.	100.00	n.d.	n.d.	n.d.	n.d.	n.d.	n.d.	n.d.
TiO2	0.16	n.d.	n.d.	0.28	0.47	0.08	0.36	0.09	98.52	n.d.	n.d.	n.d.	n.d.	n.d.	n.d.	0.00
expected values	n.d.	n.d.	n.d.	n.d.	n.d.	n.d.	n.d.	n.d.	100.00	n.d.	n.d.	n.d.	n.d.	n.d.	n.d.	n.d.
USGS BHVO-2	2.16	6.46	14.50	48.04	0.09	0.15	0.56	12.57	2.71	0.02	0.04	0.17	12.35	0.05	0.01	n.d.
expected values	2.24	7.30	13.62	50.36	0.27	0.00	0.52	11.50	2.76	0.03	0.03	0.13	11.17	0.04	0.01	0.00
USGS GSP-2	2.69	1.17	14.71	66.97	0.22	0.18	6.00	2.27	0.56	n.d.	0.01	0.04	4.81	0.03	0.07	0.01
expected values	2.83	0.98	15.16	67.75	0.30	0.00	5.47	2.14	0.67	0.01	0.00	0.03	4.49	0.02	0.13	0.00
USGS Nod-A-1	1.38	6.95	4.13	5.08	1.58	1.80	0.90	21.13	0.60	0.20	0.04	31.55	21.94	0.26	0.15	0.15
expected values	1.41	6.71	5.46	5.37	1.97	0.00	0.85	21.71	0.75	0.11	0.00	33.70	19.79	0.25	0.21	0.12
ZnO RM	n.d.	n.d.	n.d.	0.74	n.d.	0.16	n.d.	n.d.	n.d.	n.d.	n.d.	n.d.	0.23	n.d.	n.d.	n.d.
expected values	n.d.	n.d.	n.d.	n.d.	n.d.	n.d.	n.d.	n.d.	n.d.	n.d.	n.d.	n.d.	n.d.	n.d.	n.d.	n.d.
Swedish slag	0.99	0.32	6.27	22.86	0.12	0.42	1.14	1.49	0.24	0.01	0.02	2.84	63.08	0.01	0.05	n.d.
expected values	0.63	0.39	7.41	25.67	0.27	0.10	1.06	1.47	0.33	0.02	0.01	3.12	59.27	0.00	0.07	0.00

Table 5.2 Measured and expected values of Certified Reference Materials and prepared standards for the analyses performed by XRF according to the Slag Fun method.

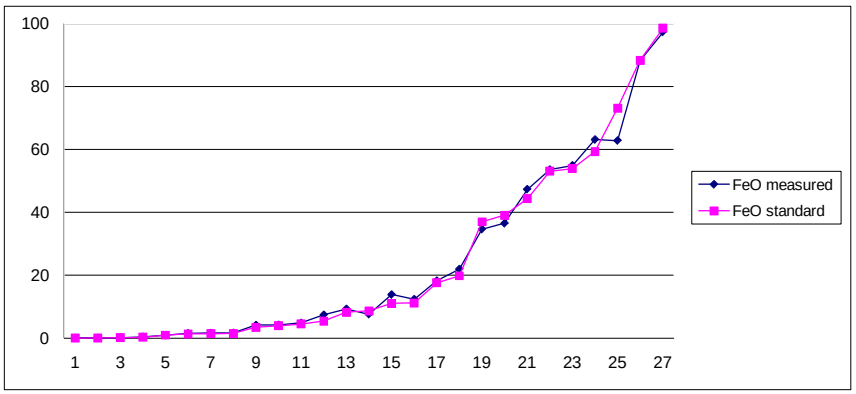

A

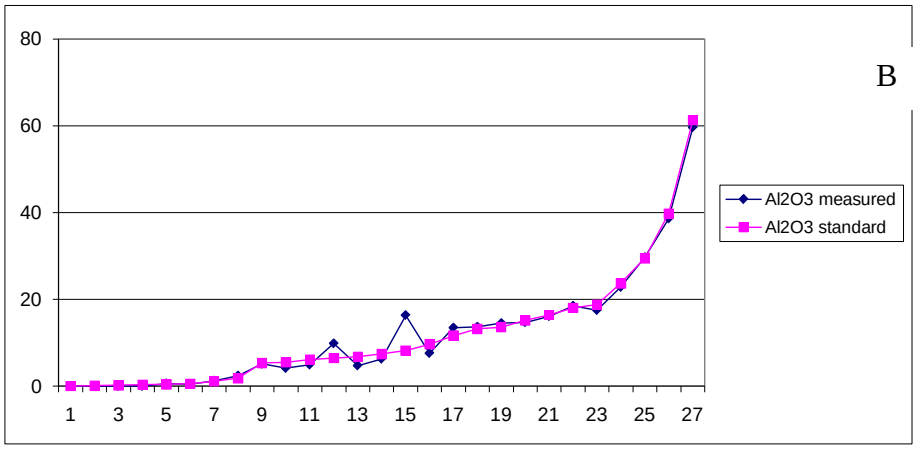

B

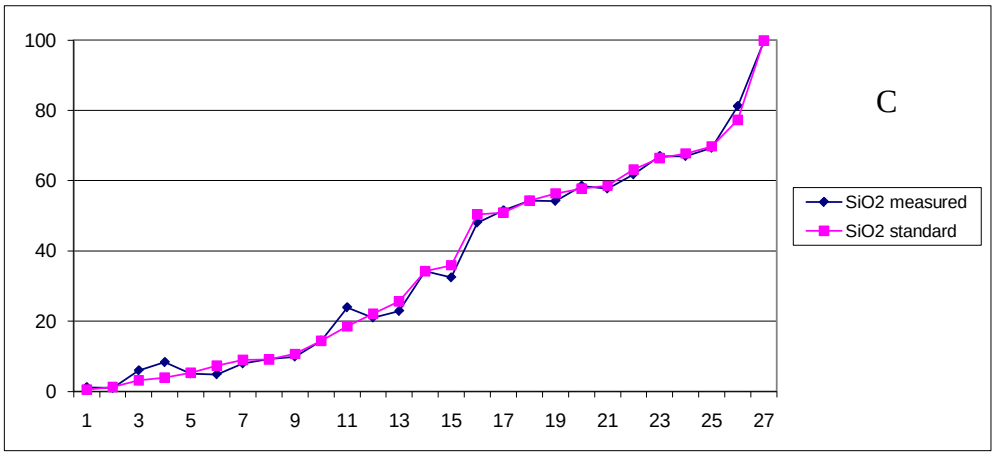

C

Figure 5.7 Diagrams presenting the results for the main compounds (A – iron oxide, B – alumina, and C – silica) measured by XRF using the Slag Fun calibration method, in comparison with the expected values (standard). The x axis is given only as a growing number, since it is preferable to show the calibration curve in relationship with the increase in concentration in order to render the differences in calibration at different concentrations more clearly visible.

Element	Na2O	MgO	Al2O3	SiO2	P2O5	SO3	K2O	CaO	TiO2	V2O5	Cr2O3	MnO	FeO	SrO	Ba	PbO
Dimension	%	%	%	%	%	%	%	%	%	%	%	%	%	%	%	%
1) BCS301/1 10PbO	0.13	0.84	5.85	10.1	0.54	n.d.	0.26	25.86	0.18	0.11	0.02	1.47	19.08	0.02	0.00	8.02
expected value		2.17	5.33	9.27	0.45		0.40	28.30	0.19			1.57	34.53			11.97
2) BHVO2 10BaSO4	2.68	4.50	14.79	44.93	0.16	3.79	0.41	9.14	2.17	n.d.	n.d.	0.22	10.99	0.18	4.74	0.00
expected value	1.91	6.22	11.95	42.90	0.23	8.27	0.45	9.80	2.35			0.11	8.54		6.29	0.00
3) BHVO 2	2.29	4.83	16.49	48.81	0.19	n.d.	0.47	10.38	2.14	0.05	0.04	0.19	12.54	0.05	0.01	n.d

Table 5.3 Measured and expected values of known samples obtained with Turbo Quant.

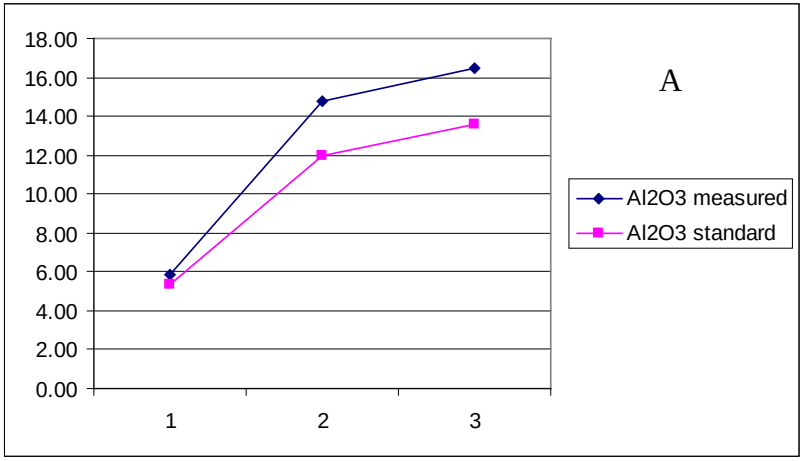

1) BCS301/1 10PbO

2) BHVO2 10BaSO4

3) BHVO 2

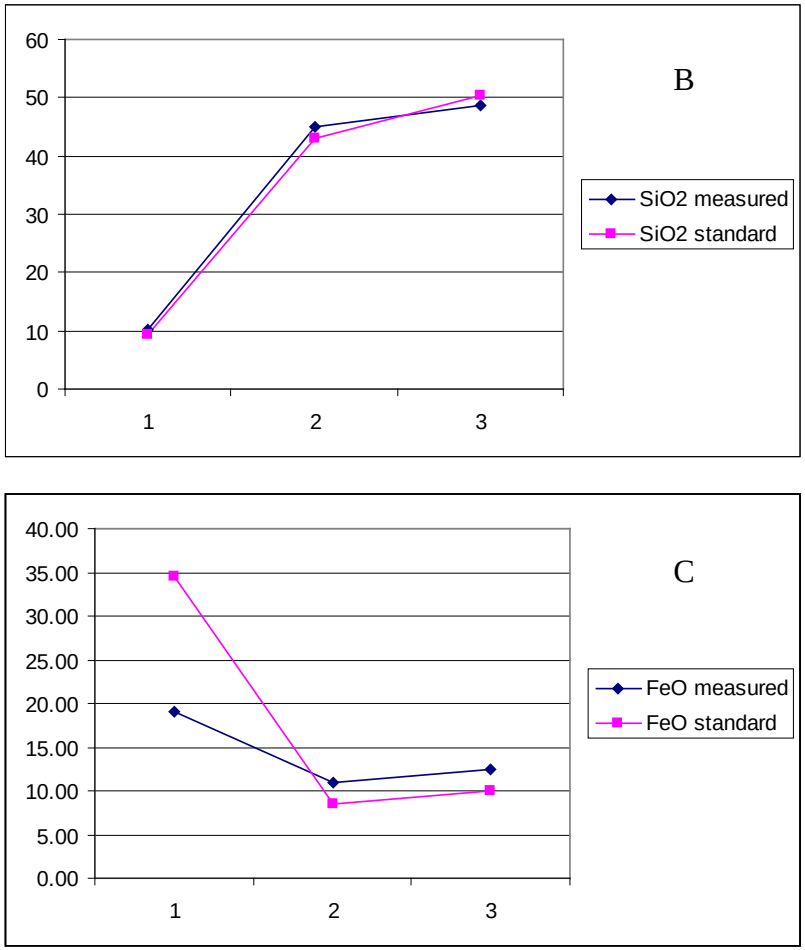

Figure 5.8 Diagram presenting the variance between measured and expected values for the main compounds (A – alumina, B – silica, and C – iron oxide) using the Turbo Quant method.

	RT16		
	SEM	**Slag Fun**	**Turbo Quant**
MgO	0.49	0.66	3.32
Al_2O_3	6.78	5.84	4.12
SiO_2	39.69	31.28	23.15
P_2O_5	0.39	0.35	0.26
SO_3	0.94	0.52	0.49
K_2O	1.35	1.11	1.18
CaO	4.67	2.95	3.67
TiO_2	0.46	0.52	0.3
FeO	39.41	48.63	52.99
CuO	0.12	0.46	0.55
As_2O_3	0.08	1.25	0.75
BaO	4.63	3.06	5.33
PbO	0.76	3.35	4.21

Table 5.4. Comparative table showing the results obtained by the three methods (SEM, Slag Fun and Turbo Quant) for sample RT25 L101 S16 (randomly chosen). In the SEM analysis, the overestimation of SiO_2 over the underestimation of FeO, critical in the determination of the smelting temperature, is noticeable.

	PbO	expected value
	%	%
BCS301-1, 8.5-1.5	5.38	15.00
BCS381, 4.5-5.5	16.58	55.00
BCS381, 5.5-4.5	1.80	45.00
BCS381, 7-3	2.31	30.00
BCS381, 8-2	2.16	20.00
BCS381_30PbO	3.06	30.00

Table 5.5 Lead oxide concentration in known samples. The numbers following the standard identification name indicate the amount of standard and the amount of lead oxide (in grams) used to produce the known sample mixture, explicated in the expected value.

	date	method	Na2O %	MgO %	Al2O3 %	SiO2 %	P2O5 %	SO3 %	K2O %	CaO %	TiO2 %	V2O5 %	Cr2O3 %	MnO %	FeO %
RT 5 FUN	29/01/2006	Slag Fun	0.36	1.35	3.74	18.02	0.22	3.30	1.01	2.88	0.29	0.03	0.01	0.09	49.66
RT 5 FUN_r01	29/01/2006	Slag Fun	0.41	1.33	3.61	17.74	0.23	3.31	0.99	2.86	0.29	0.03	0.01	0.09	48.86
RT 5 FUN_r02	29/01/2006	Slag Fun	0.32	1.36	3.71	17.89	0.22	3.37	1.00	2.89	0.30	0.03	0.01	0.09	49.71
RT 5 FUN_r03	29/01/2006	Slag Fun	0.44	1.34	3.66	17.86	0.21	3.38	0.99	2.87	0.30	0.03	0.01	0.09	48.50
RT 5 FUN_r04	29/01/2006	Slag Fun	0.21	1.44	3.78	18.26	0.32	3.48	1.03	2.96	0.30	0.03	0.02	0.10	51.08
average			0.35	1.36	3.70	17.95	0.24	3.37	1.00	2.89	0.30	0.03	0.01	0.09	49.56
normalised			0.39	1.55	4.19	20.35	0.27	3.81	1.14	3.28	0.34	0.03	0.02	0.11	56.19
RT 5	09/02/2010	Slag Fun	0.25	2.11	5.75	36.32	0.49	5.46	1.62	4.61	0.44	0.04	0.03	0.16	76.87
RT 5_r01	09/02/2010	Slag Fun	0.22	2.01	5.65	36.33	0.33	5.37	1.61	4.65	0.38	0.02	0.03	0.16	77.11
RT 5_r02	09/02/2010	Slag Fun	0.36	1.98	5.74	36.57	0.47	5.49	1.61	4.65	0.39	0.02	0.03	0.16	76.92
average			0.28	2.03	5.71	36.41	0.43	5.44	1.61	4.63	0.41	0.03	0.03	0.16	76.97
normalised			0.19	1.37	3.85	24.55	0.29	3.67	1.09	3.12	0.27	0.02	0.02	0.11	51.91

	date	method	Co3O4 %	CuO %	ZnO %	As2O3 %	SrO %	ZrO2 %	Mo %	Ag %	SnO2 %	Sb %	Ba %	PbO %	Sum %
RT 5 FUN	29/01/2006	Slag Fun	0.04	0.17	0.03	0.26	0.02	0.03	0.02	0.02	0.16	0.10	4.81	1.64	88.34
RT 5 FUN_r01	29/01/2006	Slag Fun	0.06	0.16	0.03	0.24	0.02	0.03	0.02	0.02	0.15	0.09	4.73	1.61	87.00
RT 5 FUN_r02	29/01/2006	Slag Fun	0.05	0.17	0.03	0.23	0.02	0.03	0.01	0.02	0.16	0.09	4.84	1.65	88.31
RT 5 FUN_r03	29/01/2006	Slag Fun	0.04	0.16	0.03	0.24	0.02	0.04	0.02	0.02	0.15	0.09	4.64	1.60	86.81
RT 5 FUN_r04	29/01/2006	Slag Fun	0.05	0.17	0.03	0.26	0.02	0.03	0.02	0.02	0.16	0.09	4.95	1.69	90.59
average			0.05	0.17	0.03	0.25	0.02	0.03	0.02	0.02	0.16	0.09	4.79	1.64	88.21
normalised			0.06	0.19	0.04	0.28	0.02	0.04	0.02	0.02	0.18	0.11	5.44	1.86	100.00
RT 5	09/02/2010	Slag Fun	0.05	0.24	0.05	0.34	0.03	0.08	0.03	0.03	0.41	0.17	9.98	2.55	148.27
RT 5_r01	09/02/2010	Slag Fun	0.08	0.24	0.05	0.35	0.03	0.08	0.03	0.03	0.41	0.17	9.96	2.56	148.05
RT 5_r02	09/02/2010	Slag Fun	0.11	0.24	0.05	0.34	0.03	0.07	0.04	0.03	0.41	0.17	9.88	2.58	148.49
average			0.08	0.24	0.05	0.35	0.03	0.07	0.04	0.03	0.41	0.17	9.94	2.56	148.27
normalised			0.05	0.16	0.03	0.23	0.02	0.05	0.02	0.02	0.27	0.11	6.70	1.73	100.00

Table 5.6 Comparative table showing results of XRF analyses using the Slag Fun method at two different times during the project. The sum is visibly different between the two methods.

Element	Line	App. Conc	k ratio	Intensity corrn.	Weight%	Weight% sigma	Atomic%	Compound	Formula
Mg	K_SERIES	0.36	0.00245	0.4751	0.74	0.09	0.87	1.23	MgO
Si	K_SERIES	10.25	0.0827	0.7232	13.94	0.15	14.27	29.83	SiO2
Ca	K_SERIES	1.07	0.00961	1.0584	0.99	0.06	0.71	1.39	CaO
Fe	K_SERIES	48.27	0.48273	0.9041	52.51	0.25	27.01	67.55	FeO
O					31.81	0.23	57.13		
Total					100				

Table 5.7 Results of an SEM-EDS analysis of an one olivine crystal randomly taken. The atomic concentration shows how close to the stoichiometry of olivine the analysis is.

5.1.7. Multi Collector Inductively Coupled Plasma Mass Spectrometry (MC-ICP-MS)

For the Inductively Coupled Plasma technique, the sample is brought into solution, which is then injected into a stream of argon gas in order to form an aerosol. A radio frequency coil is then used to heat the aerosol to 6000 °C. Due to the high temperature, the sample becomes plasma, defined as a gas in which some or all of the electrons are separated from their nuclei. The aerosol is then ionised and accelerated, due to an electric field difference. The ionised plasma moves through a curved magnetic field where the ions are separated depending on their mass and collected in different collectors (Thirlwall 2003, 258).

In total, 46 samples from Corta Lago, 2 from Tharsis and 1 from Lavrion were analysed by MC-ICP-MS for their lead isotope signatures. The samples from Lavrion and Tharsis were all slags, while the samples from Corta Lago included slag, litharge, ores and ingots. The following samples from Corta Lago were chosen: 3 ball slags, 5 Phoenician tapped slags, 2 Ibero-Punic tapped slags, 9 Republican tapped slags from the first period, 8 Republican Plate slags from the middle period, 2 Republican tapped slags from the last period, 5 Imperial tapped slags, 3 ingots and 9 samples of semi-reacted ores. The samples were prepared following the procedure described in Appendix 2 (section 2.1.).

The instrument used was the Multi Collector Inductively Coupled Plasma Mass Spectrometer at Royal Holloway, University of London. This MC-ICP-MS uses a hexapole collision cell flushed with argon to reduce the energy spread of ions produced in the plasma torch, instead of using an electrostatic analyser to focus the ion beam into the multi-collector array.

The samples were analysed for lead isotopes, measuring ^{204}Pb, ^{206}Pb, ^{207}Pb and ^{208}Pb. Lead has only one non-radiogenic isotope (^{204}Pb), so there is no ratio for which a constant natural value can be assumed to allow correction of all other measured isotope ratios for the observed mass bias during analysis. Since the mass bias of an element is similar to that of another with similar atomic number (Thirlwall 2003, 256), thallium, with isotopes ^{203}Tl and ^{205}Tl, has been used to correct the Pb mass bias in the first run of the samples (Thirlwall 2003, 256; Müller et al. 2003).

Some of the samples were run again with an external double Pb spike normalisation, because this method is more precise than the one involving the addition of thallium for verifying the quality of the results. The cross-check of the methods provided satisfactory results also for the sample corrected with thallium only. The error was very low, of the order of $5e^{-4}$.

Isotopes of mercury were collected at the same time, because ^{204}Hg is isobar with ^{204}Pb and mercury is present in most of the oils used in the machine, and thus it needs to be subtracted.

The sequence used during the analysis was: a blank to calculate the background, then the sample for which the result of the background was subtracted, and then a lead-free washing solution run until the signal of ^{208}Pb was around zero. Every five samples, a standard (SRM981) was measured.

5.1.8. Lead isotopes and their use in archaeometallurgy

A stable atom of any element is fundamentally composed of two parts: the nucleus, formed by protons and neutrons, where the mass of the atom itself is concentrated, and electrons. The elemental identity of the atom is defined by its number of protons, given as the atomic number, and the variable number of neutrons, the neutronic number. Together, these two values determine the atomic mass. There are many elements that present stable atoms with different masses; in the case of lead, they are ^{204}Pb, ^{206}Pb, ^{207}Pb and ^{208}Pb. These are called isotopes: atoms which have the same atomic number but a different mass, due to the fact that their nuclei contain a different number of neutrons.

Of the stable lead isotopes, only ^{204}Pb is non-radiogenic, and the quantity of this isotope has been the same since the formation of the Earth. The other three stable lead isotopes, ^{206}Pb, ^{207}Pb and ^{208}Pb, are of a radiogenic origin. They are the final stable product of the radiogenic decay of the radioactive isotopes ^{238}U, ^{235}U and ^{232}Th, respectively (Hamilton 1965, 174-175; Russel and Farquhar 1960, 2-3). The lead found on Earth today is a mixture of the lead present when the Earth was formed (or 'primeval lead') and the lead produced since then by radioactive decay of uranium and thorium (or 'radiogenic lead'). The overall concentrations of these isotopes increase with time due to the ongoing decay of uranium and thorium. As a

result, the ratios between the various lead isotopes changes continuously over geological time.

At the formation of a mineral deposit, common lead would be composed of the above-mentioned mixture in the proportions prevailing at the time. The formation process of the deposit would thus have drawn from a given isotopic ratio, which would reflect the moment of the formation of the deposit itself.

With regard to artificial processes, the isotopic ratios do not change during the different transformations to which an ore is subjected (smelting, refining, etc.), during its conversion into a final object, whether lead is the main component or only present at trace level, as has been demonstrated empirically (Gale 1989, 476-477; Pernicka et al. 1990, 269). Thus, the lead isotope composition does not depend on the distribution of lead in the different phases of the sample, because lead isotopes do not fractionate. As a result, even if the presence of lead is of different orders of magnitude in different parts of the object, its isotopic composition will remain the same.

The analysis of the isotope compositions of the slags in this project is used to trace an isotope path in the remains, and to verify the possibility of the addition of material (containing lead metal) from different sources, then to attempt the identification of the sources themselves and verify any possible changes of sources through time.

5.1.9. Preparation of the samples as powders

Three of the analytical techniques required a powdered specimen: X-Ray Diffraction, X-Ray Fluorescence and Inductively Coupled Plasma Mass Spectrometry. For these, the selected sub-sample was crushed, and then ground in a planetary mill equipped with agate pots and balls into a fine powder. The use of agate instead of tungsten carbide equipment was necessary because part of the powder was destined for isotopic analysis.

From the prepared powder, around 1 g was taken for XRD analysis. This powder was then placed in a steel ring-shaped container, taking care to produce a completely flat surface, and then introduced into the machine.

For XRF analysis, 8 g of powder (Fig. 5.9) were accurately weighed and carefully mixed with 0.9 g of wax. The mixture was then placed in an aluminium dish, and pressed into a tablet using a weight of approximately 15 tonnes in a mechanical press. The pellets (Fig. 5.9) produced were then introduced into the machine.

Figure 5.9 Powder and pellets for the XRF.

The samples for the ICP-MS required a further process in order for the powder to be dissolved in solution. The powder was treated with HNO_3, HF and HCl alternatively and in different concentrations, with subsequent cycles of heating and evaporating, to destroy all chemical bonds and obtain an ionic solution (see Appendix 2). The solution obtained was then passed through a specific ion-exchange resin in order to keep only the lead in solution. This final lead solution was then diluted to 50 ppb and used for the analysis. The sample preparation process is comprehensively described in Appendix 2 of this thesis.

5.1.10. Preparations of the samples as mounted polished sections

Two analytical techniques require a mounted polished section: Optical Microscopy and Scanning Electron Microscopy.

For X-ray analysis and BSE imaging it is extremely desirable to avoid topographic effects: specimens should therefore be flat and well polished (Reed 1996, 179). The samples were placed, with their own labels, in plastic moulds (Fig. 5.10), where they

were embedded in resin. The resin was a two component cold-setting epoxy resin (four parts resin and one part hardener). The samples thus mounted were then left to cure over night for the resin to achieve maximum hardness (Fig. 5.11). They were then ground with wet silicon carbide paper, on rotary wheels, with progressively finer grit size to a minimum of ≈ 4 μm, sufficient for the observation of the mineralogical structure and texture considering the size and the hardness of the grains. At this point the samples were washed with IMS (Industrial Methylated Spirit) and then dried.

These prepared samples were then ready for the Optical Microscope. For the Scanning Electron Microscope, the samples need to be carbon coated because the instrument needs a conductive surface when used in high vacuum, as was decided for this project.

Figure 5.10 Samples in the cups embedded with resin.

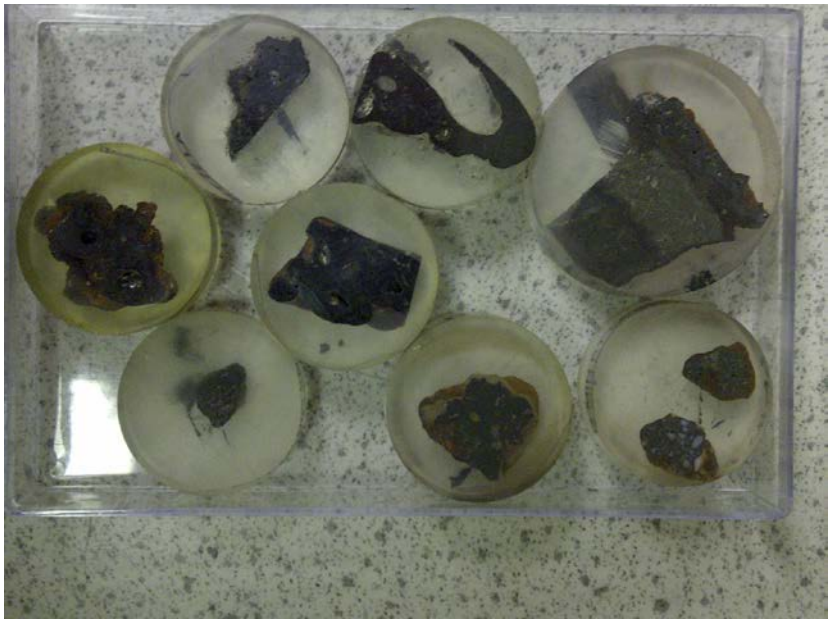

Figure 5.11 Mounted samples polished and ready for OM and SEM analysis.

Having described the preparation of the samples and the analytical techniques used to analyse them, the following sections provide the results obtained and their interpretation.

5.2 Interpretative methods

5.2.1 Olivine cooling rate

Some mineral morphology can be used as a tool to estimate the cooling rates of the melt; in particular, "olivine morphology changes systematically as a function of the degree of melt super cooling rate and of the normative olivine and water contents of the melt" (Donaldson 1976, 188). The mineralogical association of the slags under consideration in this thesis, regardless of the typology they belong to, is dominated by fayalite (Fe_2SiO_4). Fayalite is a simple silicate (nesosilicate, the simplest way to concatenate the SiO_4^{-2} tetrahedron with cations, normally Fe, Mg and Mn) which crystallises at a moderately high temperature (~ 1200 ºC for the pure iron end member). The morphology of the fayalite crystal depends greatly on the cooling temperature of the liquid mass, and, following Donaldson (1976, 188, 189), the different morphologies can be divided into 6 groups (Fig. 5.12):

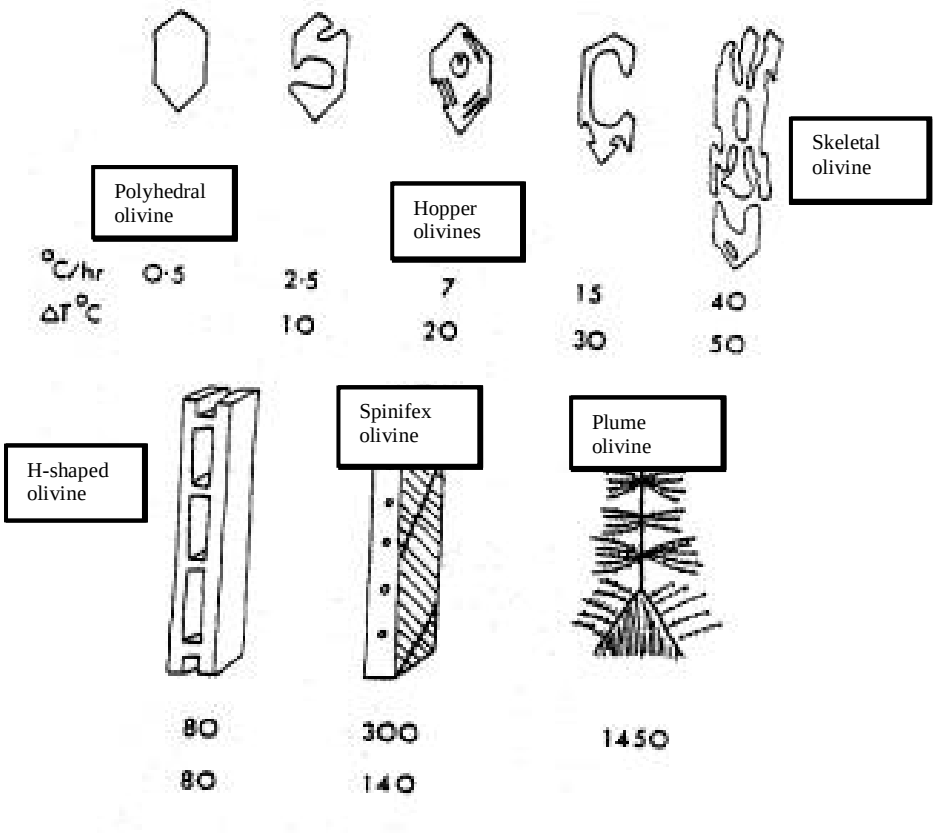

Figure 5.12 Schematic summary of Donaldson's (1976) olivine morphology groups and relative cooling speed.

- Polyhedral: the cooling speed is slow enough (0.5 ºC/h) to allow the olivine to crystallise with its fully formed habit;

- Hopper: the temperature decrease is slow, but not enough to complete the polyhedral shape. The result is a polyhedral ghost shape with some 'missing' parts. The quantity of 'missing' parts is linked to the cooling speed: thus, if only some external parts are missing, the cooling rate would be in the range of 2.5-10 ºC/h; if part of the core also begins to be missing, then the range is between 7 and 20 ºC/h, and if almost all the core is missing, leaving only the polyhedral shape, then the range of cooling speed would be in the range of 15-30 ºC/h. This last morphological type is the intermediate step between the hopper morphology and the skeletal one.

- Skeletal: this morphology looks like a chain of polyhedral olivines with their cores missing, and not yet separating into proper polyhedral crystals. The

cooling speed at which they are generated, still quoting Donaldson (1976, 189), is 40-50 ºC/h.

- H-shaped: this morphology consists of an acicular shape where the crystallisation occurred along the edges and at regular intervals between them, as a link, forming several H shapes, one on top of the other. This is a very poor crystalline structure that forms quickly, at the specific rate of 80 ºC/h (Donaldson 1976, 189).

- Spinifex: this texture indicates a very quick crystallisation (140-300 ºC/h) and it consists of a very fine, preferentially oriented group of crystals forming at the same time. They form perpendicular to the cooling surface, and hence they provide an indication of that surface.

- Plume: consist of even finer aciculae, all connected to each other, forming a plume-like shape. This morphology crystallises at quenching conditions and is mainly observable in the slags studied in this thesis as second generation fayalite, formed at the end of the cooling of the slag from the residual interstitial liquid.

In the following sections, the morphology of the olivines will be identified as polyhedral, hopper, skeletal, H-shaped, spinifex and plume without any further explanation.

The cooling rates reported above (Donaldson 1976) are the results of statistical studies of rapidly crystallised rocks of the basalt-picrite-peridotite family, including submarine lavas, lunar mare basalts, minor mafic and ultramafic intrusions, ‘spinifex’ ultramafic lavas, meteorite chondrules, and rapidly crystallised skeletal and dendritic olivines in crescumulate (or comb-layered) rocks from layered plutons. The studies were associated to laboratory experiments involving melts of mafic and ultramafic rocks: two peridotites, one olivine eucrite, two ocean ridge tholeiites and three lunar mare basalts. The materials just described, employed in Donaldson’s experiments, are much richer in MgO (between 7 and 22%; Donaldson 1976, 196) as compared to the materials studied in the context of this project (MgO between 0.3 and 1.5%). These parameters, considering the entire bulk chemistry of the system, surely influence the cooling rate, as already stated by Donaldson and reported above (“olivine morphology changes systematically as a function of the degree of melt

super cooling rate and of the normative olivine and water contents of the melt"), and emphasised by Ettler et al. (2009, 1005). Ettler and co-authors also draw attention to the fact that "smelting slags are generally cooled more rapidly than large lava flows" (Ettler et al, 2009, 1005). This statement is obviously acceptable for what concerns Donaldson's observations of natural rock formations. However, his experiments, where a low amount of material was cooled or super cooled, indicate the reaction of a small amount of melt to certain cooling parameters and may approximate the cooling of slag.

Certainly, the chemical differences, not only among the olivines but also of the bulk of the material, need to be taken into consideration. Donaldson himself, as already mentioned, emphasises the fact that the normative concentration of the phases influences the cooling rate: for example, at 5 ºC/h in the eucrite (viscosity 4.1, olivine 40%) we observe the crystallisation of chain olivine. On the other hand, in one of the basalts (viscosity 45 and olivine normative 18%), there is no actual formation of olivines.

The cooling rate of olivine is a complex matter, depending, as we have just seen, not only on the temperature gradient, but also on chemical composition, viscosity and normative mineral composition.

Ettler and co-authors maintain that the temperature ranges presented in Donaldson (1976) and described above are much slower than the ones actually intervening in the formation of slag. They argue that hopper and polyhedral morphologies (the slowest ones to form) can be obtained with a range of around 100 ºC/h, because slag solidifies almost immediately at tapping outside the furnace. On the contrary a speed around 5 ºC/h suggested by Donaldson for a well-formed hopper morphology would imply 10 hours for a slag to solidify, considering a range of 50 ºC for the slag to completely solidify (Bachmann 1982). This is true if we consider the system to move from liquid to solid outside the furnace.

Looking at slags of different origins, we always observe a dominant morphology, a secondary morphology, normally localised, and very often a second generation of olivines with a different morphology, normally more skeletal. These observations suggest different steps of crystallisation. Considering only the olivine system in order to simplify the observation, at the average chemical composition observed in the slags under examination (Mg around 0.8%), the temperature range between the *liquidus* and *solidus* curve is around 20 degrees, a range at which a first solid purely

fayalitic olivine crystallises and stays in equilibrium with a liquid impoverished in fayalitic phase. This would result in two different compositions of the olivine in the slag, the hopper polyhedral variety being crystallised in the first conditions, and the skeletal second generation ones being crystallised from the residual forsteritic enriched liquid. The composition of the two generations would be the same if the crystallisation started from a completely molten phase and occurred concurrently for the whole amount of material. The comparison of the compositions of the different generations of olivines will be used together with the study of the morphologies to identify the cooling range and the crystallisation regimes, one or two crystallisation steps, nucleation inside the furnace, etc., in order to determine whether the temperature was always above the *liquidus* curve, and also the extent to which the system was controlled.

In the results chapter (chapter 6), Donaldson's aforementioned categories will be used in a first approximation to indicate faster or slower cooling. Subsequently, the morphology will be discussed in association with the viscosity index (presented in the following section) and the internal variability (chemical variability inside each sample), in order to identify when the crystallisation started, how this would have affected the efficiency of the process, and what factors affected it.

5.2.2 Bulk chemical composition, viscosity, melting temperature and reducing conditions

Slags generated by metal production are capable of yielding significant information about the technological processes that produced them. This information is present in their bulk chemical composition, phase composition, and to some extent their morphology. The bulk chemistry of a slag specimen is derived from the chemistry of ore, fuel, furnace wall and fluxing agents. Bulk chemistry is thus well suited to studies focussing on possible variability in natural resources used in smelting technologies and variation in furnace operating procedures when the resources themselves remain constant.

Chemical variation within the assemblage is caused by: the heterogeneous character of slag derived from single smelts, more or less random differences between smelts, and the use of multiple smelting procedures during assemblage accumulation.

The three most significant sources of variation in slag chemistry are here assumed to be:

1) ore selection and preparation;
2) furnace operation;
3) addition of lead metal for the extraction of silver.

Two indices (F and G) characterise aspects of slag chemistry and may be useful for generating approximate measures of those behaviours that would also have visible consequences to the ancient metallurgists (Charlton 2007, 157). F is the ratio of silica to alumina in a slag specimen, and it aids in the detection of extreme ore variability. The F value will also be sensitive to contributions from the furnace lining.

The G value is an empirically derived index of slag glassiness, containing primarily fuel ash related oxides in the numerator and ore related oxides in the denominator. For the purposes of this project, the G value has been modified in order to take into consideration the fact that the contribution of potash is both from the fuel and the ore, and lead oxide from the ore, and it will be used as an index indicating variation in the ore and the fuel ash contribution, and not of the glassiness.

$$F = SiO_2/Al_2O_3$$

$$G = (CaO+ P_2O_5+K_2O+MgO)/(FeO+MnO+BaO+K_2O+Na_2O+Al_2O_3+PbO)$$

Since both the F and the G values are reflections of ore selection/preparation and furnace operating conditions, and the expected error ranges around each value increase to ±25%, assuming a 5% error rate in copying (Charlton 2007), then a history of experimentation is shown in the fluctuation of the values, while uniformity of the value would indicate a more standardised recipe. For instance, if there is no overlap between the error ranges of the G values, this would suggest a theoretical varying glass content. This would likely be a reflection of variable reducing conditions and fuel ash contributions, furthermore indicating that heavy experimentation of some sort was taking place at the site.

A third index, S, considers oxides specifically related to ideal slag formation. This index is formed by multiplying the weight percentage (wt%) of SiO_2 by the molar ratio of FeO to SiO_2 in fayalite and dividing this product by the sum of the cations that could enter the fayalite lattice, in this case FeO, MnO, MgO and CaO:

$S= 2.39*SiO_2/(FeO+MnO+MgO+CaO)$

An S value of 1 is equivalent to a pure fayalitic slag, while those greater than 1 are increasingly glassy, and those less than 1 are increasingly rich in wüstite. Reducing conditions are expected to be positively correlated with the value of the index.

The fourth parameter used to describe the slag is the viscosity, presented as log η, and calculated following the model proposed by Giordano et al. (2006). The model is described by the formula:

$Log\eta=b1+[(b2+b3)/b3+SM)]+b4$

where b1, b2 and b3 are constants depending on the chemistry of the melt (only the chemistry of the molten portion of the slag is used for this calculation, avoiding the residual aggregates) described by the SM parameter defined as $(Na_2O+K_2O+CaO+MgO+MnO+FeO)/2$, and b4 is sample dependent. Considering the melt chemistry, the constants were chosen as follows:

b1 = -1.4734

b2 = 14.0392

b3 = 13.4508.

Since each assemblage is derived from multiple smelting events and potentially multiple generations of metallurgists, it should be possible to monitor adaptive trends in smelting efficiency. Directional selection can be hypothesised when changes are systematic and can be shown to be increasingly adaptive relative to the environment. Stabilising selection can be hypothesised when stasis is observed in the index values through time and the slag chemistry can be shown to be an optimal solution with respect to the environment and within specific geological constraints.

As Charlton (2007) describes, craft guilds or specialist kin-groups will favour technological variants that reduce resource costs and increase product quality, while tending to reject those that increase resource expenditures or reduce the need for skilled labour. As resource costs increase or become fixed, control over the production process shifts towards individuals or groups that own supplies and away from those who own skills. This reduces the inflated benefits associated with monopolistic or oligopolistic control over a particular market. Similarly, labour-saving mechanisms reduce the need for, and therefore devalue, investments in skilled

workers (Charlton 2007). This being said, Charlton (2007) develops the hypothesis that two optima are present in iron working systems, and they can be identified through bulk chemical analyses of slags: the two optima are the two eutectic points defining the olivine field in the alumina/silica/FeO thermodynamic diagram, optimum 1 at a temperature of 1088 ºC, and optimum 2 at 1148 ºC. According to Charlton (2007), optimum 1 is at the base of a very steep temperature precipice and borders a high viscosity phase; creating slag with this chemical signature, without introducing significant contributions of silica from the furnace wall, demands exact control of both reducing conditions and temperature. Optimum 2, on the other hand, has a much gentler surrounding temperature gradient for free-running slag with varying chemistry. The phases that it borders are also relatively docile in their viscosity effects. This increases the range of permissible variation in the smelting recipe, while minimising the risk of failure. In his consideration of iron smelting, Charlton (2007) confers yet another connotation to these two optima: in fact, optimum 1 would waste 20% less iron than the less risky optimum 2.

In the case under consideration in the present study, we are not interested in the amount of iron wasted or produced by the system, since the metal produced in this context was silver-rich lead. However, we are definitely interested in the recipe selected across different periods of time in order to achieve the best conditions for recovering the lead from an iron-rich system in different geological conditions (variation in the ore chemical composition) and environmental constraints (fuel abundance).

What needs to be taken in consideration is that, given the importance of economic behaviour to an individual's fitness, selection is expected to play an important part in the evolution of metal production strategies. For what concerns bloomery iron production, for instance, economic environments where the costs of acquiring resources are low, the benefits of producing metal are high, but where demand is low (or very little competition exists between ironworkers), selection favours slag chemistries that approximate optimum 2. Less energy and labour are required to maintain the temperatures and reducing conditions for this optimum (Charlton 2007).

If the economic control of the metal is monopolistic or oligopolistic (as it is expected to have been the case in Imperial Rome), the benefits to the metallurgist might actually decrease with increasing industrial scale. Selection favours the development of a bloomery process towards optimum 1 when the demand for metal is high and the

cost of procuring resources is also high relative to the benefits of production, or when both demand and competition are high. Greater energy and more skilled labour are needed to maintain the more exacting reducing conditions. Socio-economic environments such as this should experience increasing returns to scale (Charlton 2007). This discussion is significant for iron production, since the difference between the two optima is around 20% of iron produced, and a more or less skilled professional labour force is employed.

The discussion of silver production within this framework is not exactly the same, since the higher or lower expertise in producing silver is not definable according to the same pattern, since the amount of iron loss is not indicative of the level of skill. Thus, the valuation of the optima will be used only as an index of the change in the recipe used for smelting.

CHAPTER 6

The material: morphological, chemical, petrographic and mineralogical observations

The metallurgical debris excavated at the site of Corta Lago can be allocated to different periods. The distinctions were made by dating and by macro-morphological distinctive features within the same historical periods. The dating was carried out using ceramic typology and radiocarbon dating (only two dates), and the stratigraphic and chronological grouping was discussed in detail in Chapter 4. This chapter will focus on the materials and the morphological groups identifiable within the different chronological periods. The periods are all chronological and within the Republican period we also observe a morphological subdivision that we highlight here as three groups. The groups studied are divided as follows:

- Bronze Age, 'ball' slags;
- Phoenician tapped slags;
- Ibero-Punic tapped slags;
- Iberian tapped slags;
- Republican Phase I tapped slags;
- Republican Phase II plate slags;
- Republican Phase III tapped slags;
- Imperial tapped slags.

Samples from each of the different periods have been analysed with different analytical techniques, described in Chapter 5, and details of the techniques used for each sample are presented in Table 6.1. The results will be presented and preliminarily discussed in this chapter.

Before presenting and discussing the results, however, the introduction of some terminology and concepts that will recur in the following text appears necessary. First of all, the macro-morphological features of 'free silica', tapped, plate and ball slag are described as follows.

The term 'free silica' is taken from the archaeometallurgical literature on the area and refers to slag with macroscopically visible translucent aggregates, typically

identified as quartz (see Appendix 1 for the chemical composition of the minerals referred to in the text), that have not reacted during the smelting process. To be accurate, these quartz aggregates should be called residual silica. The term 'free silica' will be used only to describe samples from the literature and not samples from the Corta Lago section, which will be identified as 'ball' slags instead (Fig. 6.1), as we will see later on in this chapter.

Figure 6.1 Sample of ball slag recovered in Rio Tinto at the site RT 24, dated as Imperial.

Tapped slag is the slag produced by the process of tapping the liquid/semi-liquid slag out of the furnace through a tapping hole (Fig. 6.2). The tapping of the slag makes it possible to continuously charge the furnace without wasting heat, and hence processing several charges of ore increases the final amount of metal produced at the end of one smelt. The tapping process generates slag with characteristic features similar to lava. 'Streams' of material with a certain width, determined by the tapping hole diameter, flow one on top of the other out of the furnace. The external layer cools very quickly and the thermal gradient from outside-in may vary greatly depending on the width of the flow. The high cooling speed of the surface of the slag flow freezes the flow coming out of the tapping hole. This effect implies that the width of the slag flow is representative, to a certain degree, of the diameter of the tapping hole. The rigidity imposed by the cooling of the surface limits the expansion

of the liquid/semi-liquid slag, exactly like a lava tunnel would do in nature. Observing microscopic images of this type of slag, the first 100 µm seem to be 'frozen' surface, below which the morphology of the minerals show a much slower cooling rate. The absence of cracks in the 'frozen' surface and the relative high fluidity of the silicatic slag seem to indicate that there would not be such a high degree of expansion from the tapping hole diameter to the lava flow-like diameter of the tapped slag structures, to the extent that I would suggest the ratio is almost one to one. Observing Figure 6.2, we see that the diameter of the final 'rivulets' of material is in fact very similar in terms of area to the amount of material at the level of the tapping hole itself, even if in this case the shape of the rivulets is more ellipsoidal than the tapping hole.

Figure 6.2 Modern slag tapping during a bloomery smelting experiment. The tapping hole is opened with an iron bar and allows the slag to flow from the furnace when all the charge is smelted and the bloom is produced.

Furthermore, returning to the explanation of the thermal gradient issue, the width of the slag flow is linked to the tapping hole diameter and the amount of material flowing out of the furnace; hence, the bigger the tapping hole, the larger the amount of slag flowing out of the furnace, and the longer the material in the internal areas of the tapping flow is kept hot. This is a qualitative observation prompted by the lack of

numeric data on the difference in cooling rate as related to difference in size of the same morphological typology of fayalitic olivines. The data reported to date (Donaldson, 1976; Dević and Marčeta, 2007; Faure and Schiano, 2004; Faure and Schiano, 2005; Faure et al., 2007; Faure et al., 2003; Ivliev et al., 2004; Kamenetsky et al., 2007; Kohut and Nielsen, 2004; O'Driscoll et al., 2007) relate only to differences in shape and consider a chemical composition more enriched in magnesium, which could invalidate the conclusions, as discussed in Chapter 5.

However, this variation in thermal gradient will result in the crystallisation of morphologically different olivines in different parts of the solidified slag flow, as will be described in more detail in the following paragraphs.

Plate slag is the name given to slabs of slag with a round disc shape, several decimetres (~60-70 cm) in diameter and few centimetres thick (~1-2 cm), with flat lower and upper surfaces (Figs. 6.3 and 6.4). These slags probably solidified in a forehearth, a 'pit' in front of the furnace where the molten material accumulated after the smelting had produced a satisfactory quantity of metal. It can be that both metal and slag were tapped into the forehearth, and the slag was then removed, almost 'peeled' layer after layer following the cooling, avoiding the build-up of too heavy a lump of slag on top of the metal. There is also the possibility that only the slag was tapped in the forehearth and the metal was still left to accumulate in the furnace. Those two hypotheses will be discussed in section 6.6. This process would allow the furnace to operate a virtually continuous process while the metal and the slag are separating in the forehearth, or the slag accumulate in the forehearth and then get discarded, while the furnace continues the smelting operation. The slag produced by such a process shows high crystallinity, with oxidised layers at the top and bottom and increasing crystal size towards the centre. The layer of oxidation at the top is self-explanatory, since the top surface of the slag is in contact with air. On the other hand, the layer at the bottom of the slag is produced when the act of 'peeling' occurs, and a 'patina' of still liquid slag quenches when touched with the tools used for the "peeling" process, favouring more oxidised phases in the dendritic texture to crystallise (Figs. 6.27 and 6.29).

Figure 6.3 Bottom surface of a plate slag formed in a forehearth (RT25 L52 S100).

Figure 6.4 Top surface of sample RT25 L52 S100, showing the smoothness and porosity due to the quenching of the superficial layer, and the rim due to the contact with the cooling pit.

As the name suggests, ‘ball slag’ is a round, ball-shaped slag. The use of the term is parallel to ‘free silica’ slag, because the latter typically looks ball-shaped, but the

employment of the term ‘ball slag’ eliminates the chemical connotation. This choice is motivated by two observations: the first is that the ball slags described in this chapter were found outside of the stratigraphic context where the ‘free silica’ slags are normally found and described in the literature (i.e., the Bronze Age, local or first Orientalising period; see following section). The second reason is that the ball slags studied here are very rich in residual aggregates of barite, as well as quartz, and therefore the term ‘free silica’ would have been chemically incorrect in this case, as already mentioned by Kassianidou (1992, 181). For this reason, two different sections are presented in this chapter: one is a short literature review of the ‘free silica’ slags, their characteristics, metallurgical explanations, sites where they were recovered and archaeological associations, to provide a taste of the debate about their provenance: local pre-Phoenician tradition or the first Phoenician jarosite smelting attempts. The second section is focussed on the ball slag samples recovered from the Imperial layers at the Corta Lago section and analysed as part of this project. As will be argued below, I believe that both terms refer to the same material, and that ‘ball slag’ is a more appropriate term than the previously used ‘free silica’.

	Sample ID	Stratigraphic layer		Period	Sample type	Analysis performed			
15	RT25 L101 S75	101	pre-Roman	Phoenician	Tapped slag		XRD		
	RT25 L101 S57	101	pre-Roman	Phoenician	Tapped slag		XRD		
	RT25 L101 S52	101	pre-Roman	Phoenician	Tapped slag		XRD		
21	RT25 L101 S39	101	pre-Roman	Phoenician	Tapped slag	XRF	XRD		LIA
19	RT25 L101 S35	101	pre-Roman	Phoenician	Tapped slag	XRF	XRD		LIA
7	RT25 L101 S16	101	pre-Roman	Phoenician	Tapped slag	XRF	XRD	SEM	LIA
9	RT25 L101 S5	101	pre-Roman	Phoenician	Tapped slag	XRF	XRD	SEM	LIA
	RT25 L104 S54	104	pre-Roman	Phoenician	Tapped slag		XRD		
13	RT25 L126 S74	126	pre-Roman	Phoenician	Tapped slag	XRF	XRD		
11	RT25 L126 S58	126	pre-Roman	Phoenician	Furnace lining fragment	XRF	XRD		
17	RT25 L126 S22	126	pre-Roman	Phoenician	Tapped slag	XRF	XRD		LIA
33	RT25 L124 S12	111/b/c/124	pre-Roman	Ibero-Punic	Tapped slag	XRF	XRD	SEM	
37	RT25 L120 S33	120	pre-Roman	Ibero-Punic	Tapped slag	XRF	XRD		
	RT25 L120 S37	120	pre-Roman	Ibero-Punic	Tapped slag		XRD		
39	RT25 L120 S40	120	pre-Roman	Ibero-Punic	Tapped slag	XRF	XRD		
41	RT25 L120 S61	120	pre-Roman	Ibero-Punic	Tapped slag	XRF	XRD		
	RT25 L120 S64	120	pre-Roman	Ibero-Punic	Tapped slag		XRD		
	RT25 L120 S68	120	pre-Roman	Ibero-Punic	Tapped slag		XRD		
	RT25 L120 S72	120	pre-Roman	Ibero-Punic	Tapped slag	XRF	XRD		
	RT25 L120 S77	120	pre-Roman	Ibero-Punic	Tapped slag		XRD		
43	RT25 L121/124 S63	121/124	pre-Roman	Ibero-Punic	Tapped slag	XRF	XRD	SEM	
	RT25 L121/131 S80	121/131	pre-Roman	episode of erosion	Tapped slag			SEM	
35	RT25 L132 S17	132	pre-Roman	Ibero-Punic	Tapped slag	XRF	XRD		
	RT25 L132 S21	132	pre-Roman	Ibero-Punic	Tapped slag		XRD		
29	RT25 L115 S55	115	pre-Roman	Iberian	Tapped slag	XRF	XRD		LIA
31	RT25 L115 S56	115	pre-Roman	Iberian	litharge	XRF	XRD		LIA
27	RT25 L115 S59	115	pre-Roman	Iberian	litharge		XRD		
23	RT25 L115 S20	115	pre-Roman	Iberian	Tapped slag	XRF	XRD		
25	RT25 L119 S50	119	pre-Roman	Iberian	Semi-reacted ore	XRF	XRD		
50	RT25 L114 S84	114 A	Republican phase I tapped		Tapped slag	XRF	XRD		LIA
	RT25 L2 S75rtm	2 B	Republican phase I tapped		Tapped slag	XRF	XRD		LIA
	RT25 L3 S74rtm	3	Republican phase I tapped		Tapped slag	XRF	XRD		LIA
52	RT25 L3 S85rtm	3	Republican phase I tapped		Tapped slag	XRF	XRD	SEM	LIA
54	RT25 L3 S86rtm	3A	Republican phase I tapped		Tapped slag	XRF	XRD	SEM	LIA

Table 6.1 (part)

	Sample ID	Stratigraphic layer	Period	Sample type	Analysis performed			
	RT25 L6 S67	6	Republican phase I tapped	Tapped slag			SEM	
46	RT25 L6 S73rtm	6	Republican phase I tapped	Tapped slag			SEM	
	RT25 L6/8 S13	8/6	Republican phase I tapped	Tapped slag	XRF	XRD		
	RT25 L9 S70rtm	9	Republican phase I tapped	Tapped slag			SEM	
48	RT25 L31 S83rtm	31	Republican phase I tapped	Tapped slag	XRF	XRD	SEM	LIA
60	RT25 L31 S7	31	Republican phase I tapped	Tapped slag	XRF	XRD		LIA
58	RT25 L31 S19	31	Republican phase I tapped	Tapped slag	XRF	XRD		LIA
56	RT25 L31 S18	31	Republican phase I tapped	Tapped slag	XRF	XRD		LIA
62	RT25 L52 S79rtm	52	Republican phase II plate	Plate slag	XRF	XRD		LIA
66	RT25 L52 S1	52	Republican phase II plate	Plate slag	XRF	XRD		LIA
70	RT25 L52 S2	52	Republican phase II plate	Plate slag	XRF	XRD		LIA
72	RT25 L52 S3	52	Republican phase II plate	Plate slag	XRF	XRD		LIA
68	RT25 L52 S17	52	Republican phase II plate	Plate slag	XRF	XRD		LIA
74	RT25 L52 S4	52	Republican phase II plate	Plate slag	XRF	XRD		LIA
64	RT25 L55 S82rtm	55	Republican phase II plate	Plate slag	XRF	XRD	SEM	LIA
77	RT25 L72 S72rtm	72	Republican phase III tapped	Tapped slag		XRD	SEM	LIA
76	RT25 L87 S77rtm	87	Republican phase III tapped	Tapped slag	XRF	XRD		LIA
79	RT24 S1		Imperial	Lead bullion (carbonatised)	XRF	XRD	SEM	
81	RT24 S2		Imperial	Tapped slag	XRF	XRD		LIA
83	RT24 S3		Imperial	Tapped slag	XRF	XRD		LIA
85	RT24 S4		Imperial	Tapped slag	XRF	XRD	SEM	LIA
87	RT24 S5		Imperial	Tapped slag	XRF	XRD	SEM	LIA
89	RT24 S6		Imperial	Tapped slag	XRF	XRD	SEM	LIA
1	RT24 S7		Imperial ? Bronze Age (redeposited)	Ball slag	XRF	XRD		LIA
3	RT24 S8		Imperial ? Bronze Age (redeposited)	Ball slag	XRF	XRD	SEM	LIA
5	RT24 S9		Imperial ? Bronze Age (redeposited)	Ball slag	XRF	XRD	SEM	LIA

Table 6.1 List of the samples analysed, their stratigraphic layer, their dating and the technique used for the analysis. Some of the samples are from the collection of the Rio Tinto Museum, and they have the suffix 'rtm' after the sample number. The integer numbers on the firs column of this table will be used in chemical graphs in chapter 8 (Figs. 8.12, 8.13 and 8.14)

6.1 Late Bronze Age 'Free silica' slags

Slags of the "free silica" type were recorded for the first time in the 1960s, in the excavations carried out in the town of Huelva. The material was named at the time "de turron", a typical Spanish sweet almond paste, similar in appearance to this "formation of grains of quartz cemented together by slag" (Garrido Roiz, 1968, 12). It is important to mention that, on occasion, free silica slags have been found accompanied by another type of slag that is similar to it but has no unreacted crystals, as in the case of Cerro de la Tres Aguilas (Hunt Ortiz, 2003). At this site, right next to the Rio Tinto mines, of the 60 individual samples collected on the surface, 15% corresponded to furnace slag, which is porous and without visible particles, while 85%

corresponded to fragments of free silica slag (Hunt Ortiz 1987, 35). Kassianidou (1992, 210) describes the free silica slag as being the first step in the process, followed by a high barium tapped slag with no residual aggregates debris. According to the available data, slags of the free silica type have been recorded at the following sites, and their principal features and proposed chronology are provided in Table 6.2:

SITE NAME	**DATE**	**REFERENCE**	**ASSOCIATED FINDS**
Cerro Salomon	8th-7th century BC	Blanco and Luzon 1969, 131	
Quebrantahuesos	8th century BC	Pellicer 1983	
Corta Lago	8th century BC	Amores 1986, 715	"Phoenician elements"
	7th century BC	Harrison (pers. comm.)	"elements of local Final Bronze Age tradition associated with Phoenician amphorae"
	Pre-Phoenician	Perez Macias 1996, 81-82	"no wheel-made pottery", "atypical pottery"
	End of the 2nd millennium BC	Perez Macias 1996, 82	
Cerro de las Tres Aguilas	Orientalising Period	Hunt Ortiz 2003	
Castillo de Aznalcollar	Late Bronze Age	Hunt Ortiz 2003	
Torre del Viento	8th-5th century BC	Hunt Ortiz 2003	Hand-made carinated, burnished pottery
Castrejones	8th-5th century BC	Hunt Ortiz 2003	Hand-made carinated, burnished pottery
Las Mesas	7th century BC	Hunt Ortiz 2003	Hand-made pottery
Gerena	7th century BC	Hunt Ortiz 2003	Orientalising wheel-made pottery
Tejada la Vieja	8th-7th century BC	Rothenberg and Blanco-Freijeiro 1981, 170	
Peñalosa	800-750 BC	Fernández Jurado et al. 1993	Phoenician pottery sherds
Cabezo de Esperanza	7th century BC	Garrido Roiz 1968, 31	

Huelva city	First half of the 8th century BC	Fernández Jurado 1993, 138	
El Pozancon	First quarter of the 1st millennium BC	Gómez Toscano et al. 1994	
El Tejar	Late Bronze and Colonisation periods	Gómez Toscano et al., 1994	"material" datable to the Late Bronze and Colonisation Period
Niebla	Orientalising Late Bronze Age	Belén and Escacena 1990, 213-214	Wheel-made pottery and *cruciales*.
San Bartolomé de Almonte	8th century BC with Phoenician influence	Ruiz Mata and Fernández Jurado 1986, I, 257	Remains related to silver smelting
Monte Romero	Second half of the 7th and beginning of the 6th century BC	Rothenberg et al. 1986; Perez Macias 1996; Kassianidou 1992.	Stone mining hammers
Tharsis	5th century BC (8th-7th century BC?)	Domergue 1987, 209	

Table 6.2 List of the sites where 'free silica' slags were identified. The table includes the reference to the publication of the site and the material correlated to the 'free silica' slag, where available.

There are contradictory opinions concerning whether 'free silica' slags belong to either the local Bronze Age tradition or to Phoenician smelting processes. The coincidence of the presence of Phoenician elements with the discovery of free silica slags in every site mentioned supports the idea that a Phoenician technique was linked to the metallurgical process producing them, but this hypothesis is not definite.

The first finds of this free silica slag were interpreted as the result of lack of control, of a bad smelting practice (Blanco and Luzon 1969, 14; Flores Caballero 1981, 38). Later on, when new finds were identified and the analyses provided more reliable data, new interpretations were put forward, that slags were made more fragile to facilitate:

- the extraction of the metallic globules they contained (Rothenberg and Blanco-Freijeiro 1981, 177);
- the separation by gravity of the metal through the slag (Rothenberg et al. 1986, 4);
- the separation of the slag from the metallic mass (Hunt Ortiz 1987, 54);

- the thickening of the slag "to take it out like water with a sponge" (Tylecote 1987, 306-307).

The study of Kassianidou (1992) on the samples from Monte Romero is perhaps the most complete on this type of slag, and reached the conclusion that they were the result of the treatment of the ores from the nearby mine with the same name, since these slags contained polymetallic ore globules and even phases rich in silver (Kassianidou 1992, 273). With regard to its mineral phases, although celsian appeared in the slags richer in barium (Kassianidou 1992, 193), fayalite was the most abundant (Tylecote et al. 1974, 32). The intentional production of this type of slag was clear for Monte Romero, where the free silica slag was later re-smelted to recover its lead and silver content, a process that also produced at this site fluid tapped slag, in this case with celsian as the principal phase (Kassianidou 1992, 240).

Slags of the free silica type have a characteristic composition. The common elements considered definitive in the samples analysed by Hunt Ortiz and reported in the literature have been summarised by Hunt Ortiz (2003) as follows:

1) The presence of high proportions of silica compounds, a large part in a 'free' (residual) state (between around 10 and 30% by volume of free, non-reacted quartz).
2) The presence of high proportions of iron (between around 15 and 30%).
3) Low copper content (<0.1%).
4) A certain silver content (<0.2%).
5) High lead content (between 5 and 10%).
6) The presence of barium, sometimes in large amounts (between around 1 and 30%).

The heterogeneity of the slags causes the SEM-EDS area analyses to vary greatly within a single sample, and with it the concentration of metallic lead droplets (with occasionally very high concentrations of silver; up to 30% Ag in metallic lead globules have been detected by SEM in Las Casetillas – Hunt Ortiz 2003) also differs from area to area of the same slag sample. There are cases in which the sample analysed showed no detectable silver, although this result could be attributed to their heterogeneity. Free silica slags are always related to extractive silver metallurgy (Hunt Ortiz 2003).

Free silica slags are thought to be the result of the use of a specific technology for extracting silver, applied to various types of argentiferous ores, although the principal one would be jarositic earths, both from large massive sulphide deposits (such as Rio Tinto, Tharsis or Aznalcollar) and small deposits with gossan on the surface, such as Hondurillas (Hunt Ortiz 2003).

Samples showing strong similarities with the ones just described are found in the Imperial layers of the Corta Lago section. Despite the author's opinion that these samples belong to the Late Bronze Age phase at Corta Lago, their redeposition in the layers of later chronology leaves a doubt about their origin. The samples will be then presented in section 6.9 following the presentation of the Imperial samples and hypothesis for their presence in the Imperial phase are also presented and discussed. For the same reason (the recovery of the samples in layers stratigraphically non conforming to the morphology and chronology described in the literature) the samples will not be identified as Free silica slag but as Ball slag following their macroscopical morphology.

6.2 Phoenician samples

The lowest layers of the Corta Lago section have been dated as Phoenician by pottery and coins: layer 101 dated to the 7^{th} century BC, layers 102, 104 and 105 dated to the Final Bronze Age, and layers 129 and 130 dated to the $6^{th}/5^{th}$ century BC (Harrison personal communication). The Phoenician tapped slags are fragments of tapped slag of a few centimetres in size, with a lava-like aspect of cord-like flows, dark grey with a reddish patina (Figs. 6.5 and 6.6). The fresh fracture is black and no crystals are visible.

Figure 6.5 Sample RT 5 showing the typical cord-like morphology of tapped slag and a red patina.

Figure 6.6 Sample RT 35 showing the typical cord-like morphology of the tapped slag.

The 11 samples, analysed using the different techniques described in Chapter 5, are taken from three layers (101, 104 and 126) and do not present macro-morphological differences.

6.2.1 Furnace lining

Sample RT25 L126 S58 is a furnace lining fragment showing superficial interaction with slag. The ceramic body presents subangular/rounded shaped quartz grains with reaction bays. Linear porosity sub-parallel to the surface seems to indicate the presence of organic material (such as straw, for example) in the original mixture Fig. 6.7). The chemical composition of the ceramic is characterised by high alumina, high potash and high magnesia.

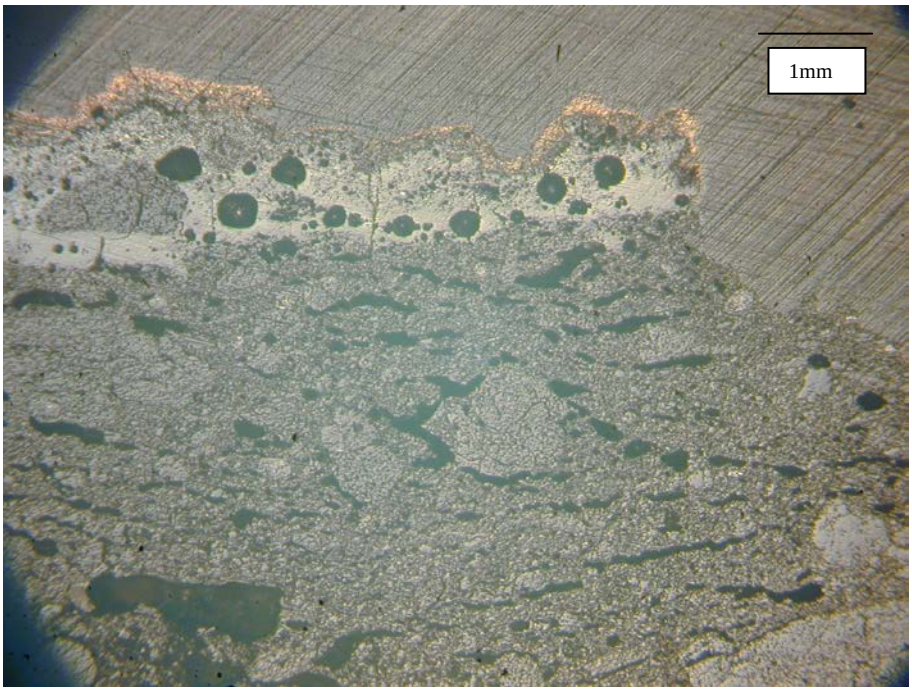

Figure 6.7 Interaction slag (on the surface) and ceramic body in sample RT25 L126 S58. Visible in the ceramic body are quartz aggregates and elongated porosity.

6.2.2 Slag samples

The other samples, all slags, show a bulk chemical composition that is not very homogenous, as obtained by XRF (see Table 6.3). The results indicated that the two main components, silica and iron oxide, vary by around 10%. Worthy of notice are the concentration of lead oxide – between 1.5 and 3.5 wt%, mostly around 1.5/1.7 wt%, barium oxide – around 5-7 wt%, and sulphur – between 0.05 and 1.5 wt% in the slag samples and as low as 0.1 wt% in sample RT25 L126 S58, composed of slag and associated ceramic (section 6.2.1, Fig. 6.7). The other metals present in the samples are copper – between 0.1 and 0.6 wt%, arsenic – mainly between 0.2 and 0.5 wt%, with sample RT L101 S16 showing 5.8 wt%, antimony – mainly around 0.1 wt%, with sample RT L101 S16 showing 1 wt%, and tin – between 0.2 and 0.4 wt%. The concentration of silver detected with the XRF varies between 200 and 700 μg/g.

All the samples suggest that the raw material was polymetallic, containing lead, tin, copper, zinc, silver and antimony. RT25 L101 S16, however, is richer in lead oxide, arsenic, silver and antimony as compared to the other samples, even though it still presents a typical fayalite composition. The reason for this is the presence of unreacted/residual ore aggregates (Fig. 6.8).

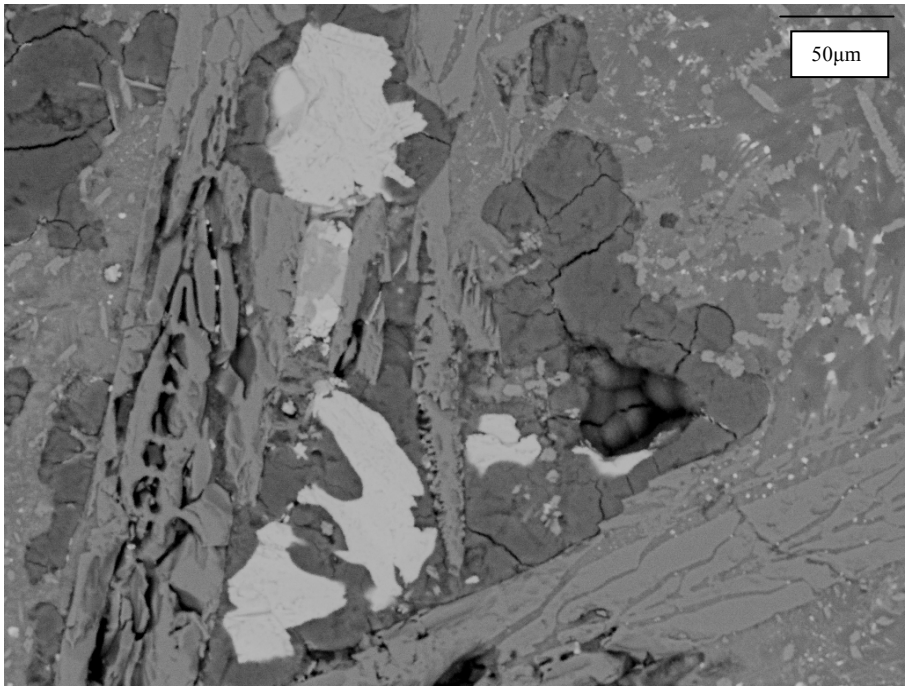

Figure 6.8 SEM backscattering image of sample RT25 L101 S16 showing the association of residual quartz (dark grey) and residual ore (white) interacting through fractures and residual bays with each other, forming olivine (lighter grey) skeletal crystals.

The hypothesis – mentioned in the free silica section above – of tapped slags deriving from a re-smelting of free silica slags should be confirmed by a higher concentration of barium oxide in the tap slag, following the partition of the residual barite into the melt (Kassianidou 1992). However, in this material the concentration of barium is fairly low as compared to the concentration of the same element in the free silica slags, and is comparable with the concentration of barium oxide in the slags of later periods. Thus, it is unlikely that this tap slag formed from the re-smelting of ball slag.

The mineralogical association is dominated by fayalite, with a low concentration of magnesia varying between 0.3 and 0.7 wt% and lime varying from 0.5 to 1.3 wt%. The crystals are skeletal/H-chain around 300 µm long and 20-30 µm wide, indicating a fast cooling speed. Fayalite is associated with magnetite with a concentration of titania around 3%, celsian and residual quartz. Lead, copper and iron sulphides and

iron arsenides have been detected, indicating an incomplete oxidation of the raw material. The main oxygen fugacity can be calculated at between 10^{-8} and 10^{-12} atm due to the coexistence of fayalite, magnetite and quartz. The interstitial glass has a calculated formula placing it near the composition of pyroxene (XSi_2O_6, where X is K, Ba, Fe and Al with various concentrations). Residual grains of quartz of a few micrometres in size are detected, indicating that the charge was not completely melted.

The area analyses show variability mainly concerning iron oxide and silica. In one of the samples, these two components have standard deviations higher than 1 (Table 6.4), and these are also the two components that vary the most between samples.

Areas of overlapping subsequent tapping are visible in the slags, with a layer of magnetite and a subsequent crystallisation of skeletal olivine perpendicular to it (Fig. 6.9).

Consequently, I hypothesise that these tapped slags are the result of primary smelting of jarositic ore associated with polymetallic sulphides, typical of the pyrite alteration area, as expected from the literature and explained in Chapter 4.

The main components ratio compared with the diagram alumina / iron oxide / silica indicates a smelting temperature of 1100/1200 °C in the fayalite field close to what has been defined as optimum 1 (t = 1088 °C – Charlton 2007, Fig. 6.62). Four of the samples create a homogenous plot, while one presents a composition more enriched in silica (RT25 L101 S35) at the eutectic (optimum 1). The variability observable in the samples, mainly for what concerns RT25 L101 S35, and the presence of residual aggregates of quartz indicate that the system was not completely homogenised and melted; quartz was in excess and it could not be used to form a crystalline pyroxenitic phase, possibly due to a too rapid cooling (hypothesis sustained by the crystallisation of H-chain and skeletal olivines).

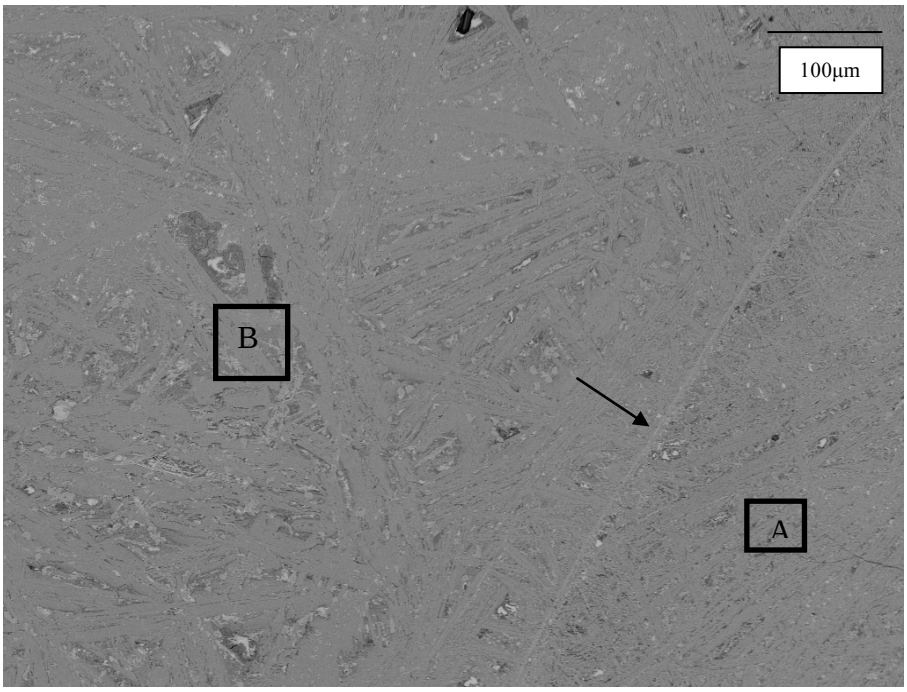

Figure 6.9 Backscattered scanning electron microscope image of one area of sample RT25 L101 S5. The areas A and B are separated by the oxidation layer (indicated by the arrow).

		Na2O %	MgO %	Al2O3 %	SiO2 %	P2O5 %	S %	K2O %	CaO %	TiO2 %	MnO %	FeO %	BaO %	PbO %	SnO2 %	CuO %	ZnO %	As %	Ag µg/g	Sb µg/g	Bi µg/g
RT25 L101 S39	Phoenician	0.32	1.61	4.56	28.03	0.24	0.41	1.22	1.76	0.30	0.14	51.00	6.84	1.85	0.29	0.16	0.02	0.19	226.85	1177.65	n.d.
RT25 L101 S35	Phoenician	0.47	2.13	9.97	37.00	0.70	0.54	0.89	2.11	0.73	0.12	37.51	4.58	1.46	0.19	0.15	0.03	0.18	416.05	1040.19	n.d.
RT25 L101 S16	Phoenician	0.22	2.72	3.41	25.63	0.25	0.23	1.03	3.23	0.25	0.10	45.22	6.08	3.57	0.39	0.44	0.03	2.20	725.97	9597.17	n.d.
RT25 L101 S5	Phoenician	0.19	1.38	3.86	24.63	0.29	1.47	1.09	3.13	0.27	0.11	52.07	6.73	1.73	0.27	0.16	0.03	0.09	170.40	1144.27	n.d.
RT25 L126 S58	Phoenician	0.06	2.00	14.36	74.62	n.d.	0.04	3.30	0.33	0.31	0.03	3.20	0.09	0.77	0.02	0.55	0.04	0.07	179.78	321.71	n.d.
RT25 L126 S22	Phoenician	0.31	1.53	3.95	31.27	0.14	0.18	1.02	2.87	0.21	0.16	49.26	6.29	1.70	0.24	0.12	0.03	0.12	170.60	1213.91	n.d.

Table 6.3 Bulk analysis (measured by XRF) of Phoenician samples.

RT25 L101 S5	average %	standard deviation	RT 25 L101 S16	average %	standard deviation
MgO	0.4	0.2	MgO	0.5	0.2
Al2O3	6.8	0.3	Al2O3	6.8	0.3
SiO2	36.5	1.1	SiO2	39.8	0.5
P2O5	0.6	0.3	P2O5	0.4	0.3
SO3	1.5	0.2	SO3	0.9	0.2
K2O	1.5	0.1	K2O	1.4	0.1
CaO	2.8	0.5	CaO	4.7	0.3
TiO2	0.2	0.3	TiO2	0.5	0.3
FeO	43.8	1.3	FeO	39.5	1.4
CuO	n.d.	n.d.	CuO	0.1	0.2
As2O3	n.d.	n.d.	As2O3	0.1	0.1
BaO	5.8	0.3	BaO	4.6	0.3
PbO	n.d.	n.d.	PbO	0.8	0.9

Table 6.4 Area analyses, measured by SEM-EDS, of samples RT25 L101 S5 and RT25 L101 S16. The area analyses show the degree of heterogeneity of the samples, quantified by the standard deviation. The standard deviation is relatively low, indicating that the samples are homogenous.

6.3 Ibero-Punic tapped slags

Figure 6.10 Sample RT25 L111/124 S8, showing red and white patinas and lava flow structure.

Figure 6.11 The other surface of sample RT25 L111/124 S8, showing the red patinas between the lava flows and a fresh fracture showing massive and non-porous structure.

Layers 111B and C, 122/124 and 132 of the section have been dated as Ibero-Punic ($5^{th}/4^{th}$ century BC), post-Orientalising period and pre-Roman. The slags present in these layers are fragments of tapped slags that do not differ macroscopically from the

Phoenician tapped slags (Figs. 6.10 and 6.11). On the fresh fracture there is no visible residual grain and the surfaces are dark grey with reddish patinas.

The analysed samples show a bulk chemical composition (table 6.5, Fig 6.62) that is not completely homogenous, but almost evenly distributed along the two isotherms of 1200 and 1100 ºC in the fayalite field of stability, presenting a chemical variance of around 10% for the main components: silica, iron oxide and alumina. Lead oxide is between 0.8 and 2.3 wt%, comparable with the previous and following periods; barium oxide between 4.5 and 6 wt% (comparable with the Phoenician, and a bit lower when compared with the Iberian samples), sulphur between 0.3 and 1.3 wt% when detected (it is not detected in sample RT25 L132 S17), again lower as compared to the Iberian, but comparable with the Phoenician samples; and copper oxide around 0.1 wt%, comparable with the previous and following periods. The Iberian samples seem to show an enrichment in both barium oxide and sulphur. This enrichment is not visible in samples either from the Phoenician or the Ibero-Punic periods.

The other metals detected in these slags are arsenic between 0.05 and 0.1 wt% for most of the samples and around 2 wt% for sample RT25 L120 S33, antimony (0.04-0.2 wt%) and tin (0.07-0.3 wt%). Silver varies between 30 and 210 ppm, lower as compared to the other periods.

Sample RT25 L120 S33 shows enrichment in arsenic oxide as well as sulphur and antimony, associated with enrichment in iron oxide and depletion in silica and alumina.

Element		Na2O	MgO	Al2O3	SiO2	P2O5	S	K2O	CaO	TiO2	MnO	FeO	BaO	PbO	SnO2	CuO	ZnO	As	Ag	Sb	Bi
Dimension		%	%	%	%	%	%	%	%	%	%	%	%	%	%	%	%	%	µg/g	µg/g	µg/g
RT25 L124 S12	Ibero-Punic	0.22	1.56	3.16	27.37	0.25	0.25	0.90	3.14	0.21	0.10	54.04	5.84	1.89	0.25	0.13	0.02	0.07	64.25	1039.06	n.d.
RT25 L120 S33	Ibero-Punic	0.19	1.76	1.85	20.32	n.d.	1.28	0.30	0.16	0.22	0.05	58.99	4.46	2.35	0.10	0.15	0.02	2.13	347.09	2101.51	n.d.
RT25 L120 S40	Ibero-Punic	0.22	0.64	3.32	28.73	0.01	1.00	0.67	0.13	0.24	0.07	57.17	5.10	0.82	0.07	0.13	0.01	0.05	226.41	445.16	6.04
RT25 L120 S61	Ibero-Punic	0.19	0.78	1.89	27.67	n.d.	0.61	0.46	0.14	0.23	0.07	60.49	4.82	1.05	0.16	0.15	0.01	0.08	391.95	1027.90	8.46
RT25 L121/124 S63	Ibero-Punic	0.22	0.73	3.61	24.23	0.03	0.55	0.63	0.65	0.20	0.12	61.63	4.79	0.86	0.11	0.18	0.01	0.16	211.57	1547.03	6.89
RT25 L132 S17	Ibero-Punic	0.24	1.89	3.33	31.01	0.11	n.d.	0.97	3.01	0.24	0.09	50.13	5.93	2.34	0.27	0.14	0.02	0.06	123.68	1173.05	n.d.

Table 6.5 Bulk chemical analyses of Ibero-Punic samples, measured by XRF.

RT25 L124 S12	Average %	Standard deviation	RT25 L121/124 S63	Average %	Standard deviation	RT25 L121/131 S80rtm	Average %	Standard deviation
Na_2O	0.1	0.2	Na_2O	n.d.	0.0	Na_2O	n.d.	0.0
MgO	0.5	0.3	MgO	n.d.	0.0	MgO	0.2	0.3
Al_2O_3	5.5	0.1	Al_2O_3	5.4	0.1	Al_2O_3	4.5	1.1
SiO_2	35.9	0.3	SiO_2	28.4	0.6	SiO_2	37.6	1.6
P_2O_5	0.1	0.2	P_2O_5	n.d.	0.0	P_2O_5	0.1	0.2
SO_3	1.2	0.1	SO_3	1.3	0.2	SO_3	3.4	0.7
K_2O	1.2	0.1	K_2O	0.9	0.1	K_2O	1.2	0.4
CaO	4.6	0.2	CaO	1.0	0.2	CaO	1.1	0.2
TiO_2	0.2	0.3	TiO_2	n.d.	0.0	TiO_2	0.2	0.3
FeO	45.5	0.5	FeO	59.1	0.6	FeO	47.4	4.1
As_2O3	0.0	0.1	As_2O3	n.d.	0.0	As_2O3	n.d.	0.0
BaO	3.8	0.3	BaO	4.0	0.3	BaO	4.0	1.1
PbO	1.3	0.2	PbO	n.d.	0.0	PbO	0.2	0.6

Table 6.6 Area analyses of Ibero-Punic samples showing the standard deviation, indicative of the homogeneity of the sample.

The area analyses of samples RT25 L124 S12 and RT25 L121/124 S63 show a very low variability, with the highest standard deviation of 0.5 verified only for iron oxide (Table 6.6), indicating that the samples are chemically homogenous. In contrast, sample RT25 L121/131 S80rtm shows a much higher standard deviation, mainly concerning FeO, indicating an uneven distribution of this component inside the sample. The difference observed at a chemical level between the samples is associated to a mineralogical difference. Samples RT25 L124 S12 and RT25 L121/124 S63 are mainly composed of skeletal/H-chain olivines around 500 µm long and 100 µm wide, while sample RT25 L121/131 S80rtm is mainly composed of polyhedral/hopper olivines 100 µm in size. This morphology produces a different packing of the crystals inside the matrix, inhibiting the chemical movement, and hence determining the heterogeneity in FeO distribution. Furthermore, the skeletal morphology implies a rapid cooling from the melt, while the polyhedral one indicates a slower cooling of the melt, possibly starting when the material is still in the furnace, initiating a process of stiffening of the melt, and impeding in this way the further homogenisation of the system.

The mineralogical association is dominated by the presence of fayalite, with both lime and magnesia around 1 wt% (Fig. 6.12, Table 6.7). The interstitial glass has a pyroxene-like composition, for what concerns the silicatic part, while the cation can vary ($XFeSi_2O_6$, where X is Ca, K, Ba, Al). Few crystals of residual barite are detected (Fig. 6.14, Table 6.9). The oxide phases vary greatly in their composition, from pure antimony oxide to copper and copper/iron oxide (Fig. 6.13, Table 6.8). All of them contain lead, arsenic and silver.

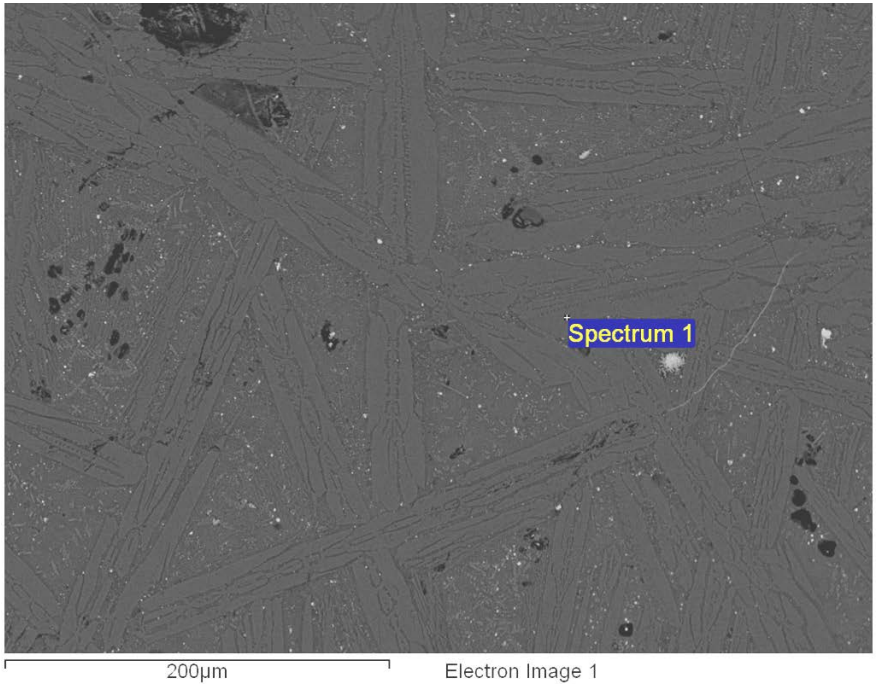

Figure 6.12 H-Chain fayalite in sample RT25 L124 S12; the H-chain morphology is visible.

Spectrum 1:

Element	Weight%	Atomic%	Compound%	Formula
Mg K	0.63	0.74	1.05	MgO
Si K	14.28	14.57	30.55	SiO_2
Ca K	0.72	0.51	1.00	CaO
Fe K	52.39	26.88	67.40	FeO
O	31.98	57.29		
Total	100.00			

Table 6.7 EDS spectrum showing the typical composition of the fayalite in the Ibero-Punic samples analysed.

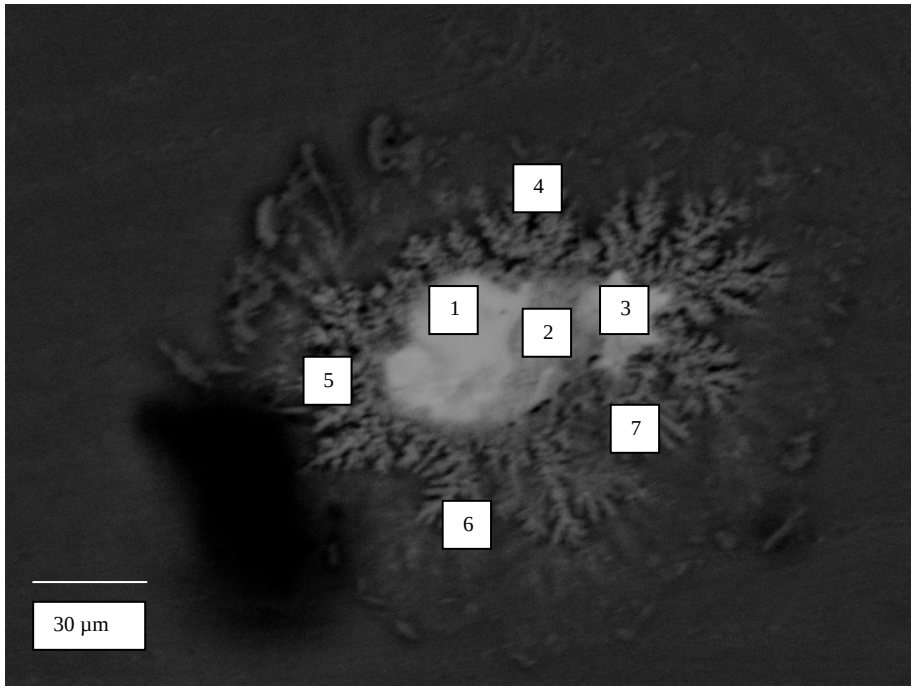

Figure 6.13 Droplet of antimony/copper associated with copper arsenate. The dendritic phase associate is mainly a copper sulphide.

	O	Al	Si	S	K	Ca	Fe	Cu	As	Ag	Sb	Ba	Pb
spectrum 1	2.63			3.71			2.32	13.21	6.25	1.22	67.99		2.66
spectrum 3	2.59			4.99			3.72	16.8	7.77	1.28	60.39		2.47
spectrum 4	19.5	1.37	9.32	8.29	0.55	1.6	26.3	29.41		1.32		2.39	
spectrum 5	10	1.08	7.54	9.83	0.55	2.1	27.95	36.97		1.51		2.5	
spectrum 6	16.1	1.02	8.2	8.89	0.47	1.7	24.56	33.27		1.67		2.54	1.53
spectrum 2	3.22			6.11			3.52	58.27	22.67	1.96	4.24		
spectrum 7	10.5	0.9	6.21	12.3	0.44	1.2	20.74	44.32		1.93		1.4	

Table 6.8 Analyses of the three phases composing the droplets and four points on the dendrites. Silver is detected in every analysis and shows a concentration always higher than 1 wt% (between 1 and 2 wt%).

	O	S	Ca	Fe	Ba
spectrum 1	27.2	13.38	0.77	1.61	52.63
spectrum 2	25.9	12.74		1.88	49.76

Table 6.9 SEM-EDS chemical analyses of residual barite.

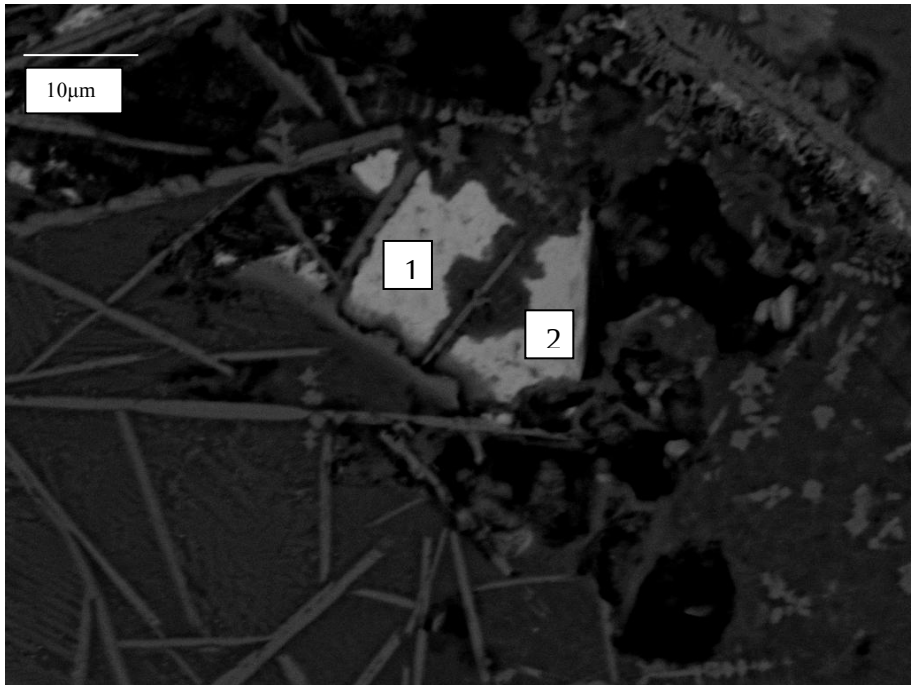

Figure 6.14 Residual barite (light grey) associated with iron oxide (grey) and iron silicate (dark grey).

6.4 Iberian samples

Figure 6.15 Sample RT 60 showing the massive, non-porous aspect of the slag and its black colour. Patinas are almost absent.

Figure 6.16 Sample RT25 L115 S60, the other surface, showing a black, glassy aspect.

Three layers of the Corta Lago section (119 – 115 – 116) are dated to the Iberian period (4th to mid-2nd century BC). Five samples analysed with different techniques, as shown in Table 6.1, were collected from layer 115 and one from layer 119. The

selected samples were of slag, litharge and semi-reacted ore. The litharge samples will be described in section 6.4.1.

6.4.1. Iberian slag samples

The slags (RT25 L115 S20 and RT25 L115 S55) in these layers are fragments of tapped slags of dark grey colour and reddish patinas (Figs. 6.15 and 6.16). The fresh fracture is black, with no macroscopic residual grains and glassy aspect.

The main components of the slags have an average composition comparable with the fayalite stability field (Fig. 6.62), close to the cotectic line at 1100 °C, bordering the field of fayalite on the side richer in iron. The two samples show different chemical characteristics: lead oxide varies between 1 and 3 wt%, sulphur varies between 0.1 and 6.3 wt% (see Table 6.10). The other metals present in the slags are copper (0.1-0.3 wt%), arsenic (between 0.2 and 2.6 wt%), and antimony (between 0.07 wt% and 0.7 wt%). Barium oxide is around 8 to 9 wt% in both samples, considerably higher than in the Phoenician samples, and tin is around 0.1 wt%, lower than in the Phoenician samples. Both these oxides are comparable in the two Iberian samples. The concentration of silver varies by one order of magnitude, from 0.01 to 0.1 wt%, in the two samples. The sulphur concentration is relatively higher than in slags from the previous periods, while the amount of silica is lower.

The two slag samples analysed (RT25 L155 S20 and RT25 L115 S55) present a mineralogical association dominated by olivine associated with pyroxene, (Ti and Mg) magnetite and residual quartz.

		Na2O	MgO	Al2O3	SiO2	P2O5	S	K2O	CaO	TiO2	MnO	FeO	BaO	PbO	SnO2	CuO	ZnO	As	Ag	Sb	Bi
		%	%	%	%	%	%	%	%	%	%	%	%	%	%	%	%	%	µg/g	µg/g	µg/g
RT25 L115 S55	Iberian	0.21	0.88	3.19	20.94	0.08	1.32	0.53	0.44	0.22	0.07	60.53	7.82	1.06	0.10	0.11	0.02	0.16	158	798	7
RT25 L115 S56	Iberian	1.65	0.94	0.62	6.11	0.01	6.27	0.29	6.93	0.11	0.02	0.26	0.02	95.16	0.17	0.67	0.03	0.31	103	3569	6880
RT25 L115 S20	Iberian	0.26	3.63	0.60	14.15	n.d.	3.49	0.20	0.51	0.03	0.08	51.90	8.98	2.74	0.07	0.32	0.03	2.63	1287	6976	n.d.
RT25 L115 S59	Iberian	2.27	1.58	0.43	4.37	0.01	0.04	0.11	3.92	0.11	0.01	0.43	0.03	99.70	0.04	0.31	0.01	0.81	61	1868	250
RT25 L119 S50	Iberian	0.25	0.49	1.72	4.82	n.d.	0.09	0.05	0.08	0.03	0.02	89.70	0.04	0.52	0.04	0.13	0.03	0.62	1141	1161	10

Table 6.10 Bulk chemical analyses of Iberian samples, measured by XRF. RT 20 and RT 55 are slag, RT 59 and 56 are litharge samples, RT 50 is a semi-reacted ore sample. The litharge samples were analysed in order to acquire a measure of the effectiveness of the process, indicated by the loss of silver.

The concentration of the main components in the two slag samples analysed is consistent with a smelting temperature calculated between 1100 and 1200 ºC. In this case though, we observe that the samples plot closer to the eutectic at 1148 ºC (optimum 2 – Charlton 2007 – Fig. 6.62) and also that the pyroxenitic phase actually crystallises in these slags, which are in fact holocrystalline. Nevertheless, we also observe residual quartz in these samples. It thus appears that the furnace was fired at a slightly higher temperature than during the previous period; in addition, the increase of sulphur indicates that there was a difference in the charge (addition of galena to the raw material) or in the shape of the furnace (height, diameter). These aspects will be further discussed later on in this chapter and in Chapter 9.

Sample RT24 L119 S50 has an iron-rich composition enriched in silver (~ 1000 ppm), and its mineralogical association is dominated by iron oxide (spinel) instead of iron silicate. The chemical and mineralogical characteristics of this sample make us infer that the sample can be identified as semi-reacted ore. Further discussion will be presented in section 6.11.2 of this chapter.

6.4.2. Iberian litharge samples

Samples RT25 L115 S59 and RT25 L115 S56 are litharge, showing a composition depleted in silver, lower than 100 ppm for sample RT25 L115 S59 and around 100 ppm for sample RT25 L115 S56, values that we should consider comparable. RT25 L115 S56 shows higher concentrations in silica, sulphur and lime (all around 5 wt%), as well as a high concentration of antimony and bismuth, confirming once again the polymetallic nature of the ores. On the other hand, sample RT25 L115 S59 does not show the same contamination in sulphur. As shown above, the sulphur content in the slag is also higher (than during the Phoenician period), indicating a change in the process or in the charge. On one hand, the possibility that lead sulphide (PbS galena) was added to the system as a source of lead, thus also increasing the amount of sulphur, has to be considered. On the other hand, however, we cannot dismiss the possibility that the furnace may have been structured differently. In particular, the furnace may have been of lower height, not allowing enough space for the separation of cation X (Pb, Ag, K, Na, NH_4) from the sulphate anion.

6.5 Republican phase I tapped slags

Figure 6.17 Three fragments of sample RT25 L6/8 S13 clearly showing the lava flow structure. The patinas, not intense, are red and white.

Figure 6.18 Sample RT25 L31 S83, showing the fine lava flow structure on the top surface, over a bulky structure with red patinas.

The first Republican phase tapped slag period includes layers 114 to 119 and layers 1 to 50, dated to the 1st century BC. The samples selected for analysis were distributed

as follows: one sample from layer 114, one sample from layer 2, three samples from layer 3, four samples from layer 6, one sample from layer 9, one sample from layer 15, one sample from layer 21, and four samples from layer 31 (Table 6.1). The visual aspect of the slags is very dark grey, with a reddish patina (Figs. 6.17 and 6.18). The fresh fracture shows a homogenous material with no macroscopically visible grains.
The main components (Table 6.11) are silica, iron oxide and alumina, all showing a variation around 10%. Lead oxide is between 1 and 5 wt%, barium oxide concentration is measured in the range 1.5 to 4.5 wt%, and for samples RT25 L31 S19 and RT25 L31 S18 it is around 16/17 wt%; this concentration is not associated with the presence of residual barite grains but with newly formed ones. Sulphur is between 0.4 and 2.1 wt%. The other metals present in the slags are: copper ~0.05/0.3 wt%; arsenic around 0.5 wt% but as high as 2.5 wt%, 4 wt% and 8 wt% respectively in samples RT25 L6/8 S13, RT25 L2 S75rtm and RT25 L3 S86rtm; antimony 0.08/0.1 wt%, except for sample RT25 L2 S75rtm (0.25%), RT25 L3 S74rtm (0.45%) and RT25 L3 S86rtm (1.4%); and tin 0.05/0.2 wt%. The concentration of silver varies between 100 and 350 ppm, where the two samples with higher silver (~ 350 ppm) correspond to the two samples with higher (~ 16/17 wt%) barium oxide (samples RT25 L31 S19 and RT25 L31 S18).
Samples RT25 L2 S75rtm, RT25 L3 S86rtm and RT25 L3 S74rtm show enrichment in arsenic, antimony and lead, while the figure for silver is still within the average. Samples RT L31 S18 and RT L31 S19 show a much higher concentration of barium oxide and no residual grains of barite, but newly formed grains are observable. The high concentration of barium oxide is not only associated with a higher concentration of silver, but also with a higher concentration of sulphur and soda. This seems to indicate the use of a different source of mineral. This aspect will be discussed further later on in this chapter.

Samples from layers 2 and 3 show higher variability in terms of their composition, mainly for iron, which in the area analyses shows a standard deviation higher than 2 (Table 6.12). Samples from layers 9 and 31 and one of the samples from layer 6 show a lower variability of iron oxide (standard deviation >1.5), and the sample from layer 9 shows an even lower variability (iron oxide standard deviation >1). Only one sample from layer 3 shows a high variability of other elements, and the standard

deviation is higher than 1 for alumina, silica, sulphur and arsenic. The variability does not appear to be correlated with the date of the slags.

Element Dimension		Na2O %	MgO %	Al2O3 %	SiO2 %	P2O5 %	S %	K2O %	CaO %	TiO2 %	MnO %	FeO %	BaO %	PbO %	SnO2 %	CuO %	ZnO %	As %	Ag µg/g	Sb µg/g	Bi µg/g
RT25 L114 S84rtm	Republican tapped phase I	n.d.	1.12	2.62	28.03	n.d.	0.40	0.51	0.28	0.31	0.10	61.39	2.30	1.38	0.10	0.05	0.01	0.27	159.05	855.19	14.93
RT25 L2 S75rtm	Republican tapped phase I	n.d.	2.06	3.27	26.91	0.11	1.14	1.12	1.07	0.25	0.04	51.88	2.62	3.00	0.17	0.11	0.02	1.61	129.76	2524.02	n.d.
RT25 L3 S74rtm	Republican tapped phase I	n.d.	2.40	2.86	22.37	n.d.	0.84	0.80	0.43	0.18	0.04	53.45	3.06	3.47	0.16	0.19	0.02	3.05	123.29	4353.83	n.d.
RT25 L3 S85rtm	Republican tapped phase I	n.d.	1.21	3.36	28.44	0.02	0.43	0.45	0.31	0.20	0.07	60.95	1.77	1.62	0.10	0.07	0.02	0.08	166.93	1211.16	14.09
RT25 L3 S86rtm	Republican tapped phase I	n.d.	3.20	1.91	20.72	n.d.	2.09	0.43	0.52	0.12	0.05	55.41	3.35	4.54	0.17	0.31	0.01	1.01	286.72	13535.15	n.d.
RT25 L6/8 S13	Republican tapped phase I	0.16	0.64	2.37	23.64	0.01	0.37	0.45	0.23	0.21	0.08	65.10	4.26	0.69	0.09	0.16	0.03	0.32	109.65	836.82	4.56
RT25 L31 S83rtm	Republican tapped phase I	n.d.	1.38	2.25	20.67	0.01	0.80	0.30	0.18	0.20	0.05	65.32	4.44	1.95	0.14	0.17	0.01	0.30	290.04	940.16	n.d.
RT25 L31 S7	Republican tapped phase I	0.17	1.49	2.66	20.61	0.02	0.85	0.31	0.21	0.20	0.05	64.91	4.15	1.91	0.14	0.16	0.01	0.29	241.55	876.61	10.44
RT25 L31 S19	Republican tapped phase I	0.30	0.73	2.17	20.48	0.03	2.05	0.33	0.35	0.13	0.11	51.50	17.23	0.82	0.06	0.10	0.02	0.16	328.53	891.03	5.26
RT25 L31 S18	Republican tapped phase I	0.22	0.67	1.87	20.05	0.02	1.75	0.31	0.19	0.14	0.10	54.14	16.31	0.77	0.06	0.11	0.02	0.20	351.65	980.47	4.09

Table 6.11 Bulk chemical analyses of Republican tapped slag samples, measured by XRF.

	RT25 L3 S86rtm		RT25 L3 S85rtm		RT25 L6 S73rtm		RT25 L6 S67		RT25 L9 S70rtm		RT25 L31 S83rtm	
	average	standard deviation	average	standard deviation	average	standard deviation	average	standard deviation	average	standard deviation	average	standard deviation
Al2O3	5.5	1.2	4.4	0.7	3.3	0.3	4.5	0.3	4.6	0.3	3.4	0.3
SiO2	31.2	1.4	30.2	0.3	36.6	0.9	36.6	2.7	31.3	1.0	24.3	0.8
P2O5	n.d.	n.d.	0.1	0.2	0.3	0.3	n.d.	n.d.	n.d.	n.d.	n.d.	n.d.
SO3	4.2	1.9	1.4	0.3	3.1	0.4	2.7	0.7	1.0	0.5	2.0	0.3
K2O	0.9	0.2	0.5	0.1	1.7	0.1	0.8	0.1	0.7	0.1	0.4	0.1
CaO	0.0	0.1	0.4	0.2	1.1	0.2	0.1	0.2	0.1	0.1	0.2	0.2
TiO2	n.d.	n.d.	0.6	0.5	0.1	0.2	n.d.	n.d.	n.d.	n.d.	n.d.	n.d.
FeO	51.6	2.8	61.4	2.0	47.0	1.5	48.0	2.5	57.7	1.2	64.8	1.5
CuO	n.d.	n.d.	n.d.	n.d.	n.d.	n.d.	n.d.	n.d.	n.d.	n.d.	0.1	0.3
As2O3	0.1	0.2	0.0	0.0	0.4	0.7	n.d.	n.d.	n.d.	n.d.	0.1	0.1
BaO	6.2	1.3	0.6	1.0	3.1	0.3	6.7	0.4	4.7	0.8	4.1	0.3
PbO	0.3	1.0	0.4	0.8	3.4	0.4	0.7	0.8	n.d.	n.d.	0.8	1.0

Table 6.12 Area analyses of Republican tapped slag measured by EDS-SEM, showing the uniformity of the samples through the calculation of the standard deviation. As discussed in the text, higher standard deviations are verified for silica and iron oxide.

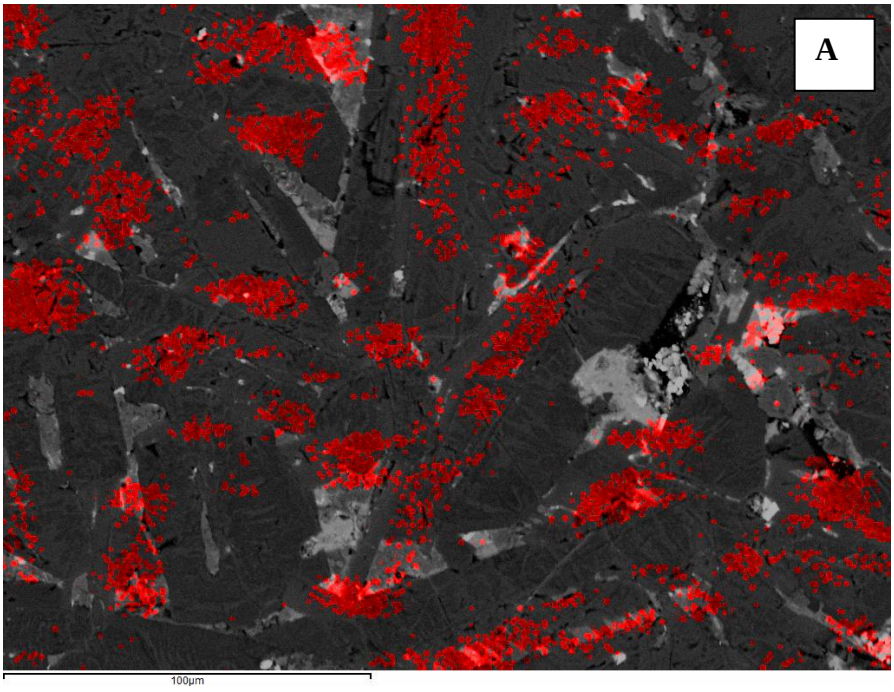
A
100µm

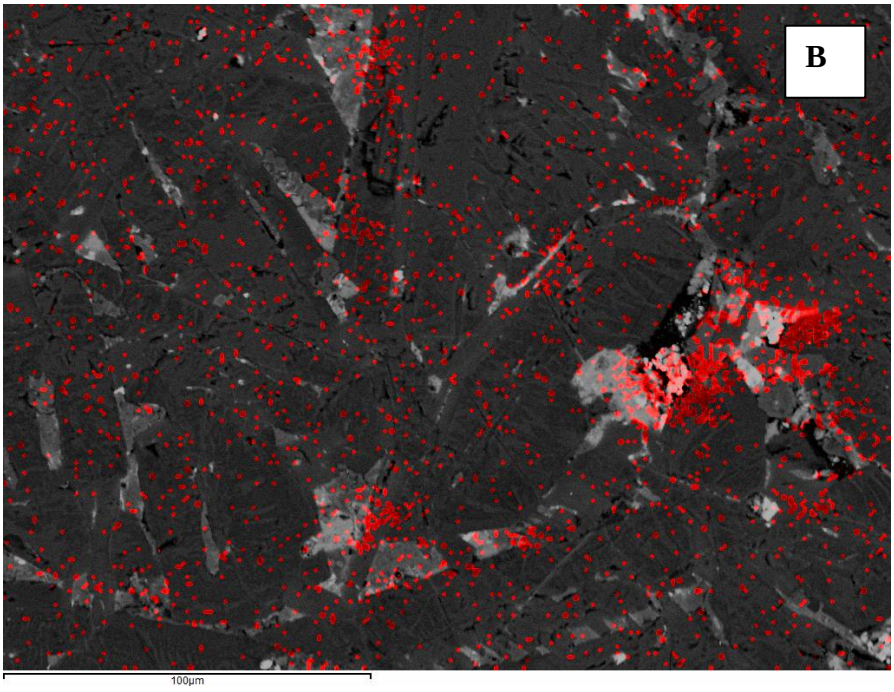
B
100µm

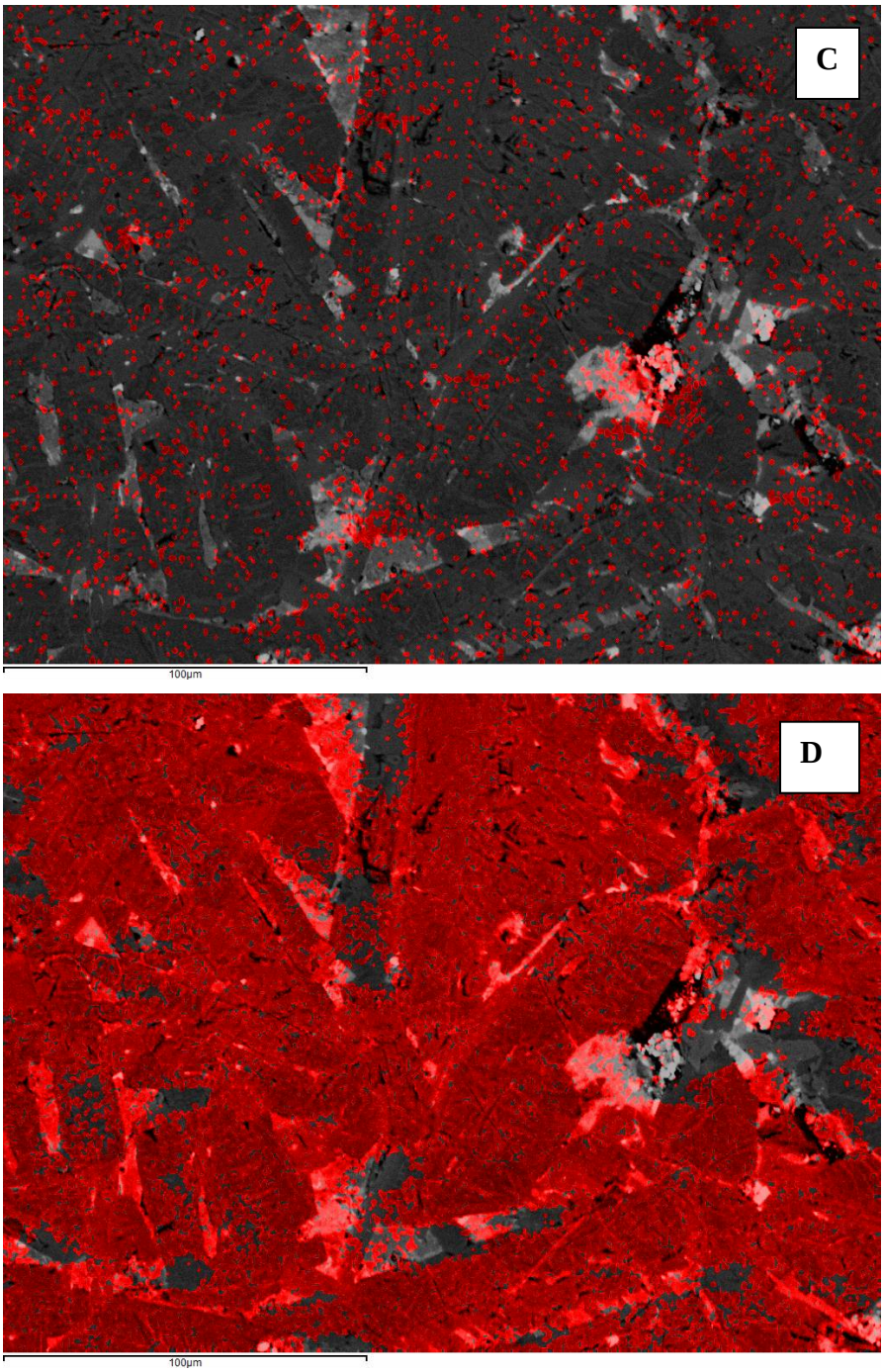

Figure 6.19 From the top: barium (A), lead (B), antimony (C) and silicon (D) chemical maps overlaid over backscattered image obtained with Scanning Electron Microscope of sample RT25 L3 S86rtm. The image shows polyhedral and hopper olivine with colour zonation, associated with iron and titanium spinel and lead/antimony bearing phases. The chemical maps show the association of lead and antimony.

The mineralogical association shows a main crystallisation of fayalite (Figs. 6.19 A to D) with no detectable trace of magnesia or lime, even though the crystals present a colour zonation in the backscattered scanning electron microscope image (Figs. 6.19A, B and C). The habit is polyhedral-hopper, with the length of the crystals around 100 µm. The other associated crystalline phases are magnetite with

polyhedral habit and Ti concentration around 0.5 wt%, and lead (and lead and iron) and barium sulphates; small droplets of silver sulphates are also detected in the same areas of the slags.

The oxygen fugacity estimated by the association fayalite/magnetite can be approximated in the range 10^{-8}-10^{-12} (Fig. 6.63).

The plot of the main components on the thermodynamic diagrams alumina/ iron oxide/ silica shows a distribution within the field of fayalite where the smelting temperature can be assessed between 1100 and 1200 °C (Figs. 6.62). The distribution shows two groups, one close to the cotectic line limiting the fayalite field on the highest concentration of iron reaching the eutectic (optimum 2), while the other is in the middle of the fayalite field, close to the 1200 °C isotherm (Fig. 6.62).

The stratigraphic layer 3 seems to be the 'watershed' between the two groups, where the more recent samples are closer to the optimum 2 cotectic, and the older ones form the group homogeneously plotting in the centre of the fayalite field. The same distinction seems to be valid for the enrichment in arsenic, lead and antimony (older samples), while the enrichment in barium and sulphur is visible in the more recent samples. These variations may be linked to a variation in the exploited ore (variations in the alkali concentrations are also visible), resulting in a variation in the process.

6.6 Republican phase II plate slags

6.6.1 Plate slag chemistry

The slags deposited in the layers from 51 to 66 are mainly of a different morphology, identified as plate slags (Figs. 6.3 and 6.4). Layer 50 was radiocarbon dated to the middle of the 1st century BC (Rothenberg and Blanco-Freijeiro 1981, 181, Harrison, R. personal communication). The fragments are bigger, with a diameter around 30 cm, and the thickness is constant, about 2/1.5 cm. The slags are dark grey with a deeper reddish patina (Figs. 6.20 and 6.21). The fresh fracture shows a homogenous grey aspect with no visible grains. The analysed samples originated from layers 52 and 55.

The main chemical components (Table 6.13) are silica, alumina and iron oxide. Lead oxide (2.5/3.7 wt%) is higher than in the second group of tapped Republican samples, while barium oxide (4.5 to 10.5 wt%) and sulphur (0.8 to 1.7 wt%) are comparable. Potash is higher than in slags belonging to the other periods, varying between 0.8 and 2.6 wt%, while phosphorous is comparable (<0.1 wt%, between 0.02 and 0.08 wt%). The other metals present in the slags are: copper (0.1 to 0.2 wt%) and arsenic (0.5 to 2.5 wt%), antimony (0.08/0.26 wt%), and tin (between 0.07 and 0.25 wt%). The concentration of silver seems to be attested in two groups: around 100/110 ppm (for samples RT25 L52 S1, RT25 L52 S4 and RT25 L55 S82rtm) and lower than 100 ppm (50 to 70 ppm) for samples RT25 L52 S79rtm, RT25 L52 S2 and RT25 L52 S3, with one outlier (RT25 L52 S17) even lower still (~ 20 ppm); considered in their ensemble, these represent the lowest concentrations observed throughout the section.

Figure 6.20 Fragment of plate slag showing the intense superficial red patina.

Figure 6.21 Bottom surface of the fragment in Figure 6.20 showing a more intense red patina.

		Na2O %	MgO %	Al2O3 %	SiO2 %	P2O5 %	S %	K2O %	CaO %	TiO2 %	MnO %	FeO %	BaO %	PbO %	SnO2 %	CuO %	ZnO %	As %	Ag µg/g	Sb µg/g	Bi µg/g
RT25 L52 S79rtm	Republican plate phase II	n.d.	1.98	2.48	20.12	0.02	1.52	0.81	1.38	0.21	0.06	54.85	10.54	2.74	0.13	0.14	0.01	0.23	46.34	1244.20	n.d.
RT25 L52 S1	Republican plate phase II	0.27	2.54	3.54	23.98	0.04	1.57	2.21	1.46	0.19	0.07	49.61	7.40	3.30	0.12	0.15	0.01	0.39	100.40	1534.17	n.d.
RT25 L52 S2	Republican plate phase II	0.31	2.71	3.41	25.02	0.03	0.81	1.61	1.33	0.17	0.05	53.39	4.48	3.67	0.24	0.14	0.02	0.43	67.47	2587.06	n.d.
RT25 L52 S3	Republican plate phase II	0.23	2.23	2.69	21.74	0.04	1.57	0.84	1.56	0.18	0.06	52.71	9.86	2.67	0.07	0.13	0.01	0.37	70.20	867.91	n.d.
RT25 L52 S17	Republican plate phase II	0.35	2.24	3.91	26.74	0.08	0.97	1.44	2.83	0.15	0.09	44.94	10.48	2.68	0.08	0.19	0.01	0.46	17.69	1397.88	n.d.
RT25 L52 S4	Republican plate phase II	0.32	1.94	3.07	26.85	0.08	1.74	2.55	1.32	0.12	0.08	45.06	8.93	2.28	0.15	0.16	0.01	0.94	101.38	2289.57	n.d.
RT25 L55 S82rtm	Republican plate phase II	0.24	2.35	3.55	24.37	0.03	1.71	1.73	1.17	0.19	0.05	49.71	7.90	3.03	0.10	0.14	0.01	0.35	112.50	1916.26	n.d.

Table 6.13.Bulk analyses of Republican plate slag samples measured by XRF.

RT25 L52 S79	average %	standard deviation	RT25 L55 S82rtm	average %	standard deviation
MgO	0.0	0.1	MgO	0.0	0.0
Al2O3	5.0	0.3	Al2O3	5.6	0.4
SiO2	29.6	1.1	SiO2	29.7	1.1
SO3	4.5	0.6	SO3	5.1	0.5
K2O	1.5	0.1	K2O	2.7	0.2
CaO	1.8	0.2	CaO	1.5	0.1
FeO	50.1	1.2	FeO	48.2	0.8
As2O3	0.0	0.0	As2O3	0.1	0.2
BaO	5.9	0.3	BaO	7.2	0.4
PbO	1.6	0.9	PbO	0.0	0.0

Table 6.14 Area analyses of Republican plate slag measured by EDS-SEM, showing the uniformity of the samples through the calculation of the standard deviation. As discussed in the text, the slightly higher standard deviations are verified for silica and iron oxide.

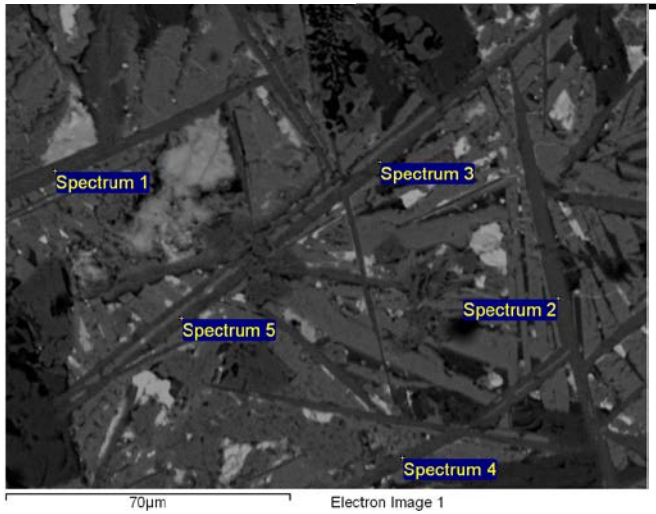

Figure 6.22 Second generation of feldspar (dark grey) crystallised over the olivine crystals (grey). Olivines show degradation of the crystals interacting with the melt, mainly in the bottom left corner of the image.

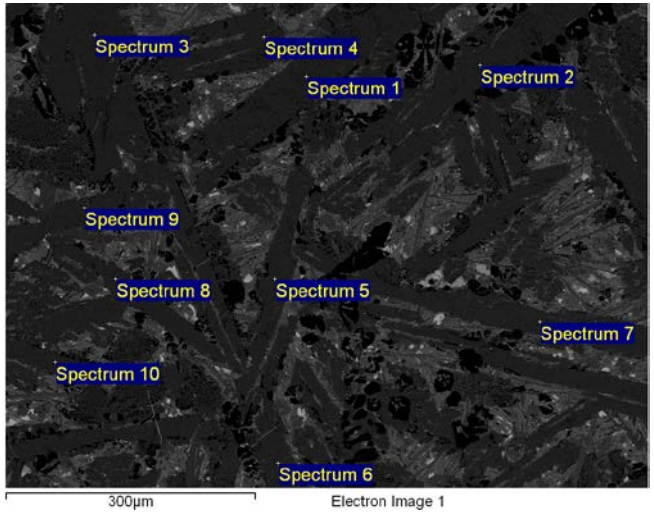

Figure 6.23 Elongated olivine (dark grey) with interstitial feldspars, and a globular barium-rich feldspar phase (black – Fig. 6.22 and Table 6.15) of second generation, visible over the olivine crystals.

Element	Weight%	Weight% Sigma	Atomic%	Compd%	Formula	Number of ions
Al K	11.28	0.17	9.22	21.32	Al2O3	1.23
Si K	26.14	0.23	20.51	55.92	SiO2	2.73
K K	17.20	0.20	9.69	20.72	K2O	1.29
Fe K	0.71	0.12	0.28	0.91	FeO	0.04
Ba L	1.02	0.20	0.16	1.14	BaO	0.02
O	43.65	0.28	60.14			8.00
Total	100.00					
					Cation sum	5.30

Table 6.15 Leucite composition (spectrum 1) of the needle-like crystals of second generation (dark grey).

Element	Weight%	Atomic%	Compd%	Formula
Mg K	0.60	0.71	1.00	MgO
Si K	14.27	14.58	30.52	SiO2
Ca K	0.32	0.23	0.44	CaO
Fe K	52.89	27.19	68.04	FeO
O	31.93	57.29		
Totals	100.00			

Table 6.16 Olivine composition (spectrum 1) of the skeletal elongated crystals of first generation (dark grey).

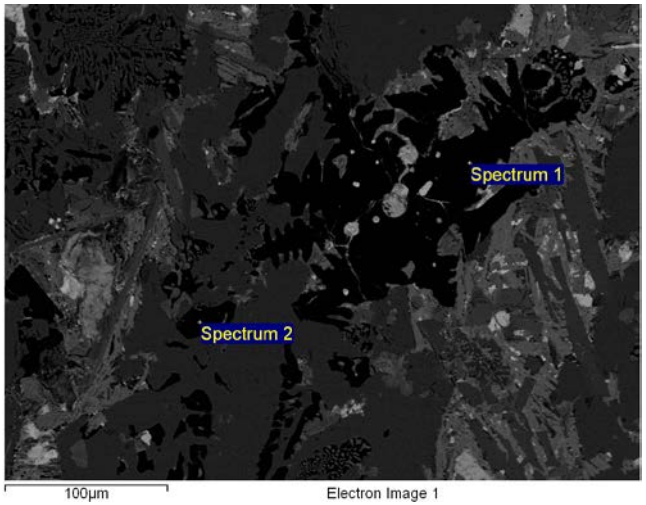

Figure 6.24 Globular barium-rich feldspar phase (black) associated with degrading olivine (dark grey).

Element	Weight%	Atomic%	Compd%	Formula
Al K	9.57	10.27	18.08	Al2O3
Si K	17.22	17.76	36.84	SiO2
K K	1.41	1.04	1.70	K2O
Ca K	0.29	0.21	0.40	CaO
Fe K	5.14	2.67	6.61	FeO
Ba L	32.57	6.87	36.37	BaO
O	33.80	61.19		
Total	100.00			

Table 6.17 EDS composition of barium-rich feldspar (spectrum 1).

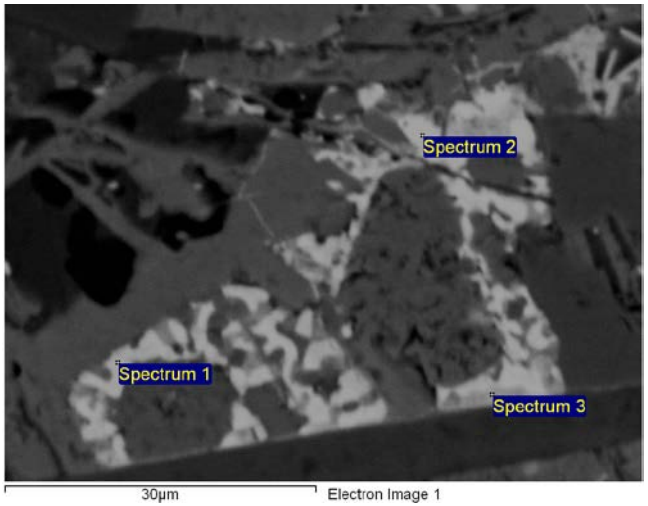

Figure 6.25 Image of residual lead sulphate 'melting' in the slag matrix.

Element	Weight%	Atomic%	Compd%	Formula
Si K	1.27	2.06	2.72	SiO2
S K	10.07	14.25	25.14	SO3
Fe K	4.51	3.66	5.80	FeO
Sn L	2.63	1.01	3.34	SnO2
Ba L	4.18	1.38	4.66	BaO
Pb M	54.15	11.86	58.34	PbO
O	23.19	65.78		
Total	100.00			

Table 6.18 Composition of residual lead sulphate (spectrum 2).

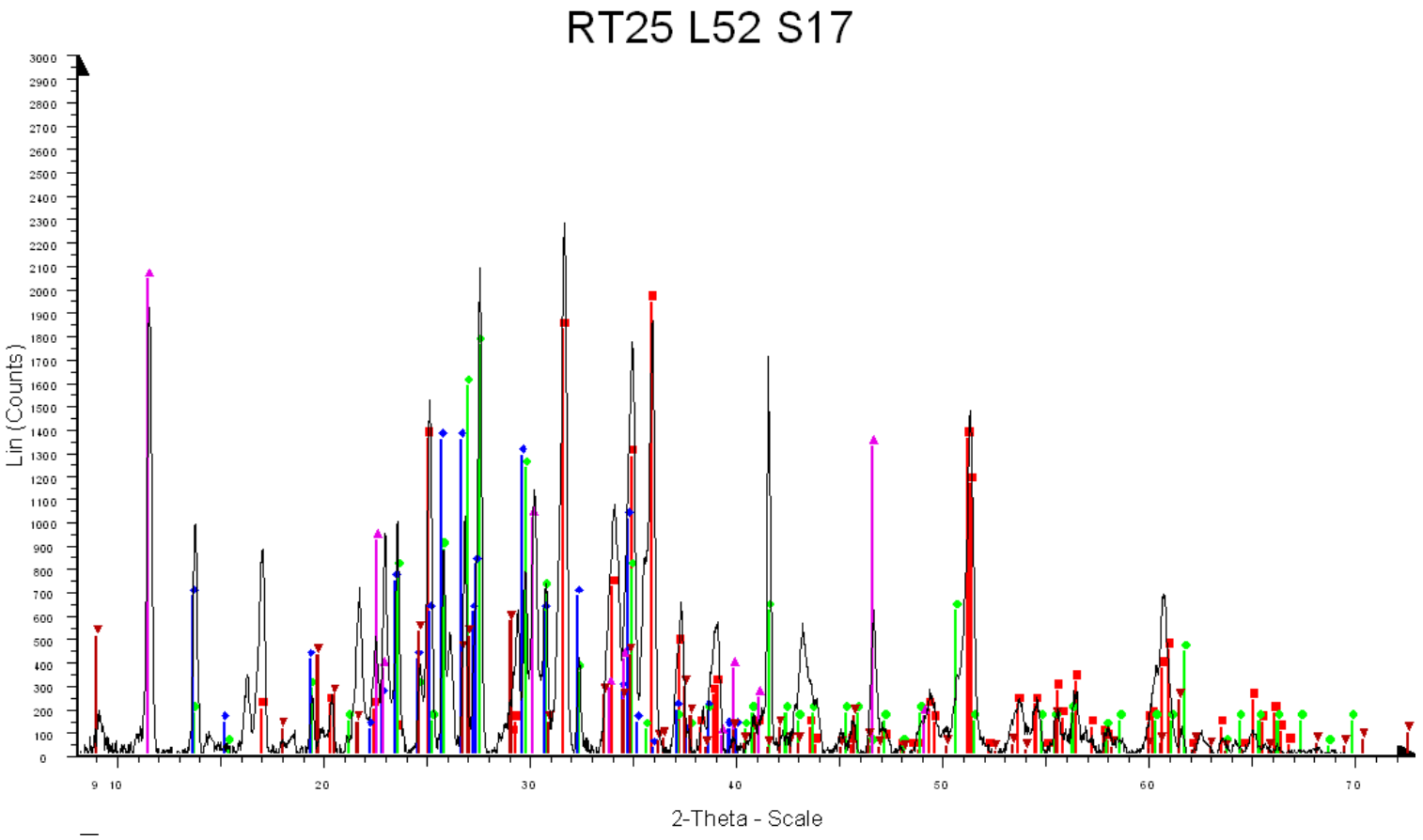

Figure 6.26 XRD pattern for sample RT25 L52 S17 showing the association of olivine and barium-rich feldspars. In details: in red fayalite, in green barian orthoclase, in blue celsian, in pink barian aluminium silicate, in dark red celadonite (see appendix 1 for the chemical composition of the mentioned minerals). The unidentified peaks belong to a hydrate phase due to alteration.

6.6.2 Area analyses and mineralogical association

The area analyses (Table 6.14) show the homogeneity of the samples; only the major components silica and iron oxide have a standard deviation around 1. This level of inhomogeneity is due to the fact that the charge was fully melted and then slowly crystallised inside the furnace, forming large crystals of iron silicate (Fig 6.23) which subsequently created a rigid structure of the system, impeding, at that point, the homogenisation of the material.

The mineralogical association encountered in these slags is dominated by the presence of fayalite (Fig. 6.23), with magnesia between 0.5 and 1 wt% and lime between 0.3 and 0.7 wt% (Table 6.16). In the central part of the slag, the crystals present an elongated but not skeletal habit around 1000 μm long and 300 μm large (Fig. 6.28). A second generation of minerals is crystallised interstitially to the olivine, overlayering them. They are elongated, measuring around 50 μm in length, and can be described by the calculated formula $KAlSi_2O_6$ (Fig. 6.22 and Table 6.15), corresponding to the feldspatoid-phase leucite,. A feldspar-like phase is crystallised overlayering the olivine, with a globular morphology. This phase corresponds to the formula $XAl_2Si_2O_8$, where X corresponds to K, Ba and Fe, and may be defined as barium-rich feldspar (Fig. 6.24 and Table 6.17), as confirmed by XRD analyses (Fig. 6.26). The metal bearing phases are sulphides (mainly pyrrhotite-like) and sulphates (mainly $PbSO_4$ – Fig. 6.25 and Table 6.18). Magnetite and tin oxide were also observed. At the surfaces, dendrites of magnetite are visible, indicating the oxidising conditions to which the surfaces were exposed during the cooling process of each layer (Figs. 6.27 and 6.29). An increase in the dimensions of the olivines is visible starting from both surfaces towards the centre. The chemical homogeneity within the samples and the increase in crystal size of the olivine towards the centre of the samples seem to indicate that the slag was completely liquid while separating from the metal in the furnace and that the high temperature and the formation of the top and bottom quenched surfaces created a good environment for the crystallisation process to continue while in the forehearth. The redox conditions enable the presence of olivine and magnetite; as a result, the oxygen pressure is estimated in the range 10^{-8} to 10^{-12} (Fig. 6.63).

The plot of the main components in the thermodynamic diagram alumina/ iron oxide/ silica shows a cloud of points within the field of fayalite, so that the smelting

temperature can be estimated between 1100 and 1200 °C (Fig. 6.62). The points can be divided into two groups, very similar to the ones described for the Republican phase I tapped slag. In this case however, there is no stratigraphic difference between the samples, since they all came from layer 52 except for sample RT25 L55 S82rtm, which is not distinguishable by any chemical peculiarities.

RT25 L52 S79rtm and RT25 L52 S3, the samples that show the highest concentration of iron, do not show enrichment in any other metal, as was observed for the samples from the previous period (barium and sulphur). The higher silver seems to be associated to high potash, sulphide and barium, between 7.5 and 9 wt%. Such a combination of high potash and high barium seems to indicate a different ore source. The high sulphur may also indicate, as seen for the Ibero-Punic samples, an addition of lead sulphide (galena) to the system to enrich the concentration of lead, or it may correspond to a change in the height of the furnace. A shorter furnace would decrease the space available for the sulphate to separate, and thus more sulphur would remain trapped in the system. The addition of lead sulphide may be a better hypothesis in this case, since the higher potash may indicate a jarosite poorer in lead, as will be further discussed in Chapters 8 and 9. For the Republican plate slag samples, the potash concentration is much higher as compared to the Ibero-Punic samples, so that the same hypothesis may not apply to the material from that period.

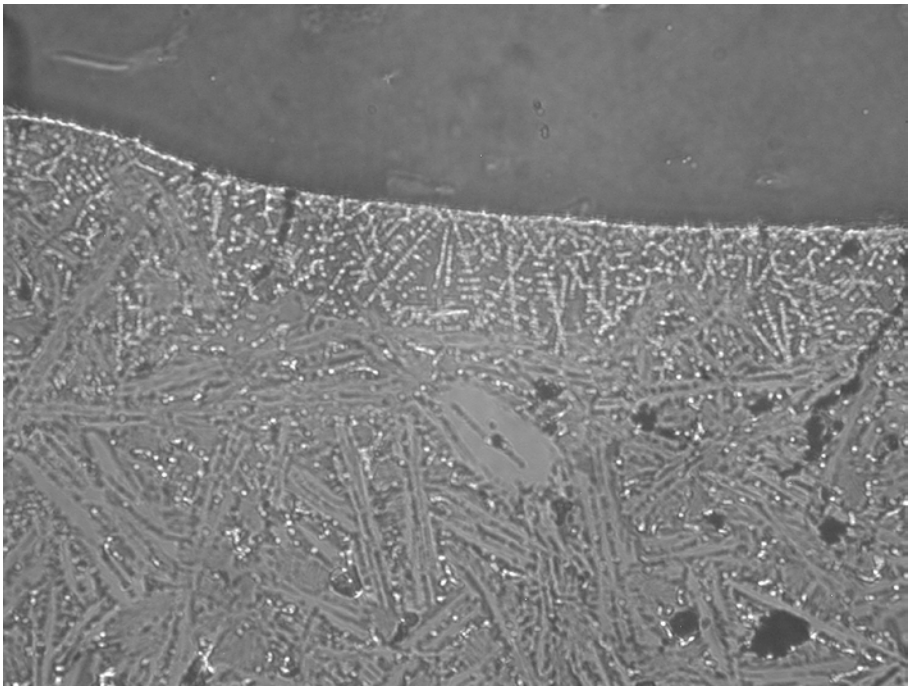

Figure 6.27 Top surface of plate slag RT25 L52 S100 showing the oxidation layer

(iron oxide – white) running all along the surface, associated to perpendicular crystallisation of dendritic iron oxide (white). The olivine crystals (grey) have mainly a skeletal-acicular morphology.

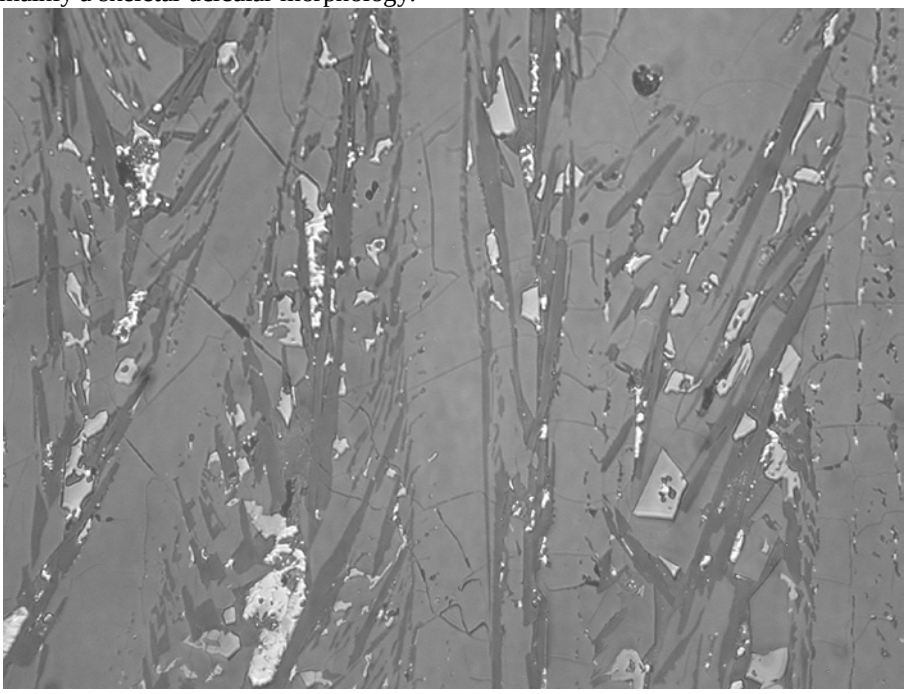

Figure 6.28 Image of an area in the middle of the plate slag RT25 L52 S100. The scale is the same as for Figures 6.27 and 6.29, and it is clearly noticeable that the size of the crystals is much larger, even though for the olivine (grey) we still observe an elongated morphology. In this case, the iron oxides are interstitial and show a tendency towards euhedral habit (light grey).

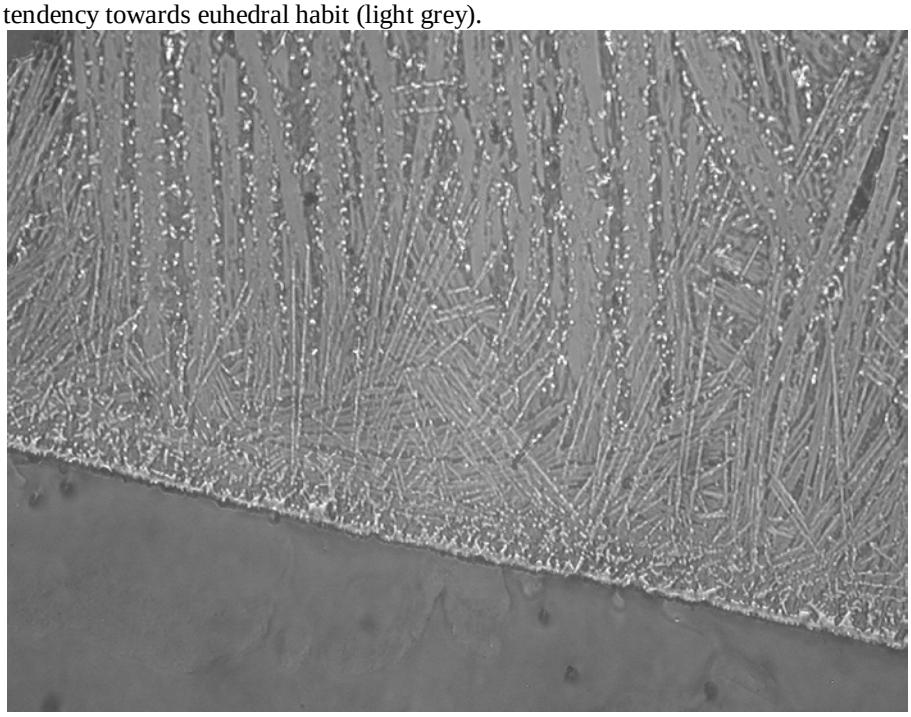

Figure 6.29 Area on the bottom surface of plate slag sample RT25 L52 S100 showing olivine (grey) elongated crystals longer than on the top surface and presenting perpendicularity with the cooling surface. The iron oxides (white) show a

layer along the surface, followed by a layer of diffused globules from which a spinifex assemblage of oxides departs, overlayering the olivine crystals. Going towards the middle of the slag, the oxides become interstitial to the olivines.

6.6.3 Cooling process hypothesis

Macro-morphologically the top surface of the plate slag can be described as a thin smooth crust almost detached from the body of the slag (Fig. 6.4) indicating a very rapid cooling of the surface in contact with the air. The bottom surface (Fig. 6.5) on the other hand, does not present these fast cooling features but is rougher, indicating a possible contact with a rougher surface, possibly the soil at the bottom of the forehearth.

The microscopic evidences show an intense oxidation layer on the top and bottom surfaces of the slag (Figs. 6.27 and 6.29) and, as already mentioned, an increase in size of the crystals in the central part of the slag itself (Fig. 6.28), due to the slower cooling speed in the central area of the slab of melted material.

There are no visible inclusion neither of metal nor of soil particles in the bottom part of the slag and this makes it difficult to point out what kind of substrate was the forehearth constituted of: soil or the actual metal produced in the furnace tapped with the slag and concentrated on the bottom of the “puddle” of melted material. The roughness observed on the bottom surface points towards the hypothesis that the slag was tapped onto the soil and not onto the metal, hence we can infer that the metal was probably left to collect inside the furnace.

Once partially or completely solidified the slag could have been removed from the forehearth living a space for the next step of tapping. This would make the plate slag just a category within the tapped slag, but still indicates a different “metallurgical school” adhering to a different “technological choice”.

6.7 Republican phase III tapped slag

Figure 6.30 Fragment of tapped slag showing intense red patina and lava-flow morphology.

From layer 67 to layer 90 a new deposition of tapped slags, still dated as Republican, is encountered. The fragments (Fig. 6.30) are bigger than in the previous tapped slag Republican phases, around 10 cm thick, and they present the typical 'lava-flow' structure of tapped slag, with flows around 1 cm in diameter. They are dark grey with reddish patina. The fresh fracture is black with no visible grain.

The main chemical compounds (Table 6.20) are silica, alumina and iron oxide, and they vary less than during the previous periods. Lead oxide (~1 wt%), barium oxide (~3 wt%) and sulphur (~0.6 wt%) are lower than during the previous periods. The other metals present in the slag have the following concentrations: copper 0.08/0.09 wt%, arsenic ~0.2 wt%, antimony 0.1 and 0.2 wt% and tin 0.09 wt%, all of them lower than during the previous periods. The concentration of silver is around 50 and 500 ppm respectively in samples RT25 L72 S72rtm and RT25 L87 S77rtm.

The area analyses (Table 6.21) show a high variance of iron oxide (standard deviation >3) and a standard deviation higher than 1 for silica and barium oxide.

The mineralogical association shows pure fayalite with neither detectable magnesia, nor lime, with a first family of skeletal-hopper olivine around 500 per 200 μm, and a

second with elongated euhedral habit around 300 μm long and 100 μm wide. The crystals present a colour zonation in backscattering images (Fig. 6.31 and Table 6.19). A difference in brightness (colour zonation) within a crystal, determined in backscattering mode, should be due to differences in atomic number in the chemical composition. In this case however, the colour zonation does not seem to have any chemical counterpart. The associated phases are iron sulphide, lead and barium sulphates, lead and iron oxides, and magnetite (Fig. 6.32).

The redox conditions allowed the crystallisation of fayalite and magnetite, so the oxygen pressure can be estimated to be in the range 10^{-8} to 10^{-12} (Fig. 6.63).

The main compounds plotted in the thermodynamic diagram alumina/ iron oxide/ silica (Fig. 6.62) fit in the fayalite field, and the smelting temperature can be estimated to have been between 1100 and 1200 °C. One of the samples plots on the cotectic linked to optimum 1 and the other in the centre of the fayalite field, following a pattern already observed for the Phoenician samples. The more recent of the two samples is the one at the centre of the field, while the older one is the one on the cotectic.

We need to bear in mind that during this period we observe a return to free tapping of the slag instead of producing plate slag by tapping the fluid material in a pit.

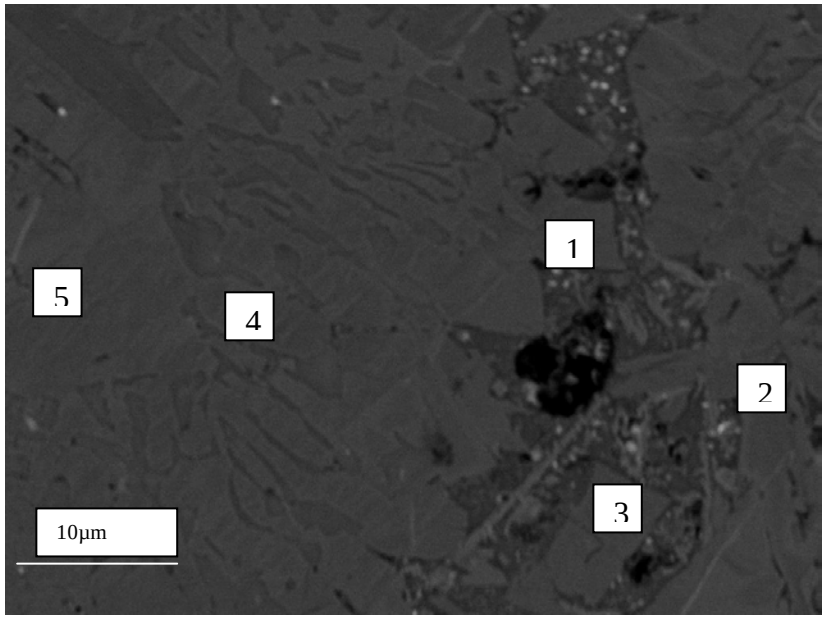

Figure 6.31 SEM backscattering image of olivine aggregates showing fine colour zonation in the polyhedral crystals (area 5).

	O	Si	Fe
spectrum 1	28.11	14.18	57.71
spectrum 2	30.84	14.95	54.21
spectrum 3	29.56	14.59	55.85
spectrum 4	30.17	14.88	54.95
spectrum 5	31.11	14.68	54.21

Table 6.19 SEM-EDS analyses of the olivines represented in Figure 6.31, showing a purely fayalitic composition despite the colour zonation visible in the backscattering imaging.

		Na2O	MgO	Al2O3	SiO2	P2O5	S	K2O	CaO	TiO2	MnO	FeO	BaO	PbO	SnO2	CuO	ZnO	As	Ag	Sb	Bi
		%	%	%	%	%	%	%	%	%	%	%	%	%	%	%	%	%	µg/g	µg/g	µg/g
RT25 L72 S72rtm	Republican tapped phase III	n.d.	0.85	2.70	27.41	n.d.	0.64	0.62	0.19	0.30	0.11	60.49	3.77	1.10	0.09	0.09	0.01	0.20	448.82	917.07	17.45
RT25 L87 S77rtm	Republican tapped phase III	n.d.	0.82	3.04	36.81	0.10	0.55	0.85	0.22	0.31	0.17	51.93	2.51	0.86	0.09	0.08	0.01	0.21	54.73	2744.24	19.90

Table 6.20 Bulk analyses performed by XRF.

RT25 L72 S72rtm	average %	standard deviation
Al2O3	5.7	1.3
SiO2	34.1	0.7
SO3	1.9	0.9
K2O	0.9	0.3
CaO	0.0	0.1
TiO2	0.1	0.2
FeO	53.5	3.3
BaO	3.7	1.2
PbO	0.1	0.4

Table 6.21 Area analyses measured by EDS-SEM of Republican phase I tapped slag sample RT72RTM, showing the uniformity of the sample according to the calculation of the standard deviation. As discussed in the text, the high standard deviation for iron oxide is due to the crystallisation of polyhedral/hopper olivines.

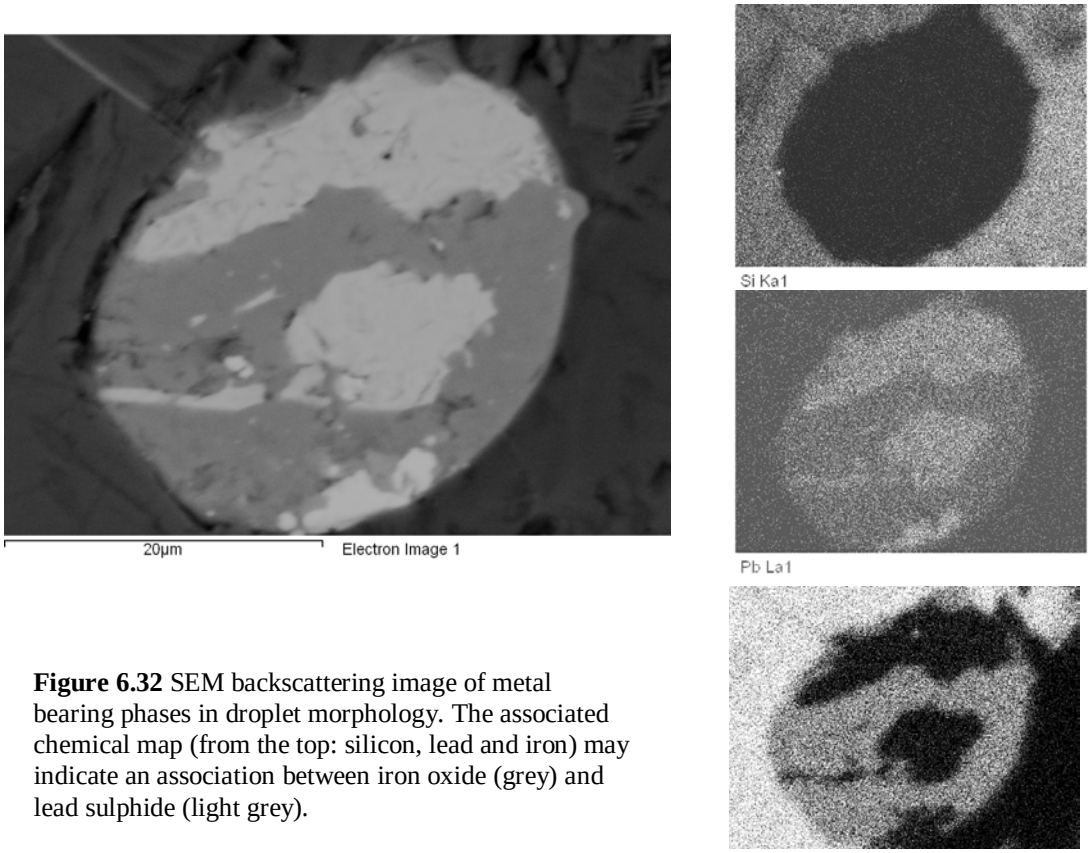

Figure 6.32 SEM backscattering image of metal bearing phases in droplet morphology. The associated chemical map (from the top: silicon, lead and iron) may indicate an association between iron oxide (grey) and lead sulphide (light grey).

6.8 Imperial samples

Figure 6.33 Fragments of slightly vesicular tapped slag. The external surfaces are affected by an intense orange/red patina, and the fresh fractures show porosity with increased size and elongated shape, oriented following the surfaces.

The top 9 layers of the section are identified as Imperial, dating up to the 2nd century AD, when the section is truncated by a wall beyond which there is no more metallurgical debris. The samples are mainly fragments (Fig. 6.33) of slag of around 5 to 3 cm in thickness (Fig. 6.34), and the lava structures are larger than the ones visible in the Republican tapped slags: they are around 2 cm wide instead of 1 cm, as measured for the Republican tapped slags. One of the samples is identified as lead bullion (carbonatised) and will be described in section 6.8.1.

Photographs taken by Paul Craddock during the excavation show the huge fragments of tapped slag as they were discovered, and provide an indication of the original thickness of the slag, around 20 cm or more (Figs. 6.34 and 6.35)

Figure 6.34 Tapped slag heap fragment as excavated. The scale is divided in units of 10cm (Photograph by Paul Craddock)

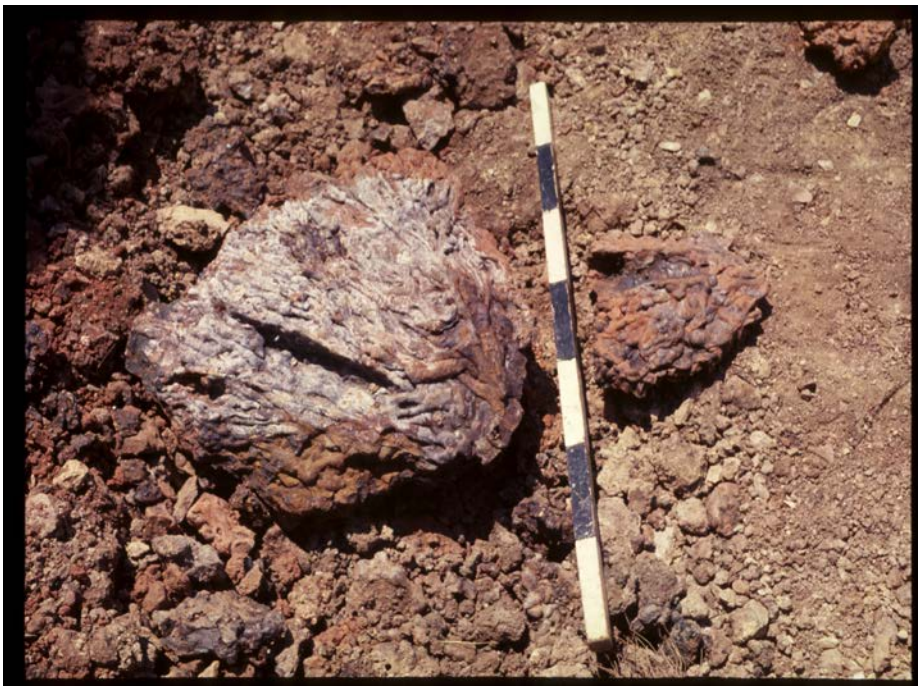

Figure 6.35 Tapped slag heap fragment as excavated, top view. The scale is divided in units of 10cm (Photograph by Paul Craddock)

The main compounds (Table 6.22) are silica, alumina and iron oxide, with a variance that is more than double as compared to the samples from the Republican phase III tapped slag period. Lead oxide (2-4 wt%), barium oxide (3-7 wt%) and sulphur (2-5 wt%) vary more than in the previous periods, and also have a higher average concentration. The other metals also show higher variance than in the previous periods: copper (0.1-0.2 wt%) and tin (0.1-0.2 wt%) are comparable in terms of their average concentrations with slags from previous periods. Arsenic (0.7 to 4 wt%) and antimony (0.2 to 0.7 wt%) are higher as compared to all the previous periods. The concentration of silver varies between 100 and 200 ppm.

		Na2O	MgO	Al2O3	SiO2	P2O5	S	K2O	CaO	TiO2	MnO	FeO	BaO	PbO	SnO2	CuO	ZnO	As	Ag	Sb	Bi
		%	%	%	%	%	%	%	%	%	%	%	%	%	%	%	%	%	µg/g	µg/g	µg/g
RT24 S2	Imperial	0.25	2.15	3.62	21.58	0.03	1.35	0.94	1.17	0.18	0.06	52.50	7.33	2.75	0.08	0.21	0.02	1.35	82.82	2102.10	n.d.
RT24 S3	Imperial	0.15	1.45	2.38	24.23	0.11	1.59	0.81	0.84	0.16	0.04	49.03	4.47	1.75	0.14	0.13	0.02	3.71	54.68	5429.70	n.d.
RT24 S4	Imperial	0.18	2.67	2.09	26.21	0.07	0.68	0.74	0.79	0.21	0.03	47.84	2.64	3.64	0.19	0.11	0.03	3.96	89.72	3944.34	n.d.
RT24 S5	Imperial	0.30	3.17	3.22	26.21	0.01	2.19	0.78	0.55	0.34	0.05	46.20	4.15	3.91	0.26	0.17	0.03	1.70	262.06	6782.44	n.d.
RT24 S6	Imperial	0.21	1.90	1.77	33.80	n.d.	0.65	0.65	0.37	0.23	0.07	48.71	2.95	2.55	0.16	0.10	0.01	1.61	90.90	6158.86	n.d.

Table 6.22 Bulk analyses performed by XRF.

	average	standard		average	standard
RT24 S1	%	deviation	RT24 S6	%	deviation
Al2O3	2.0	1.8	Na2O	0.0	0.1
SiO2	12.3	7.0	Al2O3	3.1	0.3
K2O	0.2	0.4	SiO2	46.7	1.3
CaO	0.0	0.1	SO3	1.7	0.5
TiO2	0.1	0.3	K2O	0.9	0.1
FeO	15.3	16.7	CaO	0.3	0.1
CuO	1.0	0.8	TiO2	0.1	0.2
As2O3	1.3	1.0	FeO	43.4	2.3
Ag2O	0.1	0.4	As2O3	0.1	0.2
Sb2O3	12.3	6.6	Sb2O3	0.1	0.2
BaO	0.4	1.2	BaO	2.0	0.5
PbO	54.7	24.7	PbO	1.6	0.7

Table 6.23 Area analyses performed by EDS-SEM, showing the averages and the standard deviations resulting from five area analyses.

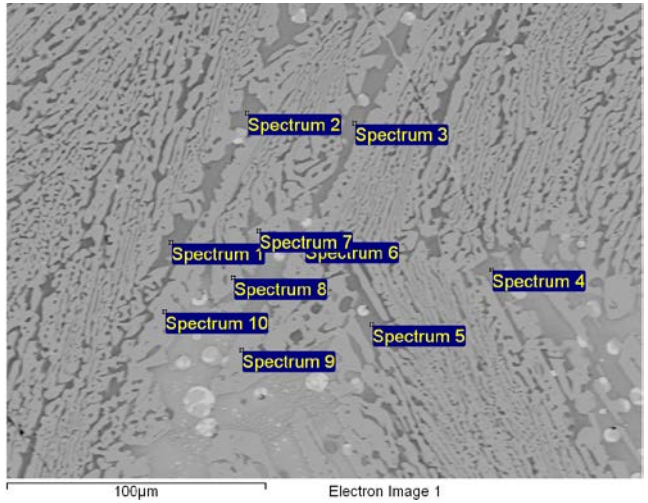

Figure 6.36 Skeletal H-chains olivine (light grey) associated with droplets of metal-bearing phases (bright white) and an interstitial glassy matrix (dark grey) – sample RT24 S6.

Element	Weight%	Atomic%	Compd%	Formula
Na K	0.29	0.28	0.39	Na2O
Al K	4.06	3.34	7.68	Al2O3
Si K	34.72	27.45	74.28	SiO2
K K	2.72	1.55	3.28	K2O
Ti K	0.28	0.13	0.47	TiO2
Fe K	5.49	2.18	7.07	FeO
Ba L	4.40	0.71	4.91	BaO
Pb M	1.78	0.19	1.92	PbO
O	46.24	64.17		
Total	100.00			

Table 6.24 Composition of the glass matrix interstitial to the olivine crystals, sample RT24 S6.

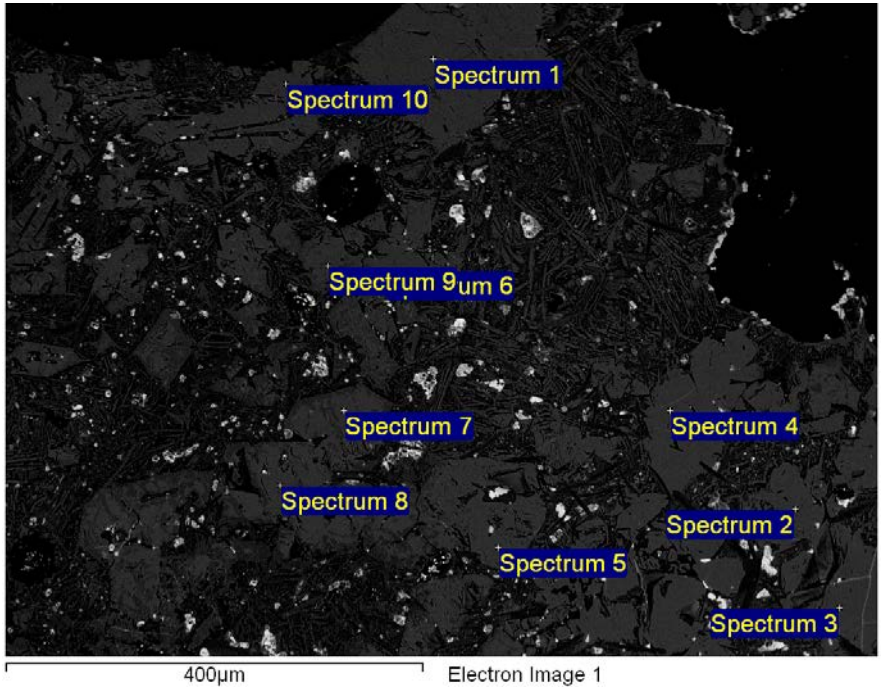

	O	Na	Al	Si	S	K	Ca	Ti	Fe	As	Sb	Ba	Pb
spectrum 1	43.44	0.24	0.77	17.91		0.66		0.16	36.83				
spectrum 2	42.3		0.93	18.36		0.71			36.65			0.72	
spectrum 3	40.04		0.89	18.11		0.79			39.3			0.87	
spectrum 4	43.69		0.86	18.02		0.63		0.19	36.62				
spectrum 5	45.07		0.78	16.36		0.55		0.15	33.2	2.57	0.82		0.5
spectrum 6	42.87		0.8	17.05		0.59		0.18	35.26	2.16	0.61		0.49
spectrum 7	44.34		0.89	18.37		0.66			34.67			0.68	0.38
spectrum 8	44.03	0.13	1.1	18.63	0.2	0.55			33.3	0		1.27	0.8
spectrum 9	42.89		0.86	16.92		0.54	0.12	0.23	35.09	1.9	0.98		0.45
spectrum 10	44.92	0.13	0.96	17.79		0.62	0.13		33.09	0.95	0.4	0.58	

Figure 6.37 and **Table 6.25** Hopper/polyhedral olivines (grey) associated with metal-bearing phases (white) and skeletal/needle-like second generation of olivine with the same composition as the polyhedral ones. This is another area of sample RT24 S6.

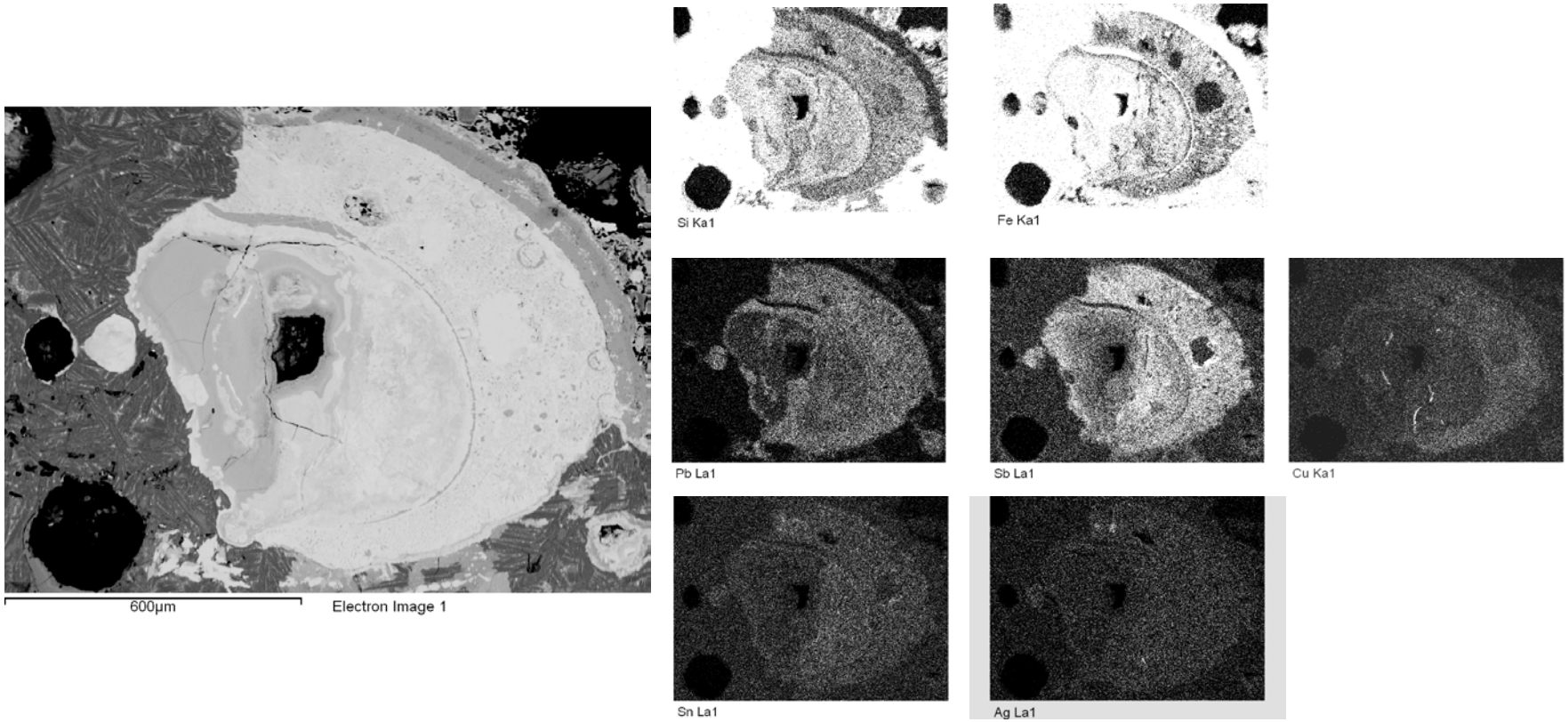

Figure 6.38 Backscattering image of a metal-bearing phase and associated chemical maps. Distinction between the areas rich in iron and the ones enriched in the other metals is visible, as well as the association mainly of lead and antimony, while copper and silver segregate in preferential droplets. Sample RT24 S6.

The area analyses (Table 6.23) of slag sample RT24 S6 show a high variance for iron and silica within the samples, with a standard deviation always higher than 1. This reflects the same behaviour as that of the samples from the Republican phase III tapped slag period.

The mineralogical association is dominated by fayalite (Fig. 6.37) with magnesia around 0.2 wt% and lime around 0.1/0.4 wt% for hopper/polyhedral olivine (Table 6.25), while neither magnesia nor lime are detected in the second generation of interstitial skeletal olivines (Fig. 6.36 and Table 6.24). The habit of the olivine is polyhedral (around 200 by 200 μm) and skeletal elongated in fairly big sizes (1000 by 300 μm). Interstitially, as already mentioned, we observe a second generation of olivine, and feldspatoid-like acicular crystals ($XAlSi_2O_6$, where X is Ba, K, Fe, and Na) are also observable. The metal-bearing phases (Fig. 6.38) are magnetite with very high titanium, between 5 and 8 wt%, higher as compared to the previous periods, and iron, copper, tin, antimony and lead sulphate with different compositions. Two different sulphides are detected associated to each other, a lead sulphide with iron around 2.5/3 wt%, tin around 2% and antimony around 0.5/1 wt%, and an iron sulphide with copper up to 8 wt%.

The association fayalite/magnetite indicates fugacity of oxygen in the range of 10^{-8} to 10^{-12} (Fig. 6.63).

The comparison between the concentration of the main components of the slags and the thermodynamic diagram alumina/ iron oxide/ silica shows a homogeneous cloud of points fitting in the field of the fayalite around the isotherm at 1200 ºC. Two points, RT24 S6 and RT24 S2, are outside the homogeneous field, but still within the fayalite field, the former on the cotectic close to optimum 1, and the latter in the middle of the fayalite field. The smelting temperature can thus be calculated between 1100 and 1200 °C (Fig. 6.62). The two outliers, RT24 S2 and RT24 S6, present respectively the highest and the lowest concentration of barium, a comparable concentration of lead (medium as compared to the other samples), and the lowest arsenic content. The concentrations of arsenic and antimony, higher on average than in the previous periods, seem to suggest that the mixture of ore used in the charge during this period was different, possibly consisting of jarosite plus sulphides and arsenates, associated or not with galena.

6.8.1. Lead Bullion

Sample RT24 S1 is not a slag, and can be identified as degraded lead bullion. The sample is mainly composed of lead carbonate (Fig. 6.39), an alteration product of lead metal (still present in the sample). Between the grains, prills of silver and antimony with eutectic texture are visible (Figs. 6.40 and 6.43). Also, a skeletal phase (Figs. 6.40, 6.41 and 6.43) enriched in iron and antimony is associated with the lead-bearing phase, even more visible in the areas where the lead is still in its metallic form. Large prills (Figs. 6.41 and 6.44 and Table 6.26) of metallic bismuth distinct from larger droplets of lead are detectable in the sample. This sample is a fortunate recovery of a fragment of the final product of the smelting at Corta Lago. The amounts of copper, antimony, bismuth and mainly silver present in the sample provide us with an insight into the tenor of metals in the raw jarositic ore. In this case, the heterogeneity of the sample (Figs. 6.40, 6.41 and 6.45) and the presence of inclusions (Fig. 6.50 and Table 6.32) indicate the SEM-EDS as best analytical method. The heterogeneity is due mainly to the presence of charcoal dust particles associated with the metal, which was possibly 'hidden' in a colder corner at the bottom of the furnace, where it incorporated charcoal dust and other particles.

The results obtained in lead carbonate areas of the sample indicate that the amount of silver in the lead bullion was around 0.2% (Table 6.27). The amount of silver in the phase still enriched in lead metal, without considering the antimony- and bismuth-rich phases, has a value one order of magnitude higher (2.7%, Table 6.28, Fig. 6.46 and 3.5% in Table 6.29, Fig. 6.47) than the composition measured in the altered carbonatised areas. This very high value of silver, recalculated at least at 20,000 g/ton (or 2 wt%) of lead, is unmatched in ancient silver production. The value is calculated using only the amount of silver in the carbonatised areas of the bullion (Fig. 6.49 and Table 6.31), while the sample is actually constituted of area richer in the precious metal (Fig. 6.48 and Table 6.30). Being the sample so heterogenous though and being only one sample, it is preferred to estimate the amount of silver at the minimum measured by the analysis.

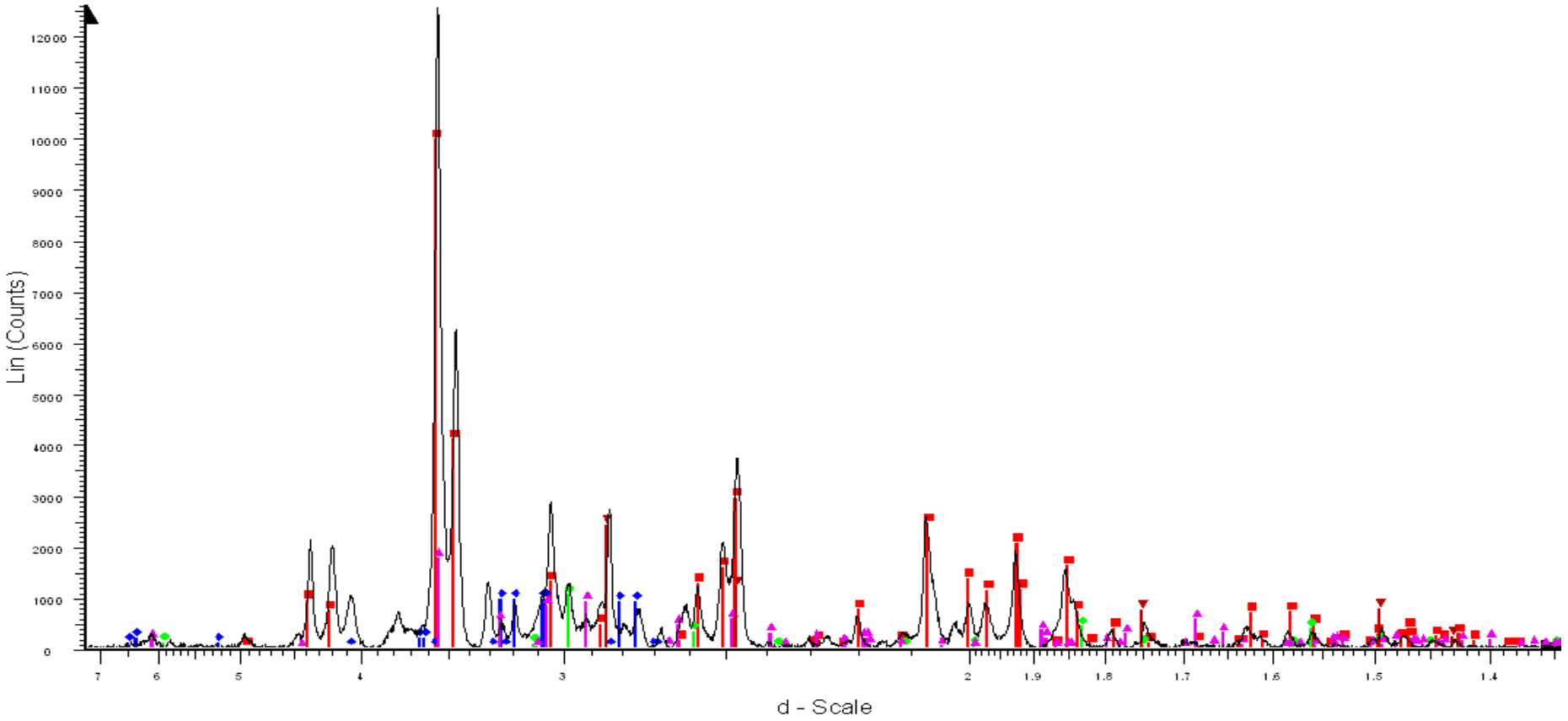

Figure 6.39 XRD spectrum of sample RT24 S1 showing Lead carbonate (red) as main compound asssociated with bismuth, antimony and silver oxides (blue, green and pink) and metallic lead (dark red).

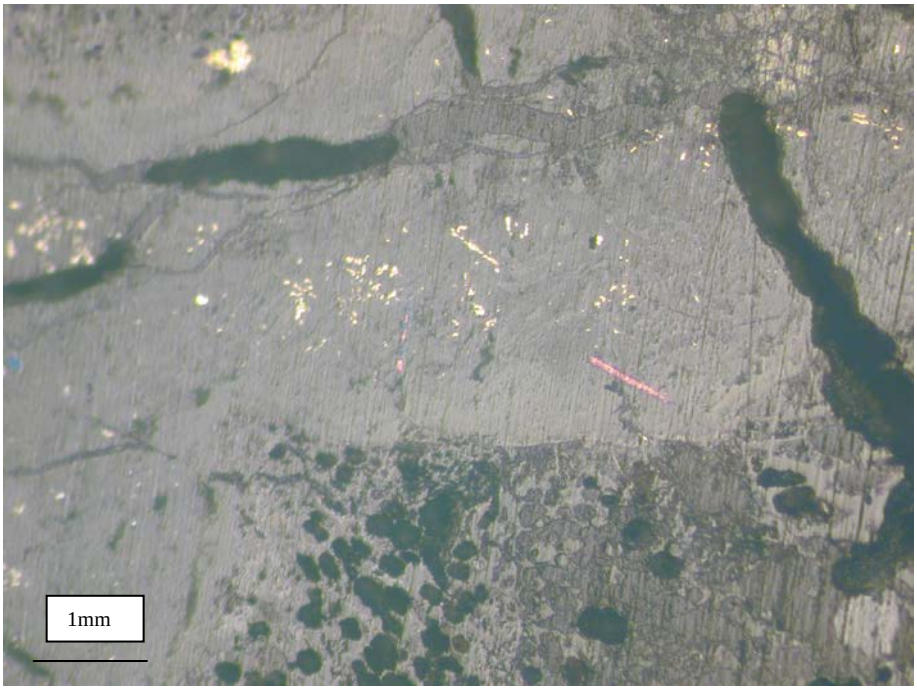

Figure 6.40 Optical microscope image (10x) of sample RT24 S1 showing eutectoid antimony/silver alloy droplets within the lead carbonate matrix. Ovoid charcoal is visible on the bottom part of the image.

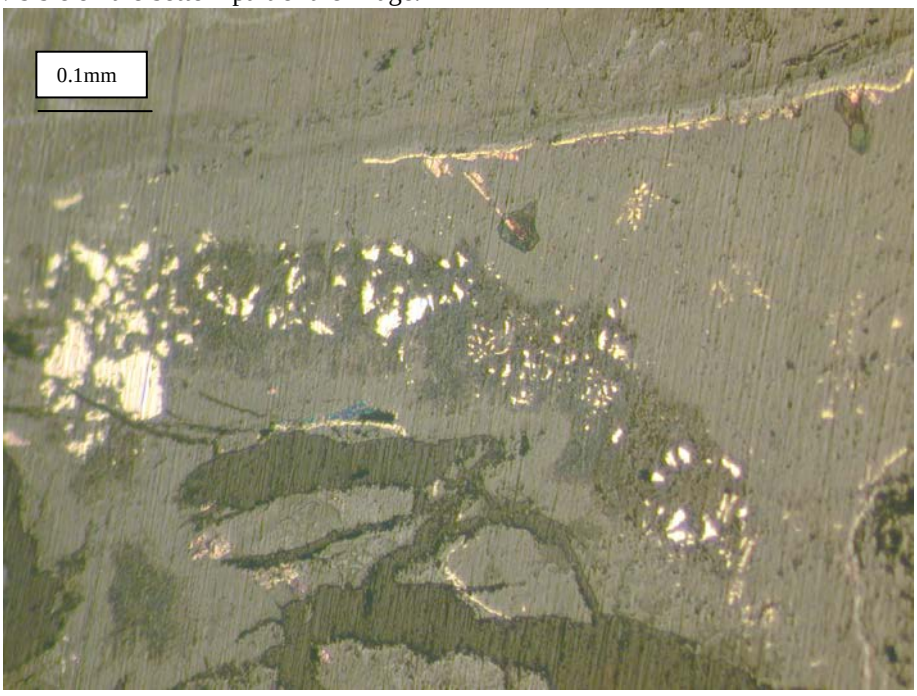

Figure 6.41 Detail (20x) of the antimony/silver alloy droplets.

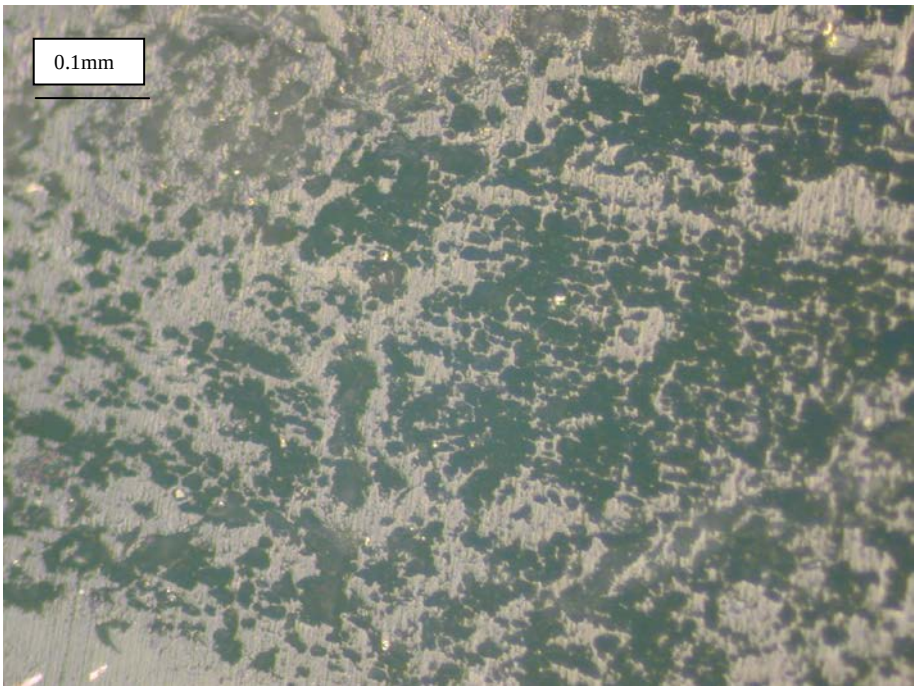

Figure 6.42 Detail of an area (20x) where the lead metal (light grey) is better conserved (with degraded oxidised portions and pitting due to the polishing – black roundish areas).

Figure 6.43 Detail (20x) of needle-like copper antimonide associated with the lead.

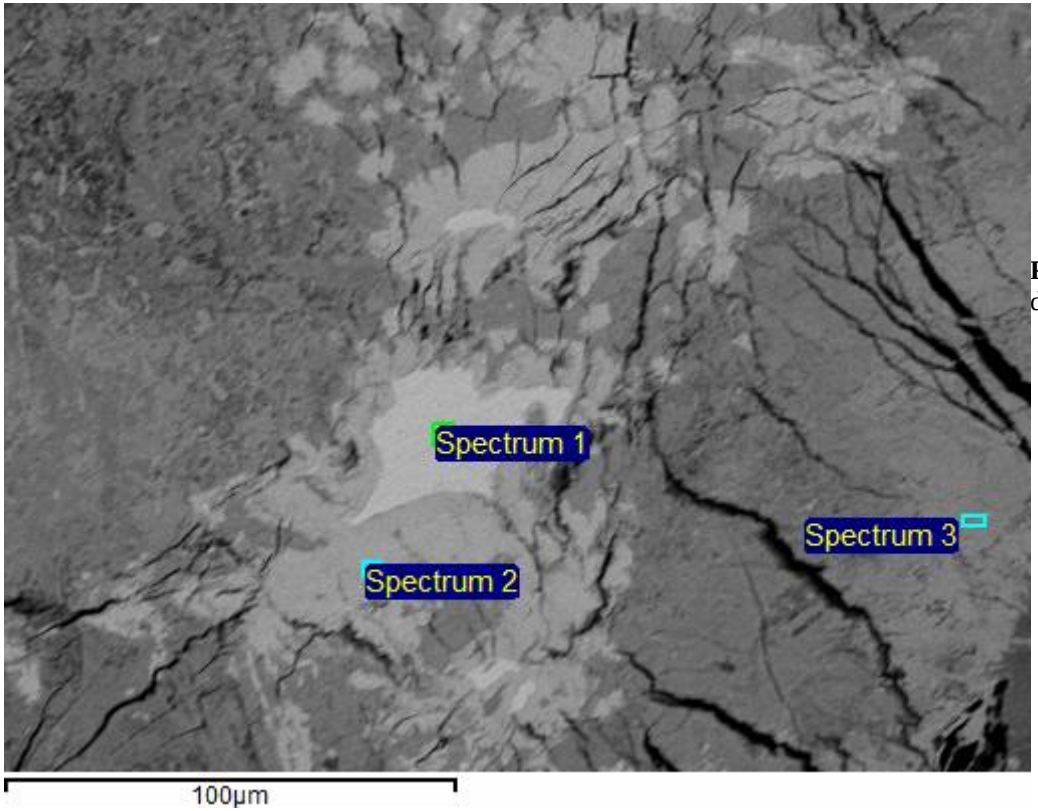

	O	Ag	Sb	Pb	Bi
Spectrum 1	5.15	n.d.	6.69	1.00	87.05
Spectrum 2	16.11	0.38	2.18	0.73	80.59
Spectrum 3	26.53	n.d.	7.97	63.85	1.77

Figure 6.44 and **Table 6.26** SEM back scattering image and EDS chemical data showing the association of a bismuth-rich phase with lead.

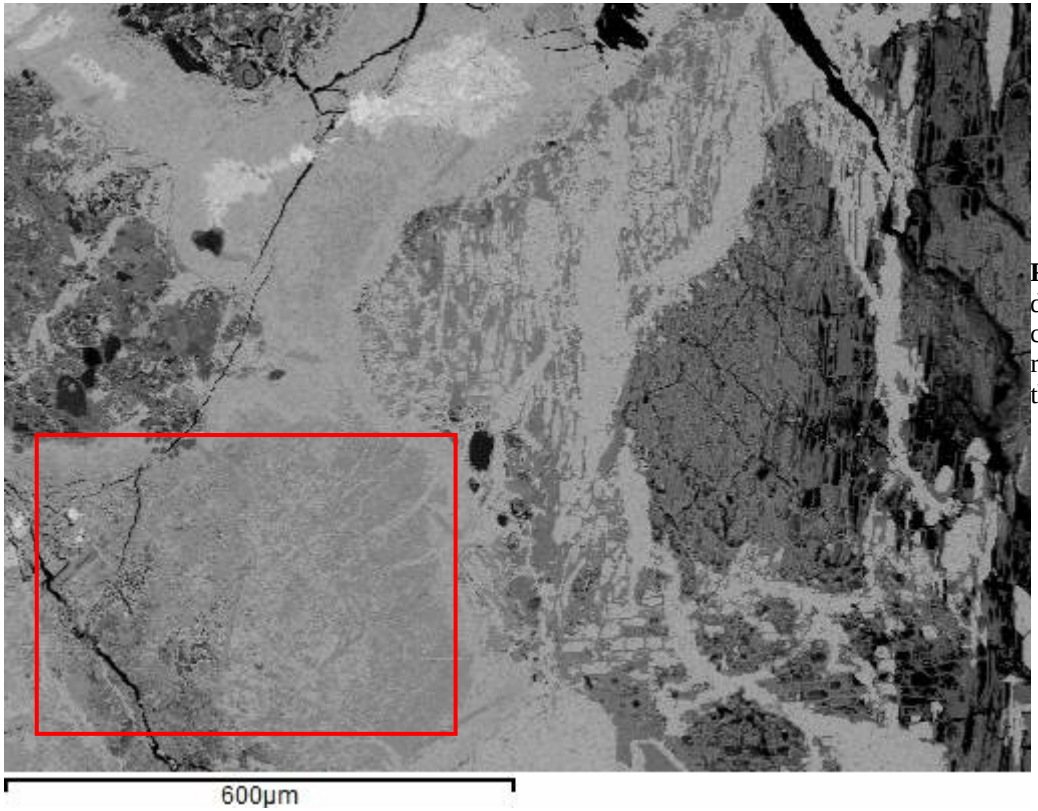

Element	Weight%	Atomic%
O	31.87	85.33
Ag	0.2	0.08
Sb	3.75	1.32
Pb	64.53	13.34
Bi	n.d.	n.d.

Figure 6.45 and **Table 6.27** SEM back scattering image and EDS chemical data showing the composition of the lead carbonate phase produced by the corrosion of lead metal. Carbon is not detected in the EDS analyses, and the result is presented as oxide. The analysis corresponds to the entire area inside the square in the bottom left corner of the image.

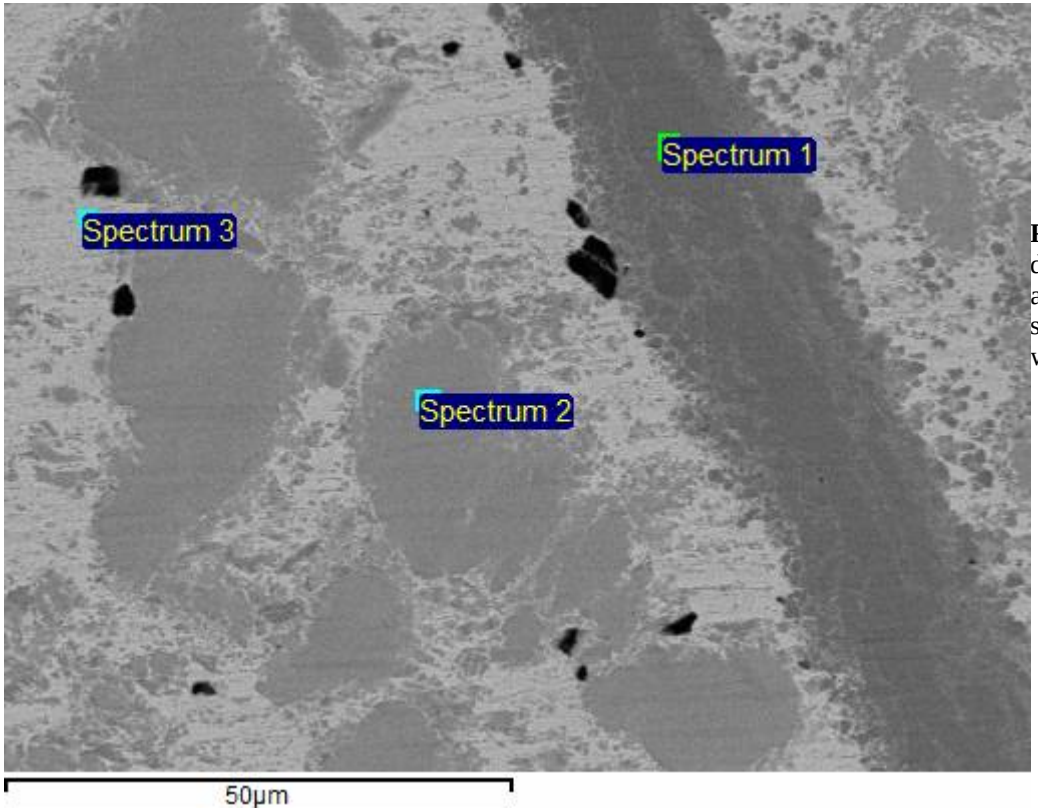

	O	Cu	Ag	Sb	Pb	Bi
Spectrum 1	1.64	40.17	0.10	46.98	9.55	1.55
Spectrum 2	1.71	0.27	n.d.	86.62	7.81	3.66
Spectrum 3	3.49	n.d.	2.69	6.72	72.36	14.95

Figure 6.46 and **Table 6.28** SEM back scattering image and EDS chemical data showing the composition of the needle-like phase (copper, bismuth/lead alloy) reported in the optical microscope image in Figure 6.44 and the separation of the antimony and lead-rich phases. Within the lead-rich phase, we can observe that the silver concentration is up to 2.7 wt%.

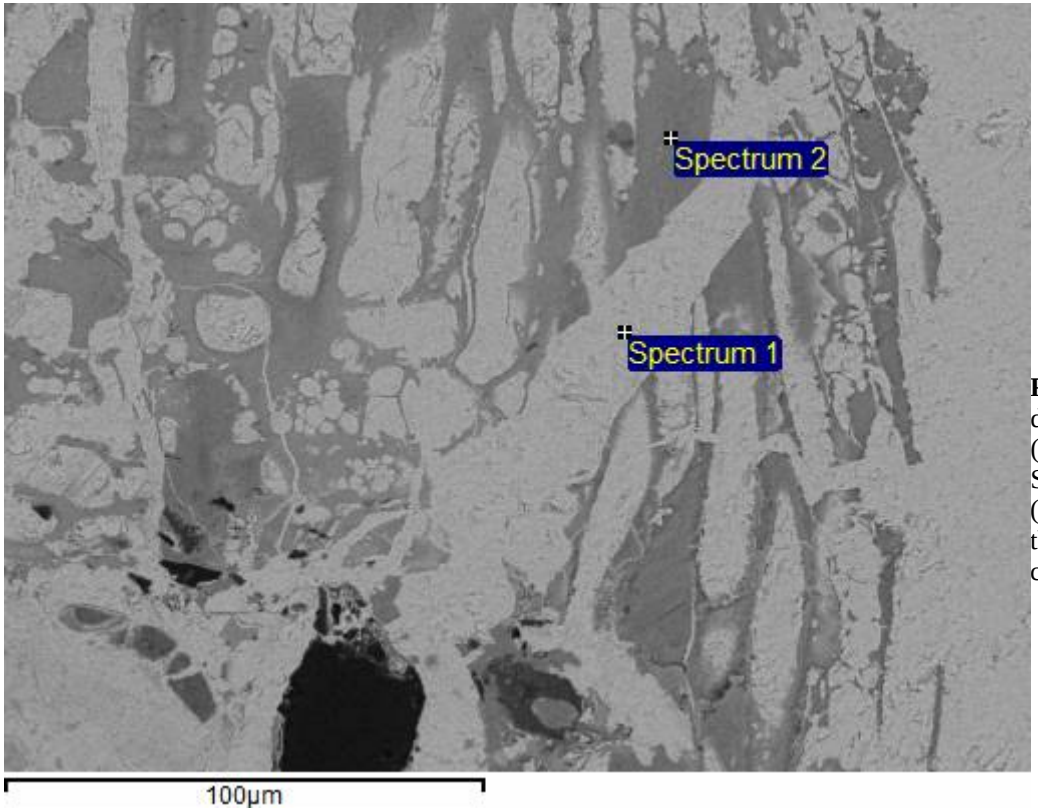

Element	Weight%	Atomic%
O	26.56	75.48
Al	0.17	0.29
Si	3.21	5.20
Fe	0.65	0.53
Cu	0.39	0.28
Ag	3.52	1.49
Sb	15.35	5.73
Pb	50.14	11.00

Figure 6.47 and **Table 6.29** SEM back scattering image and EDS chemical data showing the composition of lead carbonate (spectrum 2). In this case (spectrum 2) silver content appears very concentrated, around 3.5wt%. Spectrum 1 is lead carbonate only. Figure 6.47 shows the association of lead (spectrum 1) and lead, antimony and silver (spectrum 2). Table 6.29 shows the composition of spectrum 2. Note that the entire sample is degraded into a carbonate (the reason for such a high oxygen concentration).

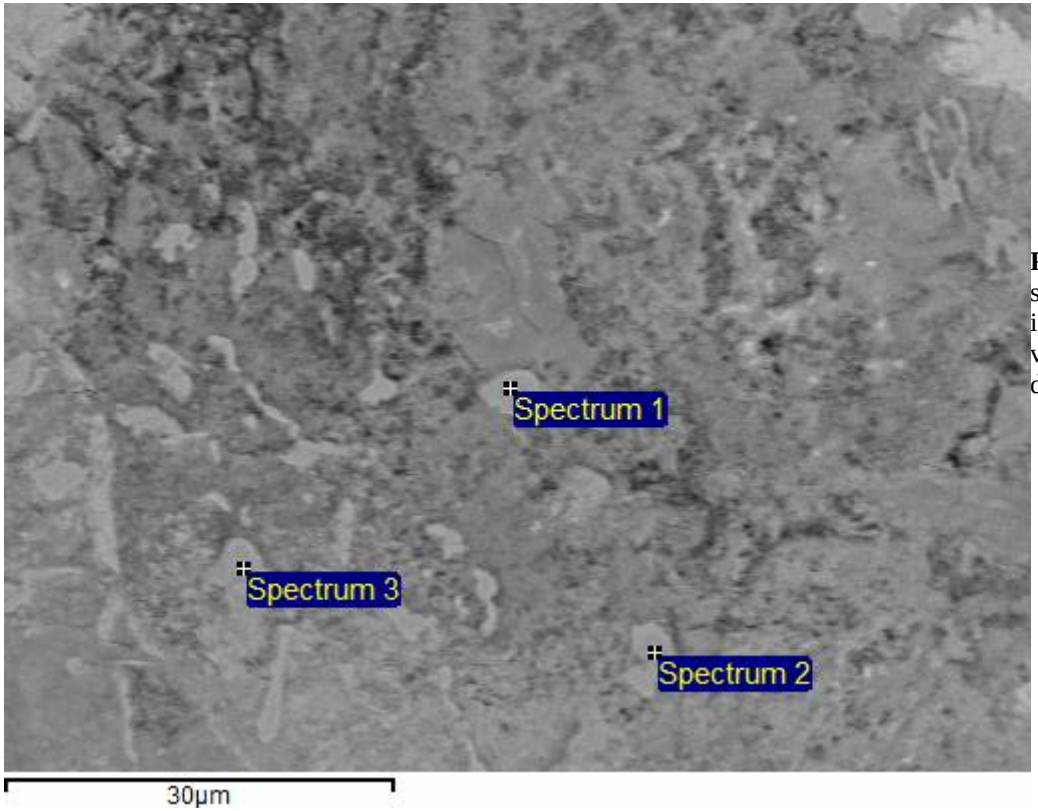

	O	Ag	Sb	Pb	Bi
Spectrum 1	9.67	66.10	17.10	6.39	0.74
Spectrum 2	22.21	33.03	14.18	30.08	0.50
Spectrum 3	26.38	8.71	14.88	49.12	0.90

Figure 6.48 and **Table 6.30** SEM back-scattering and EDS chemical data showing the composition of the silver-rich droplets also reported in the OM image in Figure 6.42. The polymetallic nature of the metal is once again visible; the very high antimony content is noticeable, and bismuth is also detected.

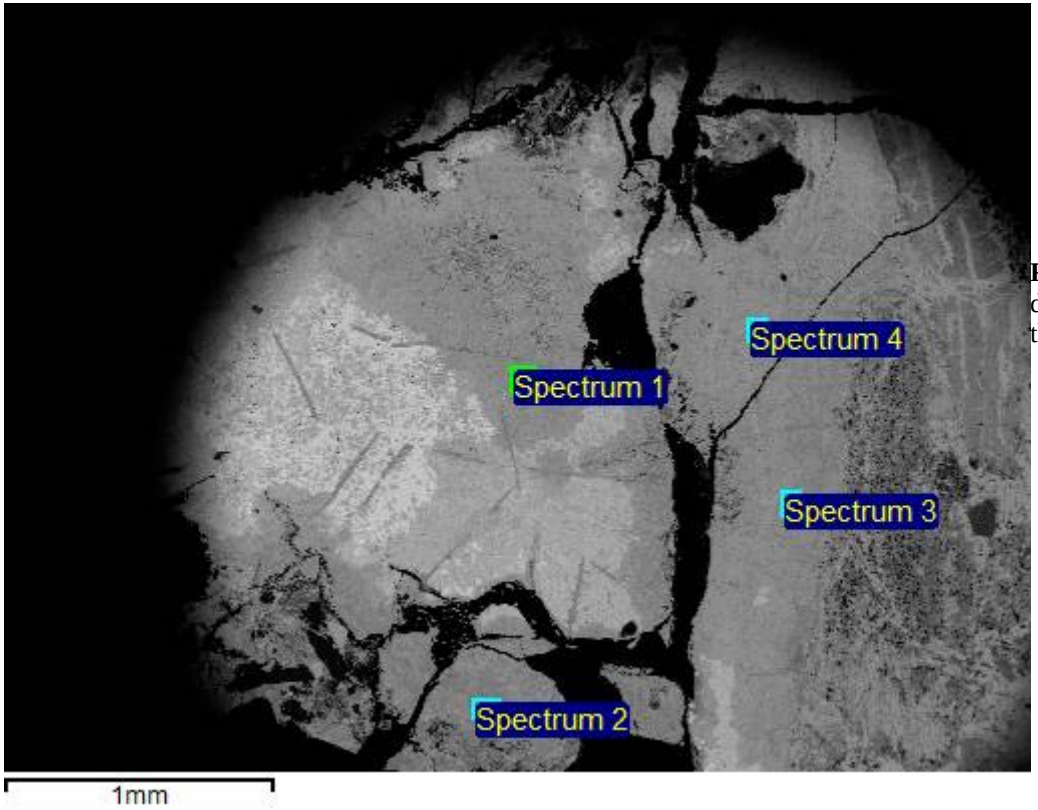

	O	Mg	Si	Cu	Ag	Sb	Pb	Bi
Spectrum 1	26.21	0.05	1.07	0.52	0.00	8.00	73.98	n.d.
Spectrum 2	25.02	0.19	2.66	1.53	1.05	17.31	49.76	2.48
Spectrum 3	23.27	n.d.	2.19	n.d.	0.33	12.31	63.53	n.d.
Spectrum 4	23.88	0.07	1.29	0.16	0.18	7.60	67.20	n.d.

Figure 6.49 and **Table 6.31** SEM back scattering image and EDS chemical data showing the area analyses of lead carbonate, indicating the variability of the silver concentration within the sample.

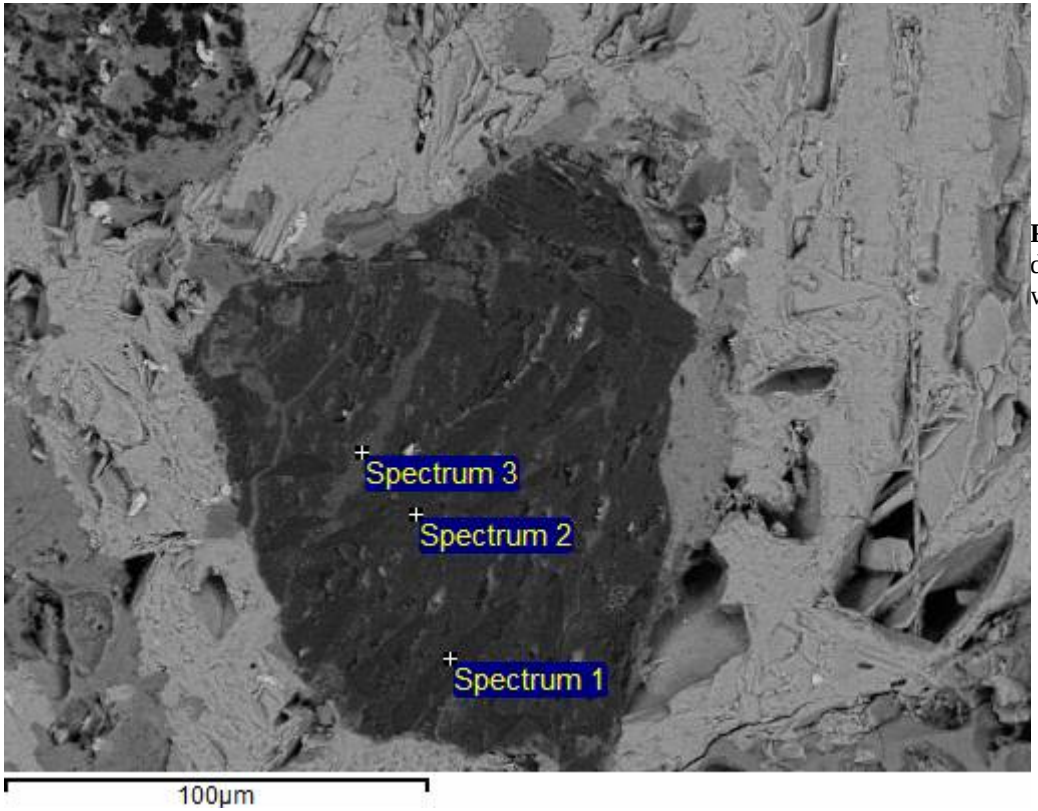

	O	Mg	Al	Si	K	Cu	Ag	Sb	Pb	Bi
Spectrum 1	55.67	n.d.	9.64	20.30	5.85	n.d.	0.30	0.82	7.81	n.d.
Spectrum 2	68.35	0.10	0.16	18.85	0.19	0.21	n.d.	1.81	11.38	n.d.
Spectrum 3	52.38	0.35	0.60	6.83	0.05	0.88	0.23	12.06	28.04	n.d.

Figure 6.50 and **Table 6.32** SEM back scattering image and EDS chemical data showing an inclusion of 'charcoal dust' from the area of the furnace where the lump of bullion was separated from the rest of the metal.

6.9. Ball slags

Three samples with a macro-morphology very similar to the characteristics of the 'free silica' slags described in the literature were identified. They originate from the site RT 24, dated as Imperial, which is the reason why they are presented in this section of the thesis. No 'free silica slag' layers identified as originating from Corta Lago are stored at the Institute of Archaeology, UCL. These samples show both differences and similarities with the characteristics summarised at the beginning of this chapter, but their stratigraphic position does not allow us to categorise them as proper 'free silica slags' and to discuss the results in comparison with those presented at the beginning of this chapter. For this reason, these slags will be referred to as '**ball slags**', due to their shape Figs. 6.51 and 6.52). For the purposes of this project, these three samples have been analysed with OM, XRF, EDS-SEM and MC-ICP-MS.

Before presenting the results obtained for these ball slags, some methodological aspects need to be discussed. The ball slags presenting crystals identified as residual need to be approached differently for bulk chemical analyses. The residual crystals did not reach a liquid state during the smelting, and thus, in order to calculate the smelting temperature, the chemical input of the residual crystal should not be considered. To measure the bulk contents of the liquid phase during the smelting, the author used the average of ten EDS-SEM area analyses, avoiding the residual crystals.

Figure 6.51 Sample RT24n7, with a round shape and a fresh fracture showing white translucent crystals.

Figure 6.52 Sample RT24n8, a fragment with a round margin and a fresh fracture showing white crystals.

The macro-morphology of this type of slag is a round shape around 10 cm in diameter, suggesting the denomination 'ball' slag (Figs. 6.51 and 6.52). The colour is grey, with visible whitish crystals and no visible porosity. On a fresh fracture one can observe residual white translucent crystals, around 1-2 mm long, identified mainly as barite crystals, which are residual, not reacted during the smelting. The samples are

very similar to each other, and the bulk chemical composition of the melt phase (determined by averaging the ten SEM area analyses, as mentioned above – Table 6.34) is characterised by a silica content around 30 wt%, alumina around 10 wt%, FeO around 20/25 wt%, alkali around 2.5 wt%, calcium oxide around 5 wt%, lead oxide as high as 15 wt%, barium oxide around 5 to 10 wt%, and sulphide around 0.2/1 wt%. The other metals present in the slag are copper, zinc and antimony, and their concentrations, obtained from XRF bulk analyses (Table 6.33), are around 0.3/0.5 wt% for copper oxide, 0.3 wt% for antimony, and 0.4 to 1 wt% for zinc oxide. The concentration of silver is around 350/450 ppm. XRF analyses of the bulk of the sample were also performed, as already mentioned earlier, and they show concentrations of barium oxide and sulphate 2-3% higher than the results presented above, since the residual aggregates were also included in the analyses. The values for the other elements are comparable for the two techniques.

Plotting the bulk chemical data of the major components on the diagram alumina/ iron oxide/ silica (using alumina/ FeO+BaO+CaO/ silica) in order to compare them with the thermodynamic data presented in the diagram alumina/ iron oxide/ silica (Figure 6.62), one can note that the points plot slightly shifted towards the alumina as compared to the homogeneous field formed by the samples from the other periods. The results are within the field of the fayalite, on the cotectic linking optimum 1 to optimum 2, plotting in the middle of it, closer to optimum 1 (as was observed for the Phoenician and the samples from the Republican phase III tapped slag period).

The area analyses carried out by SEM along the polished section (without the inclusions) indicate an inhomogeneity of the samples, and the four main components (SiO_2, FeO, BaO and PbO) have a standard deviation higher than 1 (Table 6.34).

		Na2O %	MgO %	Al2O3 %	SiO2 %	P2O5 %	S %	K2O %	CaO %	TiO2 %	MnO %	FeO %	BaO %	PbO %	SnO2 %	CuO %	ZnO %	As %	Ag µg/g	Sb µg/g	Bi µg/g
RT24 S7	Ball slag	0.42	2.74	5.96	24.76	n.d.	1.36	1.29	2.93	0.23	0.06	24.78	18.33	11.19	n.d.	0.34	0.93	n.d.	354.81	26052.19	n.d.
RT24 S8	Ball slag	0.45	2.45	6.77	24.74	n.d.	1.25	1.47	3.19	0.13	0.06	25.93	13.16	13.50	n.d.	0.39	1.01	n.d.	455.26	35543.38	n.d.
RT24 S9	Ball slag	0.95	2.83	6.60	30.42	n.d.	1.18	1.43	3.36	0.05	0.09	27.64	7.66	12.01	n.d.	0.54	0.40	n.d.	361.99	30386.74	n.d.

Table 6.33 Bulk composition obtained by XRF.

RT24 S8	average %	standard deviation	RT24 S9	average %	standard deviation
Na2O	0.20	0.27	Na2O	0.31	0.47
MgO	1.08	0.17	MgO	0.92	0.11
Al2O3	10.83	0.88	Al2O3	10.70	0.90
SiO2	31.09	2.36	SiO2	32.32	2.12
SO3	0.95	0.87	SO3	0.23	0.66
K2O	2.44	0.14	K2O	2.52	0.17
CaO	5.17	0.49	CaO	5.07	0.39
FeO	21.89	2.41	FeO	24.76	1.67
ZnO	1.34	0.47	CuO	1.25	0.61
As2O3	0.09	0.23	ZnO	0.18	0.35
BaO	10.34	1.56	BaO	5.83	1.67
PbO	14.58	2.82	PbO	15.93	3.87

Table 6.34 Average and standard deviation of ten area analyses performed by SEM-EDS avoiding the residual gangue aggregates.

The estimated temperature is indicated by the mineralogical association (Figs. 6.54, 6.55, 6.56 and 6.57 and Tables 6.35, 6.36 and 6.37) showing magnetite, feldspar ($(K,Ba,Fe,Ca,Pb)Al_2Si_2O_8$) – with different cation concentrations detected, pyroxene ($Ca(Mg,Fe)Si_2O_6$) – with traces of Pb, Ca, K and Zn, newly formed cerussite ($PbCO_3$) and lead oxide with up to 14 wt% Sb and 5 wt% Fe, and barite ($BaSO_4$). The concentration of barium oxide in these slags is between 5 and 10 wt%, and it is mainly present as feldspar (celsian). The concentration of residual barite (Fig. 53) doubles the concentration of barium oxide in the samples. The residual barite actually constitutes the majority of the crystals visible with the naked eye on the samples, even if the literature mostly talks about crystals of quartz, as we have seen above. The residual grains show signs of reactions with the molten material, mainly in the shape of fractures and reaction bays smoothing the edges of the aggregates. The linearity of the fractures seems to indicate a relatively short permanence in the melt, strongly suggesting a late addition of the 'residual' material to the system. No prills of silver are detected, and a measurement of the silver by XRF indicates an average of 350/450 ppm in each of the analysed samples, comparable with the other periods, indicating that the high lead concentration is not associated with silver.

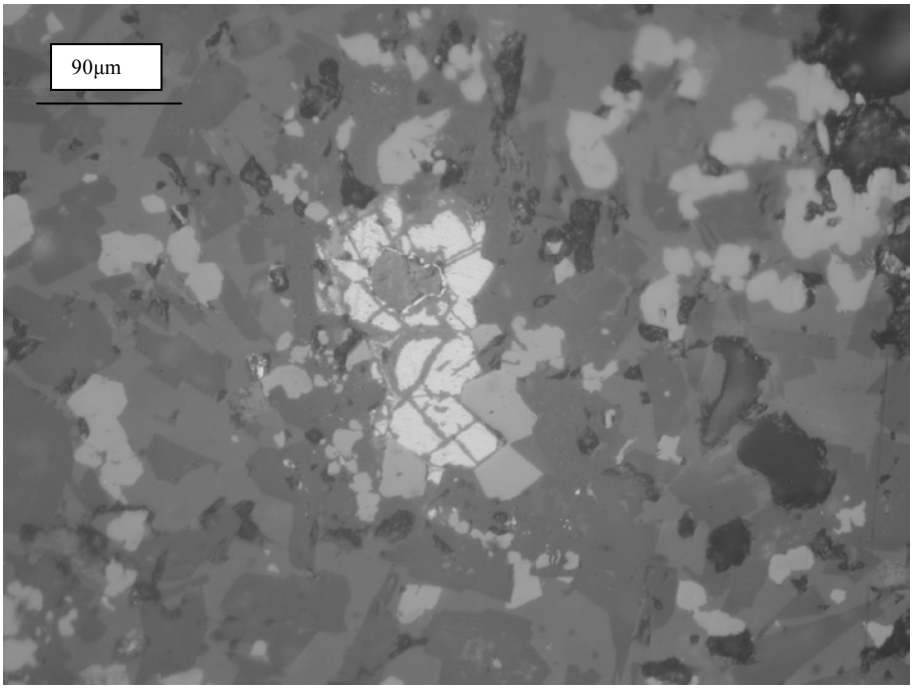

Figure 6.53 Optical microscope image of sample RT24 S8 showing a residual aggregate of barite reacting with the melted material around it through reaction bays and fractures.

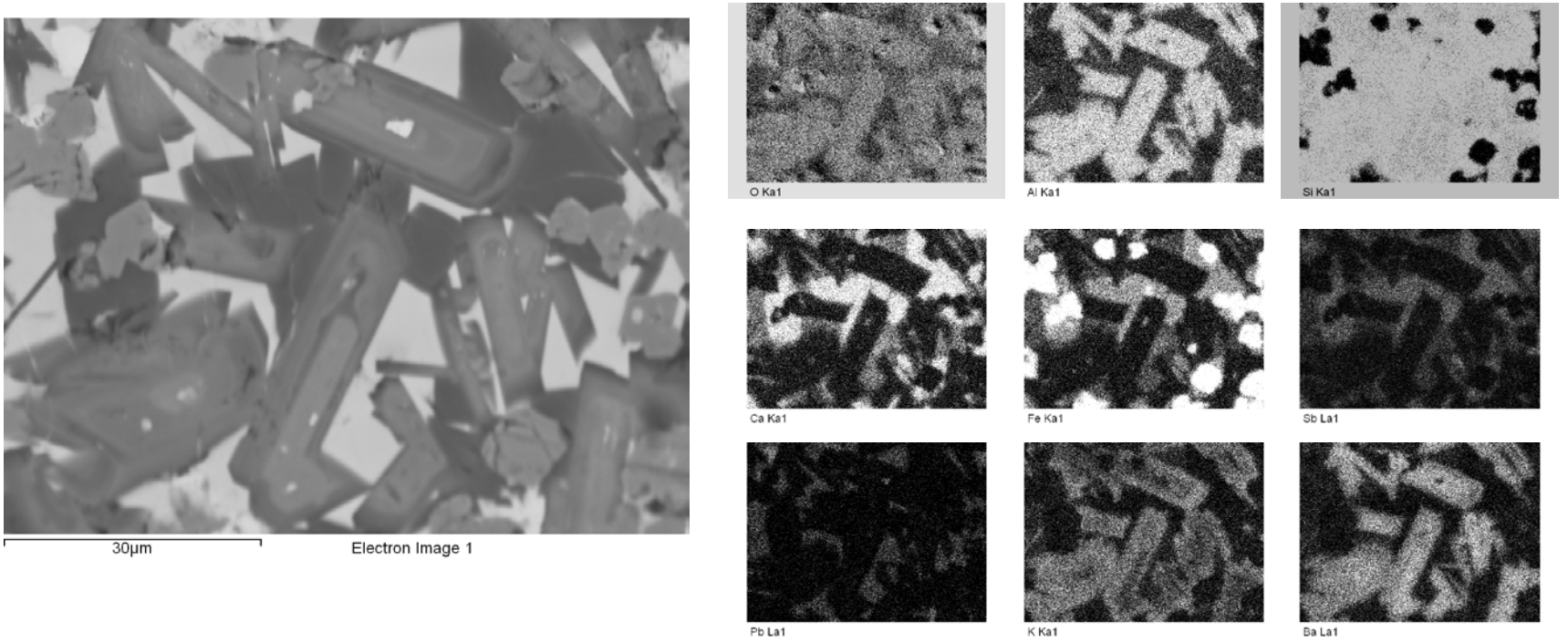

Figure 6.54 Backscattering SEM image and associated chemical maps showing the distribution of the different silicates, oxides and metals.

Element	Weight%	Atomic%	Compound%	Formula
Mg	2.0	2.0	3.4	MgO
Al	1.8	1.6	3.4	Al2O3
Si	20.7	18.1	44.3	SiO2
Ca	15.7	9.6	22.0	CaO
Fe	19.6	8.6	25.2	FeO
Zn	1.4	0.5	1.8	ZnO
O	38.8	59.5		

Table 6.35 Composition of pyroxene-like phase in sample RT24 S8 (spectrum 1).

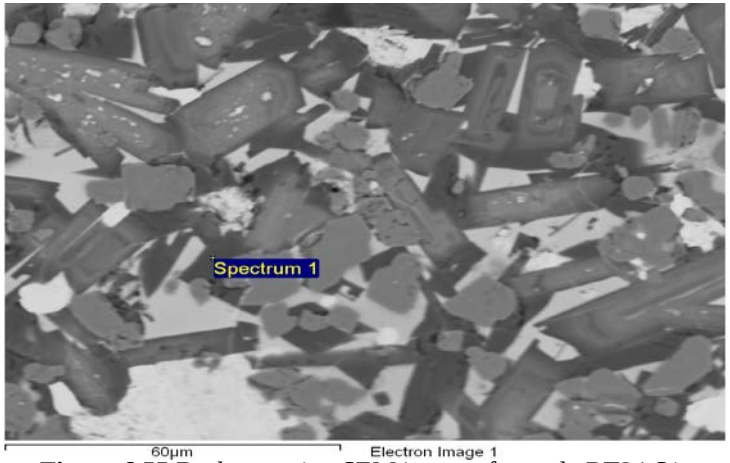

Figure 6.55 Backscattering SEM image of sample RT24 S1 showing the mineralogical association and the position of spectrum 1.

Element	Weight%	Atomic%	Compound%	Formula
Al	1.9	2.5	3.6	Al2O3
Si	13.0	16.1	27.8	SiO2
K	2.3	2.0	2.8	K2O
Ca	2.9	2.5	4.1	CaO
Fe	17.3	10.8	22.3	FeO
Zn	3.5	1.9	4.4	ZnO
As	1.2	0.6	1.6	As2O3
Ba	2.9	0.7	3.3	BaO
Pb	28.1	4.7	30.2	PbO
O	26.9	58.3		

Table 6.36 Composition of (Fe, Pb, Ca, K)(Si, Al)O_3 second generation of crystals. These crystals have a rounded shape and are crystallised mainly 'above' the pyroxenitic phase.

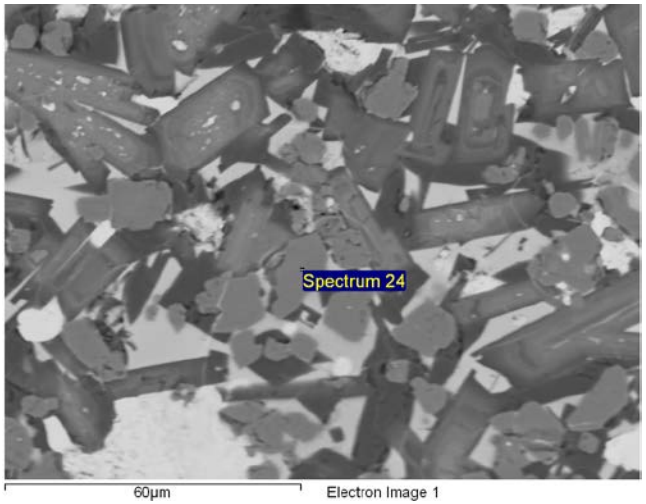

Figure 6.56 Backscattering SEM image showing the location of the spectrum reported in Table 6.36.

Element	Weight%	Atomic%
O	15.0	55.5
Al	0.5	1.1
Si	5.4	11.4
Cl	0.9	1.4
Fe	1.9	2.0
Cu	2.8	2.6
Sb	24.6	12.0
Pb	48.9	13.9

Table 6.37 EDS composition of the metal-bearing phase.

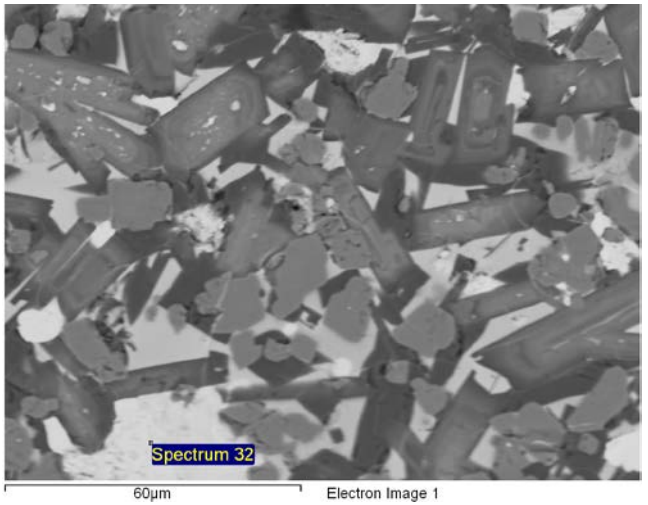

Figure 6.57 Backscattering SEM image showing the location of the spectrum reported in Table 6.37.

The presence of Ball slag in Imperial layers may be explained by the hypothesis of a re-use of the Ball slag as a source of lead, since their lead content is relatively high. It is visible in periods previous to the Imperial one, and will be discussed in more detail in Chapter 8, addressing the addition of lead to the smelting process, making the lead (in whichever form, metallic or mineral) a very important extra-component of the smelting process. According to this interpretation, the insufficiency of lead in the ore had been understood since the beginning of smelting in the area of Corta Lago (Phoenician tapped phase).

Because of their high lead content (PbO 12-14%), the ball slag would have been a valuable source of lead. However, the high barium concentration in the ball slag, of a similar level, would be detectable in the Imperial tapped slag if the ball slags were part of the raw material that produced the Imperial tapped slag as a by-product. The Imperial tapped slags do not seem to show any input of high barium material since their barium oxide concentration is average and appears consistent with the input of barium oxide from the ore itself. Furthermore, the cloud of points generated by the plotting of the BaO and PbO concentrations for all samples except the ball slag ones seems to be divided into two groups, mainly distinguished by their BaO concentration (Fig. 6.58). The group richer in BaO is mainly represented by pre-Roman samples and by the Republican plate samples, while the group poorer in BaO is represented by the Republican tapped samples and the Imperial ones. Thus, the Imperial samples show even further impoverishment in BaO as compared to the ball slag under consideration in this section.

To conclude, the similarities between the ‘free silica’ slags as summarised by Hunt Ortiz (2003) and reported at the beginning of this chapter and the ball slags described here are very strong: this points to the association of these remains to the ‘free silica’ ones, even though they are completely out of stratigraphic context.

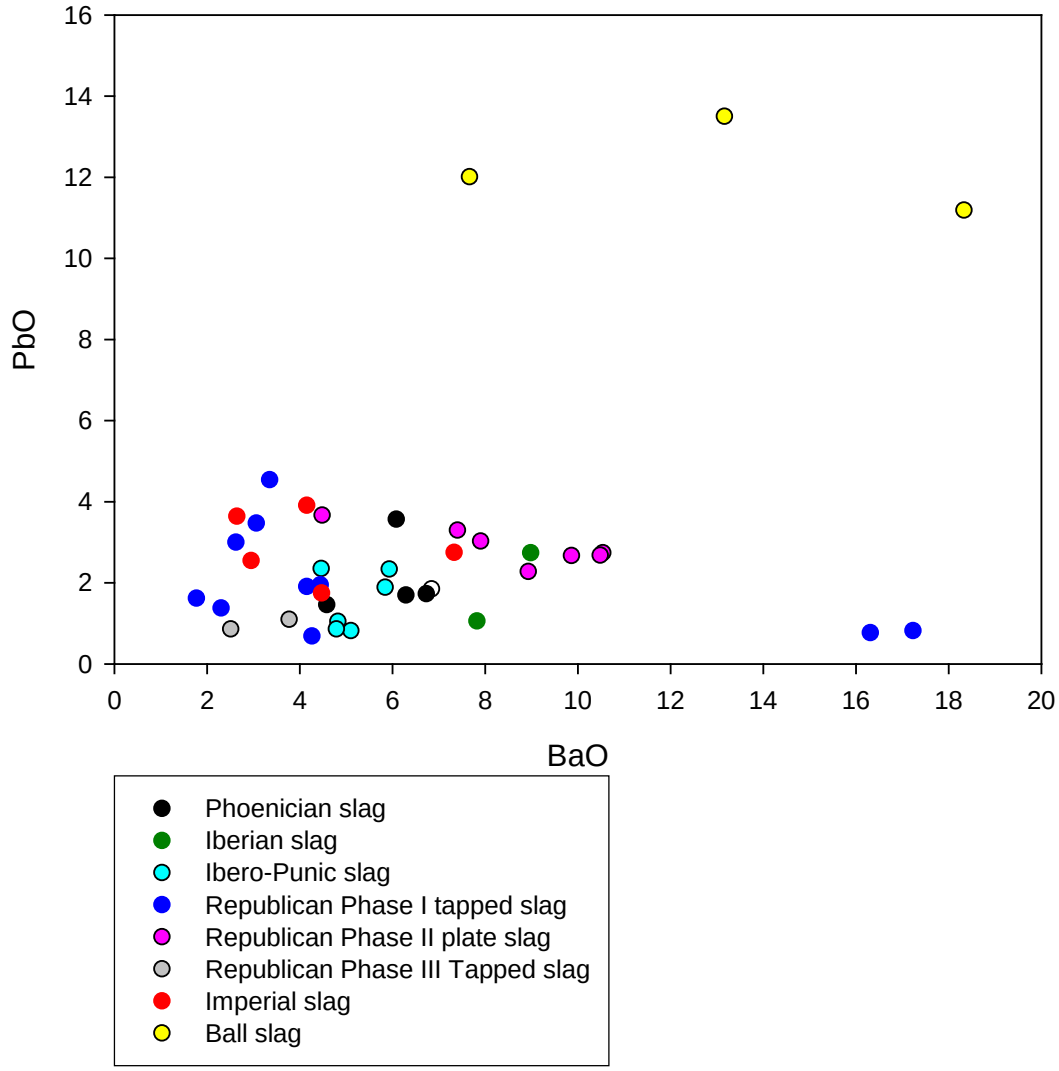

Figure 6.58 Diagram BaO/PbO.

6.10 Preliminary discussion and comparison

Several parameters are used as tools in order to achieve a better understanding of the processes under consideration and will be presented and discussed together. As identified in Chapter 5, these parameters are:

G – index of glassiness, as a reflection of ore selection/preparation and furnace operating conditions, such as the content of alkali and speed of cooling; this

parameter should have a correspondence with the olivine morphology (G = (CaO+ P_2O_5+K_2O+MgO)/(FeO+MnO+BaO+K_2O+$Na_2OAl_2O_3$+PbO)).

S – redox condition index, a reflection of the furnace operating conditions, such as the fuel/ore ratio; this parameter may also provide indications about changes in metal-bearing phases (oxides/sulphides), as well as about the concentration of sulphur in the system (S= 2.39*SiO_2/(FeO+MnO+MgO+CaO)).

Log η – viscosity calculated following the model proposed by Giordano et al. (2006). The model is described by the formula:

Logη=b1+[(b2+b3)/b3+SM)]+b4

where b1, b2 and b3 are constants depending on the chemistry of the melt described by the SM parameter defined as (Na_2O+K_2O+CaO+MgO+MnO+FeO)/2, and b4 is sample dependent.

Focusing first of all on index G, we notice from Figure 6.59 and Table 6.38 a similar distribution for Phoenician and Republican plate slags, a higher value for the ball slags, and a lower value for the Iberian and the tapped Republican phase I slags. These values are also characteristic of the majority of the Ibero-Punic samples, while two of them (RT25 L124 S12 – composed mainly of skeletal olivine, as seen in section 6.3., and RT25 L132 S17) show a higher value (comparable to the samples from the Republican phase II plate slag period). Samples from Republican phase III tapped slag period and Imperial samples show a uniform distribution around a value intermediate between the other periods. In particular, the pattern corresponding to the Phoenician and Republican phase II plate slag shows a high G value for the majority of the samples (lower only when compared with the ball slags), but three exceptions are present: one Phoenician (RT25 L126 S74) and two Republican (RT25 L52 S79 and RT25 L52 S3), with values comparable with the Republican phase III tapped slag period and Imperial slag. The period presenting the most significant internal distinctions is the Iberian period. Interestingly enough, the four samples that group at a lower value are from layer 120, while the two samples that show higher values are from more recent layers.

At a closer observation, the samples from the Republican phase I tapped slag period, even though relatively uniform as compared to the other periods, also show two samples with slightly higher values as compared to the others. These appear similar to the two older samples belonging to the same group, but in the same layer 3 we

also observe the new lower value that will be then observed in all subsequent samples.

Following Charlton (2007), a 5% of variability can be assigned to the difference in composition due to error in copying and reproducing when no experimentation takes place, meaning that 5% variability is considered acceptable in a "standardised" procedure, if experimentation is performed than the variability will be greater. Observing the values of the samples under consideration, we notice that the variability range is much lower than the expected one in case of experimentation within each period, except for the Ibero-Punic samples. In slags from this period, however, we observe a distinction in two groups and not a scattering of points as expected from experimentation, indicating a more possible change in the process or the co-existence of two different processes. In this case, the process under examination is the tapping and cooling process, and it is interesting to observe that the plate slag cooled 'in layers' in the forehearth show only a slightly higher value of this coefficient as compared to the previous and subsequent tapped examples. A more important parameter here seems to be the morphology of the olivine and consequently the moment when the crystallisation begins.

Focusing on index S (Fig. 6.60 and Table 6.38), we observe two groups within very tight ranges: between 0.4 and 1.4, indicating a mainly fayalitic slag plus a percentage of iron oxide that is very similar for all the analysed samples except the ball slag and one Phoenician sample which present an S index higher, around 2 indicating a higher presence of silica, justified by the residual aggregates. Ball slags are homogenously grouped, while for the other periods a more scattered plotting is visible. Slags from the Ibero-Punic and Republican phase I tapped slags seem to be divided into two groups. The two groups do not show correlations with stratigraphy, which may indicate the co-existence of two different processes, metallurgical traditions, or charge compositions.

The Republican phase I tapped slag shows actually a decreasing pattern (from 2 to 1), following the stratigraphy except for RT25 L31 S18 and RT25 L31 S19, which already distinguish themselves in terms of compositional characteristics (high barium and silver concentrations). No correlation is apparent between the occurrence of sulphide or oxide metal-bearing phases and the S value. The mineralogical association, highly dominated by fayalite and magnetite, seems to obliterate the presence of minor phases.

The viscosity (Fig. 6.61 and Table 6.38) shows that a homogenous range of variability is maintained throughout these periods, except for the ball slag, which presents a much lower value. The viscosity has been calculated using the composition of the melt phase only. This value would thus indicate that the ball slags are initially very fluid (more fluid than the tapped slag) and then the added quartz/barite phase thickens them in order to render them movable: this is the thickening of the slag "to take it out like water with a sponge" (Tylecote 1987, 306-307). The macroscopic observations of the ball slag show that the residual crystals are angular and fractured, demonstrating a very poor interaction with the molten material. This observation corroborates the hypothesis that the residual crystals of barite and quartz were added to the very fluid slag to facilitate its thickening and its subsequent removal. In more detail, we seem to observe a parabolic (convex) curve of which the apex is the Republican phase I tapped slag. The Imperial samples seem to be divided in two groups, one with lower viscosity as compared to the range shared by the other periods and some of the Imperial samples. One sample (RT25 L119 S50 – highly enriched in iron oxide) from the Iberian layers presents higher viscosity than the average of the other samples.

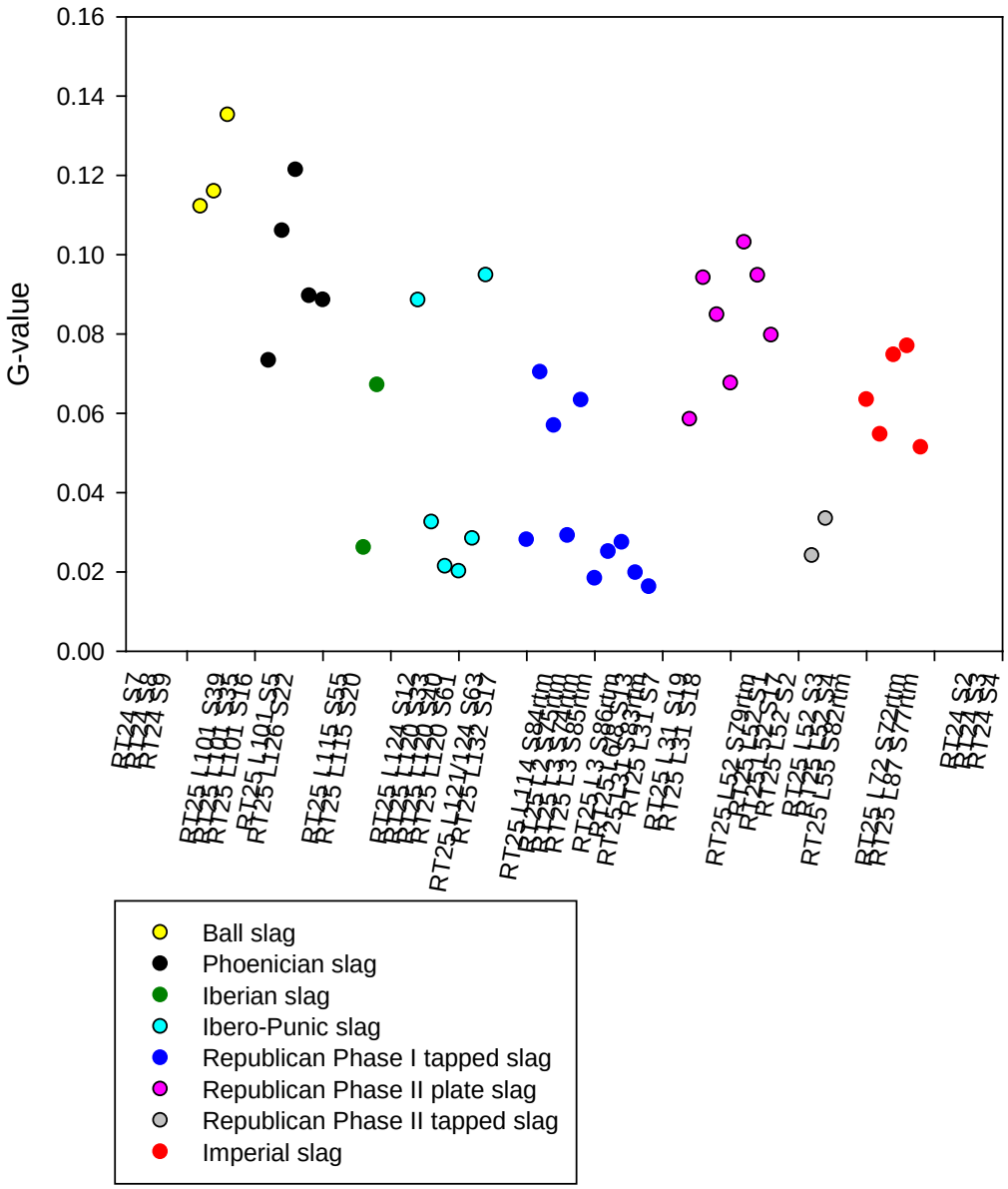

Figure 6.59 Diagram of G values for the analysed slag samples.

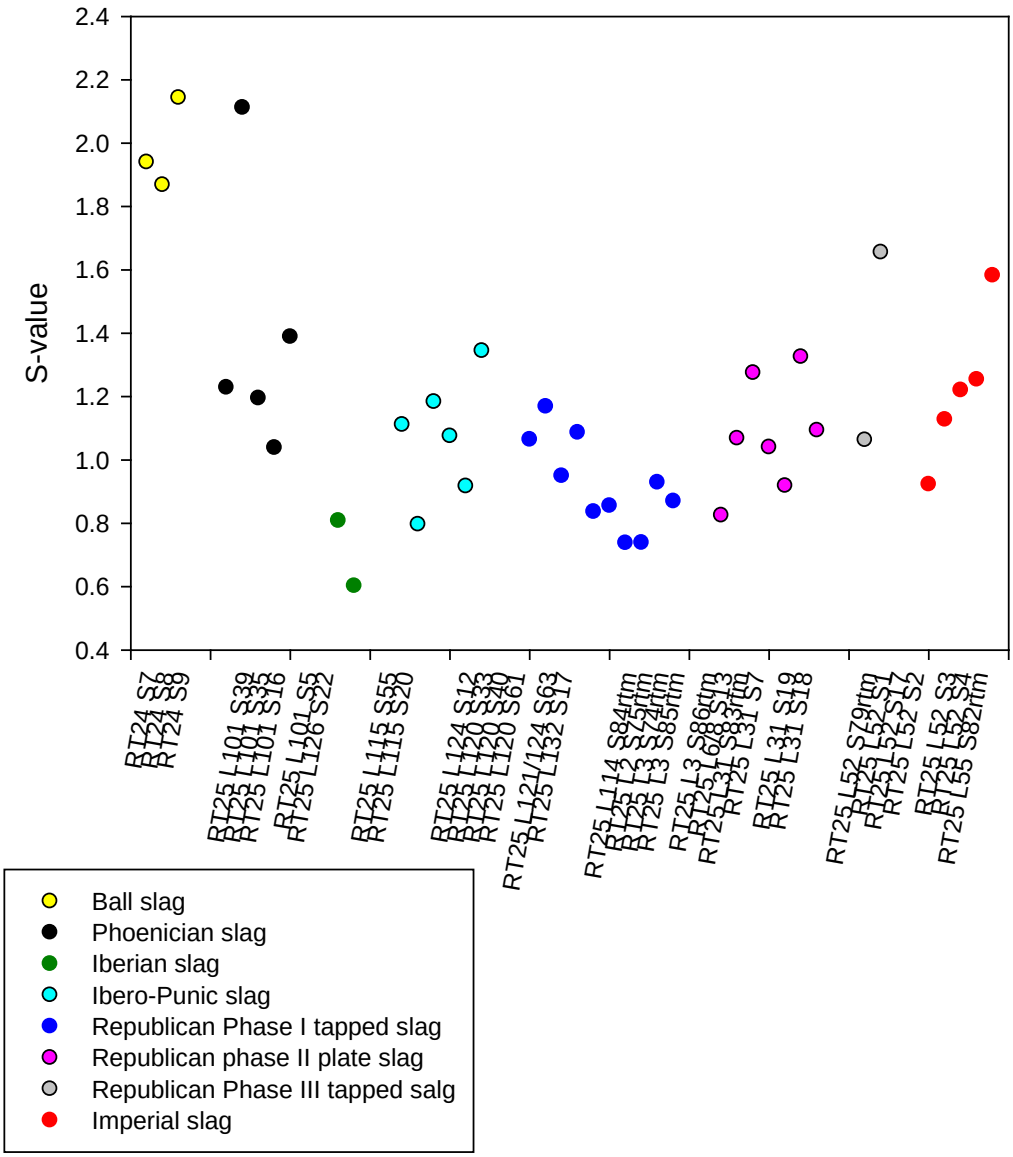

Figure 6.60 Diagram of S values for the analysed slag samples.

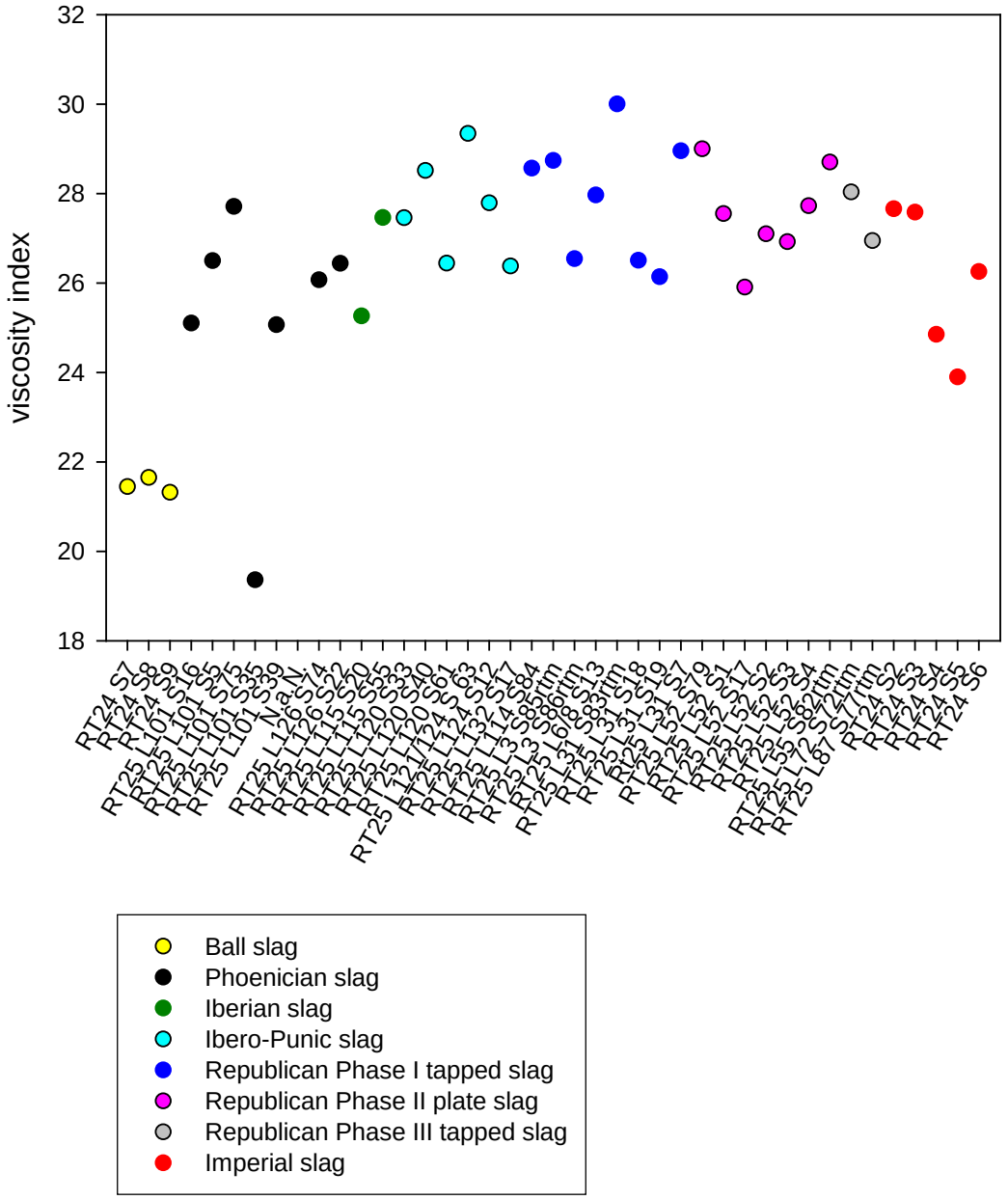

Figure 6.61 Diagram of log η for the analysed slag samples.

		log η	S	G
RT24 S7	Ball slag	21.44	1.94	0.24
RT24 S8	Ball slag	21.65	1.87	0.26
RT24 S9	Ball slag	21.32	2.14	0.30
RT25 L101 S16	Phoenician	25.10	1.19	0.19
RT25 L101 S5	Phoenician	26.50	1.04	0.16
RT25 L101 S75	Phoenician	27.71		0.15
RT25 L101 S39	Phoenician	25.07	1.23	0.15
RT25 L126 S74	Phoenician	26.07		0.15
RT25 L126 S22	Phoenician	26.44	1.39	0.16
RT25 L120 S33	Ibero-Punic	27.46	0.80	0.06
RT25 L120 S40	Ibero-Punic	28.51	1.18	0.08
RT25 L120 S61	Ibero-Punic	26.44	1.08	0.05
RT25 L121/124 S 63	Ibero-Punic	29.34	0.92	0.08
RT25 L124 S12	Ibero-Punic	27.79	1.11	0.14
RT25 L132 S17	Ibero-Punic	26.38	1.34	0.16
RT25 L115 S20	Iberian	25.26	0.60	0.08
RT25 L115 S55	Iberian	27.46	0.81	0.07
RT25 L119 S50	Iberian	32.04	0.13	0.03
RT25 L114 S84	Republican I	28.56	1.06	0.07
RT25 L3 S85rtm	Republican I	28.74	1.09	0.08
RT25 L3 S86rtm	Republican I	26.54	0.84	0.10
RT25 L6/8 S13	Republican I	27.96	0.86	0.05
RT25 L31 S83rtm	Republican I	30.00	0.74	0.06
RT25 L31 S18	Republican I	26.51	0.87	0.04
RT25 L31 S19	Republican I	26.14	0.93	0.05
Rt25 L31 S7	Republican I	28.95	0.87	0.07
RT25 L52 S79	Republican II	29.00	0.83	0.10
RT25 L52 S1	Republican II	27.55	1.07	0.16
RT25 L52 S17	Republican II	25.90	1.28	0.18
RT25 L52 S2	Republican II	27.10	1.04	0.15
RT25 L52 S3	Republican II	26.92	0.92	0.11
RT25 L52 S4	Republican II	27.73	1.33	0.16
RT25 L55 S82rtm	Republican II	28.70	1.09	0.14
RT25 L72 S72rtm	Republican III	28.03	1.06	0.07
RT25 L87 S77rtm	Republican III	26.95	1.66	0.09
RT24 S2	Imperial	27.66	0.92	0.13
RT24 S3	Imperial	27.58	1.13	0.10
RT24 S4	Imperial	24.85	1.22	0.12
RT24 S5	Imperial	23.90	1.25	0.14
RT24 S6	Imperial	26.25	1.58	0.09

Table 6.38 G, S and log η values for the analysed samples.

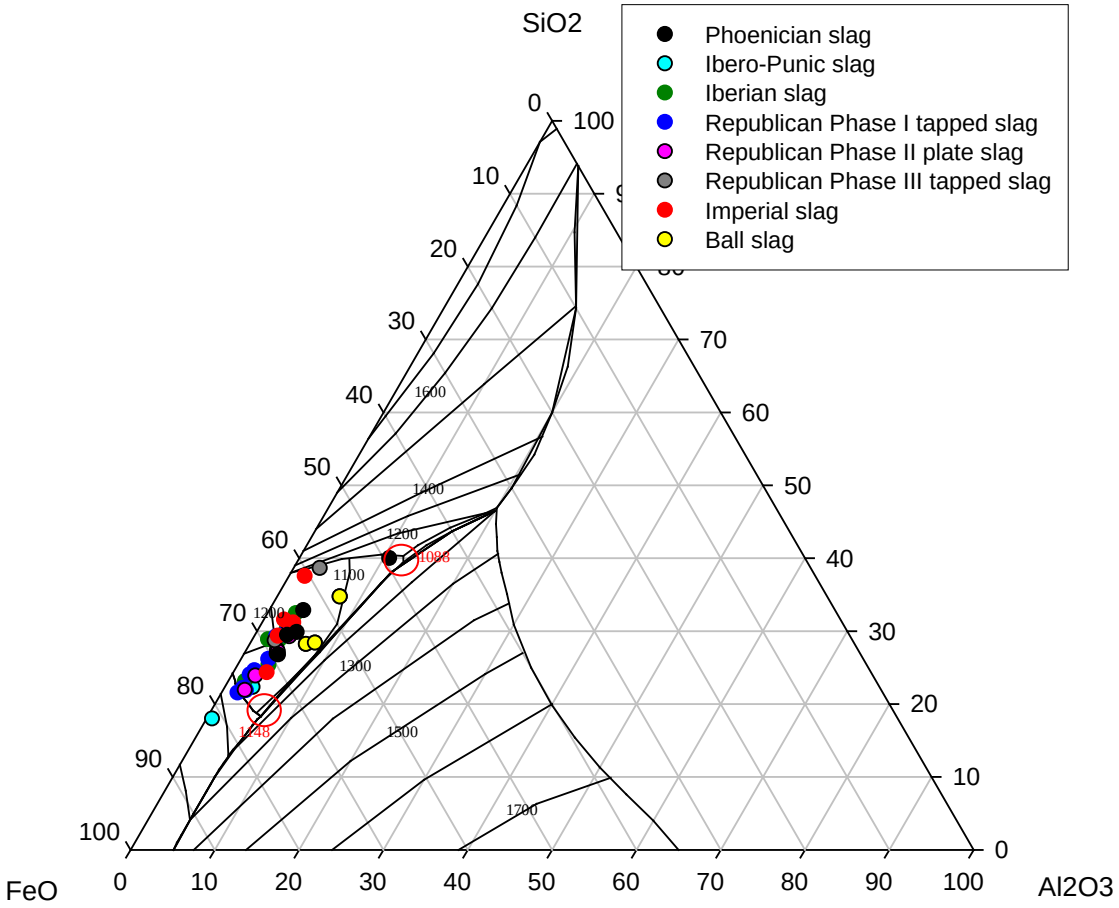

Figure 6.62 Ternary diagram of the main compounds showing the plotting of the bulk chemical composition of the samples under consideration within the valley formed by the fayalite stability field.

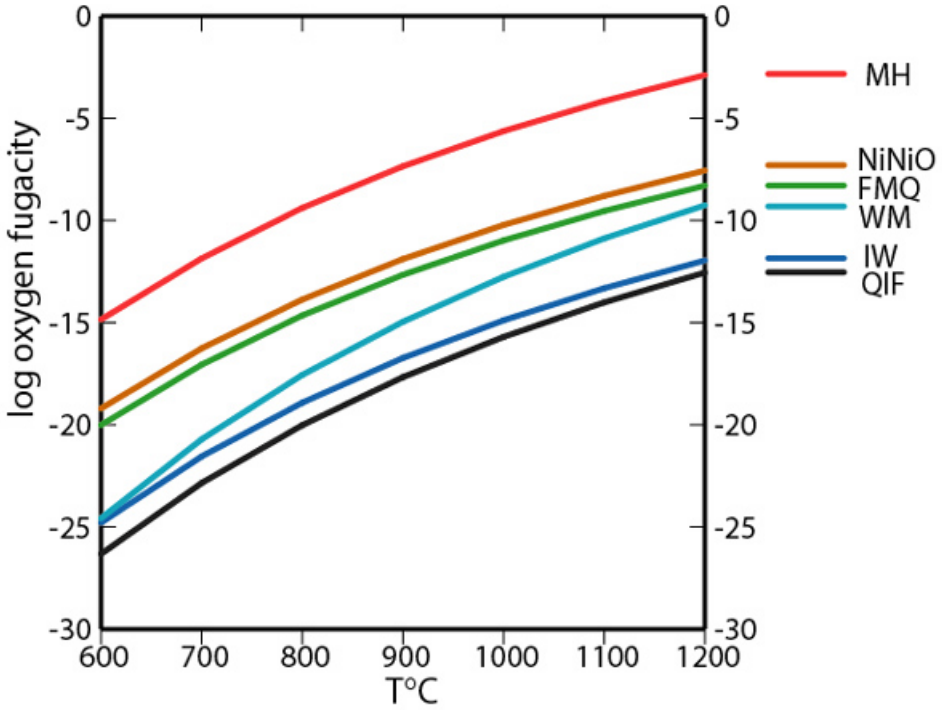

Figure 6.63 Diagram of temperature/oxygen pressure for major mineralogical phases association (MH, magnetite-hematite; NiNiO, Nickel-nickel oxide; FMQ, fayalite-magnetite-quartz; WM, wustite-magnetite; IW, iron-wustite; QIF, quartz-iron-fayalite – Frost, 1991).

The chemical and petrographical information collected suggest that different ores were exploited and used at the time, one richer in sulphides (polymetallic input) and one 'cleaner' (more concentrated) jarosite. We will see in Chapter 8 that the chemical characteristics correspond to differences in lead isotopic signature, indicating that the polymetallic input was also associated to the addition of 'foreign' lead. The Republican plate samples and the Imperial samples that seem to show some common characteristics in the principal component analysis are close to each other but not completely overlapping, indicating the presence of similarities and differences between the two groups, while the Phoenician and the Ibero-Punic samples do not show any grouping. A further discussion of the data after the presentation of the isotopic data will highlight the possible overlapping and discrepancies between these two periods. The Imperial samples show similarities with Republican Plate and Phoenician slags. The Ibero-Punic samples seem to be the bridge between Phoenician samples and one part of the Republican phase I tapped

samples, with the other part of the Republican phase I tapped positioning themselves as a virtual *trait d'union* between the two groups (Ibero-Punic and Phoenician).

6.11. Ingots, semi-reacted ores and litharge samples

A few other samples except for slag were analysed for the purposes of this project, in order to obtain some additional information on the smelting process. The analysed samples were ingots and semi-reacted ores, kindly provided by the Rio Tinto Museum to the author, and litharge samples, taken from the Corta Lago collection of material at the Institute of Archaeology, UCL. These materials were added to the assemblage under consideration in order to obtain additional information concerning the lead isotope signatures and hence contribute to the overall interpretation. For this reason, relatively little chemical information were recorded and these are presented below.

6.11.1 Ingots

Three samples (1PB RT; 2 PB RT; 3 PB RT) morphologically identifiable as ingots were recovered from the Corta Lago area and are stored at the Rio Tinto Museum. According to a personal communication with the Director of the Museum, Dr. Aquilino Delgado, they are dated to the Roman period. As already mentioned, the idea of studying these ingots is purely linked to LIA analysis. Nevertheless, EDS-SEM analysis was performed on some areas of the samples for their chemical characterisation.

The ingots have different shapes, two being elongated (Figs. 6.64 and 6.65), similar to the ones reported by Tisseyre et al. (2008), and one has a plate shape (3 PB RT) (Fig. 6.66). The chemical composition indicates that two are lead ingots, while one is an iron-copper matte (1 PB RT).

The composition of the matte shows some lead, zinc and arsenic contents, unevenly distributed in the sample. Copper droplets are visible with the optical microscope (Fig. 6.67).

The composition of the lead ingot 2 PB RT shows impurities of silica (≈ 4%), alumina (<1%) and calcium oxide (<1%), while the lead ingot 3 PB RT shows a silica content around 9% and alumina and calcium oxide levels lower than 1%. Both

silica and alumina are impurities due to the polishing process. No silver droplets are detected (Figs. 6.68 and 6.69). Overall, the lead ingots seem to be of pure lead and not of lead (silver) bullion, even though no spectroscopy was carried out on the samples. The detection limit of the SEM-EDS technique may not be sufficiently low to detect silver in the lead. Furthermore, the preparation methodology for the analytical techniques employed may have affected the visibility of silver. We cannot verify if they are the results of recycling of litharge to be re-used in the smelting process, or if they represent lead purposely smelted elsewhere.

Figure 6.64 Lead ingot 2PB RT.

Figure 6.65 Matte ‘ingot’ 1PB RT.

Figure 6.66 Lead ingot 3PB RT.

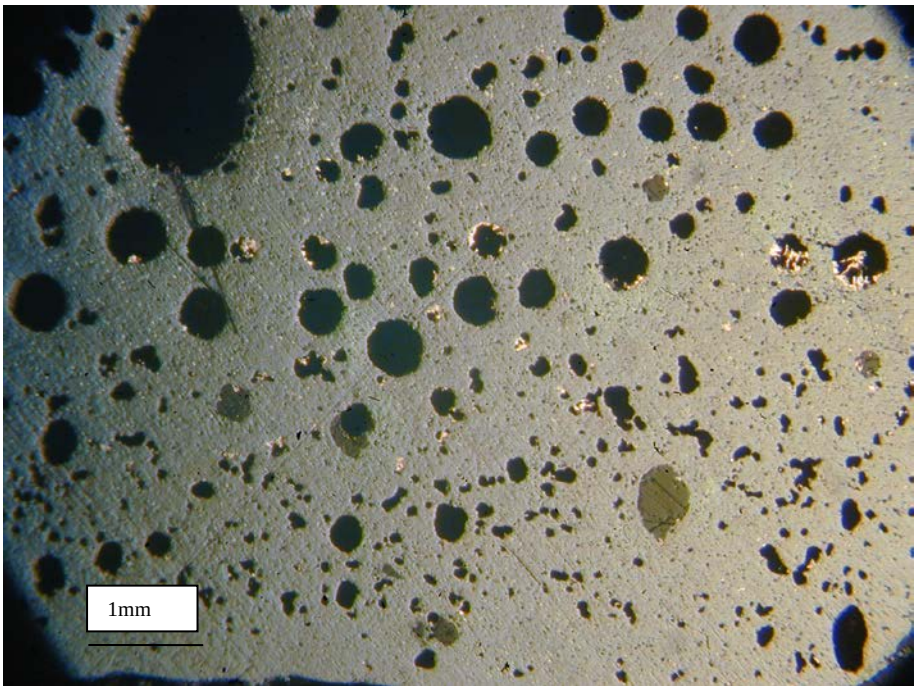

Figure 6.67 Optical microscope image of matte 1PB RT showing copper droplets (mid-tone) and porosity (dark).

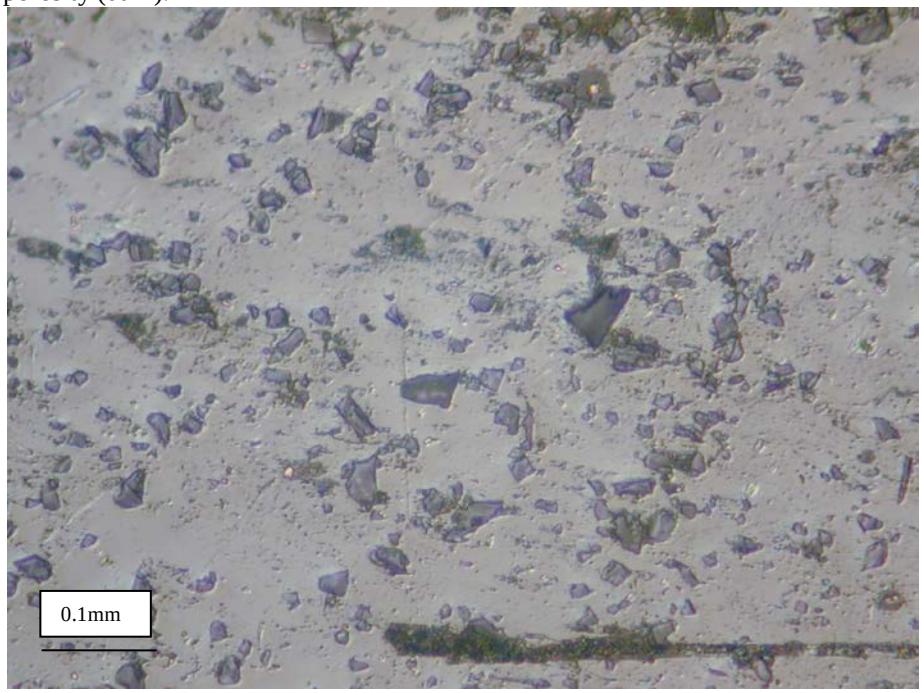

Figure 6.68 Optical microscope image of lead ingot 2PB RT showing angular impurities due to polishing.

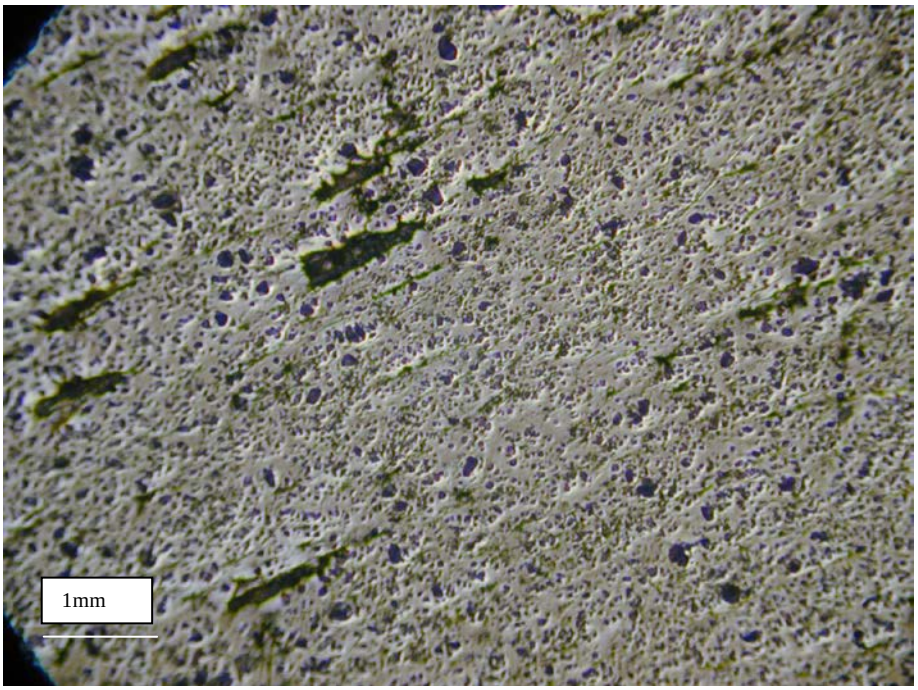

Figure 6.69 Optical microscope image of lead ingot 3PB RT showing the intense diffusion of angular impurities due to polishing.

6.11.2 Semi-Reacted Ores

The semi-reacted ores are an assemblage of slag associated to partially reacted ores recovered at the Rio Tinto Museum, in addition sample RT25 L119 S50 from the Iberian assemblage will be considered. Semi-reacted ores were studied in order to obtain an indication of the lead isotope signature of raw material from antiquity and to compare it with the literature data and the slag samples under consideration.

The main compounds (Table 6.39 and Table 6.0 for sample RT25 L119 S50) are silica, alumina and iron oxide, as for the slag, but in the semi-reacted ore samples these compounds vary greatly. Some of the samples have a characteristic composition, highly influenced by other components: for instance, samples 4MIN RT and RT25 L119 S50 both show high iron oxide associated with in one case (4 MIN RT) with high barium oxide and sulphur, indicating jarosite plus barite, and high arsenate, while sample RT25 L119 S50 shows low barium oxide, sulphur and arsenate and seem to be the result of a “roasting” process where from the jarosite only iron oxide is left with its content of silver and sntimony.

Antimony and silver contents are also very high. Sample 7MIN RT shows a comparable antimony and arsenate concentration to samples 4MIN RT and RT25 L119 S50, but much lower silver (one order of magnitude), barium oxide, and

sulphate. Samples 8MIN RT and 10MIN RT present a much higher concentration of copper oxide (~5 wt%), but, except for this compound, the two samples show a completely different chemistry: 8MIN RT shows a typical slag composition, while 10MIN RT shows a composition much closer to ceramic.

Overall, 4MIN RT seems to have the closest composition to the expected ore material (jarosite plus barite) used as charge for the smelting.

	Na2O %	MgO %	Al2O3 %	SiO2 %	P2O5 %	S %	K2O %	CaO %	TiO2 %	MnO %	FeO %	BaO %	PbO %	SnO2 %	CuO %	ZnO %	As %	Ag µg/g	Sb µg/g	Bi µg/g
4 MIN RT	0.36	2.92	0.30	7.83	n.d.	4.47	0.17	0.07	0.34	0.02	44.78	18.94	3.69	0.04	0.18	0.05	3.35	686.32	2411.22	n.d.
5 MIN RT	0.30	0.99	1.23	72.04	n.d.	0.34	0.41	0.33	0.26	0.01	19.27	1.52	0.96	0.04	0.04	0.01	0.62	65.31	905.14	n.d.
6 MIN RT	0.16	0.84	14.01	63.07	0.01	0.25	2.30	0.11	0.61	0.03	12.25	0.39	0.35	0.01	0.16	0.02	1.91	51.09	283.71	n.d.
7 MIN RT	0.10	2.01	0.33	6.45	n.d.	1.20	0.08	0.10	n.d.	0.09	75.12	0.33	3.00	0.07	0.45	0.04	3.26	20.86	2488.02	n.d.
8 MIN RT	0.54	0.37	11.81	45.36	0.03	1.53	2.23	0.40	0.50	0.07	29.44	0.29	0.25	0.01	4.48	0.17	0.06	26.43	518.41	7.94
9 MIN RT	0.45	0.40	10.15	39.02	0.06	1.05	1.53	1.16	0.38	0.08	43.13	0.17	0.03	0.00	0.62	0.07	0.05	3.17	116.74	n.d.
10 MIN RT	0.38	0.76	19.00	63.92	n.d.	n.d.	3.68	0.13	0.76	0.02	4.44	0.09	0.43	0.02	5.79	0.06	0.13	129.55	1595.99	21.88
11 MIN RT	0.22	0.48	13.47	49.66	0.08	0.90	2.09	0.25	0.51	0.07	28.78	0.33	0.08	0.01	0.81	0.14	0.29	20.26	291.15	3.99
12 MIN RT	0.47	0.03	8.35	48.96	0.06	1.41	1.55	0.63	0.31	0.07	33.66	0.27	0.01	0.00	1.71	0.26	0.02	5.24	929.81	n.d.

Table 6.39 XRF analyses of the semi-reacted ore samples.

		Na2O %	MgO %	Al2O3 %	SiO2 %	P2O5 %	S %	K2O %	CaO %	TiO2 %	MnO %	FeO %	BaO %	PbO %	SnO2 %	CuO %	ZnO %	As %	Ag µg/g	Sb µg/g	Bi µg/g
RT25 L115 S56	Iberian	1.65	0.94	0.62	6.11	0.01	6.27	0.29	6.93	0.11	0.02	0.26	0.02	95.18	0.17	0.67	0.03	0.31	103	3569	6880
RT25 L115 S59	Iberian	2.27	1.58	0.43	4.37	0.01	0.04	0.11	3.92	0.11	0.01	0.43	0.03	99.70	0.04	0.31	0.01	0.81	61	1868	250
RT25 L119 S50	Iberian	0.25	0.49	1.72	4.82	n.d.	0.09	0.05	0.08	0.03	0.02	89.70	0.04	0.52	0.04	0.13	0.03	0.62	1141	1161	10

Table 6.40 XRF analyses of the Ibero-Punic litharge and semi-reacted ores samples.

6.11.3 Litharge

Two samples of litharge were analysed within the Iberian assemblage, and have already been partially discussed in the section 6.4.2.

The composition of the two samples is slightly different (Table 6.40): RT25 L115 S59 shows a composition purer than RT25 L115 S56, but the impurities present in the two samples are consistent for typology and concentration, except for sulphur that is much higher in sample RT25 L115 S56, while RT25 L115 S59 presents higher arsenic. This seems to be an indication of the use of at least two different sources of material, one more enriched in sulphides/sulphates, and one more enriched in arsenates. There is a possibility that the arsenates are linked with the jarosite in the ore mineralogical association, and this theory would be consistent with the data regarding the semi-reacted ores presented in section 6.11.2, while the higher presence of sulphur may suggest a further addition of galena in the smelting process as silver collector.

Both of the samples present very low silver (around 100ppm), indicating a highly efficient cupellation process.

6.12 Summary

The chemical, petrographical and mineralogical analyses presented above clearly indicate that three processes were carried out at different times at the site of Corta Lago.

The main process, during the period under consideration here, is the smelting of jarosite plus quartz in a ratio of approximately 2 to 1, producing silver-rich lead bullion (also rich in arsenic, sulphur, bismuth and antimony) and fayalitic tapped slag, except for the Republican phase II plate slag period, when the slag produced had plate morphology due to the difference in slag 'tapping behaviour'. This process is a more or less continuous process performed at a temperature around 1100 ºC (Fig. 6.62) and oxygen pressure between 10^{-8} and 10^{-12} atm (Fig. 6.63). This process was carried out from approximately 600 BC (Phoenician period) to 200 AD (Imperial Roman).

Some variations were observed, mainly regarding the amount of material involved and the method of separation of the slag from the metal, and these will be discussed in

detail in Chapter 9. A major increase in production is observable during the Roman Imperial period.

The exploited ore, throughout the nine centuries under consideration, was jarosite associated with polymetallic sulphides and arsenates in different concentrations. Quartz was added to the system to separate the lead/silver bullion from the iron, producing a fayalitic slag, as explained in Chapter 3.

The Republican phase II plate slag period shows a change in the process of cooling the slag. The metal still accumulates in the furnace, but the slags are tapped in subsequent flows in a forehearth where they are left to solidify, partially or completely and then they are removed to allow a following tapping step. Mineralogically and chemically (so far as the major compounds are concerned), these slags do not differ greatly from the tapped slag; consequently, the temperature and the redox conditions reached during the process are similar, and the same is true for the viscosity level. The most striking difference is that the macro-morphology of the slag typical of this limited period indicates that the tapping of the slag and metal was performed in a forehearth where the separation between the two occurred. This is however not the only difference observed in these slags. The efficiency of the process is higher (the silver loss decreases), and, as we will discuss in Chapter 8, the isotopic signature is different from that of the samples from contiguous periods. This change in the production process will be discussed in Chapters 8 and 9 within the geological framework, but socio-economic factors may also have been the cause or contributed to this change as well.

The third process is the one producing the ball slag. In this case, an excess of barite/quartz was present, producing a web of unreacted crystals, the use of which is extensively debated by other scholars and was presented at the beginning of this chapter.

A change in the scale of the production is visible at the passage between Republic and Empire, when the scale of the tapping hole increases (doubles), indicating a possible increase in the size of the furnace.

The main chemical compositions determined during this project are in agreement with the data published by Craddock (1995) and Keesmann (1993), presented in Chapter 4. The high concentration of arsenic measured during the chemical analyses carried out in the context of this project would also corroborate the possibility of the formation of

speiss, hypothesised by both the abovementioned authors. The absence of speiss samples within the available material, with clear labelling to identify the archaeological context, did not allow the author to add examples of this material to the analytical data presented in this thesis. A discussion of the interpretation as compared with the ones provided by these two authors will follow in Chapter 9.

CHAPTER 7

Corta Lago versus Tharsis

This chapter focuses on the material recovered from Tharsis. The material is studied following the chemical, mineralogical and petrographic techniques described in Chapter 5. The analytical results are then compared with the results obtained for the materials recovered from Corta Lago. The first part of the chapter focuses on the chemical, mineralogical and petrographical discussion of the Tharsis material (the isotopic discussion will follow in Chapter 8), followed by a comparison of the results with those obtained for Corta Lago. This comparison aims to emphasise the similarities and differences between the Roman metallurgical processes in operation at the two sites, leading to an understanding of the technological responses to the different geological constraints at the two sites.

The site of Tharsis is not described in detail here, because only the comparison of the metallurgical debris from this site to that from Corta Lago is relevant to this project, a brief description of the site, its archaeology and its geology can be found in section 4.4. The site has been extensively discussed by several scholars (Gonzalo y Tarin 1886; Rothenberg and Blanco Freijeiro 1981, 172; Domergue 1987; 1990; Perez Macias 1998, 89) and the knowledge of the author derives from these eminent accounts based on fieldwork in the area. Nevertheless, I wish to highlight that Tharsis, like Corta Lago (Rio Tinto), is recognised as having been one of the main silver and copper producing sites from the exploitation of jarositic ore during Roman times (Domergue 1987). Thus, as already mentioned above, both sites can be considered as part of a bigger ‘industrial’ metal producing region. The provinces of Roman Hispania were considered as a single entity when it came to metal and ‘stone’ production (Pliny and Strabo). This consideration is important because the two sites can therefore be compared under the assumption that they were exploited using a similar technical approach.

The material from the site of Tharsis consists entirely of Roman slag and was collected by the author directly on-site, with the supervision and support of Dr. Aurelio Perez Macias, who indicated the locations of Republican and Imperial slag.
The slags were prepared for analysis according to the same procedure applied to the Corta Lago samples, following the methodology discussed in Chapter 5.
Not being as reworked as those from Corta Lago, the slag fragments from Tharsis are much larger and the macro-morphology is more visible.

7.1 Republican slag

Figure 7.1 Top surface of sample Tha-Rep 6, showing an intense red patina and lava flow structures typical of tapped slag.

Figure 7.2 Bottom surface of sample Tha-Rep 6, showing red patina, roughness, and inclusions of pebbles and soil due to tapping outside the furnace.

Figure 7.3 Top surface of sample Tha-Rep 3, showing red patina and lava flow structures typical of tapped slag.

Figure 7.4 Bottom surface of sample Tha-Rep 3, showing red patina, rough and brittle aspect, and inclusions of pebbles and soil due to tapping outside the furnace.

Figure 7.5 Top surface of sample Tha-Rep 2, showing light red/brown patina and lava flow structures typical of tapped slag.

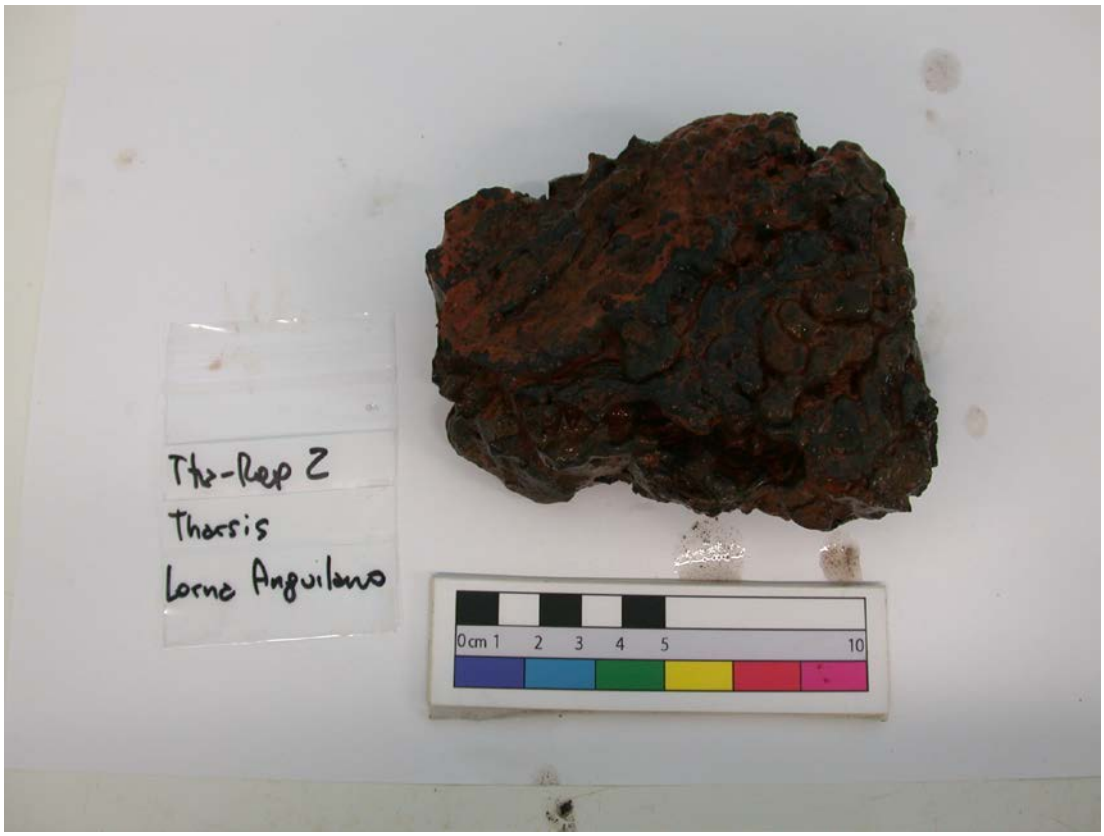

Figure 7.6 Bottom surface of sample Tha-Rep 2, showing red/orange patina and short and rounded lava flow structures. This slag does not show a brittle rough surface at the bottom but flowing structures instead.

Figure 7.7 Top surface of sample Tha-Rep 1, showing light red/brown patina and fine lava flow structures typical of tapped slag.

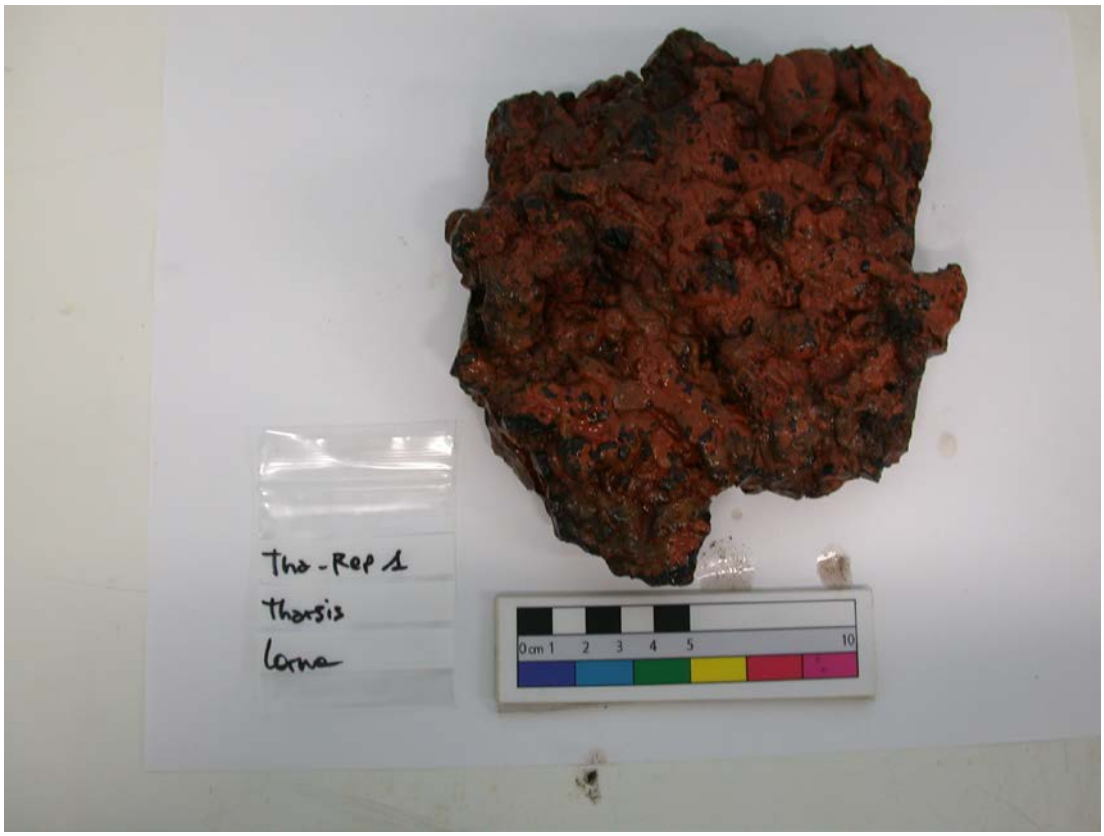

Figure 7.8 Bottom surface of sample Tha-Rep 1, showing intense red patina, rough and brittle aspect, and inclusions of pebbles and soil due to tapping outside the furnace.

The Republican slags always show red patina and lava flows (Figs 7.1 to 7.8). The lava flows, as discussed in Chapter 6, are typical of the tapping process, and are generated by flows of liquid or semi-liquid slag leaving the furnace via the tapping hole, one on top of the other, and solidifying like lava (Fig. 6.2). These morphological features range from fine (around 0.5 to 1 cm, sample Tha Rep 1 – Fig. 7.7) to greater widths (around 2 cm, samples Tha Rep 2 and 3 – Figs. 7.1 and 7.5). The thickness of the slag itself is always less than 5 cm (measured in fragments showing the originals' superior and inferior surfaces), providing an idea about the thickness of the amount of slag tapped out of the furnace. Only fragments around 10 cm in length were recovered, and thus no more information on the slag flow can be retrieved.

The mineralogical association is dominated by the presence of olivine, with a purely fayalitic composition, and only samples Tha-Rep 2, 5 and 6 present small concentrations of magnesia (between 0.5 and 1%) in a few crystals. Olivine is associated with a glass matrix and lead/iron sulphides and iron oxides. No silver was detected in the metal-bearing droplets (Fig. 7.9 and Table 7.1).

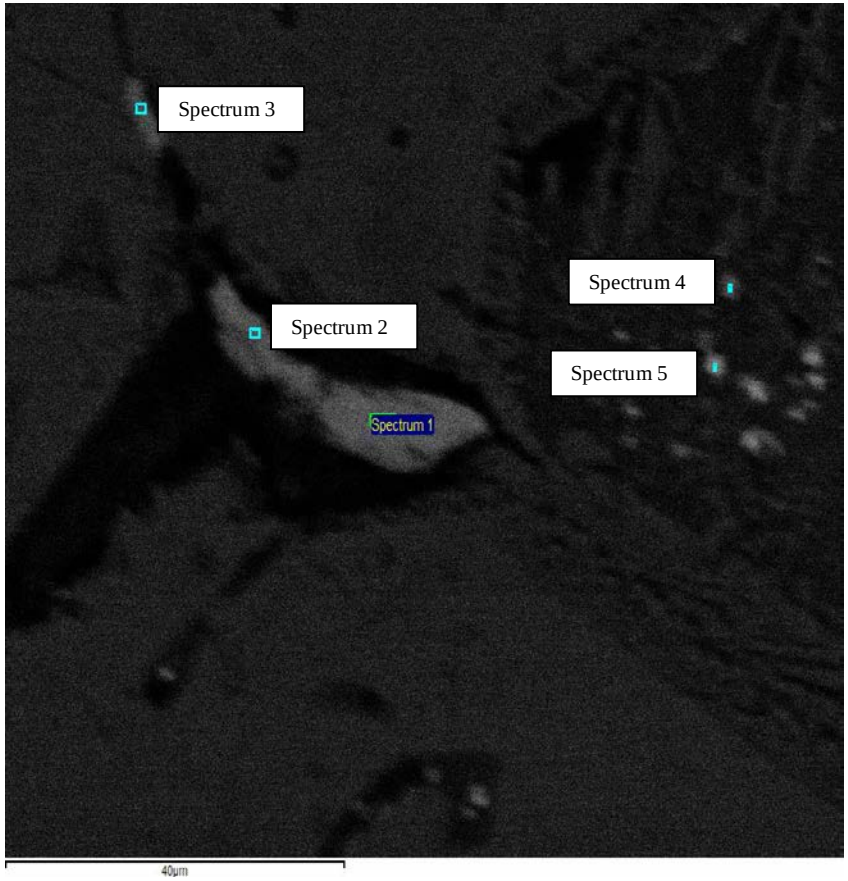

Figure 7.9 SEM backscattering image of the metal-bearing phases interstitial to the olivines.

	S	Fe	Pb
spectrum 1	13.8	39.6	46.7
spectrum 2	10.8	44.9	44.3
spectrum 3	18.0	39.8	43.2
spectrum 4	9.3	55.9	34.8
spectrum 5	19.6	65.0	15.4

Table 7.1 SEM-EDS spectra of the metal bearing droplets interstitial to the olivines in Figure 7.9.

The olivines present spinifex texture and skeletal H-chain structure (Figs. 7.10 and 7.11), and the oxides are dispersed inter-granularly. Inter-granularly we can also observe a second generation of finer skeletal olivines. The two generations of olivine are not chemically different. The skeletal structure presents an average length of 600 to 1000 μm, while the oxides present a much smaller size (around a few microns).

Overlayering of spinifex texture indicating successive tapping of slag, as already observed in the Phoenician samples from Corta Lago, is present in the samples (Fig. 7.10). The layers have different preferential orientation determined by the growth of the crystal from a different cooling surface and are separated by a layer of oxidation.

Figure 7.10 OM image showing overlayering of spinifex texture in sample Tha-Rep 1.

Figure 7.11 OM image showing H-chain skeletal structure of olivine in sample Tha-Rep 1.

Considering the correction for XRF and EDS-SEM discussed in Chapters 5 and 6, the chemical analyses of both the powder (by XRF) and the polished sample (by EDS-SEM) suggest that the Republican slags are chemically homogenous, presenting only a 0.1% difference for iron oxide and silicon oxide between two of the samples analysed by XRF (Table 7.2); a higher variance can be observed among the averages of the SEM analyses of seven samples (Table 7.3). As regards homogeneity within the samples, calculated measuring the chemical composition of 10 adjacent areas by SEM-EDS (see Chapter 5 for the analytical method), we can observe that the standard deviation of the 10 areas analysed per sample reaches 2 for FeO only in samples Tha Rep 5 and 6, while the standard deviation for silicon oxide reaches 2 in Tha-Rep 5 only, which is the sample with lower chemical uniformity than the others (Table 7.3).

The corrected chemical composition fits with the olivine field in the diagram $Al_2O_3/Fe_2O_3/SiO_2$, close to optimum 1 (Fig. 7.12), indicating a smelting temperature slightly lower than 1200 ºC. The mineralogical association fayalite/magnetite indicates oxygen fugacity in the range 10^{-8} to 10^{-12} atm (Fig. 6.63).

The loss of silver is very low, between 70 and 80 ppm (Table 7.2), indicating a very efficient process. This concentration of silver is associated to a constantly low concentration of lead, between 1 and 1.5 wt%. These numbers correspond only to the Republican phase II plate slag from Corta Lago, while all the Roman tapped phases, the two Republican phases and the Imperial, present a much higher variability for what concerns the lead oxide, and a higher loss of silver.

	Na2O	MgO	Al2O3	SiO2	P2O5	SO3	K2O	CaO	TiO2	MnO	FeO	BaO	PbO	SnO2	CuO	ZnO	As2O3	Ag	Sb	Bi
	%	%	%	%	%	%	%	%	%	%	%	%	%	%	%	%	%	µg/g	µg/g	µg/g
Tha rep 1	n.d.	1.08	3.92	34.14	0.05	0.18	0.63	0.52	0.43	0.08	57.59	0.02	1.11	0.06	0.06	0.01	0.06	71	844	12
Tha rep 4	0.27	1.16	2.51	34.43	0.11	0.53	0.44	0.32	0.32	0.05	58.30	0.02	1.34	0.05	0.05	0.01	0.02	78	560	14
Tha imp 9	0.18	1.50	1.75	28.25	0.15	1.04	0.47	1.24	0.30	0.06	62.37	0.01	1.52	0.04	0.06	0.03	0.88	53	1410	17
Tha imp10	0.41	2.14	3.05	31.04	0.16	0.82	0.83	1.52	0.53	0.05	55.95	0.02	2.48	0.03	0.05	0.02	0.76	35	1164	n.d.

Table 7.2 Chemical bulk analyses obtained by X-Ray Fluorescence for two Republican and two Imperial samples.

	THA REP 2		THA REP 1		THA REP 3		THA REP 4		THA REP 5		THA REP 6		THA REP 8	
	average	standard deviation	average	standard deviation	average	standard deviation	average	standard deviation	average	standard deviation	average	standard deviation	average	standard deviation
Al2O3	3.83	0.23	4.99	0.38	4.90	1.39	3.67	1.44	5.89	0.58	4.48	0.30	4.20	0.36
SiO2	35.79	0.74	34.31	1.14	38.83	1.98	35.60	1.22	42.36	2.07	39.86	1.85	36.91	1.22
P2O5	0.00	0.00	0.00	0.00	0.00	0.00	0.00	0.00	0.00	0.00	0.00	0.00	0.13	0.27
SO3	0.30	0.39	0.40	0.55	0.00	0.00	0.00	0.00	0.00	0.00	0.69	0.38	0.82	0.32
K2O	0.71	0.06	0.72	0.09	0.38	0.62	0.14	0.43	0.85	0.08	0.74	0.10	0.71	0.17
CaO	1.17	0.22	0.92	0.13	0.00	0.00	0.00	0.00	0.72	0.08	0.94	0.14	0.78	0.14
TiO2	0.49	0.19	0.46	0.42	0.00	0.00	0.00	0.00	0.68	0.09	0.55	0.21	0.44	0.25
FeO	54.85	0.92	58.20	1.59	55.78	4.95	62.56	1.60	49.24	2.66	50.42	2.20	55.77	1.69
As2O3	0.04	0.11	0.00	0.00	0.00	0.00	0.00	0.00	0.00	0.00	0.00	0.00	0.00	0.00
PbO	2.83	0.34	0.00	0.00	0.00	0.00	0.00	0.00	0.26	0.55	2.33	0.43	0.26	0.54

Table 7.3 Averages of chemical area analyses (10 per sample) performed by EDS-SEM, as discussed in Chapter 5.

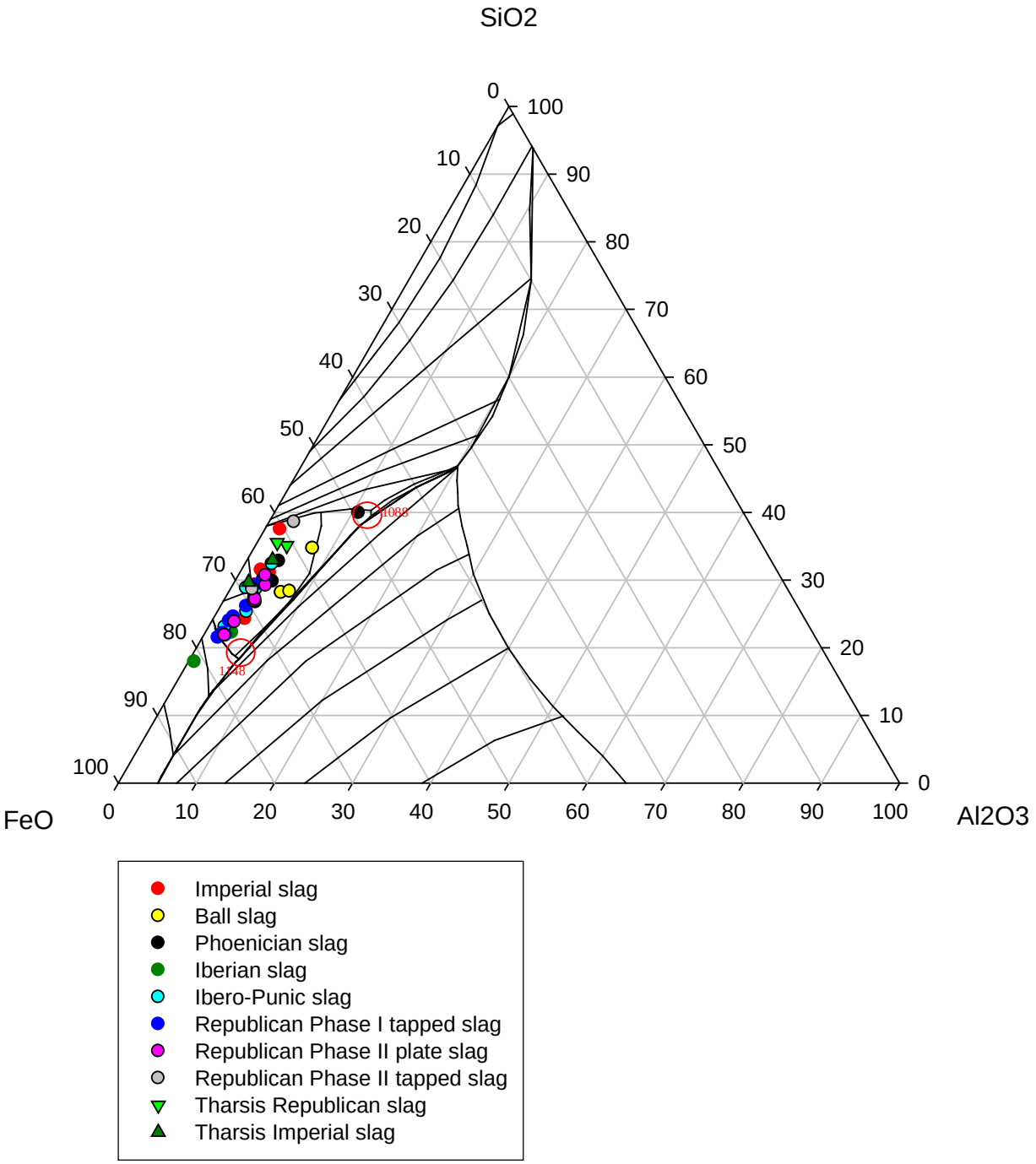

Figure 7.12 Plot of the main compounds alumina, silica, and the sum of iron oxide, barium oxide, lead oxide, calcium oxide and magnesium oxide. All the samples from Corta Lago are represented by circles, while the samples from Tharsis are represented by triangles, green for Republican and dark green for Imperial Tharsis samples.

7.2 Imperial slag

Figure 7.13 Top surface of sample Tha-Imp 5, showing light red/brown patina and lava flow structures of around 2 cm typical of tapped slag.

Figure 7.14 Bottom surface of sample Tha-Imp 5, showing brown/red patina, rough and brittle aspect, and inclusions of pebbles and soil due to tapping outside the furnace.

The Imperial slag recovered from the site of Tharsis shows the characteristic features of typical tapped slag, such as lava flows and bulky morphology. The lava flows are from around 2 cm (Fig. 7.13) to around 5 cm wide; the large ones being of a rounded shape rather than elongated/flow-like, possibly indicating a higher viscosity due to the larger amount of material. Sample Tha-Imp 5 (Figs. 7.13 and 7.14) is the biggest fragment sampled and is between 5 and 10 cm thick, indicating a large slag tapping flow from the furnace. No other size indications can be provided.

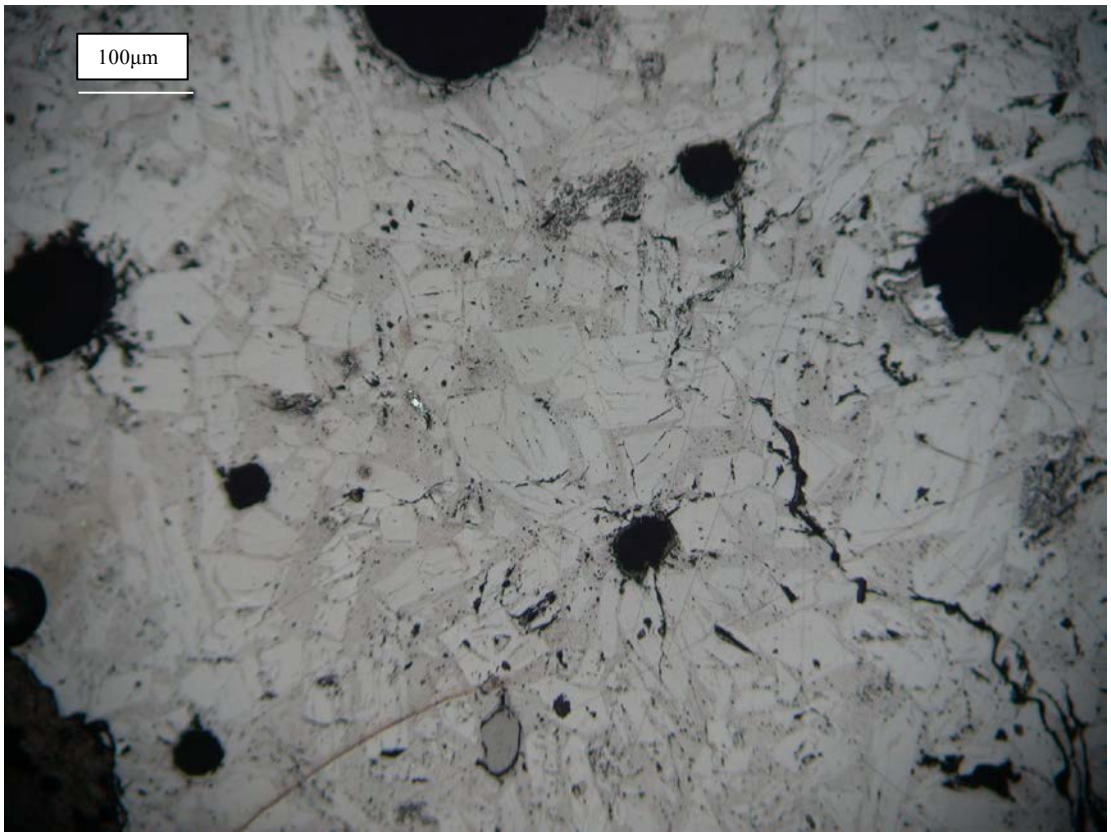

Figure 7.15 OM image of sample Tha-Imp 4, showing olivine mainly crystallised with hopper morphology.

Figure 7.16 OM image of sample Tha-Imp 4, showing that a closer look indicates the presence of two families of olivines: a larger one with hopper morphology and a smaller one, forming interstitially with skeletal morphology.

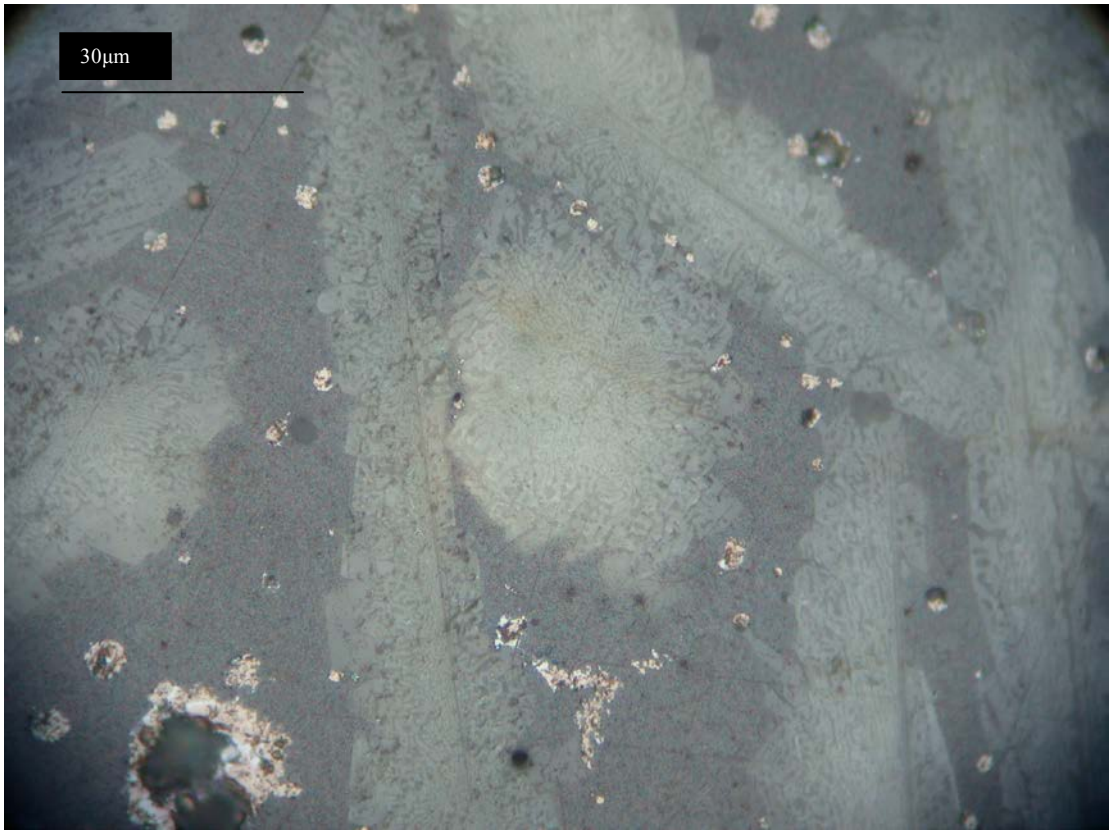

Figure 7.17 Detailed OM image of olivine associated with metallic prills. The olivines show eutectic texture.

Two generations of olivine (Fig. 7.16) can be documented, one of larger size and hopper morphology (Fig. 7.15 - Donaldson 1976), with an average size around 300 µm, and a second interstitial one of a much finer skeletal morphology (100 µm). The two generations of olivines do not show any chemical difference.

The chemical composition of the Imperial slag presents a more scattered situation in terms of the variance between the main compounds as obtained by XRF (Table 7.2); on the other hand, results similar to the ones recorded for the Republican samples can be observed in the averages resulting from SEM analyses (Table 7.4). The difference in composition between the samples reaches figures around 5% for silica and 7% for iron oxide. The chemical composition plots in the centre of the olivine stability field.

The loss of silver is very low, between 30 and 50 ppm, even lower than for the Tharsis Republican samples, and only comparable with one group of the Republican phase II plate slag from Corta Lago.

The chemical analyses carried out on each sample (ten adjacent areas were chemically analysed by SEM-EDS to assess the uniformity of the samples – see Chapter 5 for methodology) demonstrate that some of the samples are fairly uniform, presenting a low standard deviation (<1) for most samples except samples Tha-Imp 1 and Tha-Imp 2, where the standard deviation is around 2 for silica and iron oxide (using these two major components as indexes of variability – Table 7.4).

											average	standard deviation
THA-IMP 4												
Al2O3	2.31	2.16	2.80	2.41	2.36	2.41	2.97	2.34	2.16	2.18	2.41	0.27
SiO2	35.19	32.12	35.33	34.00	33.29	32.85	33.36	33.41	33.26	34.24	33.71	1.00
SO3	1.23	0.00	1.68	1.21	1.81	1.52	1.86	1.53	1.57	1.48	1.39	0.53
K2O	0.69	0.55	0.72	0.83	0.82	0.89	0.91	0.82	0.87	0.70	0.78	0.11
CaO	2.47	1.93	2.20	2.28	2.13	2.09	2.28	2.21	1.77	1.91	2.13	0.21
TiO2	0.00	0.00	0.69	0.00	0.00	0.68	0.00	0.75	0.00	0.00	0.21	0.34
FeO	59.69	61.55	56.59	59.27	59.60	59.57	58.62	58.94	60.37	59.49	59.37	1.27
PbO	0.00	1.67	0.00	0.00	0.00	0.00	0.00	0.00	0.00	0.00	0.17	0.53
THA-IMP 9												
Al2O3	2.34	2.54	1.87	2.58	2.08	1.65	2.21	2.45	2.45	1.82	2.20	0.33
SiO2	29.51	28.76	29.84	30.23	29.64	29.25	29.80	28.82	28.82	29.16	29.38	0.50
P2O5	0.67	0.75	0.00	0.00	0.73	0.00	0.00	0.00	0.00	0.80	0.30	0.38
SO3	1.35	0.94	1.15	1.46	0.90	0.87	1.25	1.66	1.66	0.88	1.21	0.31
K2O	0.89	0.95	0.74	1.09	0.79	0.58	0.67	0.81	0.81	0.59	0.79	0.16
CaO	1.62	1.69	1.65	1.44	1.45	1.23	1.77	1.71	1.71	1.20	1.55	0.21
TiO2	0.43	0.44	0.00	0.00	0.00	0.00	0.00	0.51	0.51	0.00	0.19	0.25
FeO	63.18	62.45	64.77	63.19	64.40	66.41	64.30	64.03	64.03	65.56	64.23	1.17
PbO	0.00	1.48	0.00	0.00	0.00	0.00	0.00	0.00	0.00	0.00	0.15	0.47
THA-IMP 10												
Al2O3	3.81	3.92	3.71	3.95	4.75	4.32	4.66	4.28	4.21	4.21	4.18	0.34
SiO2	34.12	33.68	33.81	34.75	33.70	34.30	34.56	33.44	33.86	33.88	34.01	0.42
P2O5	0.00	0.80	0.00	0.00	0.70	0.78	0.00	0.00	0.00	0.00	0.23	0.37
SO3	1.91	1.53	1.60	1.41	1.46	1.64	1.68	1.57	1.63	1.33	1.58	0.16
K2O	1.00	0.98	0.86	0.92	1.22	0.87	1.01	0.93	1.12	1.18	1.01	0.13
CaO	1.68	1.80	1.56	1.72	2.01	1.97	1.82	1.88	2.03	1.90	1.84	0.15
TiO2	0.63	0.53	0.48	0.58	0.73	0.77	0.66	0.48	0.72	0.58	0.62	0.10
FeO	56.85	56.77	57.97	56.67	53.26	55.35	55.61	55.11	56.44	54.92	55.90	1.32
As2O3	0.00	0.00	0.00	0.00	0.00	0.00	0.00	0.00	0.00	0.20	0.02	0.06
PbO	0.00	0.00	0.00	0.00	2.18	0.00	0.00	2.31	0.00	1.80	0.63	1.02
THA-IMP 1												
Al2O3	0.00	0.00	0.00	0.00	3.04	3.92	0.00	2.39	3.05	0.00	1.24	1.64
SiO2	33.75	30.18	35.15	31.57	31.50	33.06	37.08	30.99	33.52	32.94	32.97	2.07
CaO	1.47	0.00	1.80	0.00	0.00	0.00	2.09	0.00	1.81	0.00	0.72	0.94
FeO	60.97	65.32	56.99	63.41	62.29	58.53	56.22	58.12	56.08	57.22	59.52	3.26
PbO	0.00	0.00	0.00	0.00	0.00	0.00	0.00	3.99	5.36	2.60	1.20	2.03
THA-IMP 2												
Al2O3	2.50	4.16	0.00	3.76	0.00	3.32	0.00	3.33	3.41	3.25	2.37	1.69
SiO2	35.62	36.08	40.23	36.62	38.52	38.35	38.88	39.51	42.28	39.15	38.52	2.02
K2O	0.00	0.00	0.00	0.00	0.00	0.00	0.00	0.00	0.00	1.45	0.15	0.46
CaO	0.00	0.00	0.00	0.00	1.51	0.00	1.67	0.00	0.00	0.00	0.32	0.67
FeO	57.52	63.44	63.76	60.51	57.38	57.92	59.75	57.52	66.05	58.20	60.21	3.15

Table 7.4 (part)

THA-IMP 3											average	standard deviation
Al2O3	2.70	4.33	4.01	3.25	3.23	4.11	2.70	3.38	3.37	4.15	3.52	0.59
SiO2	36.59	37.78	38.05	37.95	37.17	38.96	35.51	36.21	38.19	38.57	37.50	1.10
SO3	1.95	3.83	2.97	3.38	1.85	2.86	1.34	1.37	1.50	3.01	2.41	0.91
K2O	0.80	0.85	0.92	0.86	1.02	1.09	0.63	0.69	0.77	0.94	0.86	0.14
CaO	0.93	1.96	1.42	1.74	1.28	1.96	1.02	1.23	1.37	1.56	1.45	0.36
TiO2	0.36	0.83	0.60	0.61	0.39	0.84	0.37	0.40	0.46	0.74	0.56	0.19
FeO	56.67	50.41	52.03	52.21	52.98	50.19	57.36	54.65	54.34	51.03	53.19	2.51
WO3	0.00	0.00	0.00	0.00	2.07	0.00	0.00	2.07	0.00	0.00	0.41	0.87
PbO	0.00	0.00	0.00	0.00	0.00	0.00	1.07	0.00	0.00	0.00	0.11	0.34
THA-IMP 5												
Al2O3	0.00	0.00	0.00	0.00	0.00	0.00	0.00	2.53	0.00	0.00	0.25	0.80
SiO2	38.39	37.63	34.29	36.47	40.35	41.02	38.21	38.95	38.24	37.90	38.15	1.88
SO3	0.00	0.00	0.00	0.00	0.00	0.00	0.00	0.00	0.00	3.32	0.33	1.05
K2O	0.00	0.00	0.00	0.00	0.00	1.29	0.00	1.57	1.46	0.00	0.43	0.70
CaO	2.29	1.91	1.60	0.00	0.00	0.00	1.65	2.27	2.29	0.00	1.20	1.06
FeO	58.45	60.50	57.98	60.94	57.96	58.12	56.16	59.13	57.47	58.34	58.51	1.40
THA-IMP 7												
MgO	0.00	0.00	0.00	0.00	0.00	0.00	0.00	0.00	0.00	0.49	0.05	0.15
Al2O3	2.68	2.59	2.96	3.01	2.14	2.59	2.85	2.91	2.83	1.89	2.65	0.37
SiO2	32.50	32.44	32.89	32.71	32.14	32.26	32.91	32.33	32.21	31.91	32.43	0.33
P2O5	0.00	0.00	0.00	0.00	0.70	0.00	0.65	0.00	0.00	0.00	0.14	0.28
SO3	1.85	1.52	1.43	1.81	1.39	1.63	1.48	1.91	1.83	1.25	1.61	0.23
K2O	0.59	0.80	0.83	0.76	0.60	0.82	0.83	0.90	0.70	0.55	0.74	0.12
CaO	1.85	1.74	1.82	1.90	1.37	1.75	1.89	1.81	1.84	1.22	1.72	0.23
TiO2	0.00	0.41	0.36	0.38	0.48	0.00	0.00	0.37	0.36	0.35	0.27	0.19
FeO	60.53	60.49	59.71	59.43	61.19	60.96	59.16	59.78	60.23	62.34	60.38	0.95
As2O3	0.00	0.00	0.00	0.00	0.00	0.00	0.22	0.00	0.00	0.00	0.02	0.07
THA-IMP 8												
Al2O3	2.88	2.42	2.55	2.68	2.37	2.62	2.75	2.40	2.61	2.28	2.56	0.19
SiO2	32.57	32.25	32.37	32.08	32.15	32.45	31.83	33.26	32.79	32.85	32.46	0.42
P2O5	0.00	0.00	0.00	0.59	0.00	0.00	0.00	0.00	0.00	0.00	0.06	0.19
SO3	1.88	1.71	1.28	1.91	1.63	1.63	1.94	2.00	2.42	1.20	1.76	0.36
K2O	0.67	0.63	0.54	0.71	0.63	0.62	0.55	0.70	0.54	0.57	0.62	0.06
CaO	1.04	0.72	0.89	0.89	0.76	0.87	0.97	0.91	0.79	0.53	0.84	0.14
TiO2	0.59	0.47	0.50	0.59	0.60	0.00	0.44	0.48	0.50	0.44	0.46	0.17
FeO	58.40	61.80	60.00	60.55	61.85	59.98	59.55	60.25	60.35	62.15	60.49	1.16
As2O3	0.00	0.00	0.21	0.00	0.00	0.00	0.00	0.00	0.00	0.00	0.02	0.07
PbO	1.99	0.00	1.66	0.00	0.00	1.83	1.98	0.00	0.00	0.00	0.75	0.97

Table 7.4 (part)

THA-IMP 11											average	standard deviation
Al2O3	2.66	2.97	3.28	3.17	2.94	2.70	3.24	3.08	2.97	2.64	2.97	0.24
SiO2	34.59	34.37	34.48	33.55	33.01	34.39	33.88	34.35	33.89	33.89	34.04	0.49
P2O5	0.00	0.00	0.00	0.00	0.91	0.00	0.00	0.00	0.00	0.00	0.09	0.29
SO3	1.22	1.47	1.31	1.28	1.12	1.26	1.29	1.39	0.00	1.20	1.15	0.42
K2O	0.53	0.58	0.77	0.68	0.52	0.49	0.83	0.63	0.61	0.58	0.62	0.11
CaO	0.88	0.97	1.00	1.05	1.17	1.08	1.17	1.08	1.05	1.01	1.05	0.09
TiO2	0.63	0.00	0.81	0.89	0.67	0.00	0.00	0.00	0.00	0.85	0.39	0.41
FeO	59.50	59.64	58.34	59.38	59.67	60.08	59.59	59.46	59.66	59.84	59.52	0.46
PbO	0.00	0.00	0.00	0.00	0.00	0.00	0.00	0.00	1.81	0.00	0.18	0.57
THA-IMP 12												
Al2O3	2.52	2.29	2.40	2.36	2.40	2.62	2.61	2.85	2.43	2.83	2.53	0.19
SiO2	30.98	32.10	32.54	32.66	32.39	33.18	33.72	33.68	33.54	33.76	32.86	0.90
SO3	1.47	1.34	1.54	1.52	1.40	1.94	2.21	2.04	1.82	1.78	1.71	0.30
K2O	0.57	0.58	0.49	0.54	0.55	0.62	0.55	0.67	0.64	0.64	0.59	0.06
CaO	0.87	0.74	0.84	0.79	0.85	0.90	1.07	1.05	1.05	1.02	0.92	0.12
TiO2	0.67	0.38	0.53	0.53	0.55	0.70	0.62	0.65	0.63	0.66	0.59	0.10
FeO	59.65	61.05	61.65	61.61	60.06	60.05	59.04	59.06	59.89	59.30	60.14	0.98
WO3	1.74	0.00	0.00	0.00	0.00	0.00	0.00	0.00	0.00	0.00	0.17	0.55
As2O3	0.00	0.00	0.00	0.00	0.00	0.00	0.19	0.00	0.00	0.00	0.02	0.06
PbO	1.54	1.53	0.00	0.00	1.79	0.00	0.00	0.00	0.00	0.00	0.49	0.79

Table 7.4 Area analyses of slag samples from Tharsis obtained by SEM-EDS. The last column indicates the standard deviation for each element.

7.3 Comparison: Republican versus Imperial tapped slag at Tharsis

Based on the analyses presented above, we can conclude that the differences between Republican and Imperial tapped slag from Tharsis are:

- Imperial tapped slag has wider lava flows;
- Imperial tapped slag is thicker;
- Silver content is comparable, but lower during the Imperial period;
- Lead content is comparable, but more variable and higher during the Imperial period;

The width of the lava flows, as already discussed for the Corta Lago material, can be linked with the diameter of the tapping hole. Therefore, an increase in the width of the lava flows should indicate an increase in the size of the tapping hole. Such an increase is likely to have been a solution for increasing the amount of charge processed per furnace, possibly alongside an increase in the size of the furnace itself. This hypothesis is supported by the increase of the thickness of the slag unit, as well as a decrease in standardisation of the waste product.

The loss of lead and silver is comparable and very low (Ag <50 ppm and Pb ~2%), even though we can observe in these values a higher variation during Imperial times, which corresponds to the variation observed in the main components. These results indicate a process that was very efficient in the recovery of silver, and also standardised. Considering both the bulk and the area analyses, we observe that the analysed samples display chemical uniformity (Tables 7.2, 7.3 and 7.4), indicating similar charge and smelting conditions on a large scale. In more detail, it seems that Republican slags show a very fine uniformity of the waste material, while the Imperial slags have a more 'approximate' composition (differences in composition between samples can be observed in Tables 7.2). The same observation is valid for the site of Corta Lago. The Republican samples also differ from the Imperial ones in terms of the concentration of antimony, higher than 1000 ppm for the Imperial samples and lower than that for the Republican. A similar pattern is identifiable for the concentrations of sulphur and calcium: the former is around 0.5 wt% and lower for the Republican samples, and between 0.8 and 1 wt% for the Imperial ones, while the latter is still around 0.5 wt% and lower for the Republican samples, but higher than 1 wt% for the Imperial ones (Table 7.2).

7.4 Comparison: Tharsis versus Corta Lago

From the results obtained from the two sites of Tharsis and Corta Lago, we can draw attention to several similarities and differences.

The similarities are on the large scale:

- chemical and mineralogical similarity (system dominated by the presence of fayalite);
- smelting temperature of 1100/1200 ºC;

- pO_2 in the range 10^{-8} to 10^{-12} atm.
- An increase in the size of the lava flows from the Republican to the Imperial period;
- No residual crystals are detected during the Roman periods;
- Alkali concentration is comparable.

The mainly fayalitic slags observed at the two sites indicate an iron-dominated system that appropriately reflects the smelting of jarosite. Jarosite being an iron sulphate, as already mentioned earlier, it needs to be processed in order to separate the iron from the lead (silver) bullion, the product of the smelting. This produces a system/debris similar to that resulting from copper and iron production, where the waste material is dominated by iron silicate. The iron silicate forming at a lower temperature is fayalite. The results indicate that the smelting was carried out at a temperature between 1100 and 1200 ºC (Fig. 7.12) in a reducing atmosphere (pO_2 between 10^{-8} and 10^{-12} atm – Fig. 6.63), conditions that allow the system to operate at the minimum temperature necessary for obtaining a completely liquid system. A fully liquid system is desirable in order to achieve the most efficient collection of the silver/lead bullion. As we have seen in the previous section, the Republican period slag at Tharsis is characterised by a system closer to optimum 1 (see section 7.1 and Fig. 7.12), similar to the situation encountered with Phoenician and Republican phase III tapped slags at Corta Lago. As the Imperial slags plot in the central area of the field, they are close to part of the Roman slag at Corta Lago. The distribution of the samples from Corta Lago is more scattered, occupying the entire field of olivine stability. Considering that only four samples from Tharsis are taken into account in terms of the XRF results, the tightness of their plot may be due to the relatively limited statistical relevance of the sample group selected for analysis. The choice of analysing only four samples by XRF is due to the fact that the main focus for this material were the SEM analyses, since we were mainly looking for analogies and differences with the material from Corta Lago, and a detailed microscopic investigation was considered the principal methodology to achieve this result.

The increase in the dimensions of the lava flow, as already discussed in the previous paragraph, indicates an increase in the size of the tapping hole, plausibly associated with an increase in the amount of material smelted and consequently the size of the furnace. The fact that we observe this increase during Imperial times both at Corta Lago and Tharsis leads us to infer that the production increased during the times of the Empire, due to an increase in the demand of silver accompanied by political stability, and the expansion of the politico-economic area ruled by the Romans, as will be discussed in Chapter 10.

The differences are:

- Corta Lago is chemically more variable both between samples from the same period and within each sample;
- Tharsis slags are poorer in Ba;
- The loss of silver in Tharsis samples is lower, comparable only with the loss observable in the Republican phase II plate slag from Corta Lago;
- Lava flows are smaller in width at Corta Lago; slag units are thicker at Corta Lago (Figs. 6.34 and 6.35 compared with Fig. 7.14);
- Sulphur content is much higher in Roman Corta Lago samples.

The chemical variability between samples at Corta Lago, and in comparison with Tharsis, seems to indicate the exploitation of jarositic ore associated with different gangue and minor minerals. The amount of barium (higher at Corta Lago) surely indicates differences in the gangue between Corta Lago and Tharsis, but the higher chemical variability at Corta Lago as compared to the uniformity at Tharsis seems to indicate that the exploited ore was highly variable at Corta Lago and more uniform at Tharsis. This can be the result of a more uniform geology at Tharsis, or of a mining choice, with a more careful ore selection carried out in the field at Tharsis.

The very efficient collection of silver at Tharsis, comparable only with the Republican phase II plate slag at Corta Lago, is indicative of the efficiency of the process rather than the ore. At Corta Lago, only the process producing the plate slags seems to have achieved the level of efficiency reached at Tharsis while producing tapped slags. This may indicate that the system was maintained in a liquid state for a longer time at Tharsis and that the lead/silver was freer to collect, as it occurred for the slag that were chosen to be cooled in the forehearths producing the Republican plate slags of Corta Lago. Within the Tharsis samples, this hypothesis is corroborated by the chemical homogeneity within each sample and the smaller size of the olivine crystals (Republican 500 µm long and less than 100 µm wide; Imperial hopper shaped 300 by 100 µm), indicating a shorter crystallisation time. In contrast, the olivine size and/or morphology at Corta Lago (Republican phase II first crystallisation skeletal >1000 by ~300 µm, and second crystallisation skeletal with smaller dimensions <500 by <100 µm; Republican phase III hopper-skeletal ~500 by 200 µm, Imperial euhedral 200 by 200 µm associated with H-chain-shaped crystals of first crystallisation sized >1000 by ~400 µm) indicates an early crystallisation of the silicates, which decreased the freedom of movement of the liquid fraction, including the lead/silver bullion. The Republican phase I at Corta Lago shows instead a smaller size for the olivines (30 by 200 µm), comparable if not smaller to the olivines observed at Tharsis. This can be an indication that during this period, similar to Tharsis, the crystallisation occurred quite late (during the tapping of the slag) and was rapid.

An increase in the lava flows is observed between the Republican and Imperial periods both at Tharsis and Corta Lago, but this increase is generally smaller at Corta Lago. This seems to indicate that within the increase of production taking place at both sites during the Imperial period, a smaller furnace was operated or a smaller amount of material per smelt was treated at Corta Lago.

This represents a fine tuning of the efficiency of the process, indicating that the skills at work in the two areas were similar in terms of their understanding of the ratio ore/gangue and temperature and redox conditions, but were slightly different in their capacity to make the process more efficient.

CHAPTER 8

The isotopic signature: a new approach to the metallurgical process

A description of the lead isotope technique is provided in Chapter 5 of this thesis, and the detailed sample preparation procedure and table of results can be found in Appendix 2. This chapter will focus on the results obtained by this technique. Before addressing the results, the need arises to discuss why in this case the interpretation of the results of the lead isotope analyses will be approached differently from the usual research of ore of origin of the exploited mineral or of the metal produced.

For the past decades, lead isotope analyses have been very important in archaeometallurgy, and several significant studies directed at building databases of metal objects, slag and ore lead isotope signatures have been carried out. The main aim of these studies was always the attempt to link the exploited ores to workshops and final objects, in order to provide a picture of the movements of the material in certain areas, permitting a better understanding of the organisation of the production.

The relevance of lead isotope data is visible by looking for instance at the studies by Gale (1989) and Stos-Gale et al. (1995), Pernicka et al. (1990), and several other scholars. However, it is also true that due to the nature of the principle behind the lead isotope analyses, there are limits to the technique. The main limit is that there is no certainty to the identification of the ore from which the mineral is exploited deriving from lead isotope analysis alone. The reason for this is, first of all, as already mentioned in Chapter 5, the nature of the method itself, which implies that ores of the same geological age would have basically the same lead isotope ratio. The second limit is that there are no complete or comprehensive databases of lead isotope signatures of ores, and the ore of origin that one is looking for could always be among the ores absent from the available databases.

For these reasons, lead isotope analyses can identify with certainty which ore is not the ore of origin, but not determine with precision which one it is.

In addition to the general observations mentioned above, the analyses carried out in the context of this project also have peculiar circumstances and background. The mineral exploited as raw material for the production of silver, both at Corta Lago and

Tharsis, is jarosite, as already mentioned on several occasions in this thesis. Better referred to as jarositic earth, the chemical variation of this mineral covers a wide range of compositions, allowing a diversity of concentrations of the different cations present in its lattice. For what concerns the lead, for instance, the concentration of plumbojarosite within jarositic earths may vary between 3 and 30% (Hunt Ortiz 2003, 35). This compositional diversity could have been the reason for the use of 'extra' lead, i.e. lead coming from sources located outside the Rio Tinto area, in order to keep the amount of lead in the charge constant. As mentioned in Chapter 3, lead has the function of silver collector. This lead metal or mineral (i.e. galena) added to the smelt will be referred to as 'extra' or 'foreign' lead.

This was the framework in which the lead isotope analysis was set. The main aim was to understand if an addition of 'extra lead' occurred, and how this addition of 'extra' lead functioned: during which period was this addition employed more extensively, and whether the addition was always from the same 'foreign' source. Furthermore, an indication of the possible source of this 'extra' lead will be provided, even if this indication of possible lead sources is not meant to be conclusive.

Until now, we have considered the technical aspects of both the lead isotope analysis method and of the metallurgical processes of the Roman and pre-Roman exploitation of jarositic earths. There are other aspects to consider, and first among these is the 'industrial' scale at which these sites were exploited. Forbes (1964) talks of a production of silver in Cartagena of the order of 9 millions *denarios* per year, specifically for the year 140 BC; and a total production of several million tons of silver in Rio Tinto and Tharsis is proposed (Blanco and Luzon 1966).

The initial difficulty is to obtain a truly representative sample of lead slag for such an extended and prolonged production of silver and lead as the one taking place during the Roman period in the Iberian Peninsula. Several mines were exploited, the production centres were spread, and the period of exploitation was long (Perez Macias1998, 192). This is the main reason why the study of the geological origin of the lead used at the various silver-producing sites is so important for tracing the connections between these industrial sites. And this is the reason why it is important in this project to at least attempt the identification of one or more areas of origin of the lead metal used for smelting at the site of Corta Lago.

Against this background, 45 samples from the Corta Lago section were analysed with Multi Collector–Inductively Coupled Plasma–Mass Spectrometry at the Department

of Geology at Royal Holloway, University of London. The samples were divided as follows:

- 3 ball slag samples;
- 6 Phoenician tapped slags;
- 2 Iberian samples (one tapped slag one litharge);
- 8 Republican phase I tapped slags;
- 7 Republican phase II plate slags;
- 2 Republican phase III tapped slags;
- 5 Imperial tapped slags;
- 9 semi-reacted ore samples;
- 3 'ingots'.

The material was first analysed by XRF to ascertain the amount of lead in the samples, in order to calculate the dilution factor necessary to obtain solutions with 50 ppb of lead to measure the isotopic ratios (see Chapter 5 and Appendix 2, where the sample preparation methodology is described in detail).

The measured isotopic signature resulting from the slag samples (Figs. 8.1 and 8.2) shows a mixing line characterising the Roman samples red regression line in Figure 8.2, the two extremes of which are identified on one side by most of the Imperial tapped slag (except sample RT24n2, which will be discussed later), and on the other side by the Republican phase II plate slag samples. The Republican phase I tapped slag phase samples can be divided in two groups, one of which plots close to one end member and one to the other end member of the mixing line. This division in two groups was already observed following the chemical and petrographic analyses and is confirmed by the isotopic analyses. These samples were chosen from a single layer of the section (layer 31), in order to establish the variance of the process within a short period of operation. The tapped slags from the Republican phase III plot closer to the area where the Imperial slags plot, one at the extreme end of the line and another where sample RT24n2, the exception among the Imperial samples, plots. The Phoenician tapped samples seem to be distributed along a different mixing line (black regression line in Fig. 8.2), and a slight offset is visible in the graph Pb208/Pb206 against Pb206/Pb204. The Iberian samples plot uniformly outside the line, and the same is true for the ball slag samples; their isotopic signature is different.

The Republican samples from Tharsis plot close to the middle of the mixing line, while the Imperial samples from Tharsis plot close to the Corta Lago Imperial extreme end of the line.

The observation that from the beginning to the end of the Roman period the isotopic signature seems to plot along the same mixing line suggests that the same two sources of lead were used during the occupation.

More interesting is the indication that the three pre-Roman periods under consideration show a different behaviour. First of all, the ball slag and the Iberian slag have a different signature from each other, and both have a uniform small plot within themselves, suggesting the use of one source only. On the other hand, the Phoenician samples already show the plot along a line, suggesting the use of two sources, one of which differs from the Roman sources (Fig. 8.2).

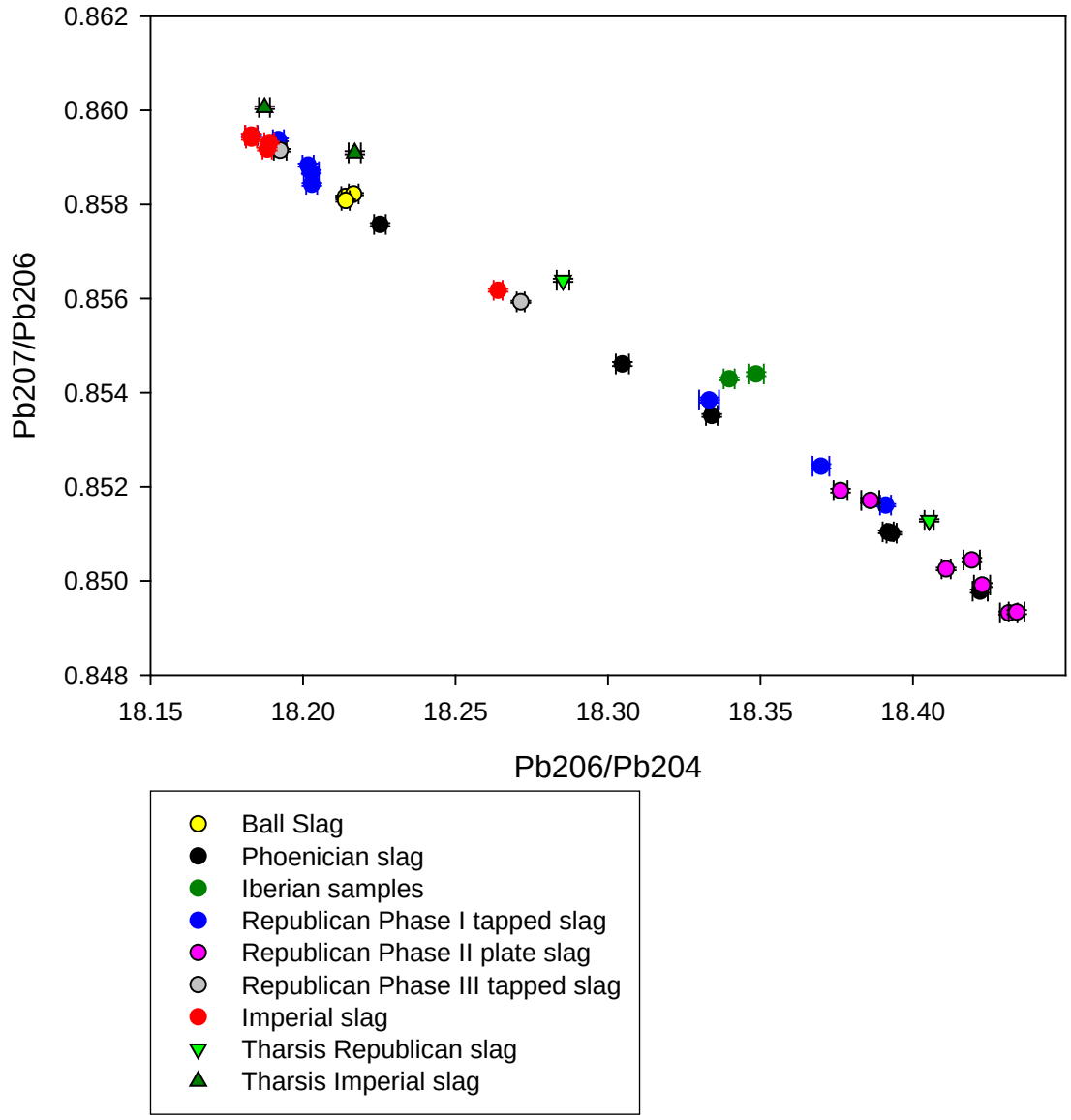

Figure 8.1 Lead isotope signatures (Pb 206/204 vs. Pb 207/206) of the slag samples from Corta Lago and Tharsis. The samples seem to plot on one line.

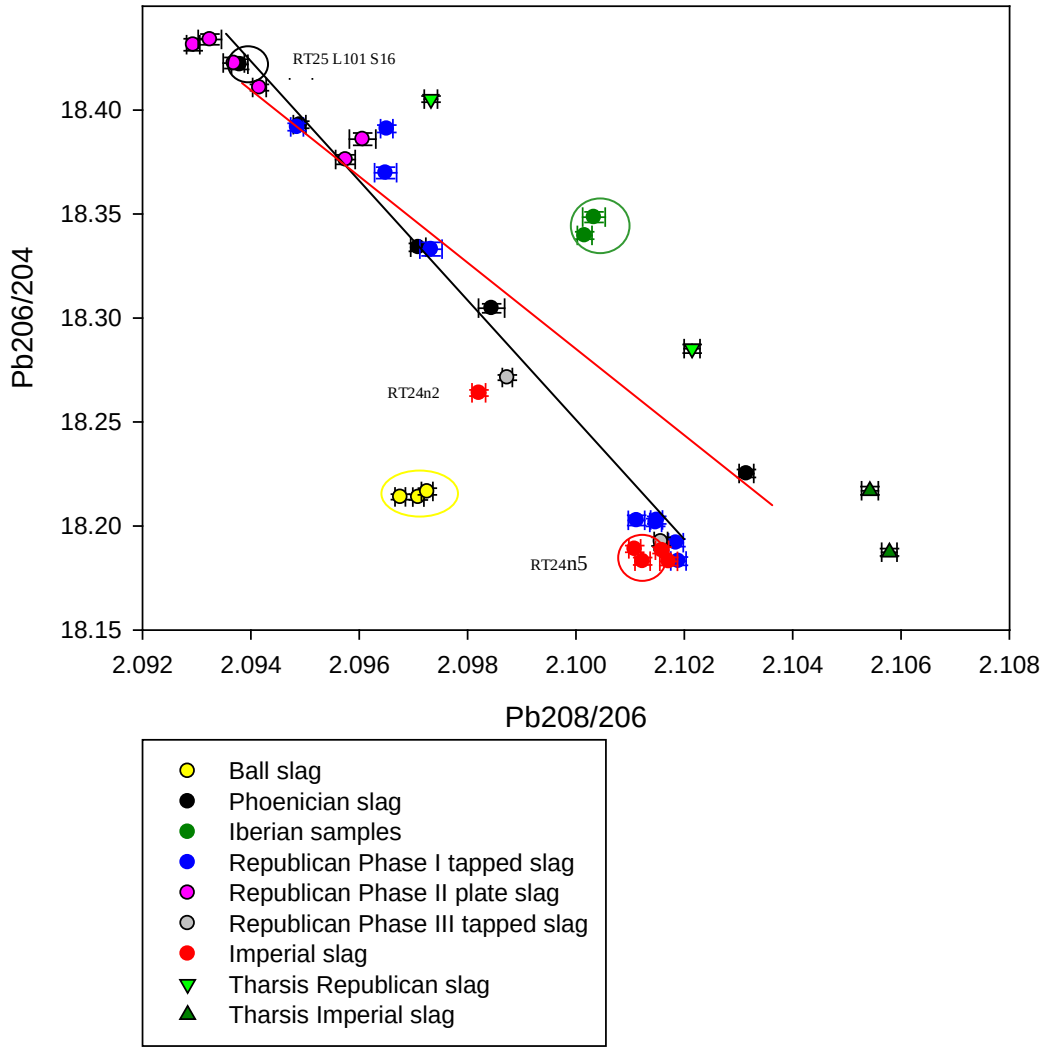

Figure 8.2 Lead isotope signatures (Pb 208/206 vs. Pb 206/204) of the slag samples from Corta Lago and Tharsis. Phoenician samples plot on a different line (red line) as compared to the Roman ones (black line).

In Figures 8.3, 8.4, 8.5 and 8.6, we can observe that the isotopic signatures of the pyritic deposits in the Rio Tinto area as presented in the literature (Stos-Gale et al. 1995) coincide with one of the extreme ends of the mixing line where the Imperial, part of the Republican Phase I tapped slag, and the Phoenician slags plot. Ball slag and Iberian samples plot slightly offset, and Republican phase II plate slag and the second part of the Republican Phase I tapped slag samples plot even further away.

A more detailed view of some part of the Rio Tinto mine is plotted in Figures 8.8 and 8.9, where it is visible that the scatter of the signature of the ores is quite large and specific small trends can be recognised. The Roman samples on this extreme of the line (the one on the side of the Rio Tinto mines) coincide with the data deriving from

the semi-reacted ores collected during this thesis (Figures 8.5 and 8.7) while the ball slag samples are still out of these areas and plot closely to the data collected from the Monte Romero samples (Kassianidou 1992; Figures 8.8 and 8.9). The proximity of the signature of the ball slag samples to the data resulting from the same typology at Monte Romero (Kassianidou 1992) seems to provide an indication of specific veins exploited to produce such a slag. The lack of punctual information of the different prehistoric mineralisations exploited may be the reason why a completely local origin can be attributed to other slags. Another explanation could be that a group of smelters using the same metallurgical traditions were operating in the area and they were using the mineralisation coming from the same site of Monte Romero. A third reason can be that these slags were collected in Antiquity in order to be exploited for lead. This hypothesis will be further discussed later in this chapter. When considering closely the data from different ores in the Rio Tinto area (Figures 8.8 and 8.9), it can be observed that the Iberian samples can be characterised by the spread of these values summed to a portion of "foreign" lead, and can subsequently be explained by the exploitation of a particular local vein in that period and addition of "extra" lead.

In order to understand if the spread of the Republican Phase II plate slag, part of the Republican Phase I tapped slag, and the Phoenician slags were linked to a different type of ore still locally present, the data were compared with the 'hydrothermal deposits' described by Marcoux and Sáez (1994), presented in Chapter 4. These deposits are described by Marcoux as not valuable economically, but the situation may have been different during Phoenician and Roman times. The results indicate that the 'hydrothermal deposits' do not actually overlap with the slag samples under consideration. Furthermore, the 'hydrothermal deposits' bring with them a strong geochemical signature, mainly manifested by enrichment in tin (Sáez, personal communication). Figure 8.14 shows that only two samples, one Phoenician (RT25 L101 S16) and one Imperial (RT24n5), show, in fact, an anomalous high concentration of tin, while all the other samples plot within a similar range. However, these two samples do not show a similar isotopic signature between each other and with the 'hydrothermal deposits'; mainly the Phoenician sample is actually very far away from the 'hydrothermal deposit' isotopic composition. Hence, the compositional anomaly and the isotopic signature do not seem to be related to an influence from the 'hydrothermal deposits' (Table 8.1).

In order to identify a possible source of the 'foreign' lead added to the process, the literary sources were consulted. Pliny and Strabo, for instance, highlight the importance of the site of Cartagena (New Carthage) for the production of silver and lead during the period under consideration. Several historical mining provinces were taken into consideration (Figure 8.10 and 8.11) in order to assess the possibility that lead was coming from further away. The lead isotope signatures of Sardinian, British and German mines would plot along a mixing line very close to the one which we are interested in, but slightly offset. The Cartagena signature conforms to this slight offset; furthermore, it is geographically closer to the Rio Tinto mining area, and it is also mentioned by the ancient sources. Thus, the isotopic data of Cartagena ores (Stos-Gale et al. 1995) were taken into consideration and examined more closely, and they show a very plausible correlation with the mixing line, highly suggesting the possibility of this mine being the second end member of the line.

Figures 8.5 and 8.6 show this correlation. A closer look at the isotopic data from Cartagena mines indicates the presence of two distinct groups, suggesting that different areas in Cartagena had slightly different isotopic signatures. Observing the trends of the Roman and the Phoenician mixing lines (Figure 8.2, red for the former and black for the latter), it seems that the cause of the difference between them can be suggested to be the exploitation of different areas of the Cartagena mines in these two important occupation periods. An analysis of the influence of polymetallic sulphide on the jarositic earths exploited has been carried out, and the results are presented in Figures 8.12, 8.13 and 8.14. The ball slags are highly enriched in antimony, in the same proportion as the Imperial slags. It is interesting to observe that the fragment of bullion recovered in the Imperial layers has a strong polymetallic character, and shows a high concentration of antimony, albeit droplets of bismuth are detectable in the sample. This observation indicates a chemical homogeneity of the ores exploited in the Rio Tinto area. This chemical characteristic does not have a counterpart in the isotopic variability; in fact, the ball slags show a peculiar and unique isotopic signature within the groups of slags under consideration.

Ore	Chemical signature	Pb206/204	Pb207/204	Pb208/204
La Ratera	Cu, Zn, Pb, Fe, Ni, Co	18,185	15,623	38,255
Masegoso	Cu, Zn, Pb, Fe, As	18,158	15,635	38,263
Masegoso	Cu, Zn, Pb, Fe, As	18.151	15,643	38,264
Los Silillos	Fe, Cu, Zn, Pb	18,200	15,627	38,215
Las Virˉias	Cu, Zn. Pb, Fe, Ni, Co	18,206	15,651	38,319
Alto Corw m.bel	Zn, Pb, Cu, Ag, As, Sb	18,142	15.607	38,205
Alto Corˉumbel	Zn, Pb, Cu, Ag, As, Sb	18,189	15,665	38,341
Bajo Corumbel	Sn, W, As	18,258	15,608	38,214
Bajo Corumbel	Sn, W, As	18,264	15,601	38,206
Tallesca	Pb, Zn, Ag	18,251	15.615	38,372
Preciosa	Cu, Pb, Zn, Ba, Sb, As	18,293	15,645	38,453
Nerön	Sb, Cu, As	18,287	15,705	38,544
EI Parador	Pb, Zn, A g	18,274	15,650	38,404
Santa Eulalia	Pb, Zn, Cu, Ag	18,373	15,602	38,485
Los Angeles	F, Pb, Zn	18,481	15,601	38,516
Aurora	Ba, Pb, Zn, Cu	18,240	15,613	38,305

Table 8.1 List of the 'hydrothermal deposits' with their main metallic components and their isotopic signatures (Marcoux and Sáez 1994).

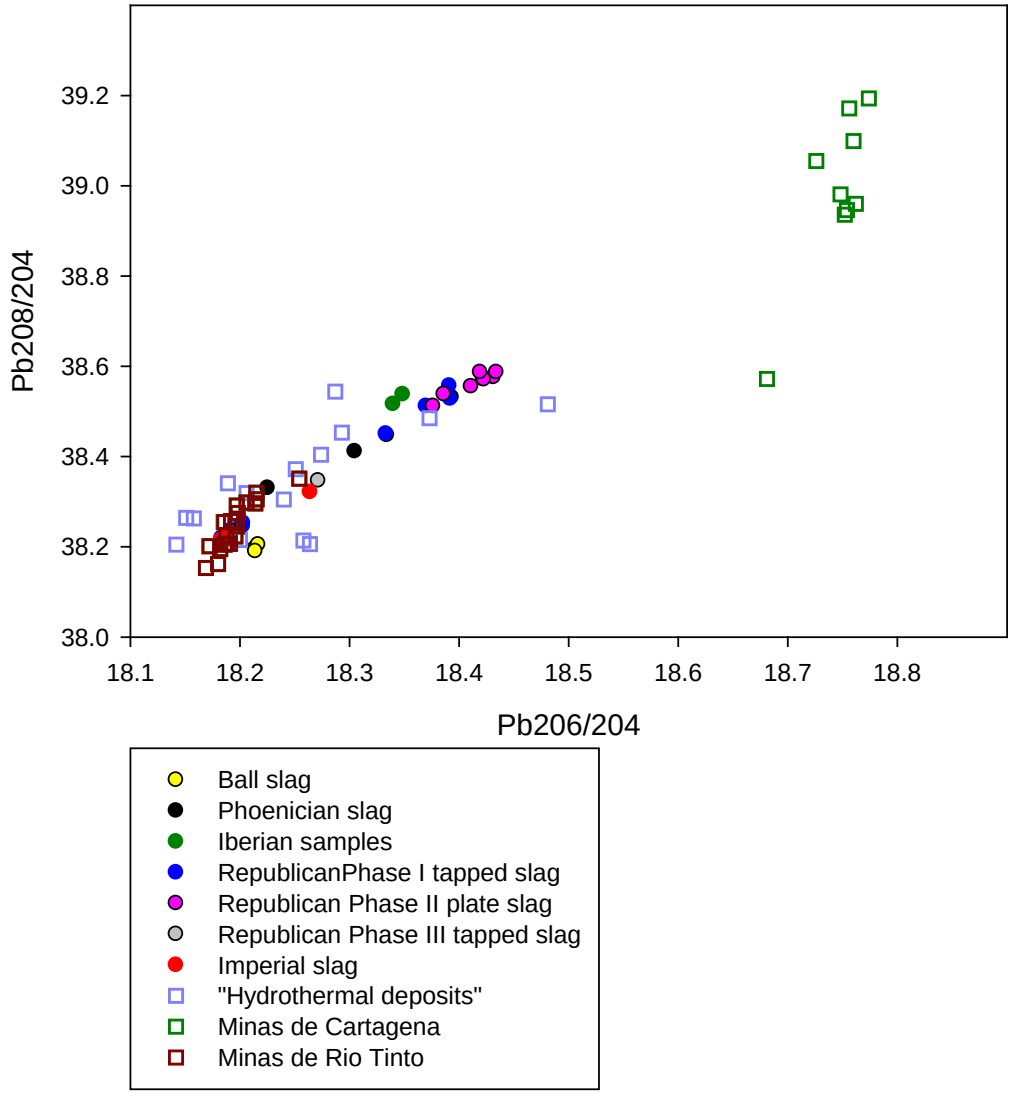

Figure 8.3 Lead isotope signature of the slag compared with the signatures of Rio Tinto ore deposits (Stos-Gale et al. 1995), Cartagena (Stos-Gale et al. 1995), and hydrothermal deposits (Marcoux and Sáez 1994) of the Rio Tinto area.

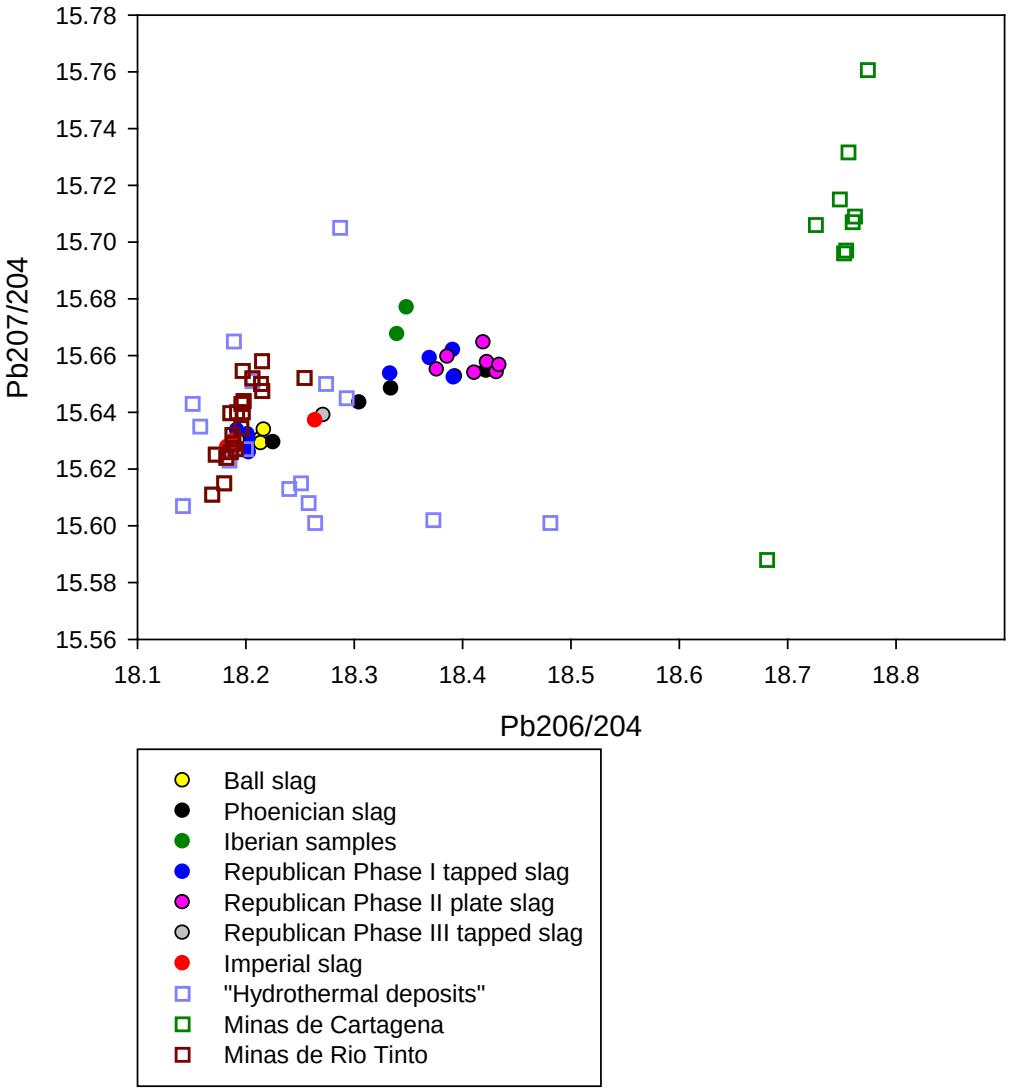

Figure 8.4 Lead isotope signature of the slag compared with the signatures of Rio Tinto ore deposits (Stos-Gale et al. 1995), Cartagena (Stos-Gale et al. 1995), and hydrothermal deposits (Marcoux and Sáez, 1994) of the Rio Tinto area.

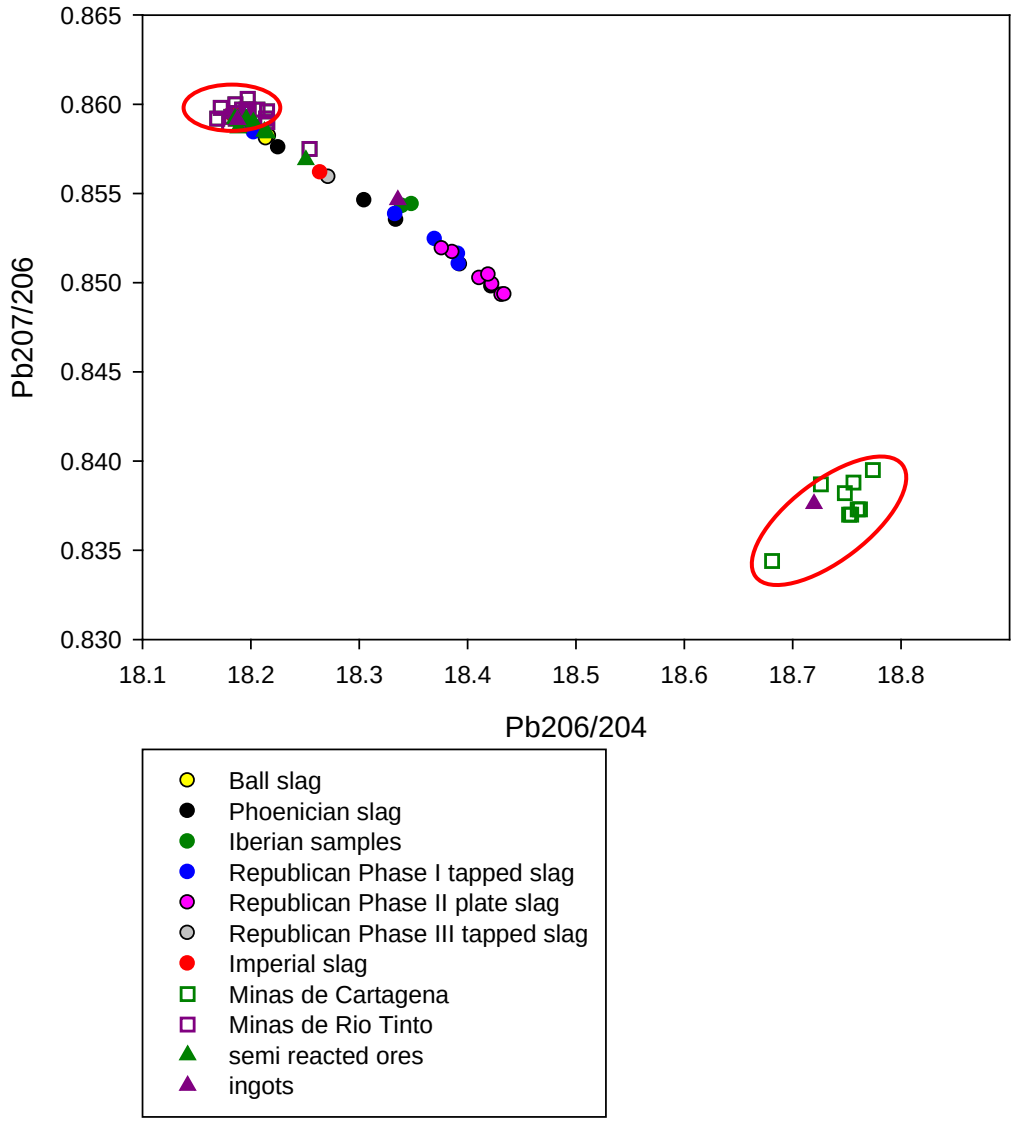

Figure 8.5 Lead isotope signatures of the slag, semi-reacted ore and ingot samples from Corta Lago compared with the lead isotopic signatures of ore samples from Rio Tinto and Cartagena (Stos-Gale et al. 1995).

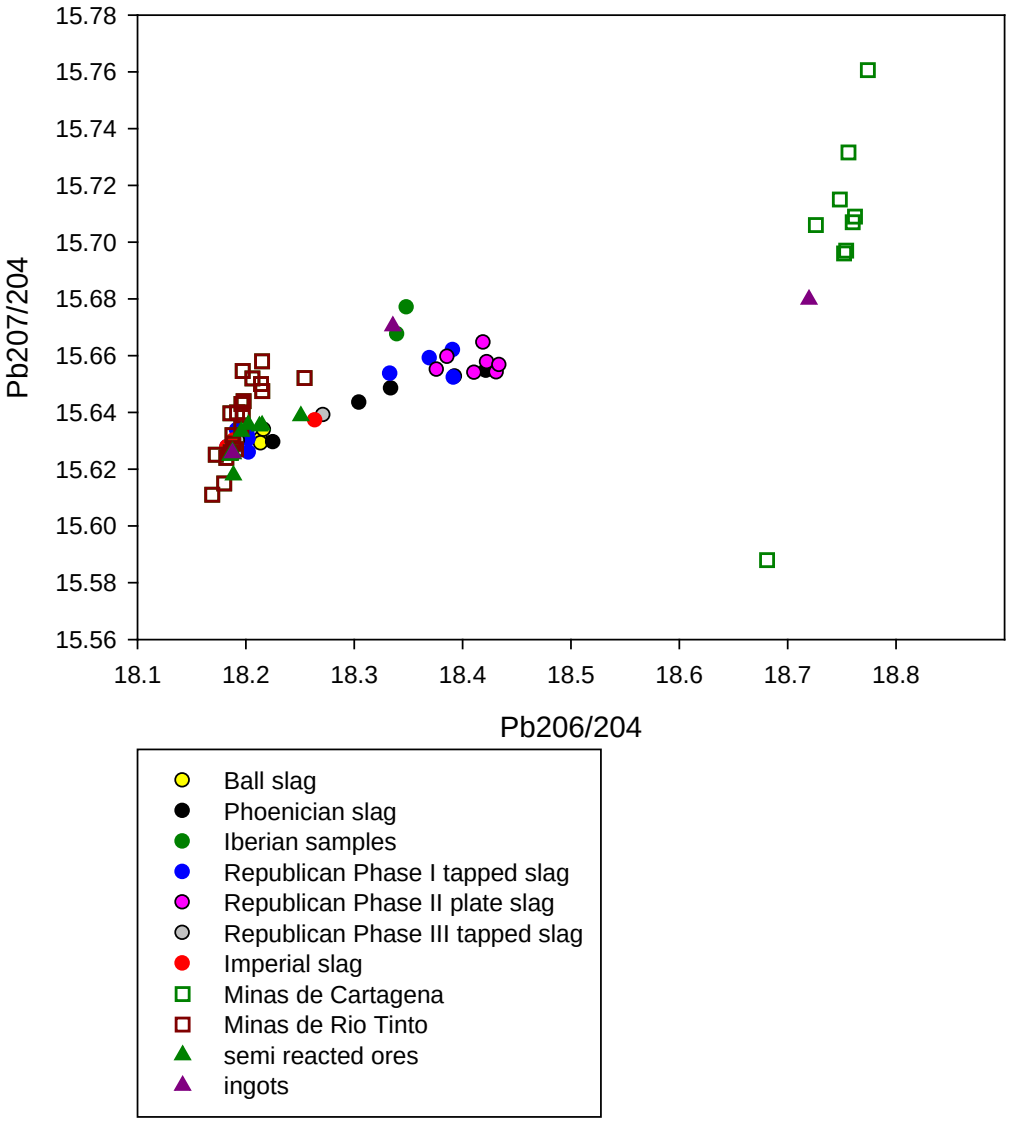

Figure 8.6 Lead isotope signatures of the slag, semi-reacted ore and ingot samples from Corta Lago compared with the lead isotopic signatures of ore samples from Rio Tinto and Cartagena (Stos-Gale et al. 1995).

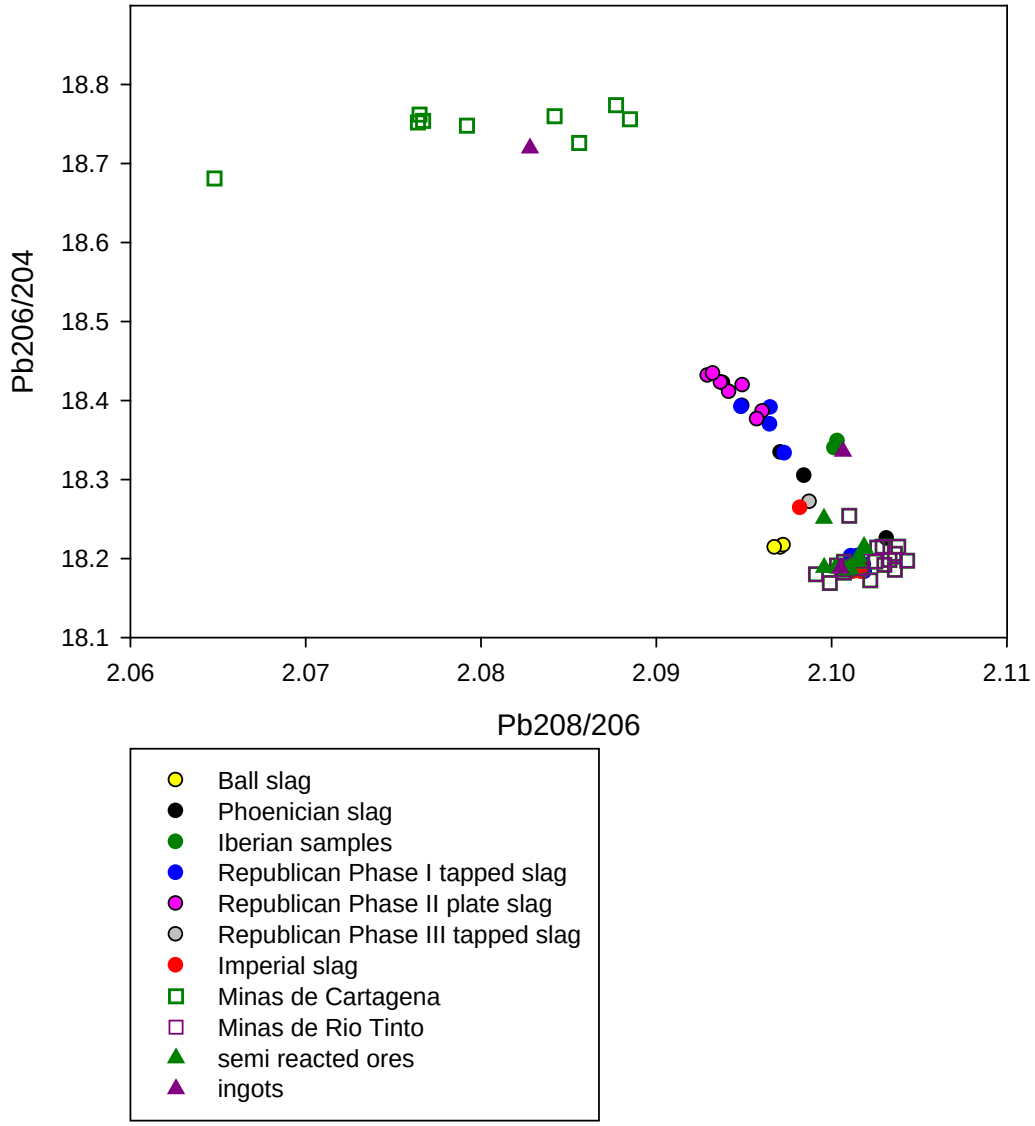

Figure 8.7 Lead isotope signatures of the slag, semi-reacted ore and ingot samples from Corta Lago compared with the lead isotopic signatures of ore samples from Rio Tinto and Cartagena (Stos-Gale et al. 1995).

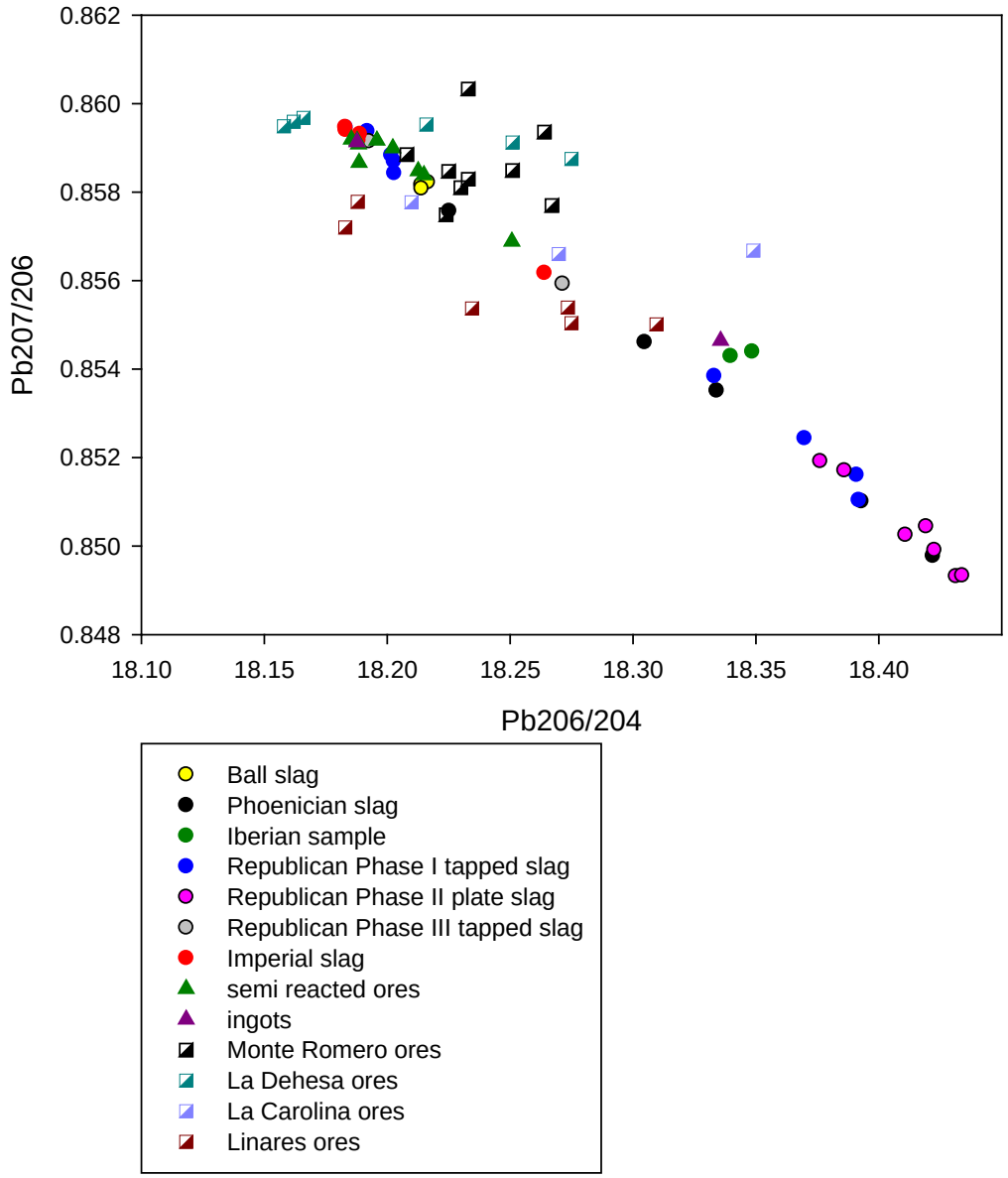

Figure 8.8 Lead isotope signatures of the slag, semi-reacted ore and lead ingot samples (the matte ingot is not plotted here) from Corta Lago compared with the lead isotopic signatures of veins from Rio Tinto (Stos-Gale et al. 1995).

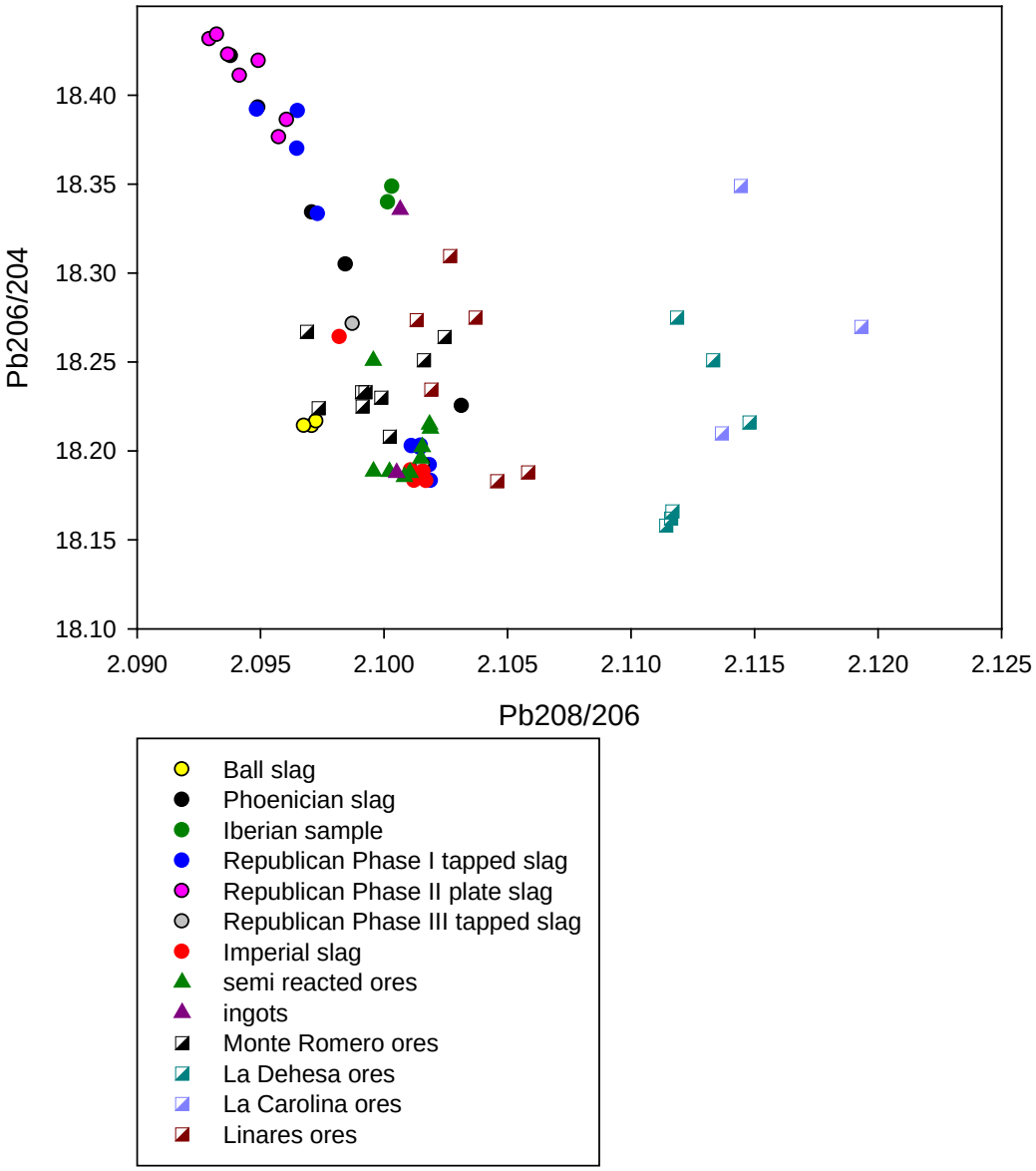

Figure 8.9 Lead isotope signatures of the slag, semi-reacted ore and lead ingot samples (the matte ingot is not plotted here) from Corta Lago compared with the lead isotopic signatures of veins from Rio Tinto (Stos-Gale et al. 1995).

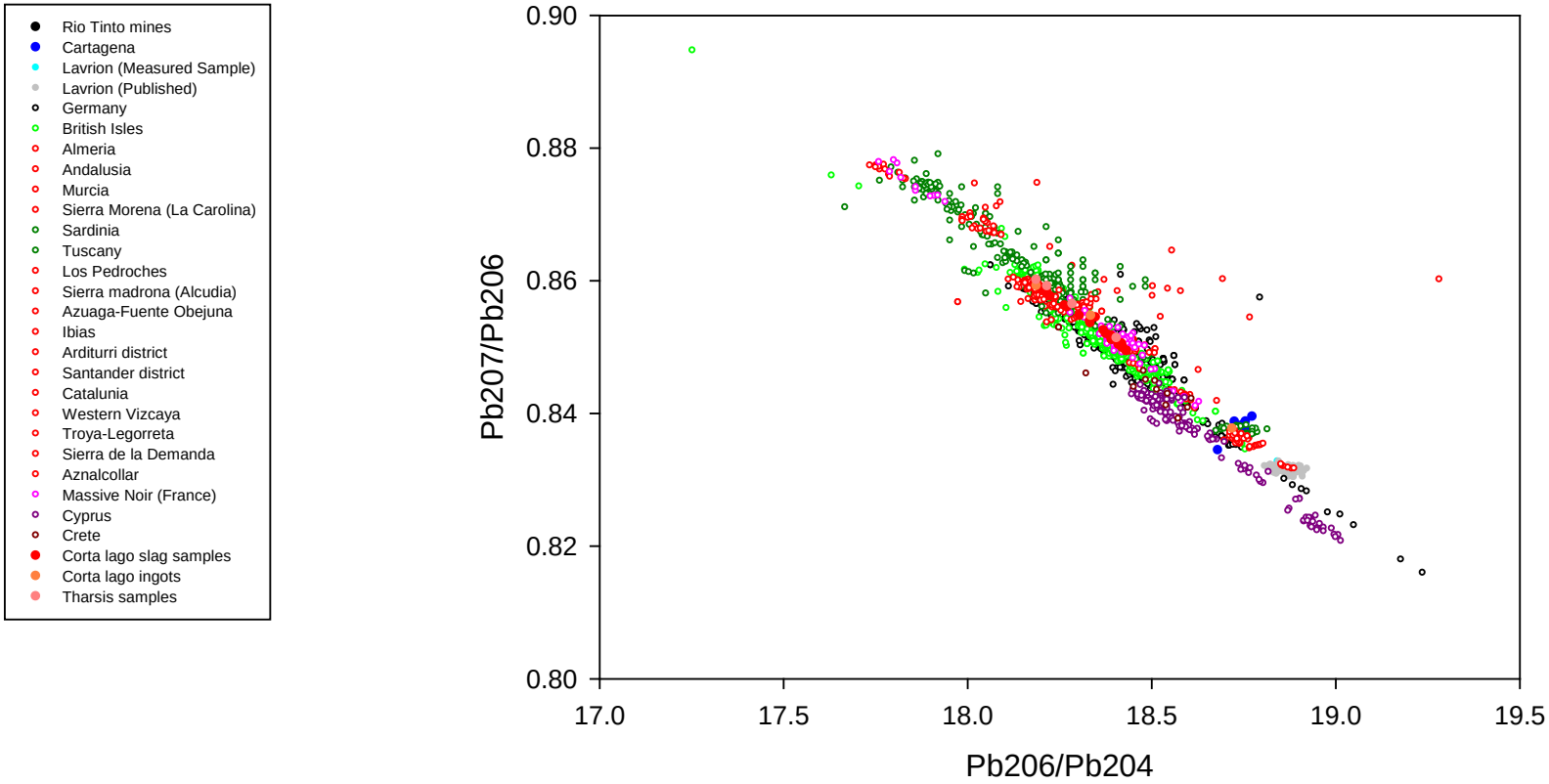

Figure 8.10 Isotopic signatures of several sources available during the Roman expansion.

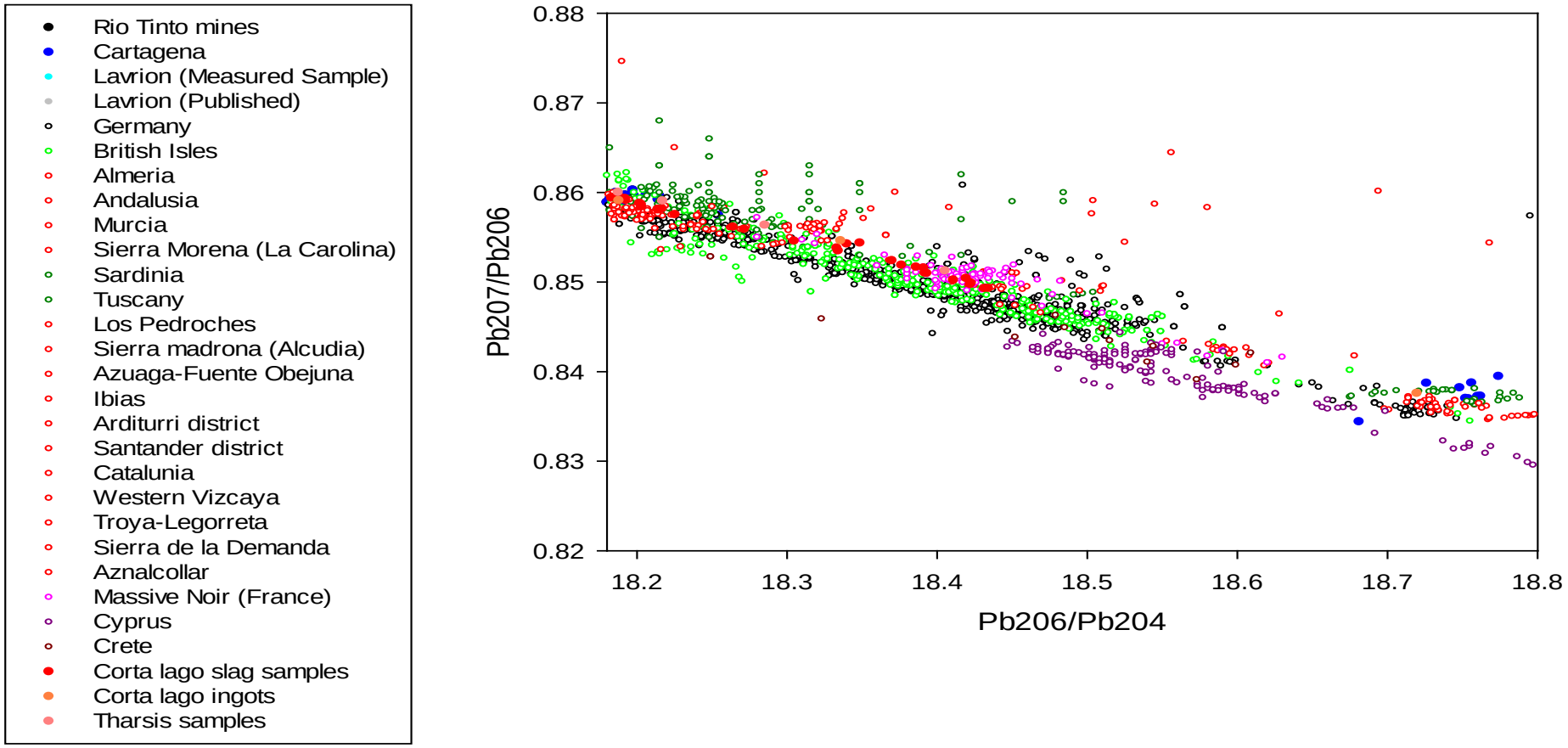

Figure 8.11 Detail of Figure 8.10.

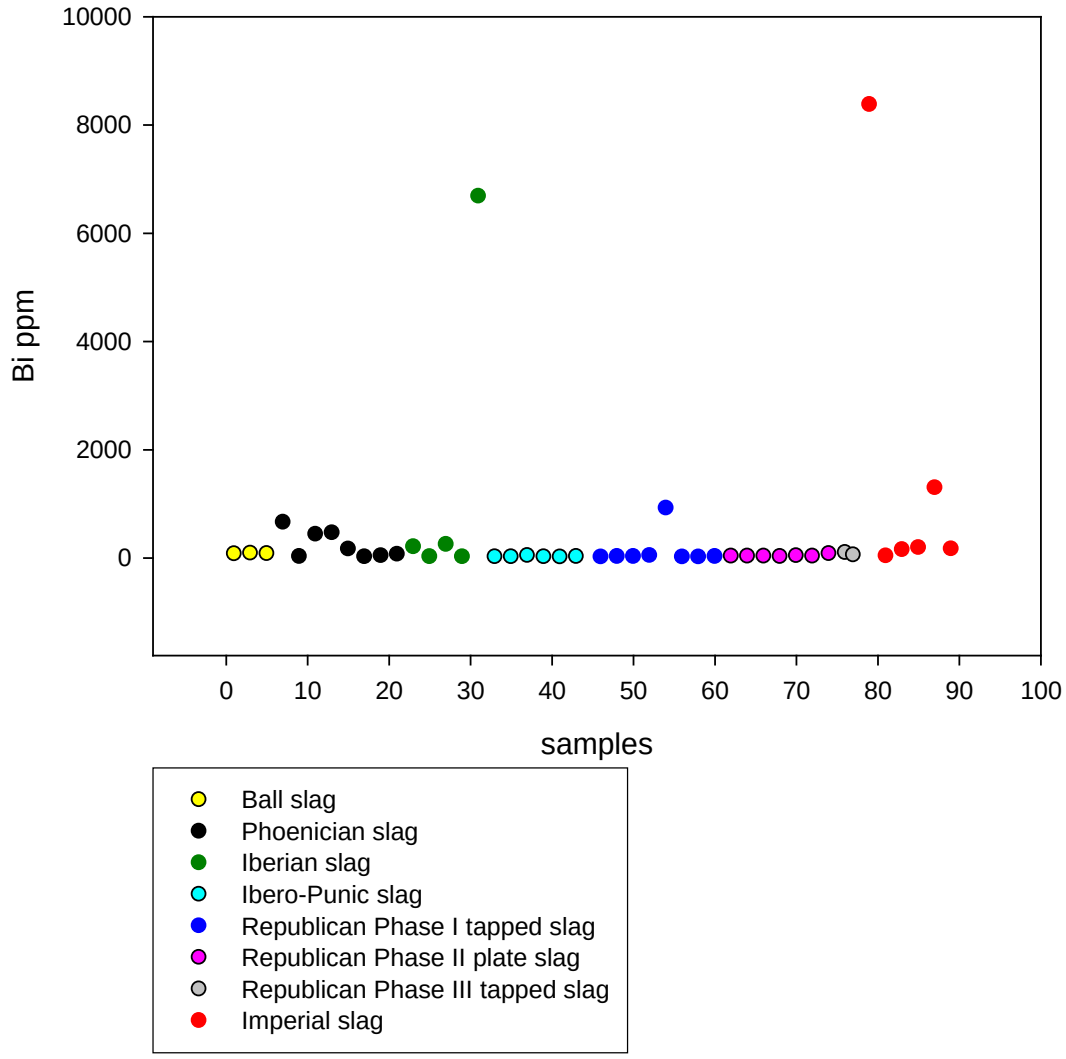

Figure 8.12 Concentration of bismuth in the analysed samples. The X-axis is a series of number corresponding to the number of the sample in table 6.1.

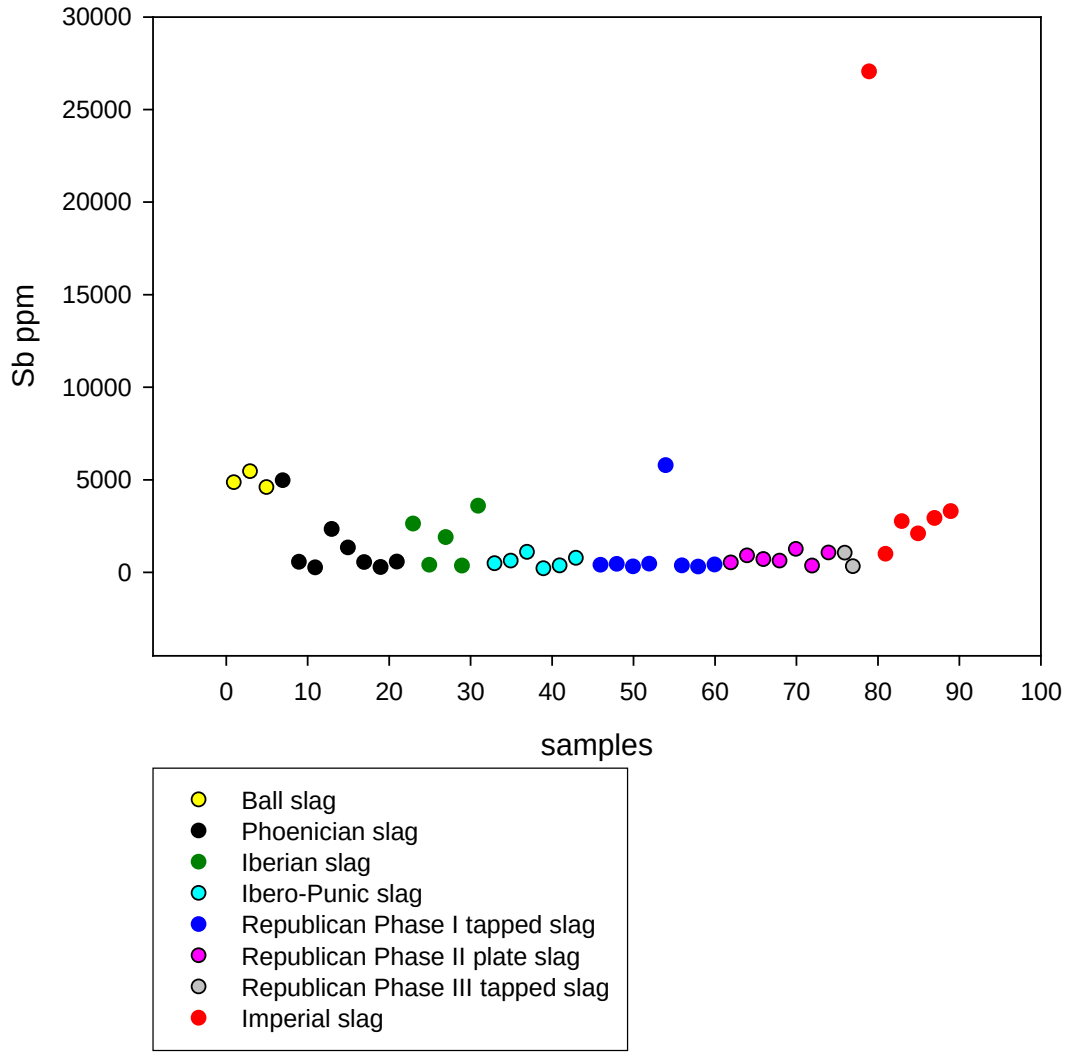

Figure 8.13 Concentration of antimony in the analysed samples.
The X-axis is a series of number corresponding to the number of the sample in table 6.1.

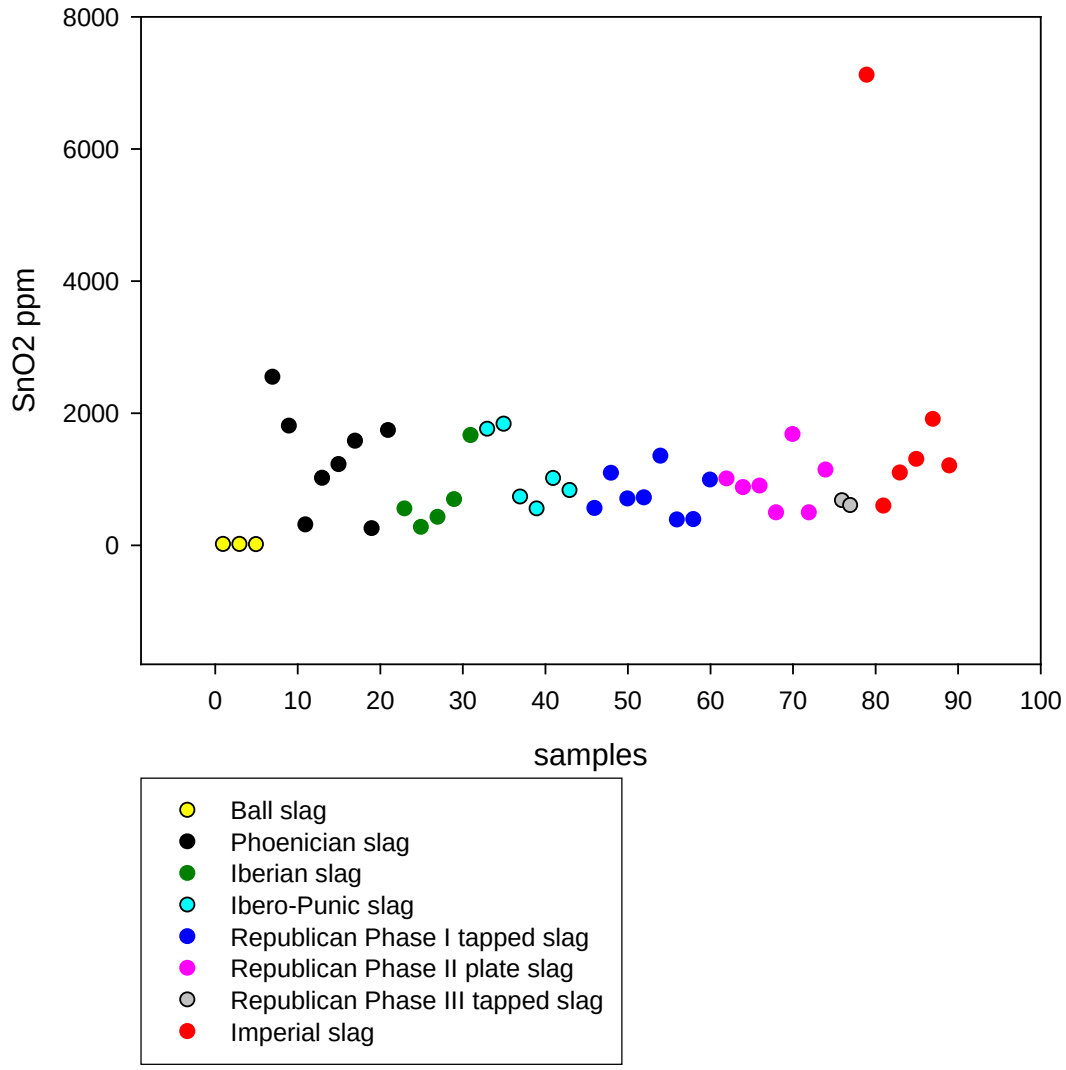

Figure 8.14 Concentration of antimony in the analysed samples. The X-axis is a series of number corresponding to the number of the sample in table 6.1.

Once established that Rio Tinto and Cartagena are the two end members of the mixing line, an empirical re-calculation of the amount of ‘extra’ lead added to the system was attempted. This calculation does not claim to be a quantitative analysis, but only a qualitative method employed to visualise which periods are associated with higher additions of ‘extra’ lead. The method is a simple proportion in which the average isotopic signature of the Rio Tinto mines is 100 and the one from Cartagena is zero; proportionally, the value for each sample is calculated. The Iberian samples are considered in this calculation, while the ball slag samples are not taken into consideration in the discussion since their isotopic signature does not fit with the other samples; however, they are graphically presented in Figure 8.15.

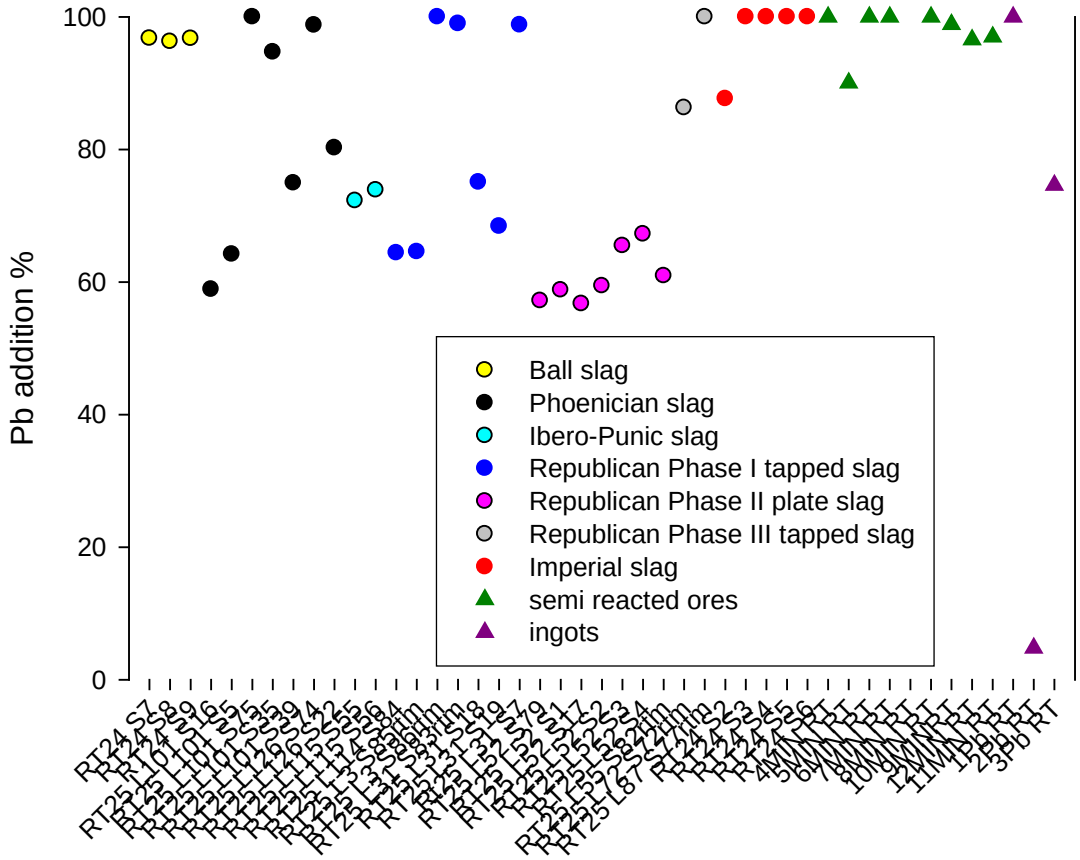

Figure 8.15 Percentage of lead coming from Rio Tinto calculated by proportion using the lead isotopic signature.

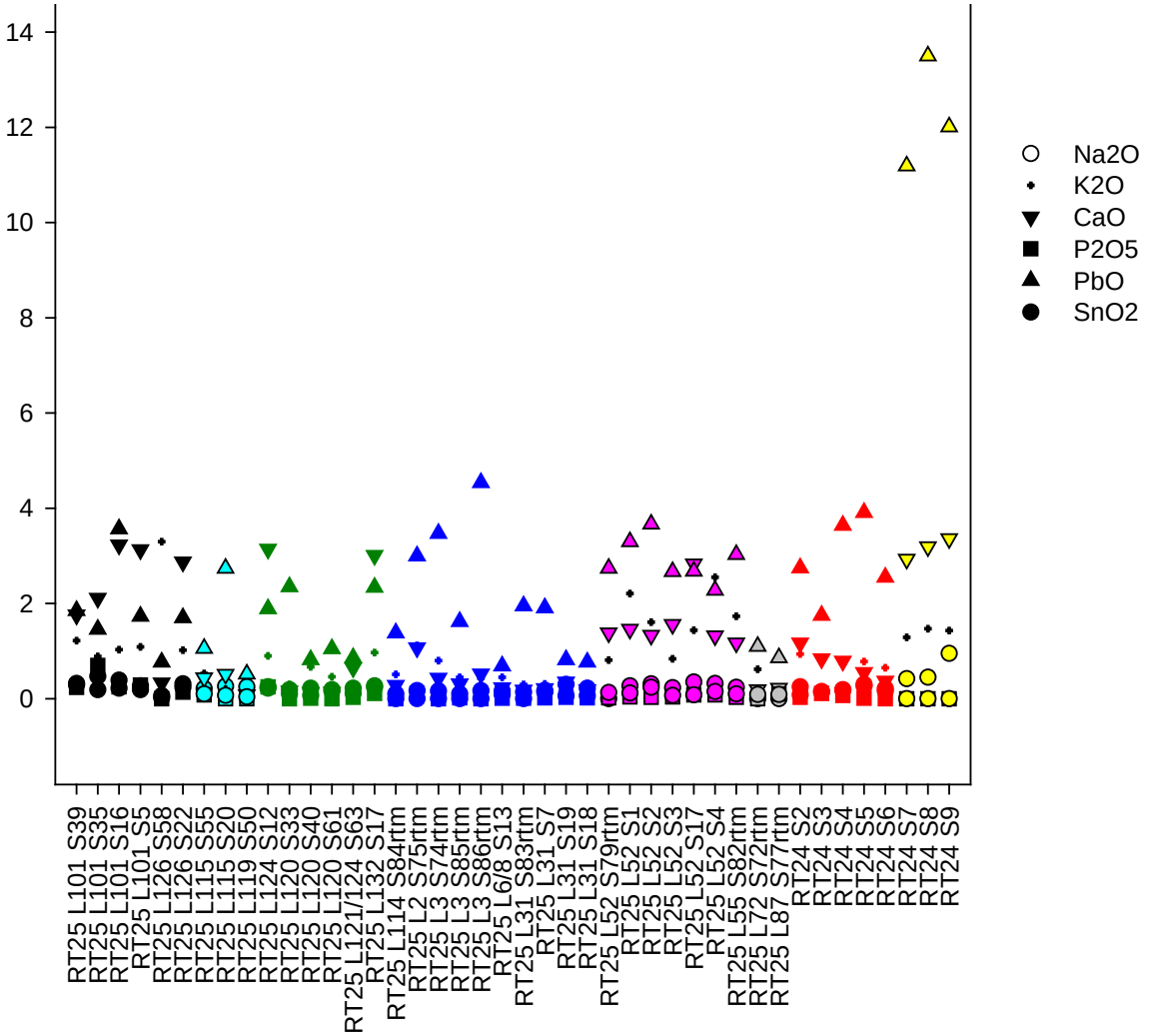

Figure 8.16 Comparison of lead and tin oxides, alkali, lime and phosphorous in the samples analysed for lead isotopes.

The samples more influenced by the addition of 'foreign' lead are the Phoenician, Iberian, a portion of Republican phase I tapped slag, and Republican phase II plate slag. The reasons why these periods show an increase in the addition of 'extra' lead needs to be addressed. Two hypotheses will be put forth: 1) A traditional method of producing silver with extra lead (as we have discussed in Chapter 3). In order to be certain that they collected all the silver, the smelters were adding an excess of lead to the system. 2) Out of necessity, the smelters being aware that the exploited ore was depleted in lead relative to the concentration of silver.

As already mentioned in the first section of this chapter, Hunt Ortiz (2003, 35) and Domergue (1990) state that, according to the Rio Tinto company archive, the concentration of plumbo-jarosite within the jarosites varies between 3 and 30 wt%. Thus, we know that there could have been veins relatively poor in lead to which lead metal needed to be added for efficient silver collection and extraction, and this was the hypothesis that we wanted to verify with lead isotope analysis. After interpreting the results, we know that lead was added to the system, but we do not know if the reason for this addition is the variation in the concentration of lead in the exploited mineralisation or something else.

Other information needs to be added in order to convincingly argue in favour of the hypothesis related to the lead concentration in the ore. The addition of lead (in metallic or mineral form) to the system does not correspond to a higher concentration of lead in the slag.

As we can see in Figure 8.16 above, there is no correlation between the addition of lead from a 'foreign' source and the concentration of lead in the slag. The lead oxide concentration in the slags is always between 1 and 4 wt%, except in the ball slags (in yellow in the diagram, Figure 8.16), presenting lead oxide concentrations around 15 wt%, mainly concentrated in a silicatic phase.

As discussed in Chapter 3, jarosite has a structure presenting large cavities that can host different cations, such as K, Na, Pb, Ag and NH_4 (Figure 8.17). The cavities are all of the same size, and there is no size selection and different lattice position for the different cations. In fact, both alkali and lead enter the structure in the same position (x=0, y=0, z=0; Hendricks 1937; Menchetti and Sabelli 1976; Groat et al. 2003). For this reason, as well as for stoichiometric reasons, it is suggested that an increase of

one cation is correlated with the decrease of the others. If this is true, then a decrease in lead should for instance coincide with an increase in alkali and vice-versa.

As seen earlier, the slags retain around the same amount of lead (between 1 and 4 wt%), because the lead is smelted as metal and should not be trapped in the slag. On the other hand, the alkali coming from the smelted ores are not trapped in the bullion, but go into the slag, so that the amount of alkali in the slag should represent the amount of alkali in the ores plus the amount originating from the fuel ash and the technical ceramics. Comparing alkali and lead oxide in two diagrams, one for potassium oxide and one for sodium oxide (because the first is more affected by the fuel than the second), it can be observed that the Republican phase II plate slags are richer in alkali than the other samples (Figs. 8.18 and 8.19).

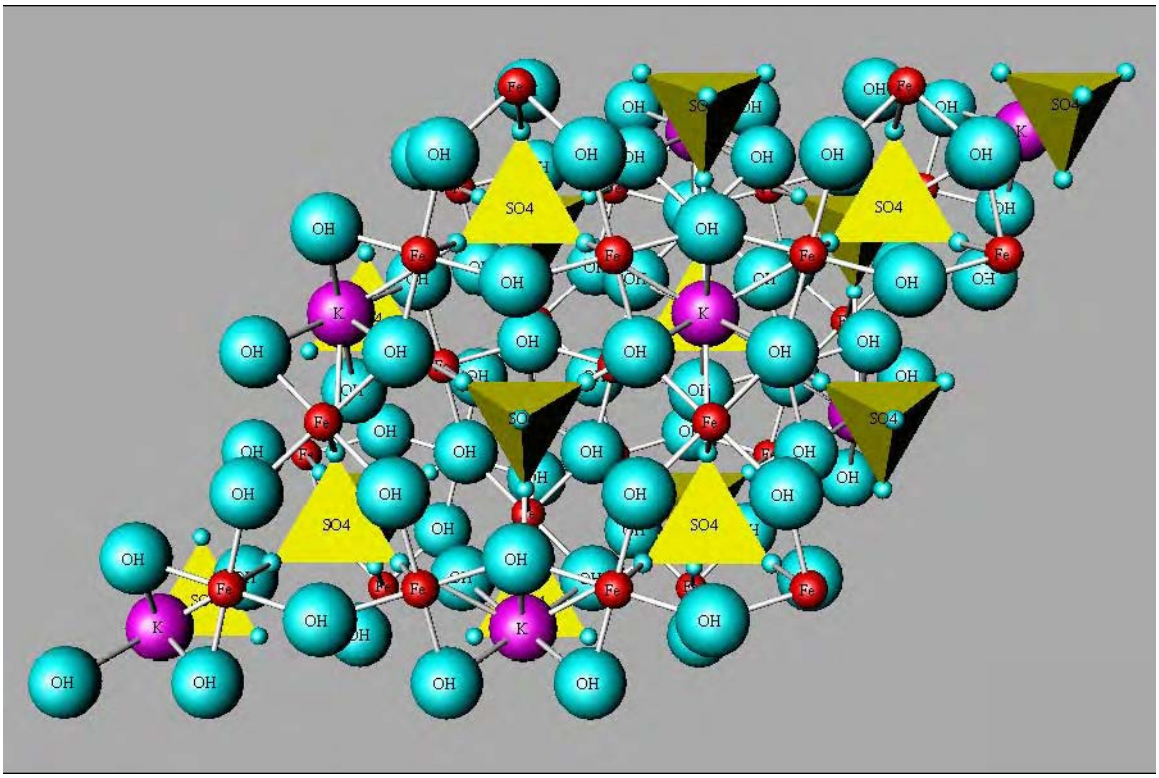

Figure 8.17 K-jarosite structure showing the position of the cation (K in this case) in the large cavities formed by the OH group.

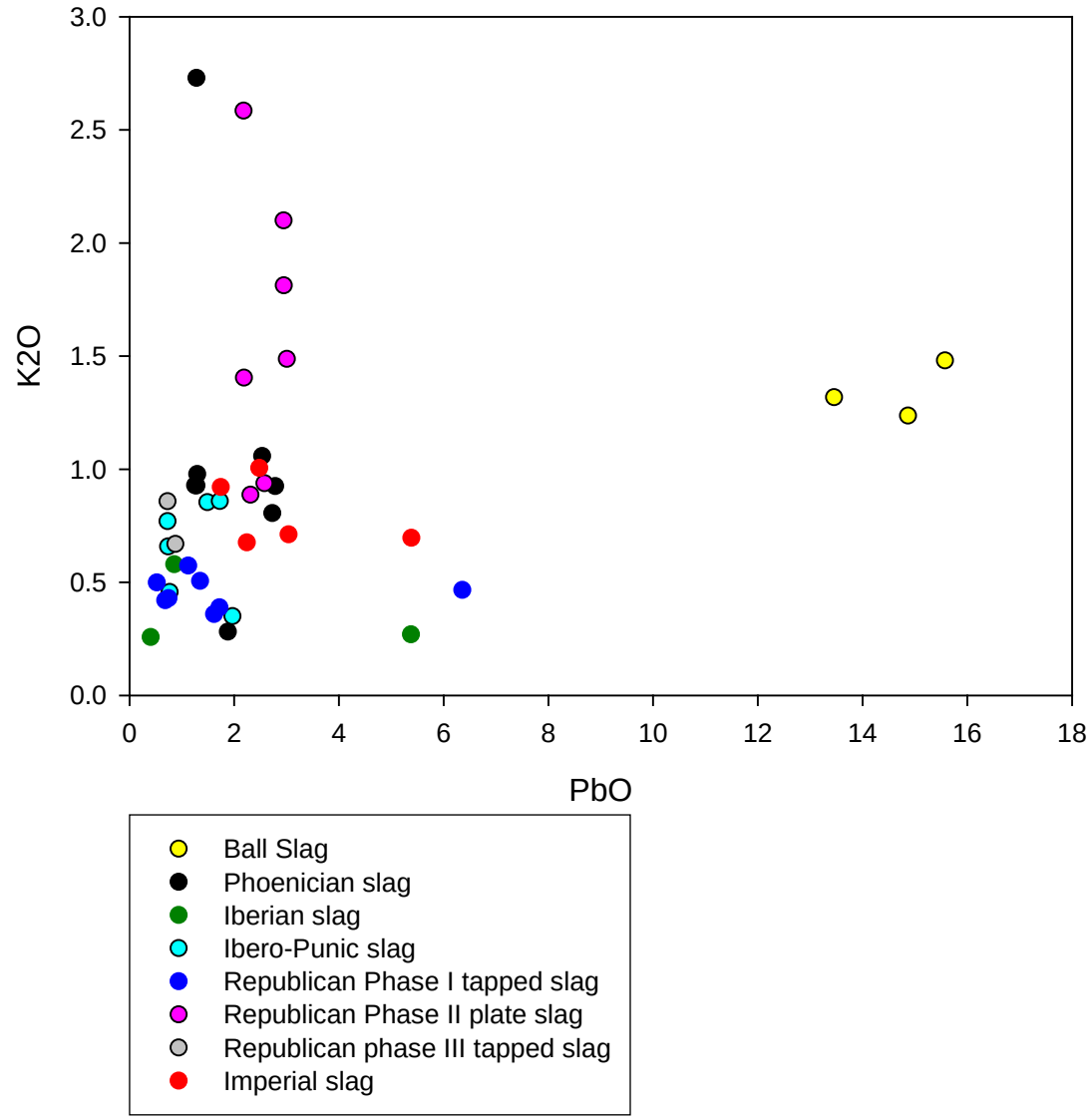

Figure 8.18 PbO/K_2O ratio in the slag samples from different periods. The Republican phase II plate slag samples show a higher concentration of potash.

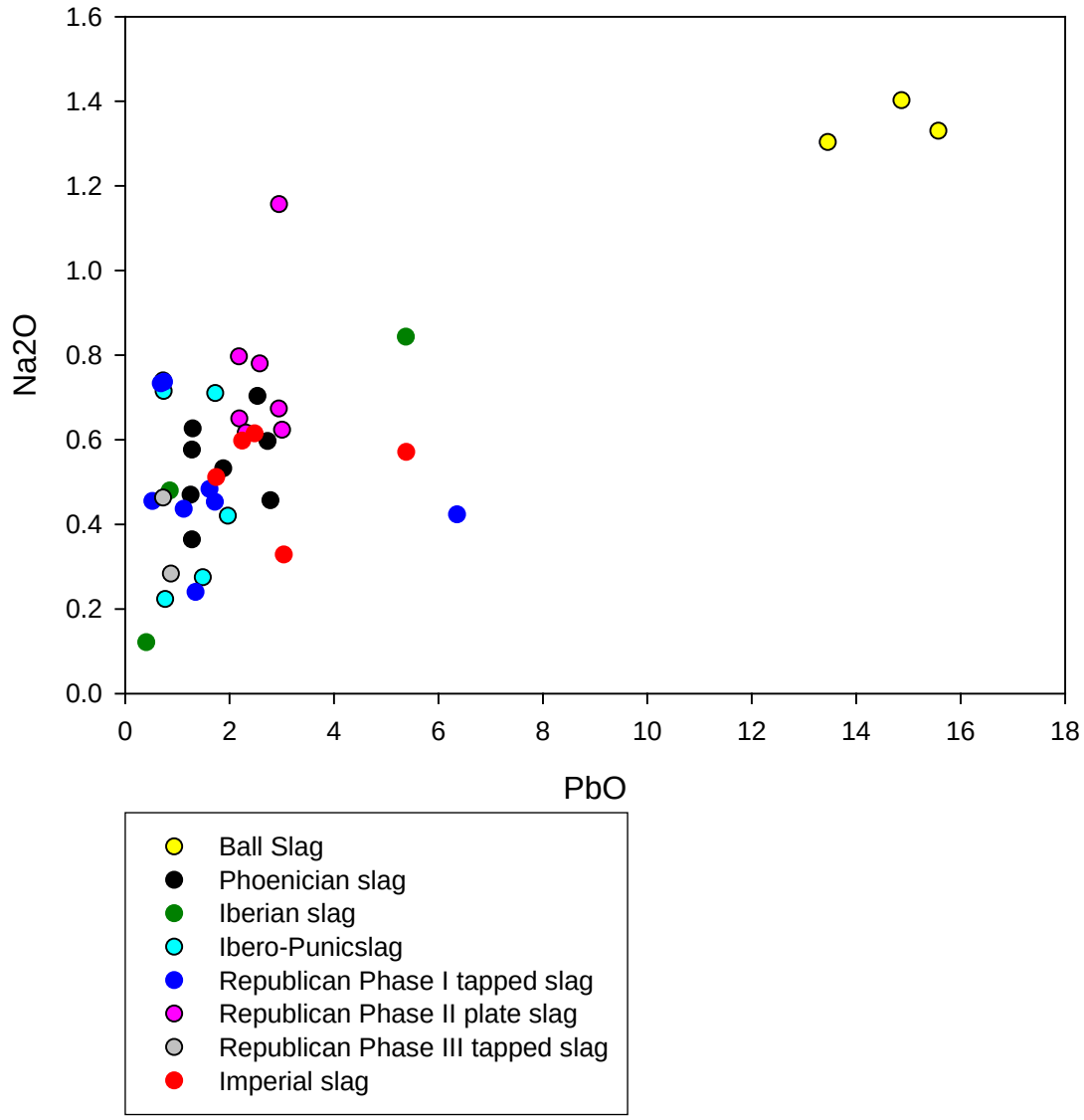

Figure 8.19 PbO/Na_2O ratio in the slag samples from different periods. The Republican phase II plate slag samples show a slightly higher concentration of soda as compared to the other samples, but the enrichment in soda is lower than the one in potash.

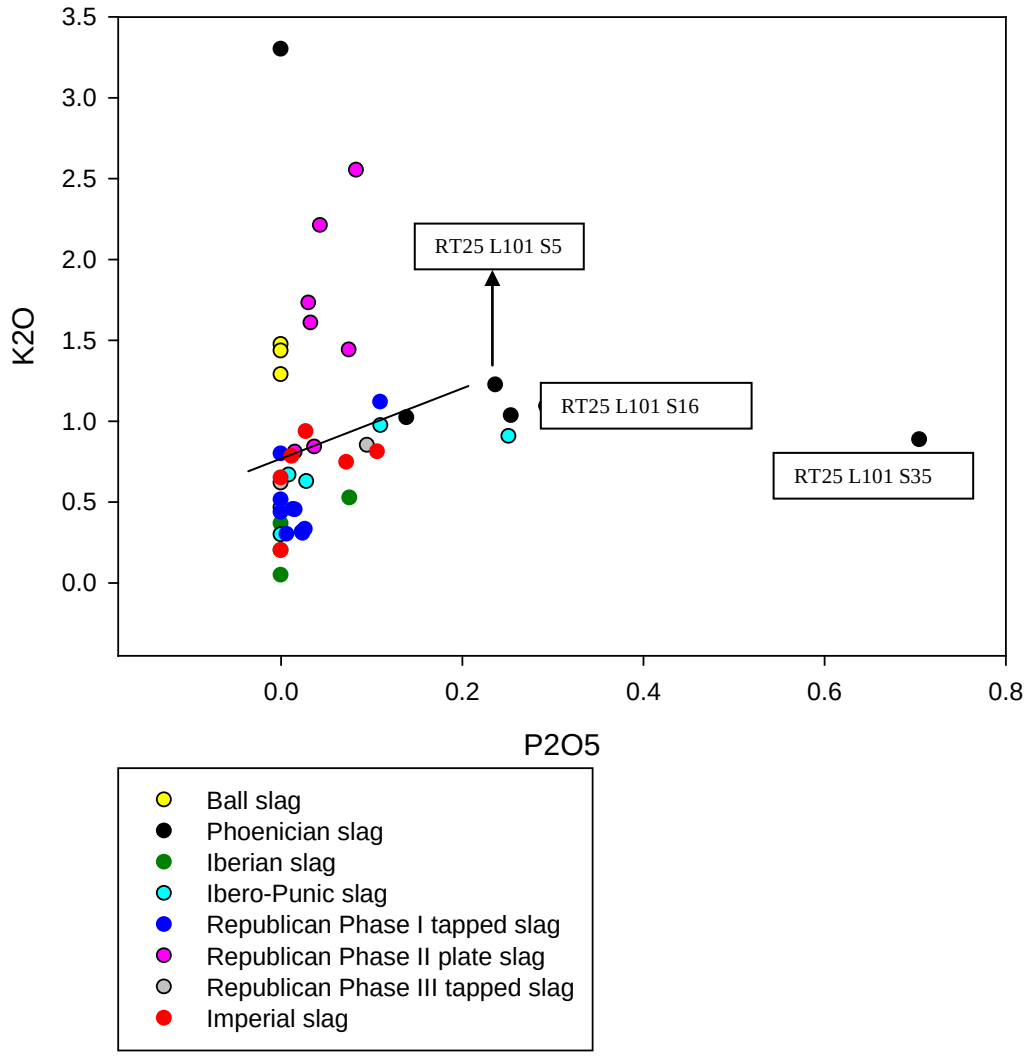

Figure 8.20 P_2O_5/K_2O ratio in the slag samples from the different periods. The Republican phase II plate slag samples show a higher concentration of potash as compared to the other samples, but the enrichment in potash is not proportional to enrichment in phosphorous, confuting the hypothesis that the enrichment in potash is linked to the use of more fuel.

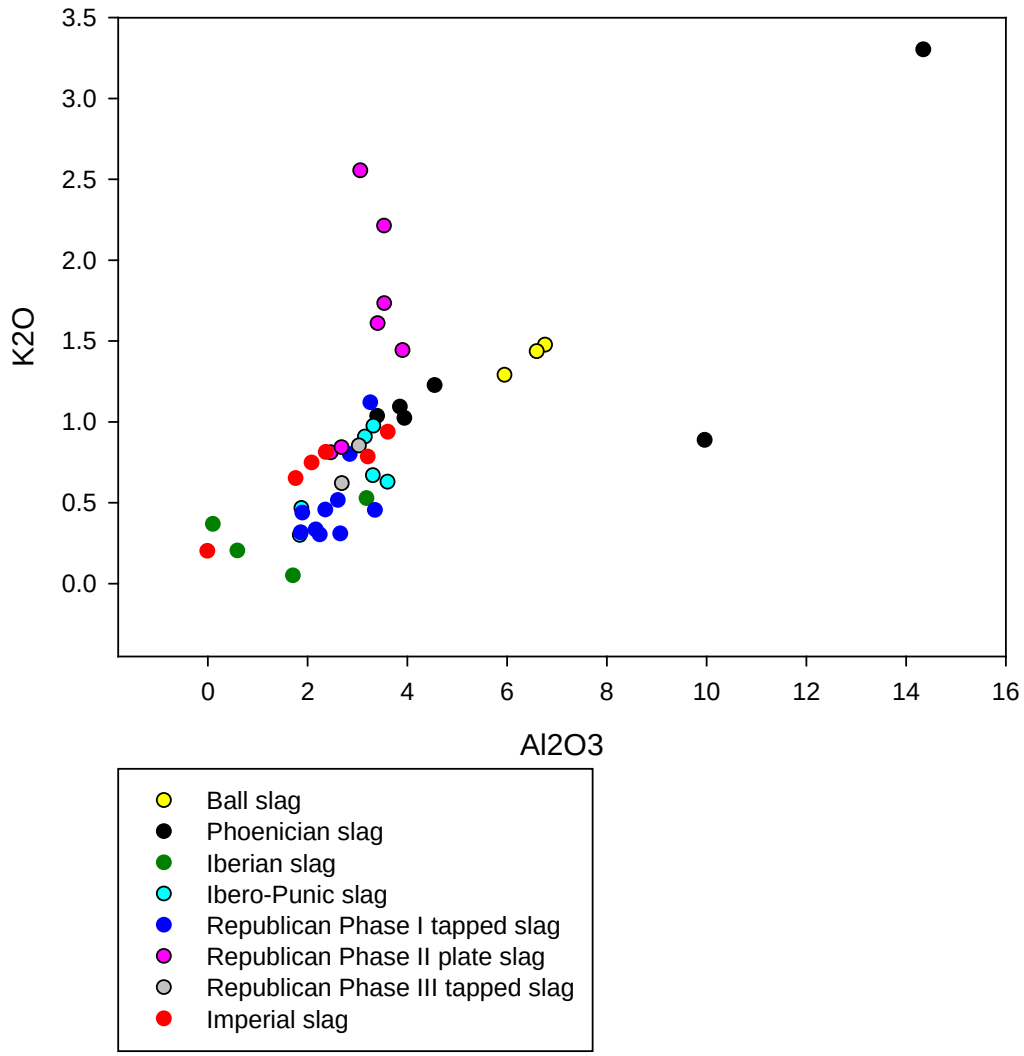

Figure 8.21 Al_2O_3/K_2O ratio in the slag samples from the different periods. The Republican phase II plate slag samples show a higher concentration of potash as compared to the other samples, but the enrichment in potash is not proportional to enrichment in alumina, confuting the hypothesis that the enrichment in potash is linked to a higher chemical influence of the technical ceramics.

These results suggest that during the Republican phase II plate slag period, the ore that was smelted was relatively richer in alkali (and perhaps in silver), and poorer in lead, and this could explain the addition of 'extra' lead to the system. On the other hand, the Phoenician and Iberian samples have an alkali/lead ratio in the same range as samples that do not show any addition of extra lead (according to the isotopic signature). This observation can lead to the argument that during the Phoenician and Iberian periods, 'extra' lead was added to an ore that was not poorer in lead. This aspect thus suggests that this addition was a result of the metallurgical tradition, because it was certainly known that silver was collected in a system with an excess

of lead and also that jarosite was not one of the usual lead minerals used for the extraction of silver (see discussion in Chapter 3).

The important difference seems to be that during the Roman period, such a high level of geological and chemical understanding of the ore – possibly acquired through assaying – existed that it allowed the metallurgists to add extra lead only when needed.

The possibility that an increase in the alkali content was due to a decrease in the ore/fuel ratio needs to be addressed. An increase in alkali correlated to an increase in fuel usage would correspond to an increase in phosphorous. A correlation between these two compounds may be seen for part of the Phoenician samples (Fig 8.20), while three Phoenician samples (RT25 L101 S16, RT 25 LT101 S5 and RT25 L101 S35) show an increase in phosphorous linked to a decrease in potash, and another sample shows only an increase in potash. Two of the three samples showing a decrease in potash and an increase in phosphorous (RT25 L101 S16 and RT 25 LT101 S5) show a marked 'foreign' signature (Fig. 8.15). The decrease in potash, possibly connected to an increase in lead in the ore, would indicate that although the addition of lead was not necessary, it was performed nevertheless.

On the other hand, the Republican phase II plate slag samples show a marked increase in alkali un-correlated with phosphorous, indicating that the source of the two compounds is different. In fact, if the source of potash was the increase in the use of fuel, we would have witnessed a positive correlation between potash and phosphorous, while in this case we observe only an increase of the potash. This indicates that the alkali must originate from the ore or from the technical ceramics. An influence from the technical ceramic should be seen in a correlated increase of potash and alumina. This correlation is not visible for the plate slag, for which we witness an increase in potash, but not in alumina (Fig. 8.21). This result, then, seems to confirm the hypothesis that the increase of alkali derives from the ore. Further confirmation comes from the Republican phase I tapped slag, where samples with a different signature, more contaminated with 'extra' lead influences (samples RT25 L31 S18 and RT25 L31 S19), clearly show a different chemistry. Even if the increase in alkali is not visible in this case, it can be inferred that the different chemistry is related to the use of a different ore/charge. Signs of use of a different ore are visible also in the Ibero-Punic samples RT25 L115 S55 and RT25 L115 S56, showing higher sulphur and higher BaO (as for samples RT25 L31 S18 and RT25 L31 S19,

mentioned in the section above). These two samples show an isotopic signature more influenced by 'foreign' lead. Could a part of the used charge have come from elsewhere? If so, would it have been in a mineral form (galena) instead of a metal form, as assumed for the Republican phase II plate slag period? If this is the case, what is the reason for it? These questions will be addressed in the following chapter.

Isotope analyses were also carried out on semi-reacted ores associated with slags from Corta Lago and on three 'ingots' kept at the museum of Rio Tinto, two lead ingots and one matte, as described in Chapter 6.

The ores all plot in the range published by Stos-Gale et al. (1995) for Rio Tinto and the three 'ingots' plot on the mixing line, considering the scattering already discussed for the Iberian samples (Figs. 8.5 and 8.7). One of the lead ingots plots in the same range as the Rio Tinto ores published by Stos-Gale et al. (1995), while the other one plots in the middle of the mixing line, where the portion of the samples from the Republican phase I tapped slag plot. On the other hand, the matte plots in the area of the Cartagena ores published by Stos-Gale et al. (1995).

The two lead ingots, as discussed in Chapter 6, are very pure and no silver is detected. These ingots could be the result of the reduction of the litharge obtained during the cupellation process. It is possible that these ingots were produced to be added to the system as lead metal for smelting, or were produced to be used as lead metal by the inhabitants of the area (see the discussion of the use of lead in Chapter 2). The recycling of the litharge resulting from cupellation, both as lead for the smelting process and lead to be used on a daily basis, would imply saving capital for the import of lead from elsewhere.

The third 'ingot' (matte) which plots within the Cartagena range is a question mark: why would the workers import such material from Cartagena? What was the use of it? One possible suggestion is that just as the modern archaeologists mistook this 'ingot' for a proper lead ingot, so too the people moving the material from Cartagena to Rio Tinto thought it was lead. Another possible explanation is that the matte was used for other purposes and was imported together with the lead ingots (on the use of matte for metal extraction, see Craddock 1995).

Based on the example of only two lead ingots and a matte ingot, we cannot perform a statistical and/or a systematic study, and thus no clear answers can be given to these issues. What we can certainly state is that the lead clearly originated from different

sources: one is certainly the ore in Rio Tinto, and the other is possibly ore from Cartagena.

Tentatively, there are three main periods when foreign ‘extra’ lead was added at Corta Lago: Phoenician, Iberian, a portion of Republican phase I tapped slag, and Republican phase II plate slag. During the first three periods we have no evidence of connections between an ore poor in lead and the addition of extra lead; while in the Republican phase II plate period, on the other hand, we have indications of such a connection in the higher potash content of the ore.

Thus, we can conclude that geological and chemical knowledge increased during the Republican phase II plate slag period, while a more approximate knowledge of the system had characterised the pre-plate smelters. This hypothesis is also confirmed by the observation of residual grains of quartz and/or barite throughout the pre-Roman samples and their disappearance during Roman times, indicating a completely melted system, in turn indicative of a better understanding of the ore/flux/fuel/time ratio of the system during smelting.

CHAPTER 9

Discussion: changes in production technologies and organisation

The archaeometric analysis of metallurgical debris from Corta Lago was carried out in order to reconstruct the metallurgical processes in areas of activity dating from the Bronze Age up to the 2nd century AD. The reconstructed processes were then compared in order to identify differences. These differences were subsequently linked to relevant geological and metallurgical knowledge and constraints.

The stratigraphic studies carried out by Harrison (personal communication) and the morphological studies of the slag carried out by the author as part of this PhD project identify seven different phases at Corta Lago:

- Phoenician phase;
- Ibero-Punic phase;
- Iberian phase;
- Republican phase I tapped slag;
- Republican phase II plate slag;
- Republican phase III tapped slag;
- Imperial tapped slag phase.

In addition to these seven phases, a few samples of different morphology were recovered from the Imperial layers. The morphology of these samples is similar to the Bronze Age 'free silica' slag as defined in the literature (see Chapter 6), even though they present some differences from the published characterisation of this type of slag (Chapter 6). These samples are treated separately from the Bronze Age material in Chapter 6, but they are believed not to be Imperial, and possibly out of their stratigraphic context, even though they could have been moved out of context in Antiquity. They are used as a case example to understand the Bronze Age process in operation before the Phoenician phase or at the beginning of the period associated with Phoenician influence.

The slag underwent morphological, chemical and petrographical analysis using different analytical techniques, as described in Chapters 5, 6 and 7. The results of

these analyses show that there is no fundamental difference in the temperature (~ 1100/1200 ºC) and the redox conditions (pO_2 between 10^{-8} and 10^{-12} atm) of the smelting processes between the different periods. As described in Chapter 6, the constant mineralogical association is fayalite and magnetite; the chemical composition for all periods under consideration indicates a relatively small range of variation: silica between 20 and 40%, iron oxide between 60 and 80%, alumina up to 10%. All samples from every period fall within the range of stability of fayalite (Fig. 6.63), indicating a temperature between 1100 and 1200 ºC. Nevertheless, several differences were also detected, such as morphology, concentration of silver and lead, concentration of alkali, barium oxide and sulphur, and isotopic signature. The discussion of these differences and their meaning will be the focus of this chapter.

9.1. Macro-Morphology

Most of the slags from the different periods, even though they exhibit different degrees of fragmentation, show the typical lava-flow structure of tapped slag. The fragmentation decreases with time, and huge slag blocks were recovered from the Republican phase III tapped slag and from the Imperial phase (Figs. 6.34 and 6.35). Not only does the size of the fragments change, but also the width of the lava flows, and during the Imperial phase we observe a doubling of this feature, from around 1 to almost 2 centimetres. The increase in the width of the lava flows can be linked to the increase of the diameter of the tap hole of the furnace, and can possibly suggest an increase of the size of the furnace itself to allow the smelt of a bigger charge.

The smaller fragment size of the earlier slags can be due to the fragmentation/crushing of the slags to recover trapped metal prills prior to the Republican phase II plate slag. The identification of almost exclusively crushed slag during the pre-Roman period in the Corta Lago section could support this conclusion even more. The observation and analysis of the slags from these periods, however, do not indicate the presence of trapped metal prills; in fact, the amount of silver and lead loss during these periods is comparable to the following ones. The fragmentation may then have been carried out for other reasons, and the fragments may have been of some sort of use during the smelting, for example as fluxing agents.

period name	sub-period name	chronology	slag morphology	silver concentration (ppm)	lead concentration (%)	alkali sum concentration (%)	BaO concentration (%)	sulphur concentration (%)	presence of residual aggregates
Late Bronze Age/Early Iron Age	Late Bronze Age	8th-7th century BC	ball	350 to 450	11.2 to 13.5	1.7 to 1.9	7.7 to 18.3	1.2 to 1.4	yes
	Phoenician	7th-6th-5th century BC	tapped	170 to 700	1.5 to 3.6	1.4 to 3.4	4.6 to 6.8	0.2 to 1.5	yes
Iron age	Ibero-Punic	5th-4th century BC	tapped	60 to 390	0.9 to 2.4	0.5 to 1.2	4.5 to 5.9	<0.1 to 1.3	yes
	Iberian	4th-mid 2nd century BC	tapped	~ 150	~ 1	0.7	7.8 to 9	1.3 to 3.5	yes
Roman Republican	Republican tapped phase I	mid 2nd to 1st century BC	tapped	110 to 350	0.7 to 4.5	0.3 to 1.1	1.8 to 17.2	0.4 to 2.1	no
	Republican plate phase II	mid 1st century BC	plate	45 to 110	2.3 to 3.7	0.8 to 2.9	4.5 to 10.5	0.8 to 1.7	no
	Republican tapped phase III	second half 1st century BC	tapped	50 and 450	0.9 to 1.1	0.6 to 0.9	2.5 and 3.8	~ 0.6	no
Roman Imperial	Imperial	up to 2nd century AD	tapped	50 to 260	1.8 to 3.9	0.8 to 1.2	2.6 to 7.3	0.7 to 2.2	no

Table 9.1 Table summarising the main characteristics from which differences are noticed between the different periods of exploitment of jarositic ores in the Corta Lago area. Note that the argument about the belonging of the Ball Slag typology to an early Phoenician phase or a local Late Bronze Age is discussed in section 6.1.

Another important morphological change is the identification of a well-defined group of layers of plate slag during the Republican period, stratigraphically located between two phases of tapped slag. This morphological change is also associated with a technological change, detectable by chemical and isotopic changes. First of all, the morphological change requires discussion. In this case, the shape difference implies an alternative tapping choice that would have brought some form of improvement to the smelting processes. This technological choice surely coincides with a very efficient process, associated with the lowest silver loss. The isotopic signature and alkali concentration of these slags also have peculiar features, mainly concerning the amount of potash.

9.2. The problem of the Republican phase II plate slags

The Republican plate slags have an isotopic signature highly enriched in 'foreign' lead, similar to the Phoenician, Iberian, and part of the samples from the Republican phase I tapped slag period; in fact, these samples plot the furthest away from the Rio Tinto signature along the mixing line (Chapter 8, Figs. 8.1 and 8.2). However, the Republican phase II plate slags are also enriched in alkali, mainly potash, a feature which the other samples with the same isotopic signature do not show.

Firstly, we will discuss the characteristics of the Republican phase II plate slag, and a discussion of the other three periods will follow. As discussed in Chapter 8, the enrichment in potash in the slags may be due to an ore vein richer in alkali and poorer in lead being exploited at the time, or to an increase in fuel use relative to the ore, or to an increase in technical ceramic influence due to, for instance, higher temperature. Jarosite-type mineral bears alkali and lead in the same crystallographic position (x=0, y=0, z=0; Hendricks 1937; Menchetti and Sabelli 1976; Basciano and Peterson 2008), so an enrichment in alkali would imply a depletion in lead due to crystallographic limitations. In contrast, some scholars recalculated that the silver cation is located in a different crystallographic position in the mineral than the alkali (x=0, y=0, z=0.5; Groat et al. 2003), so changes in these cation concentrations affect the concentration of silver, exclusively for stoichiometric reasons. However, this secondly mentioned crystallographic position of the lead (x=0, y=0 and z=0.5) is the

same as that of the silver, hence the concentration of silver and lead in the jarosite crystals are inversely proportional for crystallographic reasons. The depletion in lead could then imply enrichment in silver, limited stoichiometrically by the alkali concentration. Summarising, a depletion in lead would entail an increase in silver and alkali and vice-versa. This would mean a proportional increase of silver and alkali. However, this proportionality is not observed in the slags, not surprisingly, since the amount of silver in slag is only a function of the efficiency of the process, while the amount of alkali may be an index of both the charge and the process (fuel contamination). The hypothesis of an ore richer in silver being exploited during the Republican phase II plate slag period cannot be dismissed, but it cannot be proved either, since no visible signs of increase in silver can be found in the slag. Therefore, of these two hypotheses, only that of an ore depleted in lead and enhanced in potash will be taken into consideration.

The possibility that a different ore was processed during the Republican phase II slag period is indicated by a concentration of calcium, aluminium and barium oxide at the higher limit of the compositional range of all periods in the slag dating from this phase. This may be coming from the gangue of the ore and may be the reason for an increase in the temperature necessary for the smelting. However, calcium and aluminium oxides may also originate from a stronger interaction of the charge with the technical ceramic during the process, which could in turn also derive from the higher smelting temperature.

Thus, before expanding on the hypothesis of the benefits of an ore poorer in lead, the possibility of a fuel increase needs to be discussed. The increase in potash may also be indicative of an increase in the quantity of fuel used. As potash is a component of fuel ash, a higher consumption of fuel would lead to an increase in the amount of potash in the system. As mentioned earlier, an increase in fuel due to the need for increasing the smelting temperature may be due to an increase in lime or alumina in the system. A higher concentration of these two components would require increasing the temperature to obtain a liquid system. If this is the case, then the three oxides should be proportionally enriched in the Republican phase II plate slag. The analyses of the plate slag show that the concentrations of lime and alumina are at the higher edge of the chemical variation for all periods, but the enrichment is not as intense as the one observable for the potash (Fig. 8.7).

Since the increase in lime and alumina does not seem to be correlated to the increase in potash, indicating that a change in the ore in this direction would not be a reason for an increase in temperature, the other possibility is that a higher smelting temperature was needed to produce a higher fluidity of the slag, a lower viscosity, resulting in a better separation of slag and metal and therefore a lower concentration of metallic prills and higher silver recovery. Achieving a lower viscosity would produce slags with fewer prills of lead metal trapped in the silicatic matrix and consequently less loss of silver. Could this have been the motivation for the technological change? If lead metal prills had not been present in the slag before this technological change, then there would have been no need for an increase in temperature to improve the fluidity, because the loss of metal (both lead and silver) did not come from particles trapped in the slags due to high slag viscosity. There is no evidence of a significant concentration of trapped particles in the slags prior to the Republican phase II plate slag (but there is evidence of crushing of the slag, possibly due to the recovery of metal prills), and no evidence of a change in the concentration of trapped metallic prills is visible during the Republican phase II plate slag. The viscosity index presented in Chapter 6 does not show a marked increase in fluidity for the slags of this period, hence there is not a composition-driven change in fluidity, but this index would not provide any indication of a temperature-driven increase in fluidity. In Chapter 2, we offered the hypothesis that the Romans would not make any investment in technological change if it was not necessary, and I believe our reasoning should be set within this framework. Based on the consideration that there was no necessity to increase the temperature of the smelting since there was no significant amount of metal prills trapped in the slags, the hypothesis of an increase of fuel relative to the ore charge to increase the fluidity of the slags can be discarded.

Furthermore, the alkali enrichment is also non-proportional as compared to phosphorous. Phosphorous should show a correlated increase with potash if the increase in fuel consumption was the cause of the increase in alkali, since phosphorous is the other important component in fuel ash. The lack of a correlation between the increase in alkali and that in phosphorous seem to confute the hypothesis of a higher quantity of fuel being used during this period.

Following this discussion, the hypothesis of the enrichment in alkali being related to the processing of an ore richer in alkali seems more likely.

9.3. The addition of 'foreign' lead

As mentioned above, the evidence for enrichment in alkali, most clearly potash, was detected only for the Republican plate slags, even though the Republican phase I tapped slag, as well as the Iberian and the Phoenician phases are also characterised by a strong 'foreign' lead isotopic signature, indicating that during the Republican phase I tapped slag and the Phoenician phase something different occurred. The term 'foreign' here indicates a source of lead (metal or mineral) different from Rio Tinto ores.

Taking first into consideration the Republican phase II plate slags, several characteristics need to be considered. Not only do we observe the 'foreign' lead signature and the enrichment in alkali that could indicate the processing of an ore poorer in lead and that needed then to be added from elsewhere, but there is also the very important morphological change. As discussed above, this is linked to the technological choice of changing the tapping method without any notable improvement of the process except for a slight improvement in efficiency, corresponding to a change in the silver content in the slag from slightly above 100 ppm to slightly below 100 ppm. Would this amount have made such a difference in this period? And, if this is the case, why was that? Another factor that needs to be taken into consideration is the recovery of the aforementioned three ingots at Rio Tinto. As discussed in Chapters 6 and 8, these are two ingots composed of lead and one iron-copper matte. One of the two lead ingots has an isotopic signature closer to the Rio Tinto extreme, while that of the other one is closer to the Iberian samples. Both the Iberian samples and the ingot plot within the scattering of the signatures of Rio Tinto ores around Corta Lago (Figs. 8.8 and 8.9), combined with an input coming from "foreign" lead (see Chapter 8). On the other hand, the matte ingot has an isotopic signature in the range of the Cartagena field. The matte ingot may have been imported by mistake from Cartagena together with a cargo of lead ingots. Whether this import was accidental or intentional, the recovery of this ingot is a very important indication that material was being imported from Cartagena. The ingot was discarded and not used for any process at Rio Tinto possibly because the metallurgists noticed the mistake. However, if the two lead ingots recovered in Rio Tinto, one of which shows a mixed isotopic signature (see Chapters 6 and 8), are

taken into consideration in this discussion, then the hypothesis that lead was collected from the cupellation process and recycled in the smelt can be formulated. This hypothesis raises the question of why this process did not produce a sufficient quantity of lead during the Republican phase II plate slag period, leading to a more significant need for 'foreign' lead than in other periods.

In the author's opinion, the most convincing hypothesis for the addition of 'foreign' lead during the Republican phase II plate slag period is the exploitation of an ore poorer in lead (and possibly richer in silver). If this was the case, then a greater quantity of lead metal needed to be added to the system in order to obtain an efficient collection of the silver during smelting (because there was not enough lead in the ore and the problem would become more significant if there was more silver in the system to be collected). Moreover, the technical choice of tapping the slag into a forehearth instead of freely tapping it into heaps needs to be discussed. This issue could be approached by considering the possibility that a different 'school of smelters' became operative in the area at the time, and it looks like they brought two changes with them:

- Tapping in the forehearth and producing plate slags, maybe simply to have a more efficient way to dispose of the metallurgical debris;
- Addition of lead metal instead of lead-bearing minerals (galena) as collector for the silver.

This is in contrast to the three previous periods mentioned above, where we notice a 'foreign' isotopic signature and the coincidence of an increase in sulphur, probably indicating the addition of galena instead of lead metal to the system. The use of metal instead of mineral brings with it obvious advantages on the transport side.

In more detail, the use of extra 'foreign' lead during the other phases, Phoenician tapped slag phase, Iberian tapped slag phase and Republican phase I tapped slag, has different implications, since no differences in the alkali concentrations can be detected in the slag samples, but enrichment in sulphur and barium oxide are visible in the Iberian and the Republican samples, characterised by an isotopic signature more influenced by the 'foreign' source. If there is no difference in the alkali concentrations, then the ore is assumed not to be more enriched in potash and therefore not depleted in lead, as compared to the average observed in the periods not characterised by an isotopic signature influenced by the 'foreign' source. As a result,

there should have been no need for extra lead metal when compared with other phases. Thus, the reason for the addition of lead originating from a 'foreign' source needs to be sought elsewhere. The lead isotope signature shows a higher use of 'foreign' lead up to the Republican phase II plate slag, and only a limited one after this phase. We have discussed the indications for a change in mineralisation as well as a process change during the Republican phase II plate slag, and we have seen that these observations (both for the mineralisation – higher in alkali and poorer in lead, and the technological aspects – choice of tapping the slag in a forehearth or freely) are not verified for the periods prior to that phase. The suggested conclusion is that prior to the Republican phase II plate slag, the 'foreign' lead – in whichever form, metal or ore – was added regardless of the ore composition, as a safety measure to ensure efficient collection of the silver. Possibly, considering a continuous process, the quantity of lead available for recycling after cupellation was too low to satisfy the demand for lead metal as collector during the smelting.

9.4. The two processes during the Republican phase I tapped slag

A digression is needed to focus our attention to the Republican phase I tapped slag. During this period, we observe the coexistence of two processes, one of which has already been mentioned in comparison with the Republican phase II plate slag, since it is characterised by a lead isotope signature influenced by a 'foreign' source. We have already mentioned that the samples from this period that are characterised by a 'foreign' lead isotope signature are also characterised by high barium oxide and sulphide. It is also true that the same samples plot closer to Optimum 2 in the diagram alumina/ silica/ iron oxide (Fig. 6.63). The other samples of this period show enrichment in arsenic, lead and antimony, and plot in the centre of the fayalite field. It seems that during this period we can identify the coexistence of a 'comfortable' smelting – in the safe region (centre of the fayalite field), with no addition of 'foreign' lead – with a more closely controlled type of smelting, set to a particular region (Optimum 2) where there is a higher iron/silica ratio. Consequently, more iron is concentrated in the slags, with the same amount of silica added to the charge, plus the addition of a lead ore to improve the silver collection. As a matter of

fact, what we see here is that the barium and the iron are collected by the added silica to form the silicates, barium that appear to be added when mixed with the lead sulphide (a possible sign of the association galena/barite in the added ore). This entire change seems to worsen the efficiency of the system, and the concentration of silver in the slags increases to around 300 ppm. During the Imperial tapped slag period there is an increase in production, attested by the increase in the dimensions of the furnace, as mentioned above. During this period we observe a production of silver with no (or minimal) addition of 'foreign' lead (the isotopic signature is well within the Rio Tinto mine scatter – Figs. 8.8 and 8.9). The absence of or decrease in the addition of 'foreign' lead can be explained by two alternative hypotheses: first, a larger furnace needs proportionally less collector lead metal per unit of ore as compared to the smaller furnaces of earlier periods, due to the longer length of the process, so the lead present in the ore and the one added from recycling of litharge from cupellation was nearly sufficient for the collection of the silver. The second hypothesis is that there was an improved yield of recycled lead from litharge smelting, probably due to organisational or technical changes in litharge processing: technically independent of the increase in furnace size, but possibly part of an overall optimisation of the *chaîne operatoire*. Neither of these two hypotheses can be proved by this archaeometric study, but the latter seems more likely considering the highly organised 'industrial' production observed during the Imperial period.

9.5. Lead metal, galena and barite

At this point a digression needs to be undertaken to address the form of the 'foreign' lead added in the pre-plate slag phases. The Iberian and Republican phase I tapped slag samples showing 'foreign' lead isotope signature present chemical differences mainly concerning the concentrations of sulphur and barium oxide. The Phoenician samples, on the other hand, show high barium oxide, but do not seem to show any high sulphur distinguishing the samples enriched in 'foreign' lead from the others. It looks like the three periods all show high barium concentrations, but not the same increase in sulphur. If we consider the increase in sulphur in the system as due to addition of lead sulphide as collector for the silver, then the same cannot be said for the Phoenician period. It can then be inferred that during the Ibero-Punic period

galena was added to collect the silver, and this was also occurring within one of the processes in operation during the Republican phase I tapped slag. On the other hand, the increase of barium oxide is associated with the use of a different ore, apparently richer in the 'foreign' lead isotopic signature, and therefore possibly indicative of the geochemical signature of such an ore. As first possibility, the suggestion that smaller hydrothermal veins could have been added to the main ore to increase the amount of lead and silver in the system can be taken into account. According to Marcoux and Sáez's (1994) description of the chemical association in the hydrothermal veins, it appears that only two of them contain barium, Preciosa and Aurora (circled in red in Figs. 9.1 and 9.2 below). These show the isotopic signature of Rio Tinto and Cartagena mines (Stos-Gale 1995), hydrothermal veins (Marcoux and Sáez 1994) and slag and litharge samples studied in this thesis. Aurora (the plot on the left hand side) plots within the slags mixing line, close to the Rio Tinto end member in the 206/204 vs. 208/204 diagram, but outside it in the 206/204 vs. 207/204 diagram (Figs. 9.1 and 9.2), so its isotopic signature is not compatible with the Rio Tinto slags, and Preciosa plots out of the mixing line in both diagrams, and thus its signature is not even compatible with the slags under consideration in this study. This seems to indicate that the mineralisation enriched in barium oxide that was added to the jarositic ore in Rio Tinto has indeed a 'foreign' origin and is not related to the local hydrothermal veins. It seems then that an ore rich in sulphur and barium (barite) with an origin outside of the Rio Tinto area was added to the system. The frequent association of galena and barite seems to suggest the possibility that such a mixture was added to the system. For what concerns the Phoenician samples, where a correlation of sulphur and barium was not observed, the hypothesis suggested is that the galena/barite was added to the system after roasting.

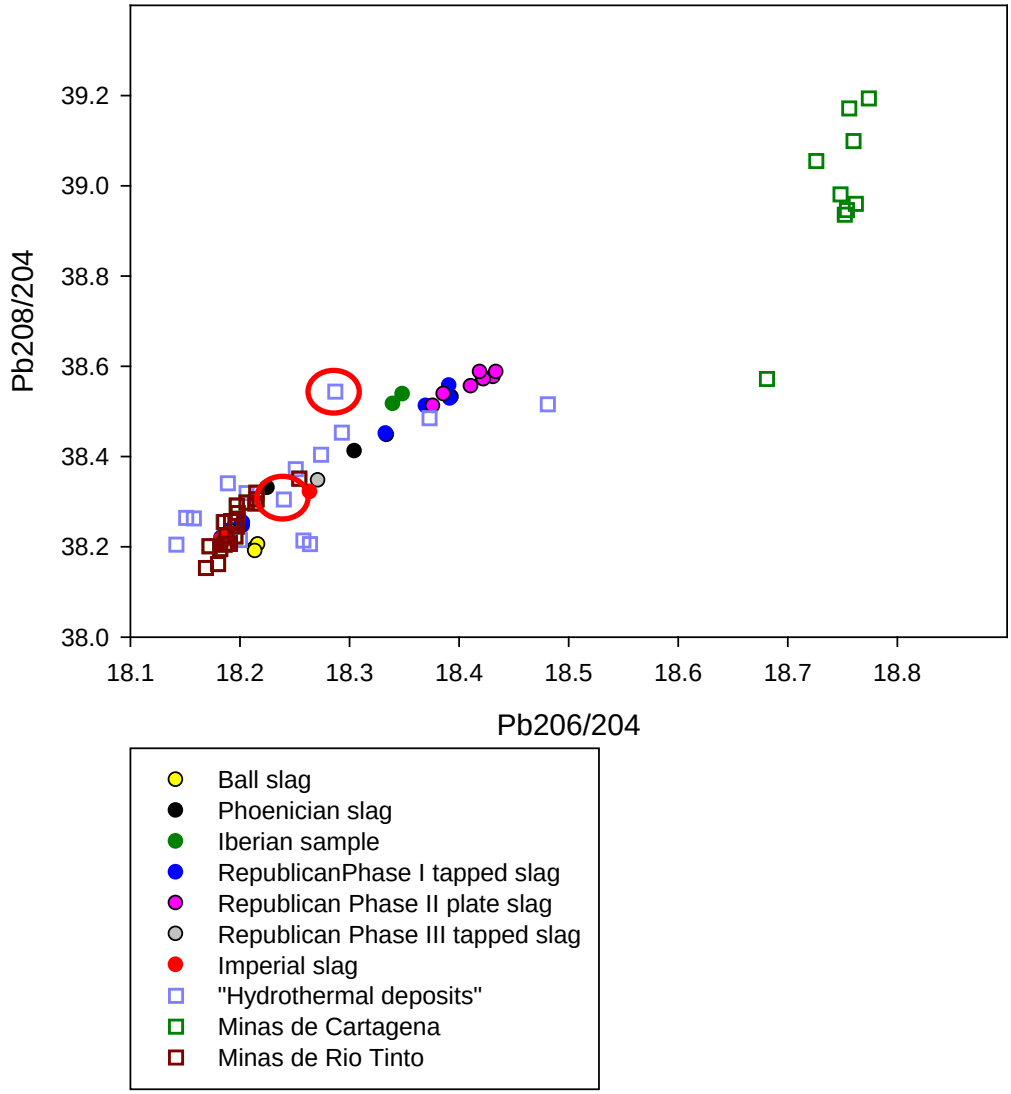

Figure 9.1 Isotopic signatures of Corta Lago samples compared with Rio Tinto and Cartagena mines (Stos-Gale 1995) and hydrothermal veins (Marcoux and Sáez 1994). The veins circled in red are Aurora (bottom) and Preciosa (top).

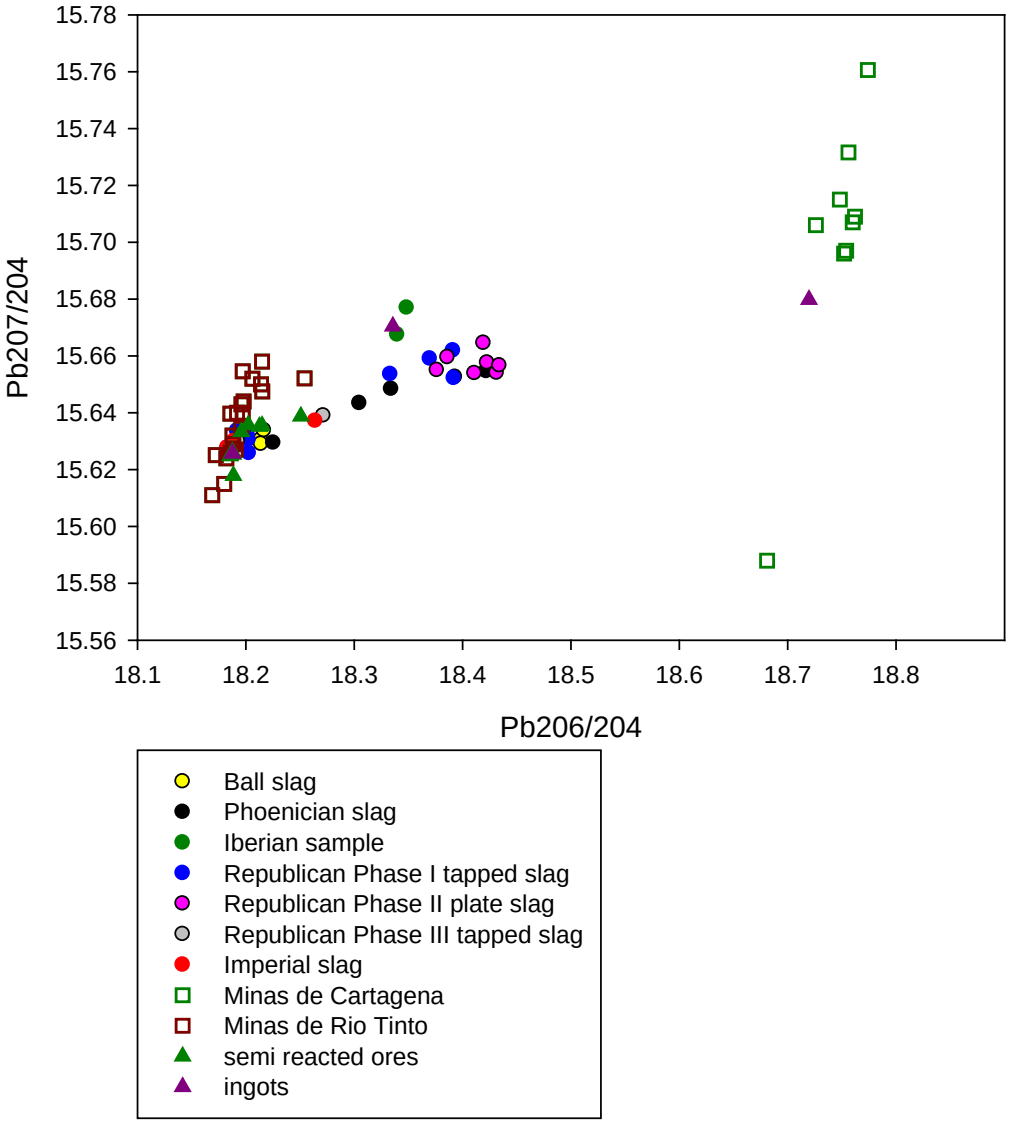

Figure 9.2 Isotopic signatures of Corta Lago samples compared with Rio Tinto and Cartagena mines (Stos-Gale 1995) and hydrothermal veins (Marcoux and Sáez 1994).

9.6. Silver loss and efficiency of the process

Observations on the efficiency of the production processes can be drawn from analysing the silver loss in the different periods. The ball slag and the Republican plate slag both indicate a very efficient process, with a loss of silver of less than 100 ppm associated with a relatively high lead loss (around 15% for the ball slag and around 3% for the Republican plate slag). This seems to indicate that the free tapping technique increases the loss of silver in some manner, at least at Corta Lago. On the

other hand however, at the site of Tharsis, freely tapped slags present a concentration of silver that is even lower (less than 100 ppm).

In general, pre-Roman slags exhibit a slightly higher loss of silver. Among the Roman slags, the Imperial ones show a greater variation in the loss of silver and lead for what concerns Corta Lago, while in Tharsis, even though we observe a larger compositional range, the loss of silver is still low. The increase in the size of the furnace, hypothesised following the observation of the increase in tap flow and slag thickness, indicates a larger process (charge/system), and the greater variation in the loss of silver may be due to the larger amount of material processed and the high amount of silver produced. The decrease in chemical homogeneity during this period seems to indicate a difficulty in the mixing of the charge, possibly due to its greater size. Thus, even though the standardisation of the process was greater, the possibility that the consequent charges of the furnaces were not uniform, and the difficulty of mixing due to the size of the furnace and consequently of the charge, resulted in non-uniform residues.

A further relevant observation concerns once again the amount of barium oxide. Regardless whether the barium oxide originated from Rio Tinto or a 'foreign' source, as discussed above, the concentration of this oxide shows relatively high variation, but this does not seem to introduce big changes in the system. The high barium oxide quantity is not correlated to the presence of residual, non-reacted grains of barite for the Roman slags. The correlation of high barium oxide and residual barite in the slag is observable for the ball slags. However, residual grains are not visible in the Republican phase II plate slag and the Republican phase I tapped slags, two samples of which show an amount of barium oxide comparable with the ball slags, and even higher, indicating that the presence of this oxide does not affect the smelting conditions (T, fO_2 and subsequently viscosity) in these proportions, and a fully melted system could still be obtained.

9.7. Chemical homogeneity

A few residual mineral grains were detected in the pre-Roman samples, quartz in the Phoenician and Iberian slags and barite in the Ibero-Punic ones, indicating that during these periods the charge was not completely melted, creating a more rigid

semi-liquid system that theoretically would trap a slightly higher amount of metallic droplets. Nevertheless, these circumstances did not increase dramatically the loss of silver, as already mentioned above. Observing the chemical variation within the area analyses carried out on the samples (see Chapter 6), and using this data to describe the chemical diffusion of the elements in the system, it can be suggested that the early crystallisation of olivines limits the diffusion of the elements more than the presence of residual crystals. Normally these olivines show polyhedral/hopper morphology, indicating a 'long' crystallisation time, and suggesting the possibility that the crystallisation was starting already in the furnace. As a matter of fact, the Roman slag samples exhibit a lower chemical uniformity (detected from the standard deviation between the area analyses in each sample), even if no residual crystals are present, but the olivines crystallised in these slags are more euhedral (hopper or euhedral) or, when skeletal, are bigger than those in the pre-Roman samples. These observations suggest that the loss of silver is linked to the diffusion of this element in the system. We observe the lowest loss of silver in Tharsis, where in the Republican samples we observe spinifex and skeletal olivines, and in the Imperial ones (characterised by a larger amount of material being tapped out of the furnace) we observe skeletal and small hopper morphologies, in both cases indicating fast cooling. Thus, the beginning of the crystallisation can be estimated to have occurred outside and not inside the furnace. Furthermore, if we take into consideration only the Imperial samples at both sites, the samples from Tharsis show lower standard deviation, considering the area analyses. It seems then that the system was kept on a molten state at Tharsis, while at Corta Lago the system was kept at a slightly lower temperature, around the *solidus* conditions. Was this due to a constraint related to saving fuel in the Corta Lago area during the Imperial period, when the production increased (as we can infer from the increase in the size of the furnaces and of the slag heaps)? A comparison of the phosphorous concentration between Imperial samples at Tharsis and Corta Lago, to be used as an indication of fuel usage, shows a similar concentration in the samples from the two sites, seeming to confute the hypothesis of the fuel constraint. In reality, the amount of phosphorous at Corta Lago may be related more to the length of the process rather than to a small variation in temperature, and perhaps the charge was kept in a *solidus* condition for longer time. This choice would still allow saving fuel, since most of the fuel is used for increasing the temperature and not for maintaining it in a heated system.

9.8. Smelting process and slag production

Overall, the smelting technology for the production of silver from jarositic ores at Corta Lago seems to have been known since the Bronze Age and not radically changed up to the 2nd century AD. The jarositic ore $XFe_3(SO_4)_2(OH)_6$, where X could be K, Na, Ag, Pb or NH_4, was smelted with the addition of quartz in order to obtain a lead bullion enriched in silver and a fayalitic slag that would free the lead from the iron and the other impurities. This process was carried out by firing a furnace to a temperature around 1100/1200 ºC (the fayalitic low temperature field in the diagram alumina/ silica/ iron oxide), maintaining an oxygen fugacity between 10^{-12} and 10^{-8} atm, while the lead (metal or mineral) addition captured the silver. The finer distinction within the fayalite stability field will be discussed in the concluding chapter of this thesis.

The mineralogical association shows a difference concerning the minor minerals. The Republican phase II plate slag seems to mark a threshold showing the first crystallisation of feldspathoids and feldspars associated with the main fayalite plus magnetite association. In geology, the crystallisation of a feldspathoid would indicate the lack of silica in the melt, leading to the crystallisation of a feldspathoid instead of a feldspar; this aspect has been previously discussed in the literature (Craddock 1995; Keesman 1993). The association of the two indicates steps of crystallisation from the melt. The correspondence of the chemical analyses performed by EDS-SEM with the XRD results confirms the detection of feldspathoids as minor phases present in the slag from the Republican phase II plate slag onwards. The firing temperature is still the same, but a longer crystallisation period seems to be involved in the crystallisation of this phase, occurring in an environment 'lacking' in silica, consumed for the crystallisation of the main olivinic and feldspar phases. Since the ratio (iron oxide/silica) used to charge the furnace was two to one, correct to form olivine, but far lower considering the feldspar ratio, hence feldspathoids crystallise, after an initial feldspars crystallisation.

The chemical variation between samples within the different phases is consistently around 10% (considering the main oxides), indicating the use of a fairly standardised

charge since the Bronze Age/Phoenician period, within the variability of the ore used and the addition of the collector considered (galena or lead metal).

The technological changes discussed above occur within this standardised charge/process, in response to geological constraints and as a result of superior metallurgical and geological knowledge, observable for instance in the response to the depletion in lead of the ore during the Republican phase II plate slag.

9.9. The amount of slag produced

As mentioned in Chapter 2, the calculation of the Roman slag produced at Rio Tinto varies greatly depending on the author calculating it. Salkield (1987, 90), for instance, calculates a total of nine million tons of slag produced as a result of silver metallurgy at Rio Tinto, considering as a starting point that the smelting of one ton of ore could produce around 4500 kg of slag. Salkield's calculation (1987, 92) is based on extreme numbers – for instance, an ore with 90% silica and a ratio of cation/silica around 2.33, with the implication of the addition of around 2100 kg of quartz for the smelting of 100 kg of ore. He continues by stating that if we consider the formula of jarosite $XFe^{3+}{}_3(OH)_6(SO_4)_2$, we observe the presence of three atoms of iron with oxidation state 3+ that we need to scorify as silicate Fe_2SiO_4 where we have two atoms of iron with oxidation state 2+. After reducing the iron from the state 3+ to 2+ in the presence of charcoal, three parts of quartz are needed for every two parts of jarosite. Thus, a ton of ore mixed with one ton and a half of quartz would be a sufficient ratio to produce fayalite plus residual quartz (Salkield 1987, 92). Since this is already an overestimation because we did not consider the OH group, the sulphate and the X cation in the jarosite, we believe that the 4500 kg of slag per ton of ore estimated by Salkield represent more than double the possible estimation. In fact, even if we consider the cation X as well as Fe^{3+} (reduced to 2+) entering in the silicatic phase and a ratio of two parts of quartz for every part of jarosite (to maintain an iron oxide/silica ratio of 2 to 1 and thus to remain in the fayalite field, as the chemistry of every sample analysed shows), then three tons of slag per ton of ore are formed, making an estimation of six million tons of slag in total more realistic. This is a simplified re-calculation of the slag produced since it does not take into

consideration the fact that iron is present in other form in the ore assemblage (as goethite or hematite for instance).

9.10. The process

The comparison between Corta Lago and Tharsis reveals that there is no major difference in the smelting process between the two sites, and, furthermore, there is a major common trend but also a few differences. The process is in both cases the one described above, smelting jarosite with an addition of quartz at a ratio of approximately one to two to obtain a chemical system that would smelt at the minimum temperature in the field of stability of the fayalite, around 1100 ºC in a reducing atmosphere (pO_2 between 10^{-12} and 10^{-8} atm).

As shown in Chapter 4, both Craddock (1995) and Keesman (1993) indicate that the smelting of the jarositic phase would produce a middle product necessary for the process, this being speiss. The slag analysed for this thesis reveals the presence of arsenic in the system, with concentrations of up to 3% (RT25 L115 S20 – Iberian) and often around 1%, and rare newly formed phases of antimony-copper arsenide/sulphide (trapping silver) are detected in the Ibero-Punic sample RT25 L124 S12. These phases are not detected in the Roman samples, even though the amount of arsenic measured does not decrease. In the lead bullion recovered from the Imperial layers, arsenic is present, as well as antimony (high concentration). The arsenic in the bullion is at least half than in the slag from the same period, and the antimony is ten times higher (like the silver). These observations seem to indicate that arsenic and antimony were part of the initial charge, suggesting the use of a polymetallic ore (sulphates plus arsenides). The formation of speiss would trap part of the silver but does not seem to be a necessary middle step, since the composition of the bullion seems to derive directly from the slag. The detection of 'speiss' phases is too rare in the samples, and the arsenic seems to be associated with the sulphidic residue on a proportion of one to ten in average, which could be representative of the ore in the charge, without indicating an enrichment in speiss before the formation of the bullion. It is believed that the bullion separates directly during the production of silicatic slags.

9.11. Ore variability and technical choices

The common trend detected between the two sites is the increase of production in Imperial times, attested by the increase of lava flows that, as mentioned above, can be used as an index for the increase in furnace size and scale of production. The lava flows are generally bigger at Tharsis than at Corta Lago, indicating that the design of the furnaces was slightly different at the two sites.

The sites present a certain variability in the chemistry of the system, within the general lines of a fayalitic slag. Tharsis slags have a lower concentration of barium, as well as a lower concentration of silver. While the former cations may be linked to a difference in the ore exploited, the amount of silver has more to do with technical choices. The barium in the system originates from the gangue of the ore, not causing any worsening in terms of system time and not requiring a waste of energy to clean it out. The barium concentration thus provides an imprint of the gangue, and the fact that the concentration at Tharsis is around hundreds of ppm while at Corta Lago it is constantly a few percent indicates that the gangue of the ore is different.

A difference is also visible in the chemical variability between the samples; while the samples from Tharsis look chemically homogenous, the samples from Corta Lago show a higher chemical heterogeneity. This variability, in light of the observation regarding the barium concentration, can be linked to a higher variability of the ore at Corta Lago as compared to the one at Tharsis, as well as to a different ore selection choice/technique in the field. Since the jarositic earths are a complex mineral assemblage, this is quite possible, and we would observe a variation in all the components that can enter in the mineral itself. However, this might not be the only difference, as the mineralogical association of the ore can also vary. An interesting chemical observation concerning the sulphur concentration can be related to this argument: in fact, the analyses of the samples from Corta Lago show a higher concentration of sulphur as compared to the analyses of the samples from Tharsis, not only in the samples discussed for their isotopic signature, but as a general observation. Sulphur enters into the system from the jarosite itself, but also from the associated sulphides, considering that the jarosite develops within a pyritic environment as alteration product. In the case when the worked veins are stockworks instead of larger deposits, more associated sulphides can enter into the system. A

charge constituted by sulphates plus sulphides may exhibit an increase in sulphur concentration even in case of pre-roasting of the ore.

The loss of silver in the slag is related to the process rather than the chemistry of the ore. The loss of silver was measured to be more variable and slightly higher in the Roman samples from Corta Lago as compared to the samples from Tharsis, except for the Republican plate slag samples, where the values are comparable. The loss of silver is understood to be linked with the degree of liquidity of the system during the process. During the time when the system is liquid, the chemicals have the freedom to move and react in the system, and thus the silver would be collected by the lead metal, forming droplets that would coalesce forming the bullion. When the system starts solidifying or when it is not completely melted, the droplets stop coalescing, getting trapped between the newly formed crystals or the residual ones.

We could then hypothesise that the geological and environmental situations are different at Corta Lago and Tharsis. Geologically speaking, the difference is in the type of deposit, a more stockwork-like deposit for Corta Lago and a more defined vein deposit at Tharsis. Where at Corta Lago we witness the exploitation of a polymetallic ore enriched in sulphides, a cleaner jarositic ore was used at Tharsis. The environmental situation seems to be different if we consider the fuel 'saving' discussed above as a necessity at Corta Lago and not at Tharsis. That would mean that the amount of available wood was much higher at Tharsis than at Corta Lago.

The responses to geological and environmental constraints, finely tuning the standardised process to the context of the site and of the time, suggest a high knowledge of the chemistry of the system during the Roman periods under consideration.

CHAPTER 10

Conclusion

In the introductory chapter we stated the aims of this project as follows:

What was the process employed for the production of silver during the Roman occupation in the Rio Tinto area?

What metallurgical and geological knowledge was applied and what was the economic and socio-political framework within which this production was contextualised?

In the previous chapters, we presented the framework within which these questions are set, and consequently the methodology and the sites chosen to answer these questions. The analytical results were then presented and discussed, and now it is time to sum up our conclusions trying to contextualise the discussed results within the socio-economic context sketched out at the beginning.

The metallurgical process as described in Chapter 6 and reconstructed in Chapter 9 is the smelting of a mineral assemblage mainly composed of the iron-rich ore (jarosite $XFe_3(SO_4)_2(OH)_6$, where X could be K, Na, Ag, Pb or NH_4) with the addition of silica, in an approximate ratio of one to two, in order to achieve a mainly fayalitic (Fe_2SiO_4) slag that would allow a minimum smelting temperature of ~1100 ºC to reach a completely liquid system, and the collection of a silver-rich lead bullion.

These smelting conditions do not undergo major changes through time, but several improvements are visible with the Roman occupation. First of all, no residual crystals of quartz or barite were detectable in the samples starting from the Republican phase I tapped slag onwards at Corta Lago, while they were detected in those from the previous periods. They were not detected in the samples from Tharsis (Roman only), indicating that only the Roman smelters achieved the optimum ratio of jarosite/quartz (both from the gangue and voluntarily added), amount of fuel and forced air (smelting conditions) allowing the quartz to react completely.

The differences between the samples from different periods can be narrowed down to four categories: morphology, concentration of silver and lead, concentration of alkali, and isotopic signature. These were discussed in association with the technological changes and choices.

10.1. Morphological changes

The morphological differences can be further divided into two categories:

1) Tapped versus plate slags. At Corta Lago, we observe the presence of several layers characterised by plate rather than tapped slags. One layer is dated around the middle of the 1st century BC, and thus in the middle of Republican Rome. This phenomenon is not observable at Tharsis, where only tapped slags are present.
2) Increase in size of the tapped slags. This is observable at both sites following the transition from the Republican to the Imperial period. During the Empire, the size of the lava flows typical of the tapped slags doubles, as does the thickness of the slag.

If we focus on the increase in the size of the lava flows first, leaving the issue of the plate slag for later in this chapter, we can say, as stated in Chapters 7 and 9, that this feature of the slags can be linked with the tap hole dimensions of the furnace. Thus, the doubling of the flow size should correspond with a doubling of the tap hole, and suggests a possible increase in the size of the furnace (that could be confirmed only observing possible changes in the size of tuyéres), as well as in the amount of material smelted. Another observation related to this is the presence of consecutive layers of slag in the samples. These layers are separated by an oxidation layer during the Republican period, while there is no oxidation layer detectable during Imperial times, indicating that there was virtually no time delay between the consecutive tappings of slag under the Empire. Also, a larger range of chemical variation is noticeable during the Empire (both at Corta Lago and Tharsis), even though the chemistry is always within the safe range of stability of fayalite.

The increase in the amount of material smelted and the continuity of the process coincides with Imperial times, and it is possibly due to a higher demand for silver for coinage, resulting from greater political stability, as well as the increase in the area dominated politically and economically by the Romans.

The plate slags, on the other hand, have a different explanation. As mentioned above, these appear only at Corta Lago, and occur between periods of tapped slag, thus indicating a temporary change in production technique at that specific time, possibly due to geological constraints (change in the ore composition). Factors relating to the

isotopic signature, alkalis imprint and silver content are all significant for the discussion of these plate slags. It seems here, as discussed in Chapters 6, 8 and 9, that a geological constraint such as the presence of a jarositic ore poorer in lead (and perhaps richer in silver) was addressed with an addition of extra lead metal produced elsewhere ('foreign' lead). The smelting conditions were allowing the crystallisation of feldspathoids and feldspars, and the smelting was followed by tapping of the molten material in a forehearth. The observation of the slag indicates that the bullion was collected inside the furnace, but in any case a more efficient collection of the bullion is observed in this period at Corta Lago, efficiency comparable to Tharsis (where only "normal" tapping debris is recovered). There are few differences visible during this period as compared to the previous ones: the first is the coincidence of a 'foreign' lead isotope signature with higher alkali in the slags. This pattern is not present in the previous periods, or in the later ones. The second difference is the tapping in the forehearth, maybe in order to achieve a more efficient disposing of the metallurgical debris. If this is the case, the indication coming from these observations is that a different smelting tradition was being enacted here (and not in Tharsis), only for a limited period, possibly because a different group of smelters were in charge. These smelters were possibly also importing lead metal, instead of lead ore, to add to the system maybe because they assayed the ore to be poorer in lead and they also attempted to render transport more efficient (the same amount of lead obviously occupies less space in its metal form than as sulphide).

This hypothesis of individual smelters or groups of smelters producing the bullion instead of a larger, 'industrial' scale production seems to be visible also in the periods antedating the plate phase. For instance, we observe grouped chemical distribution within the ternary diagram of the main compounds (Fig. 6.62) when examining the Republican phase I tapped slags at Corta Lago (two groups) and the Republican slags at Tharsis (one tight group).

Going back to have a closer look at the lead isotopic signature, we notice that, as described in Chapter 8, the slags from Corta Lago and Tharsis have an isotopic signature that plots on a mixing line, with Rio Tinto at one end and, it can be hypothesised, Cartagena at the other (the results are consistent with the data published on Cartagena – Figs. 8.3 and 8.4). Regardless of whether the identification of Cartagena here is correct, which is not the aim of this thesis, even though it seems to be the best hypothesis, it is interesting to note that not all the periods under

consideration are influenced by the addition of lead from external sources in the same manner. Phoenician, Iberian and one part of the Republican phase I tapped slag, and the Republican plate slags at Corta Lago show the greatest influence. Observations regarding the concentrations of the alkalis, developed in Chapters 8 and 9, led us to suggest that during the Republican phase II plate slag period the ore was depleted in lead as compared to the previous and following periods, and this was the reason for the addition of lead produced elsewhere. For the other periods, however, another explanation needs to be found.

The variability of the ore seems to be a constant at Corta Lago, where the chemical variability between samples is much higher than at Tharsis. This would corroborate the hypothesis that the Republican phase II plate slag period, where there is a depletion of lead and a possible enrichment in silver in the treated ores, is indicative of a metallurgical answer to a geological constraint, easily coinciding with a change in smelting traditions (forehearth tapping instead of free tapping). It would also explain the chemical variability of the slag as the result of mediation between geological changes and technical availability when the efficiency was not measured only by the loss of silver, but also by the capital invested versus the silver produced, since when the ore is poorer or very variable, this ratio changes significantly.

10.2. Process efficiency

This new morphology (plate slag) also corresponds to improved efficiency in the process and a much lower loss of silver. The same efficiency is achieved at Tharsis both during Republican and Imperial times by keeping the free tapping technology. This high efficiency can be achieved by controlling the length of time during which the system is fully liquid in order to increase the degree of mixing and provide a reaction opportunity for the silver to be absorbed by the lead metal. In one case (Corta Lago) this is achieved only when the slag cooling technique changes suggesting a different smelting school/smelter group, in the other (Tharsis) this is achieved since the beginning of the Roman exploitation of the site, during both the Republican and the Imperial periods. The increased length of time during which the system is liquid seems to be confirmed if we consider that the morphology of the olivines in the plate slag and at Tharsis exhibit a highly euhedral shape but smaller

size when compared with the skeletal big crystals present in the Roman Imperial phases at Corta Lago, indicating an early nucleation of the silicate already within the furnace, which would limit the mobility of the liquid phase during the smelting, trapping a higher amount of lead/silver.

The chemical variability within samples is another index of the precocious nucleation of crystals during smelting. Crystallisation of long chain-shaped olivines reflects early nucleation, and is normally also reflected in high chemical variability within the sample, because the presence of crystals even at early stages impedes the free movement of the chemicals and the homogenisation of the melt. This tends to coincide with higher loss of silver, as we observe during Imperial times at Corta Lago, where an early nucleated skeletal family of olivines is formed in the early stages, limiting the amount of liquid material during the smelt.

In contrast, during the Republican phase II plate slag period, for example, we still observe elongated crystals of similar dimensions to the Imperial ones, but this time they are not skeletal and should be the result of a slow cooling of the slag material and not of an early nucleation of the silicates. This allows a better movement of the chemicals, and we obtain as a result a very efficient process with a very low loss of silver (<50 ppm).

Going back again to the isotope analyses, we noted above that the Phoenician, Iberian and Republican phase I tapped slags are more influenced by a non-Rio Tinto isotopic signature as compared to those from the other periods (Figs. 8.3 and 8.4). Unlike the plate slag, the chemical analyses of these samples do not exhibit differences concerning the alkalis from the other periods, indicating, as discussed in Chapter 8, that there is no depletion of lead in the ore used as raw material during the Phoenician smeltings. This would indicate an addition of unnecessary ‘foreign’ lead for reasons other than technical ones, most likely cultural reasons which were not influential during Ibero-Punic times and certainly not during Roman times. Furthermore, an increase of barium oxide is visible in all these samples, indicating the use of two different ores added together. For the Ibero-Punic and the Republican phase I tapped slag samples, we also observe an increase in sulphur concentration, indicating the addition of sulphide to the system, an increase that is not visible where the lead isotope signature coincides with that of Rio Tinto. As a result, the sulphur and the ‘foreign’ lead signature are considered to be inter-connected features,

indicating the possibility that galena rather than metallic lead was added to the system as a source of extra lead.

10.3. Scale of production

Overall, the Romans did not bring any extraordinary new technology to the processing of jarosite in the Rio Tinto area. They continued using a technology certainly established during the Phoenician period and continued during the Ibero-Punic period. What is clear, though, is that the Romans brought a better understanding of the 'chemistry' and 'mineralogy' of the system, managing a controlled smelting where the complete charge was liquid for a length of time sufficient for an economically advantageous exploitation of the ore. If we take as examples the Republican phase II plate slag period and the Imperial phase at Corta Lago, we can hypothesise two different scenarios. During the former, we have an ore richer in silver and poorer in lead that necessitates the import of lead from elsewhere, requiring extra capital to pay for the imports. There is then a more efficient and overall slower process that produces a certain quantity of silver. During the Imperial period, however, we observe an increase in the scale of production as well as an increase in loss of silver for an ore that does not need addition of 'foreign' lead to be smelted. If the increase in the loss of silver is due, as argued above, to a shortening of the time during which the system is above the *liquidus* temperature, then we can argue that this is a result of mediation between the efficiency of the process and the consumption of fuel in an area where several centuries of ore exploitation had already depleted wood resources, and mainly at a moment when industrial scale production was needed. The situation may be different at Tharsis, where the ore might have had a lower concentration of silver that required higher efficiency for the process to be economically viable, or where fuel supply was less costly since the woodlands were not diminished by centuries of pre-Roman exploitation.

All this can be argued also if we consider the smelting as a small, medium or state-controlled enterprise, and, for instance, consider Rio Tinto and Tharsis as being under different management where the technical choices were concerned.

Slags from both Tharsis and Corta Lago plot isotopically on the same mixing line with a certain degree of separation due to the ore variability, and this seems to

suggest that lead ingots from the same sources were used as additions for silver collection in areas where jarositic ores were exploited. This entire scenario appears to be part of an extensive network of activities easy to understand within a state-controlled system, but can obviously also be explained by private 'companies' interacting with one another.

The technological responses to geological constraints show a clear pattern in industrial scale production areas such as Corta Lago and Tharsis, and even though there are no dramatic changes in production, the fine tuning of a similar process to answer the socio-economic requirements of the different periods can be observed throughout this analytical work.

10.4.Summary

To sum up: the Phoenician period slags show high barium oxide concentration and a mixed lead isotope signature, indicating the mixing of two different ores. During the Ibero-Punic period, we start observing the additional increase of sulphur, indicating the addition of concentrated galena as a source of lead as silver collector. The same occurs during the Republican phase I tapped slag, but in conjunction with the presence of samples with no 'foreign' lead signature, indicating that two processes were being carried out at the same time. Since no enrichment in alkalis was noticeable in the slags from this period, it seems that the two processes were more linked to cultural traditions than being forced by geological constraints. As such, we can infer that different groups of smelters were working in the same area. When we reach the Republican phase II plate slag, we observe a different technology (tapping in the forehearth), together with the presence of a geological constraint (an ore poorer in lead). These indicate that both the geological and chemical knowledge were more advanced, and of the efficiency of the process was improved by the import of material from elsewhere (an import that was itself linked to efficiency criteria - lead metal instead of lead mineral). This may indicate a further economic pressure on the group of smelters that needed to reduce costs and metal losses, since part of the capital was invested in the import of lead metal. A similar pattern is visible at Tharsis, where we observe a very tight chemical composition of the samples, indicative of a

highly skilled metallurgical tradition. With the advent of the Empire, the scenario changes, and we observe an increase in the waste material produced, indicating an increase in the total production, as well as an increase in variation of the chemical range observed, even though it is always in the low temperature range delimited by the fayalite field. As already mentioned in the introduction, it appears as if in this case a recipe was followed by smelters with lower skills, possibly within a state-controlled 'industrial' framework, where the 'quantity' became more important than the 'quality' (efficiency and standardisation of the process).

Overall, it looks like we are looking at centuries of fine tuning within a very similar process, showing the evolution of the process within a changing geological (ore) and natural (fuel) environment, due to the exploitation of the ore and the woodland. The Romans overlay their process on a local production without wasting investment in changing it if not necessary. It seems that during this period (Roman occupation and improvement of the process in the ratio capital invested/improvement in the efficiency), a technical knowledge superseded what was a social/cultural knowledge or habit (with regards to the addition of lead, for example).

Also, what initially seems to be a single small enterprise production (the two process contemporarily existing in the Republican phase I tapped slag and the singular process carried out during the Republican phase II plate slag) within a state-controlled economic system (the products were all 'sold' to the Roman Republic to be used for coinage) changes into a larger scale state enterprise production (the process is overall more standardised for what concerns basic parameters but leaves much more room for 'mistakes', meaning loss of silver for example). At this point, fuel (at least at Corta Lago) becomes an issue, following centuries of exploitation, and the large industrial process allows for compromise in terms of wood consumption, determining a slight decrease in temperature of the process (*solidus* instead of *liquidus* temperature).

Two samples of litharge were recovered from the Iberian assemblage, and one fragment of bullion was recovered from the Imperial assemblage. All of them are explained in a smelting context, the litharge to be re-smelted in a new charge as a recycled lead source, and the lead bullion as a lost fragment in the corner of a furnace. Their presence, though, raises a question regarding the organisation of the smelting and cupellation workshops in the area. Were the locations completely separate,

owned and run by different people in order not to compete, for example for the stock of fuel? Or, on the contrary, were the workshops intimately connected, in order to easily exchange material, like for example bullion to cupel and litharge to recycle? In such an archaeological environment like Corta Lago where the richness of material has led to almost total obliteration of the stratigraphy, the reconstruction of the organisation of work may not be possible.

The problem of the lack of stratigraphically identified material faced during this project creates an unfortunate paucity of statistics for this work, and only tentative suggestions can be made regarding the technological answers. More samples need to be stratigraphically identified through the process of re-establishing the old stratigraphy from the new labelling at the Rio Tinto Museum, for example by using the old excavation notes of Dr Perez Macias. The use of several analytical techniques to generate a comprehensive picture of the available samples analysed in this project did not allow the author to produce a new stratigraphic inventory of the samples stored and to use them to enrich the statistics of the case study. Despite these limitations a framework of changes was noticed and hypothesis to how these changes could be contextualised in a socio-economic context were advanced. Although these hypotheses may be confuted in case of a larger statistical study the proposed approach still remains valid and it could be used to improve the understanding of the economic context.

References

Geological-Mining Map of Andalusia (MGMA, 1985) and Extremadura (MGME, 1987)

Alföldy, G. *Noricum*. Routledge & Kegan Paul, London

Allan, J.C. 1968 The accumulations of ancient slags in the South-West of the Iberian Peninsula. *Bulletin of the Historical Metallurgy Group*, Vol 2 n.1, 47-50

Amoros J.L., Lunar R. and Tavira P. 1981 Jarosite: A silver bearing mineral of the gossan of Rio Tinto (Huelva) and La Union (Cartagena, Spain). *Mineralium Deposita*, 16, 205-213

Anguita Virella, F. and Moreno Serrano, F. 1991. *Procesos Geologicos Internos* Ed. Rueda, Madrid

Anguilano, L. Timberlake, S. Rehren, Th. 2010 An early medieval lead smelting bole from Banc Tynddol, Cwmystwyth, Ceredigion. *Historical Metallurgy* 44 (2), 85-103

Atkins, P.W. 1990 *Physical chemistry*. 4th edition. Freeman W.H. New York

Bachmann, H.G. 1982 *The Identification of Slags from Archaeological Sites*. Institute of Archaeology Occasional Publication, 6. Institute of Archaeology. London

Barriga, F.J.A.S. 1990 Metallogenesis in the Iberian Pyrite Belt. In: R.D. Dallmeyer and E. Martinez Garcia (Eds.) *Pre-Mesozoic Geology of Iberia*, Springer-Verlag, Berlin, 369-379.

Basciano, L.C. Peterson, R.C. 2008 Crystal chemistry of the natrojarosite-jarosite and natrojarosite-hydronium jarosite solid-solution series: a synthetic study with full Fe occupancy. *American Mineralogist* 93, 853-862.

Belén, M. Escacena, J.L. 1990 Niebla (Huelva). Excavaciones junto a la puerta de Sevilla (1978-1982). La cala 8. *Huelva Arqueológica* 12, 169-249.

Binford, L.R. 1962 Archaeology as anthropology. *American Antiquity* 28 (2), 217-25

Binford, L.R. 1972 *An Archaeological Perspective*. New York; London, Seminar Press.

Blanco, A. and Luzon, J.M. 1966 Mineros Antiguos Españoles. *Archivio Español de Arquelogia*, 114-115.

Blanco, A. and Luzon, J.M. 1969 Pre-Roman miners at Riotinto. *Antiquity* 43 n. 170, 124-131.

Blagg, T.F.C. and Read, S. 1977 The Roman pewter-moulds from Silchester. *The Antiquaries Journal* 57, 270-276.

Boulakia, J.D.C. 1972 Lead in the Roman World. *American Journal of Archaeology* 76, 139-144.

Braudel, F. 1985 *The structures of everyday life: the limits of the possible.* Fontana eds. London.

Bui, C., Confalonieri, L., Milazzo, M., and Paltrinieri, E. 1986. Basic Aspects and Limits of XRF Analysis in the case of Old Metal Objects. Comparison with the Alaysis by Absorption and Diffusion of Gamma Radiation. In: Furlan, G., Cassola Guida, P., and Tuniz, C. (Eds.) *New Paths in the Use of Nuclear Techniques for Art and Archaeology* World Scientific, Singapore, 203-228.

Calderon S. 1910 *Los Minerales de Espana*. Junta para Ampliación de Estudios e Investigaciones Científicas, Madrid.

Charlton, M. 2007 Ironworking in Northwest Wales: an evolutionary analysis. PhD thesis. University College London.

Checkland, S.G. 1967 *The mines of Tharsis: Roman, French and British Enterprise in Spain.* Allen and Unwin Ltd. London.

Cohen, C. 2009 Silver production in Porco-Potosi, Bolivia. PhD thesis. University College London.

Colls, D. Domergue, C. Laubenheimer, F. and Liou, B. 1975 Les lingots d'étain de l'épave Port-Vendres II. *Gallia* 33-*1*, 61-94.

Cope, L.H. 1971 Oxygen in Roman coinage metals and alloys. *Numismatic Circular* 79, 402-404.

Craddock, P.T., Freestone, I.C., Gale, N.H., Meeks, N.D., Rothenberg, B. and Tite, M.S. 1985 The investigation of a small heap of silver smelting debris from Rio Tinto, Huelva, Spain. In: Craddock P.T. and Hughes, M.J. (Eds.) *Furnaces and Smelting Technology in Antiquity*. British Museum Occasional Papers 48, London, 199-217.

Craddock, P.T. 1995 *Early Metal Mining and Production*. Edinburgh University Press, Edinburgh.

Crawford, M.H. 1970 Money and exchange in the Roman world. *Journal of Roman Studies* 60, 40-48.

De Launay, L. 1913 *Traité de métallogenie*. Volume 3. Libraire polytechnique C. Béranger, Paris.

Dević, S. and Marčeta, L. 2007 Differences in morphological properties between the olivine group minerals formed in natural and industrial processes. *Journal of Mining and Metallurgy* 43B, 99-105.

Domergue, C. 1966 Les lingots de plomb romains du musée archéologique de Carthagène et du musée naval de Madrid. *Archivo Español de Arqueologia.* 39, 41-72.

Domergue, C. 1987 *Catalogue des mines et de fonderies antiques de la Peninsule Iberique*. 2 Vols. Publications de la Casa de Velazquez. Madrid

Domergue, C. 1990 *Les Mines de la Peninsule Iberique dans l'antiquité Romaine*. Collection de l'Ecole Française de Rome, 127, Rome.

Donaldson, C.H. 1976 An experimental investigation of olivine morphology. *Contributions to Mineralogy and Petrology* 57, 187-213.

Douglas, G. 1924 Notes accompanying Drawing n° 14349. Prepared to show the sites of ancient slag heaps at Rio Tinto from the smelting of copper and silver ores and their relative position to the ore bodies from which this ore was mined. Unpublished.

Duncan-Jones, R. 1974 *The economy of the Roman Empire: quantitative studies.* Cambridge University Press, Cambridge.

Dusanič, S. 1977 Aspects of Roman mining in Noricum, Pannonia, Dalmatia and Moesis Superior. *Aufstieg Niedergang Römische Welt.* 2.6, 52-94

Dutrizac, J.E. Jambor, J.L. and O'Reilly, J.B. 1985 Man's first use of Jarosite: the pre-Roman mining-metallurgical operations at Rio Tinto, Spain. *Canadian Institute of Mining, Metallurgy and Petroleum Bulletin* 76, 859, 78-82.

Ettler, V. Cervinka, R. and Johan, Z. 2009, Mineralogy of Medieval Slags from Lead and Silver Smelting (Bohutín, Príbram district, Czech Republic): Towards Estimation of Historical Smelting Conditions *Archaeometry,* 51, 6, 987-1007.

Faure, F. Trolliard, G. Nicollet, C. and Montel, J.M. 2003 A developmental model of olivine morphology as a function of the cooling rate and the degree of undercooling. *Contributions to Mineralogy and Petrology* 145, 251-263.

Faure, F. and Schiano, P. 2004 Crystal morphologies in pillow basalts: implications for mid-ocean ridge processes. *Earth and Planetary Science Letters* 220, 331-344.

Faure, F. and Schiano, P. 2005 Experimental investigation of equilibration conditions during forsterite growth and melt inclusion formation. *Earth and Planetary Science Letters* 236, 882-898.

Faure, F. Schiano, P. Trolliard, G. Nicollet, C. and Soulestin, B. 2007 Textural evolution of polyhedral olivine experiencing rapid cooling rates. *Contributions to Mineralogy and Petrology* 153, 405-416.

Fernandez Alvarez, G. 1975 Los yacimentos de sulfuros polimetalicos del S.O. Iberico y sus metodos de prospeccion. *Studia Geologica*, 9, 65-102

Fernandez Caliani, J.C. and Requena Abujeta, A. 1993 *Minerales y rocas industrials de Huelva*. Universidad de Sevilla, Sevilla.

Fernández Jurado, J. and Garcia Rincon, J.M. 1988 El area minera de Tejada le Vieja. *Revista Huelva* 79 (6), 23-30.

Fernández Jurado, J. 1993 Plata y plomo en el comercio fenicio-tartesio. In: Arana Castillo, R. Muñoz Amilibia, Ramallo Asensio, Russel, A. *Metalurgia en la Península Ibérica durante el*

primer milenio a.C. Estado actual de la investigación. Ed. Universidad de Murcia, Murcia, 131-165.

Fernández Jurado, J. Garcia Sanz, C. and Rufete Tómico, P. 1992 Prospeccion con sondeo en Peñalosa (Escacena, Huelva). *Anuario Arqueológico de Andalucía* 2, 185-190.

Finley, M.I. 1973 *The ancient economy*. University of California Press, Berkeley.

Finley, M.I. 1992 *Ancient history: evidence and models*, Penguin Books, London.

Flores Caballero, M. 1981 *Las antiguas explotaciones de Rio Tinto*. Disputación de Huelva, Huelva.

Forbes, R. J. 1964 *Studies in ancient technology* Vol 9 Brill, Leiden.

Frost, B. R. 1991 Log oxygen fugacity vs temperature at 1 bar pressure for common buffer assemblages, plotted from algorithms. In: D. H. Lindsley (ed), *Mineralogical Society of America "Reviews in Mineralogy" Volume 25, "Oxide Minerals: Petrologic and Magnetic Significance"*, 1-9.

Gaitzsch, W. 1980 *Eiserne römische Werkzeuge*. British Archaeological Reports Supplementary Series 78. Oxford

Gale, N.H. 1989 Lead isotope analyses applied to provenance studies. A brief review. In: Maniatis, Y. (Ed.) *Archaeometry, Proceedings of the 25th International Symposium*, Elsevier Science Ltd, Amsterdam, 469-502.

Garcia Palomero, F. 1990. Rio Tinto deposits: Geology and geological models for their exploitation and ore-reserve evaluation. In: *Sulphide Deposits, their origin and Processing*, Institute of Materials, Minerals and Mining, London, 17-35.

Garrido Roiz, J.O. 1968 Excavaciones en Huelva. *Excavaciones arqueológicas en España* 63, 3-246.

Giordano, D. Mangiacapra, A. Potuzak, M. Russell, J.K. Romano, G. Dingwell D.B. and Di Mauro, A. 2006, An expanded non-Arrhenian model for silicate melt viscosity: a treatment for metaluminous, peraluminous and peralkaline liquids. *Chemical Geology*, 229, 42-56.

Gómez Toscano, F. Campos Carrasco, J.M. Borja Barrera, F. Castiñeira Sánchez, J. Garcia Rincón, J.M. 1994 Territorio y ocupación en la Tierra Llana de Huelva: el poblamiento de la Edad del Bronce. In: Campos, J.M. Perez, J.A. Gómez, F. (Eds.) *Arqueología en el entorno del bajo Guadiana, Huelva*, Universidad de Huelva, Huelva, 329-350.

Gonzalo Y Tarin J. 1886 *Descripcion Fisica Geologica y Minera de la provincia de Huelva. Tomo I, 1^{a} Parte: Descripcion Fisica; 2^{a} parte: Descripcion Geologica*. Memorias de la Comision del Mapa Geologico de Espana, Madrid.

Greene, K. 1986 *The archaeology of the Roman Economy*. B.T. Batsford Ltd., London.

Groat, L.A. Jambor, J.L. and Pemberton, B.C. 2003 The crystal structure of argentojarosite, $AgFe_3(SO_4)_2(OH)_6$. *Canadian Mineralogist* 41, 921-928.

Hamilton, E.I. 1965. *Applied Geochronology*. Academic Press, Berkley.

Healy, J.F. 1978 *Mining and Metallurgy in the Greek and Roman World*. Thames and Hudson, London.

Hendricks, S.B. 1937 The crystal structures of alunite and the jarosites. *American Mineralogist* 22, 773-784.

Hodder, I. 1987 *Archaeology as long-term history*. Cambridge University Press, Cambridge.

Hopkins, K. 1980 Taxes and trade in the Roman Empire (200BC – AD400). *The Journal of Roman Studies* 70, 101-125.

Hopkins, K. 1983 Introduction. In: Garnsey, P. Hopkins, K. and Whittaker, C.R. (ed.) *Trade in Ancient Economy*. University of California Press, Berkley, 9-25.

Hughes, M.J. 1977 The analysis of Roman tin and pewter ingots. In Oddy, W.A. *Aspects of early metallurgy*. British Museum Occasional Paper, 17, London, 41-50.

Hunt Ortiz, M.A. 1987 *Silver Metallurgy in the South West Iberian Peninsula, with special reference to Rio Tinto, Huelva*. M. Sc. Thesis. Institute of Archaeology. University of London.

Hunt Ortiz, M. A. 2003. *Prehistoric Mining and Metallurgy in South West Iberian Peninsula*. British Archaeological Reports International Series 1188, Oxford.

Ivliev, A.I. Kashkarov, L.L. Kuyunko, N.S. Kalinina, G.V. and Skripnik, A.Ya. 2004 Experimental research of shock-thermal history of carbonaceous chondrites by thermoluminescence and track methods. *Electronic Scientific Information Journal "Herald of the department of Earth Sciences RAS"* 1(22), 1-3.

Jenkin W.A. 1911 Copy of Notes on Ancient Slags sent to Mr. Carlyle in Jan. 1902. Unpublished.

Jones, A.H.M. 1974 *The Roman Economy: Studies in ancient economic and administrative history.* Brunt, P.A. ed. Oxford, Blackwell.

Julivert, M, Fontbote, J.M, Ribeiro, A. and Conde, L. 1974 *Mapa tectonico de la Peninsula Iberica y Baleares*. Ministerio de Industria, Madrid.

Kakavoyannis, E. 2001 The silver ore-processing workshops of the Laurion region. *Association for Business Sponsorship of the Arts* 96, 369-380.

Kassianidou, V. 1992 Monte Romero (Huelva), a Silver Production Workshop of the Tartessian Period in SW Spain, PhD thesis, Institute of Archaeology, UCL.

Kamenetsky, V.S. Kamenetsky, M.B. Sobolev, A.V. Golovin, A.V. Demouchy, S. Faure, K. Sharygin, V.V. and Kuzmin, D.V. 2007 Olivine in the Udachnaya-East kimberlite (Yakutia, Russia): types, compositions and origins. *Journal of Petrology* 49-4, 823-839.

Keesmann, I., 1993, Naturwissenschaftliche Untersuchungen zur antiken Kupfer- und Silberverhuettung in Suedwestspanien. In: H. Steuer and U. Zimmermann (eds), *Montanarchaeologie in Europa*, Thorbecke Verlag, Sigmaringen, 105-122.

Kohut, E. and Nielsen, R.L. 2004 Melt inclusion formation mechanisms and compositional effects in high-An feldspar and high Fo-olivine in anhydrous mafic silicate liquids. *Contributions to Mineralogy and Petrology* 147, 684-704.

Laubenheimer-Leenhardt, F. 1973 *Recherches sur les lingots de cuivre et de plomb d'époque romaine.* De Boccard, E. Paris

Leistel, J.M. Marcoux, E. Thiéblemont, D. Quesada, C. Sánchez, A. Almodóvar, G.R. Pascual, E. and Sáez, R. 1998 The volcanic-hosted massive sulphide deposits of the Iberian Pyrite Belt. *Mineralium Deposita* 33, 2-30.

Lo Cascio, E. 1981 State and coinage in the late Republic and early Empire. *Journal of Roman Studies* 71, 76-86.

Lopez de Azcona, J 1962, Bibliografia de mineria, metalurgia, geologia y ciencias afinos 1778-1961. Instituto Geologico y Minero de España, Madrid.

Luzon J.M. 1968. Contribucion al estudio de la mineria romana en la betica occidental Unpublished. University of Seville thesis

Madoz, P. *Diccionario Geografico-estadistico-historico de Espana y sus posesiones de Ultramar*. Madrid, 1848-1850; reprinted Ambito Ediciones, Madrid, 1984.

Maffei, E. Rua Figueroa 1871, Apuntes para una biblioteca Espanola de libros, folletos y articulos, impresas y manuscritos, relatives al conocimiento y explotacion de las riquezas minerals y a las ciencias auxiliaries. *La Mineria Hispana e Iberoamericana* 1970. Actas del VI congreso Internacional de Mineria. Vol III Catedra de San Isidoro. Leon.

Manasse, A. Mellini, M. and Viti, C. 2001 The copper slags of the Capattoli valley, Campiglia Marittima, Italy. *European Journal of Mineralogy* 13, 949-960.

Marcoux, E. and Sáez, R. 1994. Geoquímica isotópica del plomo de las mineralizaciones hidrotermales tardihercínicas de la faja pirítica Ibérica: *Boletín Sociedad Española Mineralogía* 171, 202-203.

Menchetti, S. and Sabelli, C. 1976 Crystal chemistry of the alumite series: crystal structure refinement of alunite and synthetic jarosite. *Neues Jahrbuch fuer Mineralogie*, 406-417.

Monseur, G. (1977) Mineralisation Cambriennes d''Espagne (essai de sinthese). *Mineralium Deposita*, 12, 331-352.

Mrozek, S 1977 Die Goldbergwerke im römischen Däzien. *Aufstieg Niedergang Römische Welt* 2.6, 95-109.

Mukhopadhyay, D.K. and Lindsley, D.H. 1983 Phase relations in the join kirschsteinite ($CaFeSiO_4$) – fayalite (Fe_2SiO_4). *American Mineralogist* 68, 1089-1094.

Müller, W. Fricke, H. Halliday, A.N. McCulloch, M.T. and Wartho, J. 2003 Origin and migration of the Alpine Iceman. *Science* 302 (5646), 862-866.

Noeske, H.C. 1977 Studien zur Verwaltung und Bevölkerung der dakischen Goldbergwerke in römischer Zeit. *Bonner Jahrbuch* 177, 271-416.

O'Driscoll, B. Donaldson, C.H. Troll, V.R. Jerram, D.A. and Emeleus, C.H. 2007 An origin of harrisitic and granular olivine in the Rum Layered Suite, NW Scotland: a crystal size distribution study, *Journal of Petrology* 48 (2), 253-270.

Painter, K.S. 1977 Gold and silver in the Roman world. In Oddy, W.A. *Aspects of early metallurgy*. Sheffield. 135-158.

Patiak, N.M. Seal, R.R. and Hammarstrom, J.M. 2004 Mineralogical and geochemical controls on the release of trace elements from slag produced by base – and precious – metal smelting at abandoned mine sites. *Applied Geochemistry* 19 (7), 1039-1064.

Parkes, P.A. 1986. *Current scientific techniques in archaeology* Croom Helm, London.

Pellicer, M. 1983 El yacimiento Protohistórico de Quebrantahuesos (Riotinto). *Noticiario Arqueológico Hispánico* 15, 61-91.

Perez Macias, J.A. 1996 *Metalurgia extractiva Prerromana en Huelva*. Universidad de Huleva, Huelva.

Perez Macias J.A. 1998 *Las mines de Huelva en la antigüedad* Huelva, Disputacion Provincial.

Pernicka, E. Begemann, F. Schmitt-Strecker, S. and Grimani, A.P. 1990. On the composition and provenance of metal artifacts from Poliochni on Lemnos. *Oxford Journal of Archaeology*, 9 (3), 263-298.

Pinedo Vara, I. 1963 *Piritas de Huleva*. Ed. Summa, Madrid.

Pliny *Historia Naturalis* (translated by John Bostock –www.perseus.tufts.edu, April 2010)

Ploquin, A., Allée, P., Bailly-Maître, M.C., Baron, S., de Beaulieu, J.-L., Carignan, J., Laurent, S., Lavoie, M., Mahé-Le Carlier, C., Peytavin, J. and Pulido, M. 2003 Medieval lead smelting on the Mont-Lozère, Southern France. *International Conference in Archaeometallurgy in Europe*, 1, 635-644. Associazione Italiana Metallurgia, Milan.

Pomponius Mela *De Chorographia* (translated by Romer, F.E. University of Michigan Press, Ann Arbor.)

Reed, S.J.B. 1996 *Electronic microprobe analysis and scanning electronic microscopy in geology*. Cambridge University Press. Cambridge.

Richardson, J.S. 1976 The Spanish mines and the development of provincial taxation in the second century BC. *Journal of Roman Studies* 66, 139-152.

Rickman, G. 1980 *The corn supply of ancient Rome*. Oxford University Press, Oxford

Rothenberg, B. and Blanco-Freijeiro, A. 1981 *Ancient Mining and Metallurgy in South-West Spain*. Institute for Archaeo-Metallurgical Studies, London.

Rothenberg, B. Andrews, P. and Keesman, I. 1986 Monte Romero, September 1986 – the discovery of a unique Phoenician silver smelting workshop in South-West Spain. *IAMS Newsletter* 9, 1-4.

Rothenberg B. and Andrews P. 1996 Prehistoric Copper Mining in South West Spain: The evidence from Chinflon. Unpublished manuscript.

Routhier, P. 1963 *Les gisements métallifères.* Voulmes 1 et 2. Masson. Paris.

Rua Figueroa, R. 1868 *Minas de Rio Tinto*, Cascante, E. Madrid

Ruiz Mata, D. and Fernández Jurado, J. 1986 El yacimiento metalúrgico de época tartésica de San Bartolomé de Almonte (Huelva). *Huelva Arqueológica* 8

Russel, R.D. and Farquhar R.M. 1960. *Lead Isotopes in Geology*. Intersciences Publishers, New York.

Sahama, Th.G. Siivola, J. and Rehtijärvi, P. 1973 Andremeyerite, a new barium iron silicate from Nyiragongo, Zaire. *Bulletin of the Geological Society of Finland* 45, 1-8.

Salkield, L. U. 1970 Ancient slags in the south-west of the Iberian peninsula. *Proceedings of the sixth international mining congress*. Catedra de San Isidoro, León.

Salkield, L.U. 1987 *A technical history of the Rio Tinto Mines: some notes on exploitation from pre-Phoenician times to the 1950s*. The Institute of Mining and Metallurgy, London.

Stos-Gale, Z.A. Gale, N.H. Houghton, J. and Speakman, R. 1995 Lead isotope analyses of ores from the western Mediterranean. *Archaeometry* 32 (2), 407-415.

Strabo *The Geography* Translation 1903, George Bell and Sons, London.

Strauss, G.K and Gray, K.G. 1986 Base Metal Deposits in the Iberian Pyrite Belt, In: Friedrich, G.H. (Ed.) Geology and Metallogeny of Copper Deposits, Springer-Verlag, Berlin. 304-324.

Thirlwall, M.F. 2003 Multicollector ICP-MS analysis of Pb isotopes using a (207)Pb-(204)Pb double spike demonstrates up to 400ppm/amu systematic errors in Tl normalization. *Chemical Geology* 184 (3-4), 255-279.

Tisseyre, P. Tusa, S. Cains, W.R.L. Bottacin, F.S. Barbante, C. Ciriminna, R. and Pagliaro, M. 2008 The lead ingots of Capo Passero: Roman Global Mediterranean Trade. *Oxford Journal of Archaeology* 27 (3), 315-323.

Tornos, F. González Clavijo, E. and Spiro, B. 1998 The Filon Norte orebody (Tharsis, Iberian Pyrite Belt): a proximal low-temperature shale-hosted massive sulphide in a thin-skinned tectonic belt. *Mineralium Deposita* 33, 150-169.

Tranoy, A. 1981 *La Galice romaine: recherches sur le nord-ouest de la péninsula ibérique dans l'antiquité*. Centre Pierre Paris, Paris.

Tylecote, R.F. Rothenberg, B. and Lupu, A. 1974 The examination of metallurgical material from Abu Matar, Israel. *Historical Metallurgy* 8 (1), 32-34.

Tylecote, R.F. 1987 *The early history of metallurgy in Europe*. Longman, London.

Veldhuijzen, A, 2003 Slag_Fun" A New Tool for Archaeometallurgy: Development of an Analytical (P)ED-XRF Method for Iron-Rich Materials, *Papers from the Institute of Archaeology* 14, 102-118.

Ward-Perkins, J.B. 1980 Nicomedia and the marble trade. *Papers of the British School at Rome* 48, 23-69.

Williams, D. 1934 The Geology of the Rio Tinto Mines, Spain. *Bulletin of the Institute of Mining and Metallurgy*, 43, 593-678.

Williams, D. 1950 Gossanized Breccia-Ores, Jarosites, and Jaspers at Rio Tinto, Spain. *Bulletin of the Institute of Mining and Metallurgy* 59, 1-12.

APPENDIX 1

Glossary of the chemical compositions of the minerals mentioned in the text

Alloclasite	(Co,Fe)AsS
Anglesite	$PbSO_4$
Ankerite (Ankeritic carbonates)	$Ca(Fe,Mg,Mn)(CO_3)_2$
Argentojarosite	$AgFe_3(SO_4)_2(OH)_6$
Arsenopyrite	FeAsS
Azurite	$Cu_3(CO_3)_2(OH)_2$
Barian aluminium silicate	$BaAl_2Si_2O_8$
Barian orthoclase	$(K, Ba, Na)(Si,Al)_4O_8$
Barite	$BaSO_4$
Bismuthinite	Bi2S3
Bornite	Cu5FeS4
Bournonite	PbCuSbS3
Calcite	CaCO3
Cassiterite	SnO2
Celadonite	$K(Al,Fe,Mg)_2Si_4O_{10}(OH)_2$
Cerussite	$PbCO_3$
Chalcocite	Cu2S
Chalcopyrite	CuFeS2
Chrysocolla	(Cu,Al)2H2Si2O5(OH)4*nH2O
Cobaltite	CoAsS
Cosalite	Pb2Bi2S5
Covellite	CuS
Cubanite	CuFe2S3
Dolomite	CaMg(CO3)2
Famatinite	Cu3SbS4
Fayalite	Fe_2SiO_4
Fluorite	CaF2
Galena	PbS
Giessenite	2(Cu2Pb26(Bi,Sb)2OS57
Glaucodot	(Co,Fe)AsS
Goethite	FeO(OH)

Graphite	C
Haematite	Fe_2O_3
Hammarite	Pb2Cu2Bi4S9
Ilmenite	FeTiO3
Jarosite	$XFe_3(SO_4)_2(OH)_6$ where X=K, Na, Pb, Ag and NH_4
Joseite	Bi4TeS2
Kirschteinite	CaFeSiO4
Kobellite	Pb22Cu4(Bi,Sb)3OS69
Leucite	KalSi2O6
Limonite	FeO(OH) *nH2O
Löllingite	FeAs2
Mackinawite	(Fe,Ni)9S8
Magnetite	Fe_3O_4
Malachite	Cu2(CO3)(OH)2
Meneghinite	Pb13CuSb7S24
Natrojarosite	$NaFe_3(SO_4)_2(OH)_6$
Nuffieldite	Pb2Cu(Pb,Bi)Bi2S7
Plumbojarosite	$PbFe_6(SO_4)_4(OH)_{12}$
Pyrite	FeS2
Pyrrhotite	Fe1-xS
Quartz	SiO_2
Rutile	TiO2
Scheelite	CaWO4
Scorodite	$FeAsO_4*2H_2O$
Sericite (Muscovite)	KAl2(AlSi3O10)(OH)2
Siderite	FeCO3
Sphalerite	ZnS
Stannite	Cu2FeSnS4
Stibnite	Sb2S3
Tennantite	Cu10(Fe,Zn)2As4S13
Tetradymite	Bi2Te2S
Tetrahedrite	Cu10(Fe,Zn)2Sb4S13
Wittichenite	Cu3BiS3
Zircon	ZrSiO4

APPENDIX 2

Section 2.1. Preparation of the solution for MC-ICP-MS

20 milligrams of powder were accurately weighed and mixed with 0.250 ml of nitric acid 16 molar. Subsequently 1.00 ml of hydrofluoric acid 29 molar was added, necessary to break the silicate chemical links and form the volatile SiF_4. The solutions obtained stayed then 36 hours on the hot plate at 100°C to have most of the links disaggregated. Then 0.5 ml of distilled water were added to the solution, and left to evaporate on the hot plate.

At this point a spike of ^{208}Pb in HNO_3 2 molar was added in the so called blank sample. The blank sample shows the level of contamination in the laboratory; it is an empty specimen that undergoes exactly the same steps as the samples, but does not contain any sample itself.

When the evaporation is completed 1 ml of HCl is added and then the samples are placed on the hot plates to dry again. At this point the formation of chlorides happens so the addition of 1 ml HNO_3 is necessary. The solution is left for 15 minutes to react on the hot plate and is left to evaporate on the hot plate. When the solution is dried, 1 ml of HCl 1M is added and then left to evaporate. Subsequently another 1ml of HCl 1 M is added and the solution is retained.

A column is prepared for the samples to go through an ion exchanger resin. In this case, the resin is a Sr Spec resin, which, in an acid environment keeps Sr and Pb while leaves all the other ions to pass through. Before being used, the resin is washed several times with different concentration of HCl and then the solution is poured on it and left to go through the resin. After all the acid left the resin the column is washed with water. The peculiarity of this resin is that in an aqueous environment strontium is not held anymore, so only lead is finally kept in the resin. In order to take the lead out of the resin another acidic washing is needed. HCl 8 molar is used to wash the column: at this point, lead is obtained in HCl solution. This solution needs to be diluted to a maximum level of 100ppb of lead. The dilutions were done by adding nitric acid with a concentration of 2% to obtain a 100ppb lead solution starting from the initial concentration of lead determined in the samples by XRF.

Section 2.2. LIA results

The following table includes the lead isotope measurement of the samples from Corta Lago and Tharsis

		Pb206/Pb204	Pb207/Pb206	Pb208/Pb206	Pb207/Pb204	Pb208/Pb204
Ball slag	RT24n7	18.2139	0.8582	2.0971	15.6305	38.1962
	RT24n8	18.2166	0.8582	2.0973	15.6339	38.2049
	RT24n9	18.214	0.8581	2.0968	15.6291	38.1903
Phoenician slag	RT25 L126 S22	18.3047	0.8546	2.0984	15.6434	38.4114
	RT25 L101 S35	18.2252	0.8576	2.1031	15.6295	38.3303
	RT25 L101 S39	18.334	0.8535	2.0971	15.6484	38.4481
	RT25 L101 S5	18.393	0.851	2.0949	15.6526	38.5314
	RT25 L101 S16	18.422	0.8498	2.0938	15.6547	38.5719
Iberians samples	RT25 L115 S55	18.3485	0.8544	2.1003	15.6769	38.538
	RT25 L115 S56	18.3397	0.8543	2.1002	15.6675	38.5164
Republican Phase I	RT25 L2 S75rtm	18.1919	0.8594	2.1018	15.6336	38.2366
	RT25 L3 S74rtm	18.2029	0.8584	2.1015	15.6258	38.2531
	RT25 L3 S86rtm	18.1831	0.8595	2.1019	15.6277	38.2189
	RT25 L3 S85rtm	18.391	0.8516	2.0965	15.6619	38.5569
	RT25 L31 S7	18.2027	0.8587	2.1011	15.6306	38.2461
	RT25 L31 S18	18.3331	0.8538	2.0973	15.6536	38.4505
	RT25 L31 S19	18.3698	0.8524	2.0965	15.6591	38.5121
	RT25 L31 S83rtm	18.2017	0.8588	2.1015	15.6322	38.2503
	RT25 L114 S84	18.3918	0.851	2.0949	15.6522	38.5282
Republican Phase II	RT25 L52 S79rtm	18.4314	0.8493	2.0929	15.6541	38.5757
	RT25 L55 S82rtm	18.4108	0.8503	2.0942	15.6539	38.5552
	RT25 L52 S1	18.4226	0.8499	2.0937	15.6576	38.5712
	RT25 L52 S2	18.4193	0.8504	2.0949	15.6646	38.587
	RT25 L52 S3	18.386	0.8517	2.0961	15.6596	38.5382
	RT25 L52 S4	18.3762	0.8519	2.0957	15.655	38.5119
	RT25 L52 S17	18.434	0.8493	2.0932	15.6567	38.5868

		Pb206/Pb204	Pb207/Pb206	Pb208/Pb206	Pb207/Pb204	Pb208/Pb204
Republican Phase III	RT25 L72 S72rtm	18.2714	0.8559	2.0987	15.639	38.3467
	RT25 L87 S77rtm	18.1925	0.8591	2.1016	15.6301	38.2328
Imperial slag	RT24S2	18.264	0.8562	2.0982	15.6372	38.3216
	RT24S3	18.183	0.8595	2.1017	15.6277	38.2153
	RT24S4	18.1831	0.8594	2.1012	15.6266	38.2069
	RT24S5	18.189	0.8593	2.1011	15.63	38.2165
	RT24S6	18.1883	0.8592	2.1016	15.6269	38.2243
semi-reactyed ores	4MIN RT	18.1884	0.8591	2.1002	15.6253	38.1996
	5MIN RT	18.2508	0.8569	2.0996	15.6388	38.3187
	6MIN RT	18.1878	0.8592	2.101	15.6262	38.2134
	7MIN RT	18.1855	0.8592	2.1008	15.6248	38.2044
	8MIN RT	18.1958	0.8592	2.1015	15.6333	38.2383
	10MIN RT	18.1886	0.8587	2.0996	15.6179	38.1882
	9MINRT	18.2023	0.859	2.1015	15.6357	38.2529
	12MIN RT	18.215	0.8584	2.1018	15.6355	38.285
	11MIN RT	18.2126	0.8585	2.1019	15.6352	38.2807
ingots	1Pb RT	18.1878	0.8591	2.1005	15.6257	38.2035
	2Pb RT	18.7196	0.8376	2.0828	15.6798	38.989
	3Pb RT	18.3356	0.8546	2.1006	15.6704	38.5167
Tharsis	THA-REP4	18.4053	0.8513	2.0973	15.6682	38.6019
	THA-REP1	18.2852	0.8564	2.1021	15.6593	38.4382
	THA-IMP10	18.217	0.8591	2.1054	15.6501	38.3544
	THA-IMP9	18.1874	0.8601	2.1058	15.6422	38.2987

Figure 1 table of the LIA results